Physical and Link Layer Implications in Vehicle Ad Hoc Networks

By

Ghassan Mohammed Taha Abdalla

A thesis submitted to the University of Plymouth

in partial fulfillment for the degree of

DOCTOR OF PHILOSOPHY

School of Computing, Communications and Electronics

Faculty of Technology

In collaboration with

France Telecom

August 2009

Physical and Link Layer Implication in Vehicle Ad Hoc Networks

Ghassan Mohammed Taha Abdalla

Abstract

Vehicle Ad hoc Networks (VANET) have been proposed to provide safety on the road and deliver road traffic information and route guidance to drivers along with commercial applications. However the challenges facing VANET are numerous. Nodes move at high speeds, road side units and basestations are scarce, the topology is constrained by the road geometry and changes rapidly, and the number of nodes peaks suddenly in traffic jams. In this thesis we investigate the physical and link layers of VANET and propose methods to achieve high data rates and high throughput.

For the physical layer, we examine the use of Vertical BLAST (VBLAST) systems as they provide higher capacities than single antenna systems in rich fading environments. To study the applicability of VBLAST to VANET, a channel model was developed and verified using measurement data available in the literature. For no to medium line of sight, VBLAST systems provide high data rates. However the performance drops as the line of sight strength increases due to the correlation between the antennas. Moreover, the performance of VBLAST with training based channel estimation drops as the speed increases since the channel response changes rapidly. To update the channel state information matrix at the receiver, a channel tracking algorithm for flat fading channels was developed. The algorithm updates the channel matrix thus reducing the mean square error of the estimation and improving the bit error rate (BER). The analysis of VBLAST-OFDM systems showed they experience an error floor due to inter-carrier interference (ICI) which increases with speed, number of antennas transmitting and number of subcarriers used. The update algorithm was extended to VBLAST-OFDM systems and it showed improvements in BER performance but still experienced an error floor. An algorithm to equalise the ICI contribution of adjacent subcarriers was then developed and evaluated. The ICI equalisation algorithm reduces the error floor in BER as more subcarriers are equalised at the expense of more hardware complexity.

The connectivity of VANET was investigated and it was found that for single lane roads, car densities of 7 cars per communication range are sufficient to achieve high connectivity within the city whereas 12 cars per communication range are required for highways. Multilane roads require higher densities since cars tend to cluster in groups. Junctions and turns have lower connectivity than straight roads due to disconnections at the turns. Although higher densities improve the connectivity and, hence, the performance of the network layer, it leads to poor performance at the link layer. The IEEE 802.11p MAC layer standard under development for VANET uses a variant of Carrier Sense Multiple Access (CSMA). 802.11 protocols were analysed mathematically and via simulations and the results prove the saturation throughput of the basic access method drops as the number of nodes increases thus yielding very low throughput in congested areas. RTS/CTS access provides higher throughput but it applies only to unicast transmissions. To overcome the limitations of 802.11 protocols, we designed a protocol known as SOFT MAC which combines Space, Orthogonal Frequency and Time multiple access techniques. In SOFT MAC the road is divided into cells and each cell is allocated a unique group of subcarriers. Within a cell, nodes share the available subcarriers using a combination of TDMA and CSMA. The throughput analysis of SOFT MAC showed it has superior throughput compared to the basic access and similar to the RTS/CTS access of 802.11.

Contents

List of Figures

List of Tables

Glossary

AC	Access Category
ACK	Acknowledgment
ADAS	Advanced Driver Assistance Systems
AIFS	Arbitrary Inter-Frame Space
AOA	Angle of Arrival
AOD	Angle of Departure
AODV	Ad hoc On-Demand Distance Vector
AP	Access Point
AR	Auto Regressive
ARMA	Auto-Regressive Moving Average
ASK	Amplitude Shift Keying
ASTM	American Society for Testing and Materials
ATIM	Ad hoc Traffic Indication Messages
AWGN	Additive White Gaussian Noise
BEB	Binary Exponential Back-off
BER	Bit Error Rate
BLAST	Bell Labs Layered Space Time
BTMA	Busy Tone Multiple Access
CBF	Contention Based Forwarding
CBMAC	Cluster Based Medium Access Control
CBR	Constant Bit Rate
CDM	Code Division Multiplexing
CDMA	Code Division Multiple Access
CFP	Contention Free Period
CH	Cluster Head
CP	Contention Period
CSI	Channel State Information
CSMA	Carrier Sense Multiple Access
CSMA/CA	Carrier Sense Multiple Access with Collision Avoidance
CTS	Clear To Send
CW	Contention Window
DBLAST	Diagonal Bell Labs Layered Space Time
DBTMA	Dual Busy Tone Multiple Access
DCA	Dynamic Channel Assignment
DCF	Distributed Coordination Function
DFE	Decision Feedback Equaliser
DIFS	Distributed Inter-Frame Space

DRGS	Dynamic Route Guidance System
DSRC	Dedicated Short Range Communications
DSSS	Direct Sequence Spread Spectrum
eCall	Emergency Call
EDCA	Enhanced Distributed Channel Access
EDCF	Enhanced Distributed Coordination Function
EIFS	Extended Inter Frame Space
FDM	Frequency Division Multiplexing
FDMA	Frequency Division Multiple Access
FFT	Fast Fourier Transform
FHSS	Frequency Hopping Spread Spectrum
FI	Frame Information
GBSB	Geometrical Based Single Bounce
GSM	Global System for Mobile Communications
GyTAR	Greedy Traffic Aware Routing
HBLAST	Horizontal Bell Labs Layered Space Time
HMI	Human-Machine Interaction
ICI	Inter-Carrier Interference
IDFT	Inverse Discrete Fourier Transform
IEEE	Institute of Electrical and Electronic Engineers
IFFT	Inverse Fast Fourier Transform
IP	Internet Protocol
ISI	Inter Symbol Interference
LSE	Least Square Error
MAC	Medium Access Control
MANET	Mobile Ad hoc Networks
MH	Must-Have
MIMO	Multiple Input Multiple Output
ML	Maximum Likelihood
MMAC	Multi-Channel Medium Access Control
MMSE	Minimum Mean Square Error
MRC	Maximal Ratio Combining
MSE	Mean Square Error
NAV	Network Allocation Vector
OBU	On Board Unit
ODMA	Opportunity Driven Multiple Access
OFDM	Orthogonal Frequency Division Multiplexing
OFDMA	Orthogonal Frequency Division Multiple Access
PBF	Position Based Forwarding

PCF	Point Coordination Function
PDA	Personal Digital Assistant
PDF	probability density function
PIFS	Priority Inter-Frame Space
PSK	Phase Shift Keying
PTP	Point To Point
QAM	Quadrature Amplitude Modulation
QoS	Quality of Service
QPSK	Quadrature Phase Shift Keying
R2V	Roadside to Vehicle communications
R-ALOHA	Reservation ALOHA
RES	Reserve
Res-Req	Reservation Request
RI-BTMA	Receiver Initiated Busy Tone Multiple Access
RS	ReServation slot/period
RSU	Road Side Unit
RTS	Request To Send
RTTI	Real-time Traffic and Travel Information
S-ALOHA	Slotted ALOHA
SDMA	Space Division Multiple Access
Seq	Sequence Number
SIFS	Short Inter-Frame Space
SINR	Signal to Interference plus Noise power Ratio
SIR	Signal to Interference power Ratio
SISO	Single Input Single Output
SNR	Signal to Noise power Ratio
STBC	Space Time Block Code
STC	Space Time Code
STTC	Space Time Trellis Code
TBLAST	Turbo Bell Labs Layered Space Time
TCP	Transmission Control Protocol
TDD	Time Division Duplexing
TDM	Time Division Multiplexing
TDMA	Time Division Multiple Access
TS	Transmission Slot
TTL	Time To Live
UDP	User Datagram Protocol
UTRA	Universal Terrestrial Radio Access
V2V	Vehicle to Vehicle communications

VANET	Vehicle Ad hoc Networks
VBLAST	Vertical Bell Labs Layered Space Time
VICS	Vehicle Information and Communication System
VMESH	Vehicular Mesh
WAVE	Wireless Access for Vehicular Environment
WBSS	Wave Basic Service Set
WiMAX	Worldwide Interoperability for Microwave Access
WLAN	Wireless Local Area Network
WTRP	Wireless Token Ring Protocol
ZF	Zero Forcing

Acknowledgement

First of all I would like to thank my supervisors Dr Mosa Ali Abu-Rgheff for his continuous support and guidance throughout this project and Dr Mohammed Zaki Ahmed for his valuable discussion and advice. My sincere gratitude is due to Dr Sidi-Mohammed Senouci from France Telecom for his remarks, ideas and support during these last three years. I am deeply grateful to The University of Plymouth and France Telecom for supporting this work. I wish also to thank the staff at the School of Computing, Communications and Electronics for their support. Finally, I would like to thank my family and friends for their encouragement, understanding and patience. To all of you, thank you.

Author's Declaration

At no time during the registration for the degree of Doctor of Philosophy has the author been registered for any other University award.

This study was funded in part by France Telecom and a University bursary.

Publications:

Conference Papers

[1] G. M. T. Abdalla, M. A. Abu-Rgheff, and S.-M. Senouci, "Current Trends in Vehicular Ad Hoc Networks," in *UBIROADS Workshop, IEEE GIIS Conference,* Marrakech, Morocco, 2-6 July 2007.

[2] G. M. T. Abdalla, M. A. Abu-Rgheff, and S. M. Senouci, "A Channel Update Algorithm for VBLAST Architecture in Vehicular Ad-hoc Networks," in *Wivec 2008* Calgary, Canada, 21–22 Sep 2008.

[3] G. Abdalla, M. A. Abu-Rgheff, and S. M. Senouci, "Space-Orthogonal Frequency Time Medium Access Control (SOFT MAC) for VANET," in *IEEE GIIS*, Hammamet, Tunisia, 22-26 June 2009.

Journal Papers

[4] G. M. T. Abdalla, M. A. Abu-Rgheff, and S. M. Senouci, "Current Trends in Vehicular Ad Hoc Networks," in *UbiCC Journal-Special Issue of UbiRoads 2007*. vol. UbiRoads -Special Issue, March 2008.

[5] G. M. T. Abdalla, M. A. Abu-Rgheff, and S. M. Senouci, "An Adaptive Channel Model for VBLAST in Vehicular Networks," *EURASIP Journal on Wireless Communications and Networking,* vol. 2009, 2009.

[6] G. Abdalla, M. A. Abu-Rgheff, and S. M. Senouci, "Channel Tracking for VBLAST," *IEEE Vehicular Technology Magazine,* vol. 4, pp. 71-77, March 2009.

[7] G. M. T. Abdalla, M. A. Abu-Rgheff, and S. M. Senouci, "Joint Channel Tracking and ICI Equalisation for VBLAST-OFDM in VANET", *Accepted for IET Intelligent Transport Systems*, Jan 2009

[8] G. M. T. Abdalla, M. A. Abu-Rgheff, and S. M. Senouci, "Evaluation of SOFT MAC for VANET", *Submitted for IET Communications*, October 2009

Patent

[9] M. A. Abu-Rgheff, G. M. T. Abdalla, and S.-M. Senouci, "Space-Orthogonal Frequency-Time Medium Access Control (SOFT MAC) for VANET," French patent INDI FR #0951620, France, 13 March 2009, p. 24.

Word count of main body of thesis: 55,896

Signed .....

Date ..12/01/2010.....

Chapter 1

Introduction

1.1. Motivations

Millions of accidents occur around the world and thousands of lives are lost in car crashes every year. A large number of these accidents can be avoided if information about traffic and road conditions ahead is provided to the driver. Sensors can be installed in cars to inform drivers of road conditions but their operation range is limited to a few tens of meters. By receiving information about the road from cars ahead via wireless communication systems, the effective sensing range can be increased to several kilometers. For these reasons, safety applications, route guidance and traffic control applications have received special research interest. Governments estimate the losses due to traffic jams in millions of pounds every year. Traffic jams usually occur due to the inefficient use of the road network. Drivers tend to use similar routes leading to high traffic in certain roads while alternative routes experience low traffic. A dynamic route guidance system which takes into account the current traffic density will calculate the best route for that particular time.

Although a large number of these applications are already available to users, they are provided as distributed unrelated solutions. The aim of Vehicle Ad hoc Networks (VANET) is to provide safety, route guidance and other traffic related applications along with commercial applications using a unique communication system. The vision is to provide free safety and basic traffic information to all the users on the road while commercial and advanced traffic related applications are provided upon subscription with service providers. This motivated governments, car manufacturers and

communication service providers to backup research in the area of VANET and push towards establishing a single worldwide standard.

VANET is a special type of Mobile Ad hoc Networks (MANET). VANET is characterized by high speed nodes with a predictable topology constraint by the geometry of the road. The high speed encountered in VANET is a major issue in the design of the wireless system. Since the communication time will be very short, high data rates are required to exchange as much information as possible in this limited communication duration. Moreover the communication system should work without the intervention of the driver. VANET, on the other hand, has a number of advantages compared to MANET. Space is not an issue in VANET, therefore advanced multiple antenna systems can be deployed in the nodes. Nodes in VANET also have no power and weight constraints hence complicated algorithms and hardware can be employed. This research investigates the physical and link layers to identify their limitations and challenges, and propose solutions to achieve high data rates in VANET.

1.2. Aims and Objectives

The aims of this research are to investigate and identify the limitations of the physical and link layers in VANET and develop algorithms to overcome these limitations and achieve high data rates in VANET. Towards these aims the project took the following line of research:

Physical Layer

- Review in detail the literature to identify the available standards and proposals, their strengths, their limitations, and develop an understanding of the main issues and problems in VANET. Based on this review, MIMO-VBLAST systems were chosen as the most feasible solution to achieve high data rates.
- To investigate the applicability of VBLAST to VANET, a channel model to simulate the performance of antenna arrays was developed. The statistics of the channel model were compared to measurement statistics from the literature to verify its applicability to VANET. The performance of VBLAST with a narrow

band channel and perfect channel knowledge at the receiver was then simulated in Matlab using the developed channel model. The results were compared with mathematical expressions and showed reasonable agreement.

- The bit error rate of VBLAST with channel estimation via a training sequence was examined via simulations and found to be quite poor. To enhance the performance of the system, a channel tracking algorithm was developed and evaluated. The channel tracking algorithm enhanced the performance of VBLAST and improved its bit error performance.
- The proposed physical layer standard for VANET uses OFDM. We extended our Matlab model to VBLAST-OFDM systems and studied their performance. Beside the requirement for channel tracking, OFDM systems are limited at high speeds by Inter-Carrier Interference (ICI). We mathematically analysed the ICI for VBLAST-OFDM. Then the channel tracking algorithm was extended to OFDM and an algorithm to reduce ICI was also developed and evaluated.

Link Layer

- Review in detail the standards and proposals for the link layer and identify their advantages and shortcomings. A standard based on IEEE 802.11 standards is under development for the link layer of VANET.
- Investigate the connectivity in VANET and identify the required node density to achieve high connectivity and the expected number of neighbours.
- The performance of 802.11 standards were analysed both mathematically and via simulations using NS2 to identify their limitations. 802.11 standards perform poorly under high traffic and high node densities and have little support for quality of service. To ensure high performance the number of nodes should be controlled and the number of hidden nodes should be minimised.
- A link layer protocol for VANET was developed and evaluated. The protocol limits the number of neighbours by dividing the road into cells and allocating subcarriers to cells. A combined TDMA-CSMA method is then used to organize access within the cell. Nodes exchange information about ongoing transmissions

to minimise the number of hidden terminals. The protocol showed superior throughput performance compared to 802.11 standards.

1.3. Thesis Structure

The rest of the thesis is organized as follows:

Chapter 2 provides an overview of VANET communication architecture and protocols and reviews the available standards and proposals for the physical and link layers. It also highlights the challenges, requirements and limitations found in VANET.

Chapter 3 introduces our channel model and studies the applicability of VBLAST systems to VANET. The bit error performance of VBLAST is also investigated with perfect channel knowledge and using training sequence channel estimation at the receiver.

Chapter 4 describes and evaluates our channel tracking algorithm for VBLAST in a flat fading channel. The algorithm is then extended to VBLAST-OFDM systems and, afterwards, an ICI cancellation algorithm is proposed and evaluated.

Chapter 5 discusses the wireless connectivity of nodes in VANET. The connectivity model used is first introduced then the connectivity in highways and within city's roads and roundabouts is investigated in detail. The results are compared with those from the literature.

Chapter 6 analyses the throughput performance of 802.11 standards. Mathematical models are first introduced and then the results are presented and analysed. Results from a simulation model are also presented.

Chapter 7 introduces the proposed link layer protocol and discusses its rules and implementation in detail. A mathematical derivation for the design of its parameters is developed followed by a mathematical analysis of its throughput performance. The throughput performance is then evaluated and compared with the performance of 802.11 standards.

Finally chapter 8 draws the conclusions of the work and highlights some open issues and future work.

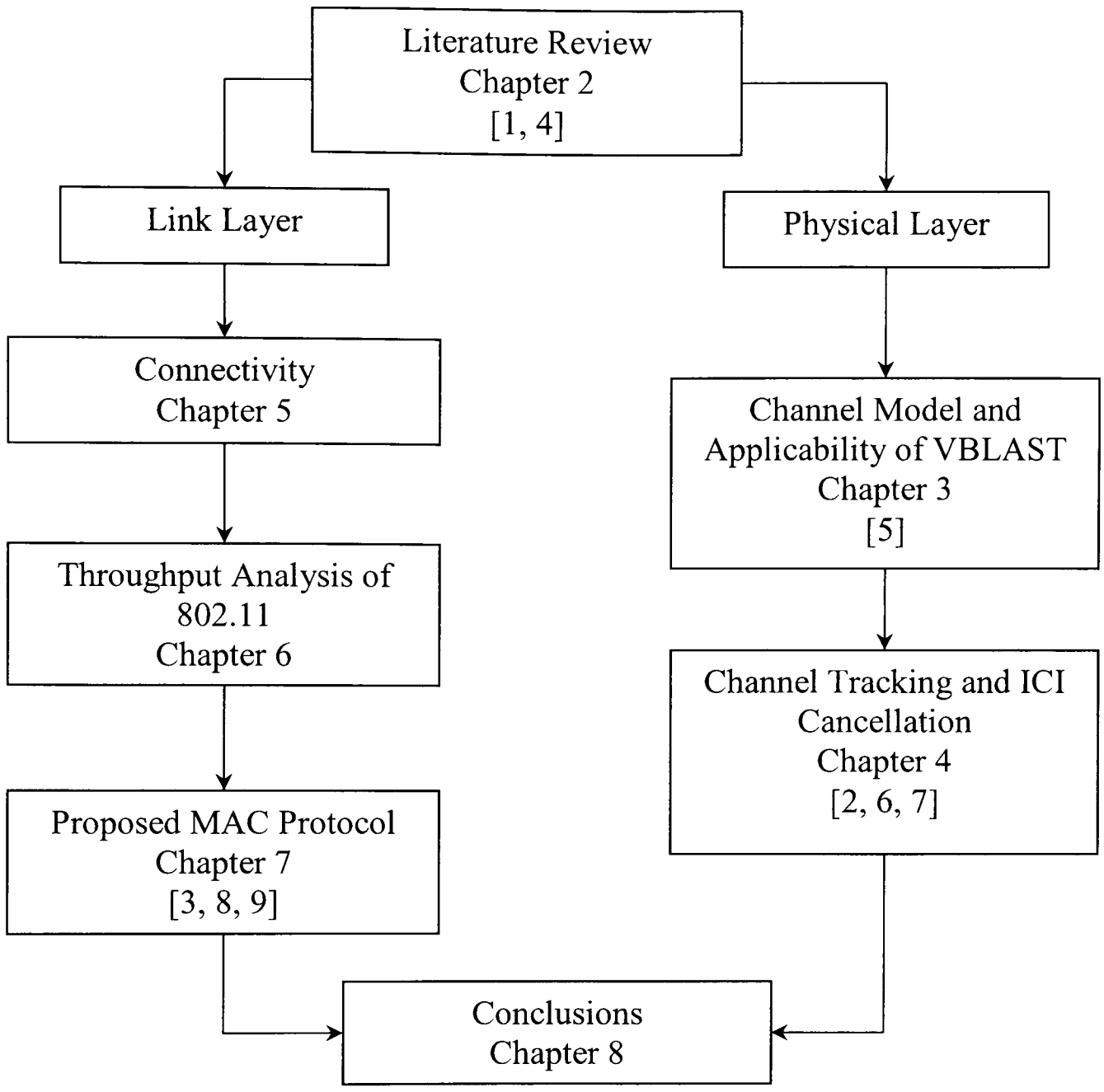

Figure (1.1): Thesis Structure

Chapter 2

Literature Review

2.1. Overview

A lot of research work has been conducted recently on vehicular communications. The research is backed up by government authorities, car manufacturers as well as the communication industry. The aim is to develop a complete communication system that can provide Vehicle to Vehicle communications (V2V) as well as Roadside to Vehicle communications (R2V). Through this system, cars would receive information about accidents, traffic status and weather conditions to prevent car crashes and traffic jams. Along with these, several commercial applications can be provided by vendors such as internet access, route guidance and tourism information provision. Several implementations for the VANET communication system have been proposed [10-13]. In this chapter we review the work on vehicle ad hoc networks (VANET) related to the project and investigate the issues facing VANET that need to be resolved. We identify the challenges and discuss the existing solutions and standards for VANET communications. The chapter is partially based on the publications [1, 4].

2.2. VANET Architecture

The Institute of Electrical and Electronic Engineers (IEEE) released in 2006 a draft for the VANET communication protocol architecture shown in figure (2.1) [12]. The architecture consists of a data plane and a management stack. The data plane consists of two stacks, one is the ordinary Internet Protocol (IP) stack using User Datagram Protocol (UDP) and IP version 6 and the other is a new stack known as the Wireless Access for Vehicular Environment (WAVE) stack. The IP stack is used to communicate user data whereas the WAVE stack is used for communicating safety and traffic related

information. Both stacks share the physical and link layers. The management plane manages the different layers of the stack and responds to service announcements received from Road Side Units (RSU). The functions and operations of the different layers and protocols are not yet finalised [11, 12, 14].

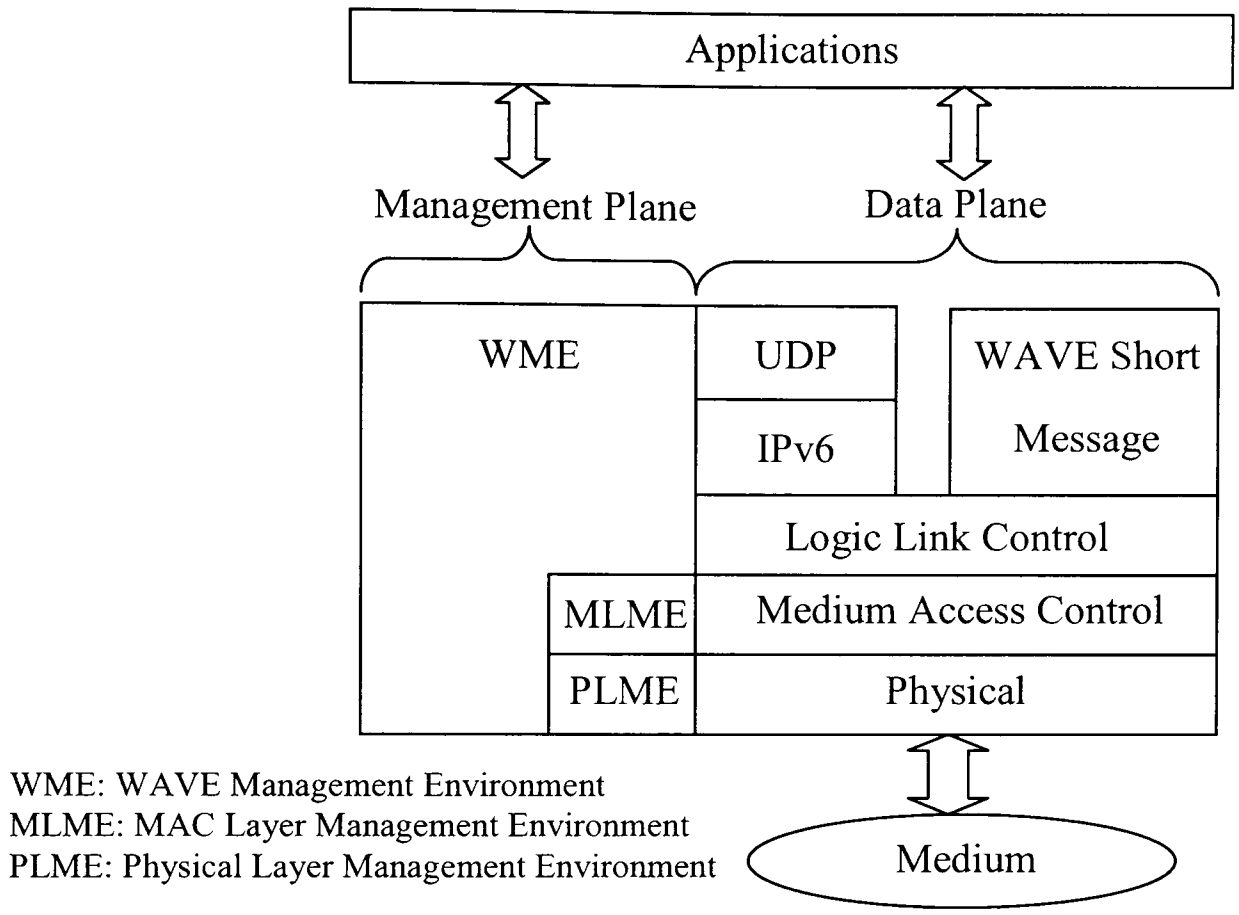

Figure (2.1): IEEE VANET Architecture

The IEEE is working on a standard for the Medium Access Control (MAC) layer and has recently released the WAVE standards of the upper layers for trial use [11, 14]. The WAVE standards are shown in figure (2.2). Standards P1609.1, P1609.2 and P1609.4 were recently released for trial use whereas standard P1609.3 is still under further development. P1609.1 is the standard for WAVE Resource Manager. It defines the services and interfaces of the WAVE resource manager application as well as the message and data formats. It provides access for applications to the rest of the architecture. P1609.2 defines security, secure message formatting, processing, and message exchange. P1609.3 defines routing and transport services. It provides an alternative for IPv6. It also defines the management information base for the protocol stack. P1609.4 organises how the multiple channels specified in the Dedicated Short

Range Communications (DSRC) standard should be used. The WAVE stack uses a modified version of IEEE 802.11a for its Medium Access Control (MAC) known as IEEE 802.11p [11, 12]. In the following sections we review the standards and related research work for the different layers of the VANET protocol stack.

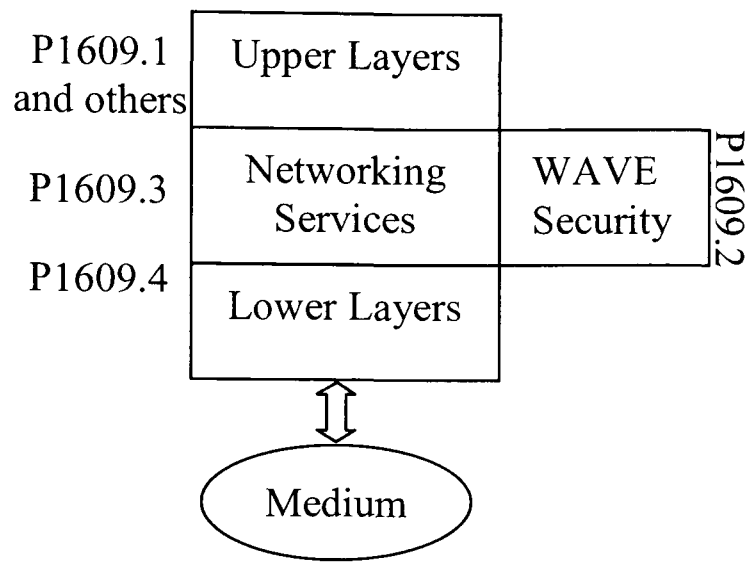

Figure (2.2): WAVE Standards

2.3. VANET Physical Layer

In 1999, the Federal Communications Commission licensed a 75MHz bandwidth, known as Dedicated Short Range Communications (DSRC) band, at 5.9GHz for inter-vehicle communications in USA. The bandwidth is divided into seven communication channels as shown in figure (2.3) [15]. The central channel is dedicated for safety and control messages whereas the other six channels can be used by other applications. The American Society for Testing and Materials (ASTM) released the physical layer standard ASTM DSRC E2213-03 for DSRC. The standard uses Orthogonal Frequency Division Multiplexing (OFDM) with Quadrature Amplitude Modulation (QAM) and has a maximum data rate of 27Mbits/s for a 10MHz channel. It is designed to operate for a range up to 1 km [11, 14, 16].

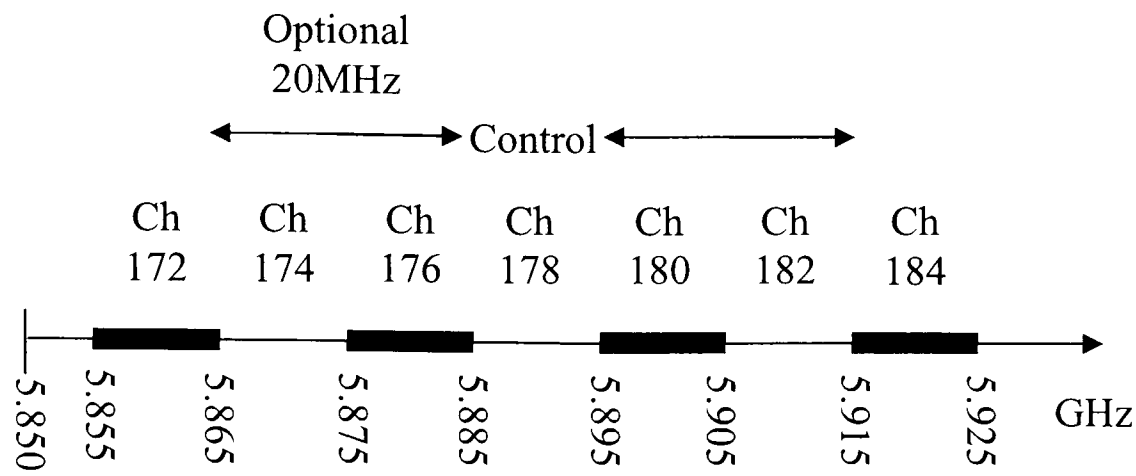

Figure (2.3): DSRC Band in North America

In Japan, the standard ARIB STD-T75 is being developed. It has 7 downlink and 7 uplink channels, as shown in figure (2.4), and a range of 30m. Each channel is shared between cars using Time Division Multiple Access with 8 time slots, thus the standard can provide service for up to 56 cars simultaneously. The standard uses Amplitude Shift Keying (ASK) to provide a data rate of 1Mbits/s and Quadrature Phase Shift Keying (QPSK) to provide 4Mbits/s [13]. In Europe the spectrum shown in figure (2.5) has been proposed. Initially two channels, each 10 MHz wide, will be allocated (labelled as part 1 in figure (2.5)). The rest of the spectrum will be assigned later. The spectrum is in line with the spectrum allocated in the US [17, 18].

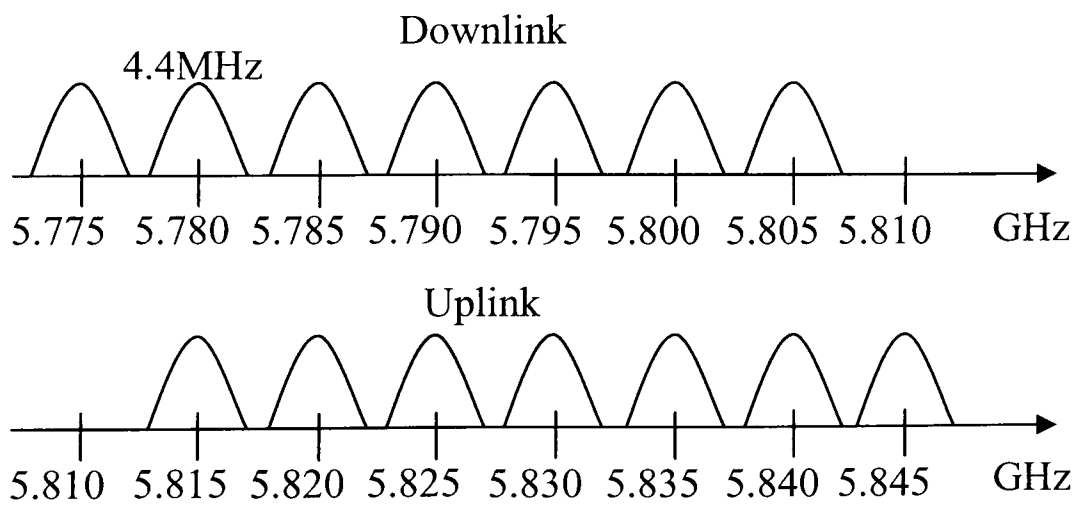

Figure (2.4): ARIB STD-T75 Frequencies

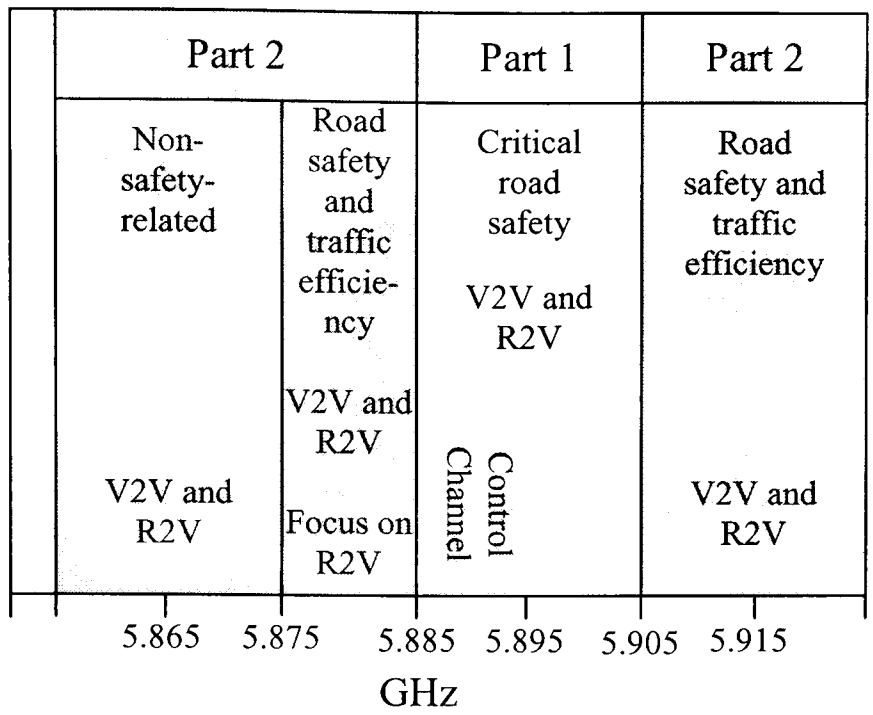

Figure (2.5): Proposed Spectrum in Europe

In VANET nodes move at high speeds and the communication time can be limited to a few seconds. This places a major challenge on the communication system of VANET, especially the physical and link layers, since the system must provide a high data rate in a fast-varying channel. To study the performance of VANET, a good understanding and an accurate representation of the channel is required.

2.3.1. VANET Channel

The transmitted signal in wireless channels experiences attenuation due to the distance between the transmitter and receiver, shadowing due to objects obstructing the line of sight, and multipathing due to reflection from objects in the vicinity of the receiver and/or transmitter. The simplest attenuation model is the free space model which calculates the attenuation due to the distance (R) between the transmitter and receiver assuming no shadowing or multipathing. For the free space model, the path loss (L_p) for a signal with wavelength (λ) is given by [19].

$$L_p = \left(\frac{4\pi R}{\lambda} \right)^2 \quad (2.1)$$

The free space model is ideal for satellite links and short range communication with no multipathing. However in long terrestrial links, there is usually a wave reflected from the ground. The two-ray model, shown in figure (2.6), takes into account this reflected wave. The minimum distance for the first Fresnel zone to touch the ground and, thus, for a ground reflection to exist is given by (2.2) [20, 21]. The path loss is then calculated using (2.3) [19]:

$$R \geq \frac{4\pi . h_t h_r}{\lambda} \qquad (2.2)$$

$$L_p = \left(\frac{R^2}{h_t h_r} \right)^2 \qquad (2.3)$$

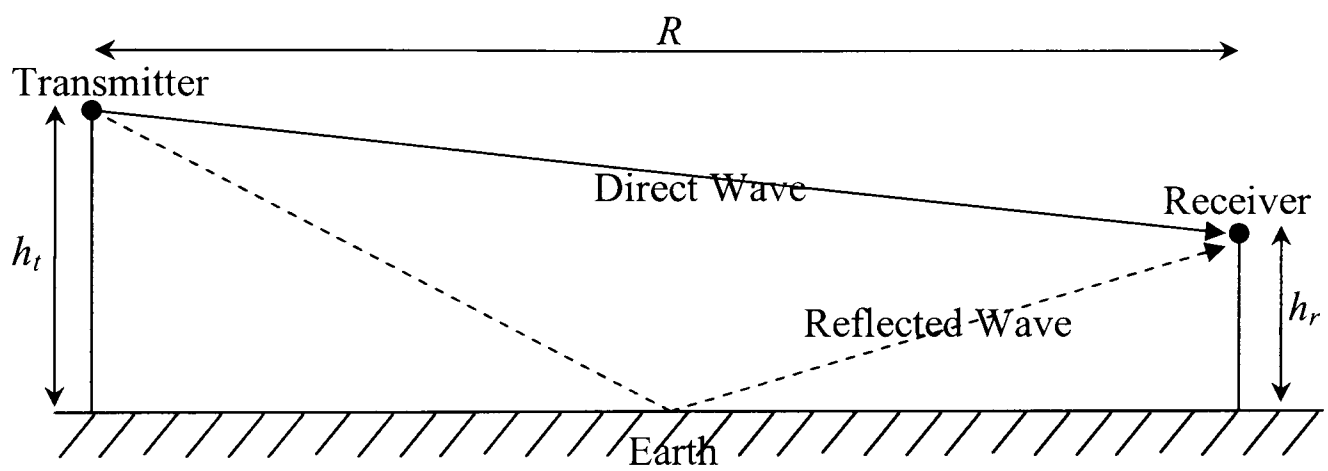

Figure (2.6): Two Rays Model

The received signal power (P_R) is calculated for transmit and receive antenna gains G_T and G_R respectively using Friis equation [19]:

$$P_R = \frac{P_T G_T G_R}{L_p} \qquad (2.4)$$

where P_T is the transmit power and the path loss is calculated from (2.1) or (2.3).

In mobile links equation (2.4) gives an estimate of the average received signal power [19]. The channel in mobile links experiences shadowing, when an object blocks the line of sight, thus reducing the received power. This phenomenon is known as slow fading. Moreover several waves may be reflected from objects surrounding the mobile terminal, beside the ground reflection. Depending on the delays experienced by these

waves, they may be in phase or out of phase with respect to the line of sight thus enhancing or extremely reducing the received signal. Since the phase relations between the waves may change over distances as small as a fraction of λ, this fading is known as fast fading. When a large number of waves exist, i.e. rich scattering, the amplitude of the received signal is a random variable and is usually approximated by statistical models [19, 22].

In rich scattering environments with no line of sight, the distribution of the amplitude of the received signal follows the Rayleigh distribution given by (2.5) [19]. When a line of sight exists, the amplitude distribution is given by the Rician distribution of (2.6) [19].

$$f(r)=\frac{r}{\sigma^2}e^{-\frac{r^2}{2\sigma^2}} \qquad r\geq 0 \qquad (2.5)$$

$$f(r)=\frac{r}{\sigma^2}e^{\frac{-(r^2+\mu^2)}{\sigma^2}}\mathrm{I}_0\left(\frac{r.\mu}{\sigma^2}\right) \qquad r\geq 0 \qquad (2.6)$$

where r is the amplitude, μ is the mean, σ^2 is the variance and I_0 is the zeroth-order modified Bessel function.

An important parameter in mobile links is the Doppler Shift. The Doppler shift (f_D) increases with speed and is calculated using (2.7) for a carrier frequency f, relative speed v and incident angle θ with respect to the direction of motion. λ is the wavelength while c is the speed of light [23].

$$f_D=\frac{v}{\lambda}\cos(\theta)=f\frac{v}{c}\cos(\theta) \qquad (2.7)$$

Doppler shift affects the channel coherence time (T_c). The relationship between the channel coherence time and the maximum Doppler shift for a single antenna system was found in [24, 25] to be given by (2.8). When the Doppler shift is high, the channel coherence time becomes small. For basestation-mobile links, the Doppler spectrum ($P(f)$) is the well known U shaped spectrum given by (2.9) and shown in figure (2.7) as found by Jakes [26].

$$T_c \leq \frac{0.5}{f_D} \tag{2.8}$$

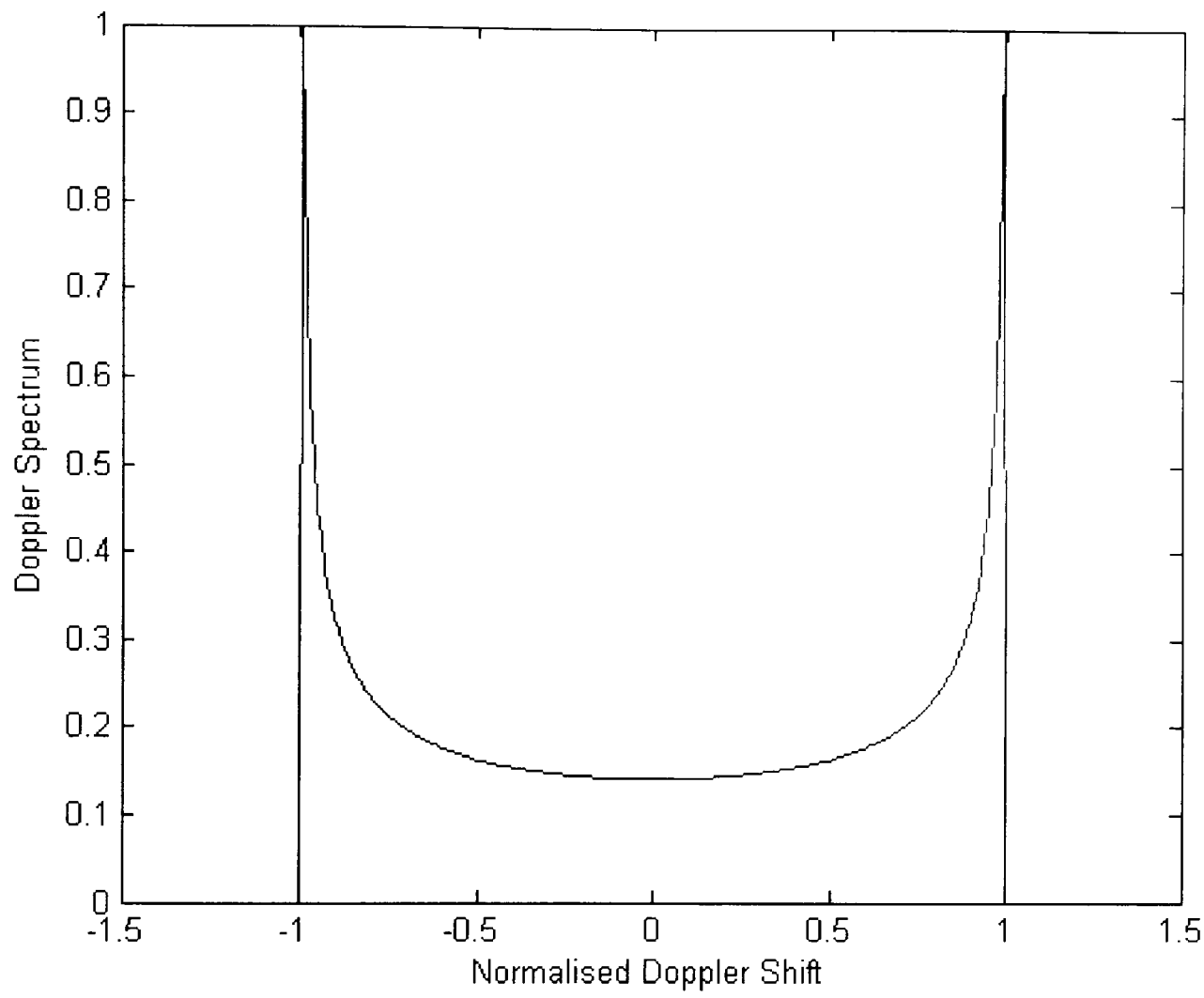

Figure (2.7): Jakes' Doppler Spectrum

$$P(f) = \begin{cases} \dfrac{1}{\pi . f_D} \dfrac{1.5}{\sqrt{1-\left(\dfrac{f}{f_D}\right)^2}}, & |f| < f_D \\ 0, & otherwise \end{cases} \tag{2.9}$$

Several models to approximate the wireless channel were developed [19, 27-29] each focusing on certain aspects of the channel. The widely used Lee's model, shown in figure (2.8), simulates a channel between a basestation and a mobile terminal in macrocell, city environment. Basestations are usually located at high positions with a small number of surroundings whereas mobile terminals are typically surrounded by a large number of scatterers and a line of sight rarely exists [27, 28].

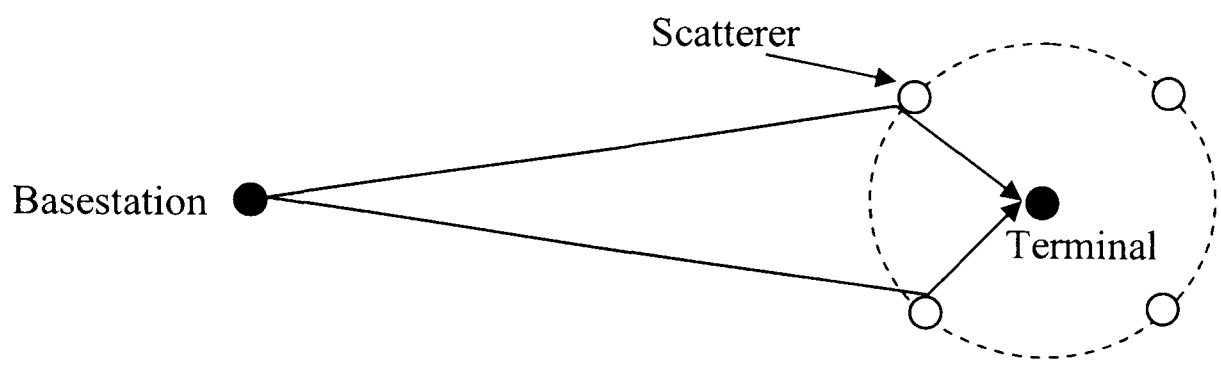

Figure (2.8): Lee's Model

The geometrical model, shown in figure (2.9), was developed by Liberti *et al.* for microcells to study the angle of arrival (AOA) and angle of departure (AOD) as well as the performance of antenna arrays at basestations [29]. In microcells the basestation is usually at lamp post height and the probability of line of sight communication is greater than in macrocells [19, 27, 29]. The basestation and the scatterers are all fixed and the transmitter and receiver are placed at the foci of the ellipse. The primary (a_m) and secondary (b_m) radii of the ellipse are calculated from the maximum delay spread of interest as follows [27]:

$$a_m = \frac{c\tau_m}{2}$$
$$b_m = \frac{1}{2}\sqrt{c^2\tau_m{}^2 - R^2} \qquad (2.10)$$
$$\tau_m = 3.244\sigma_t + \tau_0$$

where τ_m is the maximum delay to be considered, σ_t is the delay spread, τ_0 is the minimum delay (line of sight delay), R is the distance between the transmitter and the receiver and c is the speed of light.

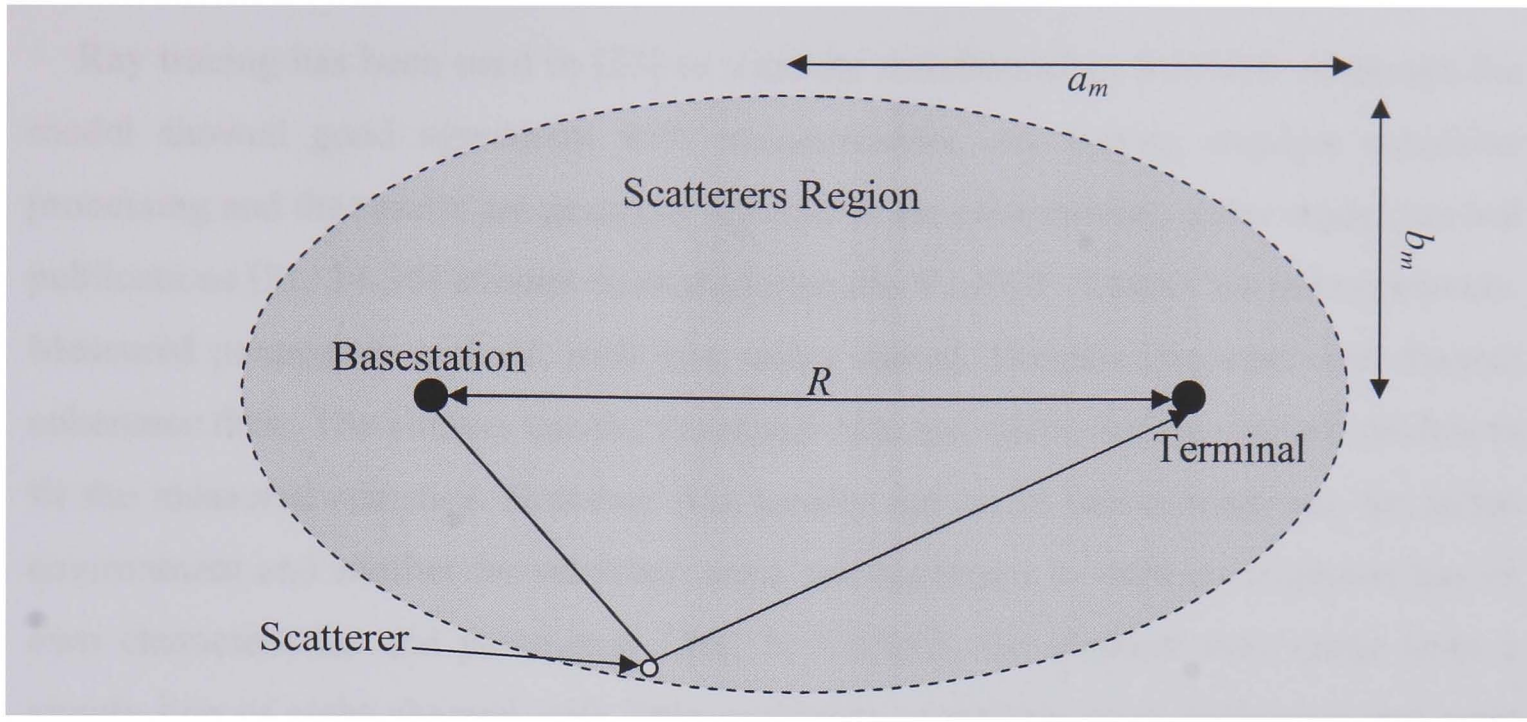

Figure (2.9): Elliptical Channel Model

In [30], the authors extended Lee's model to mobile ad hoc networks by using two rings of scatterers, one around each terminal, with no line of sight as shown in figure (2.10). The model, known as the two rings model, approximates nodes in city environment with rich scattering. In highways the number of scatterers is small thus using a ring around each terminal becomes a poor approximation. Moreover in highways it is very likely that no obstacle blocks the line of sight while the model assumes Rayleigh fading [30]. Another limitation of this model is the assumption of fixed scatterers which lead to inaccurate representation of the Doppler spectrum [31]. To study the performance of vertical antenna arrays, the authors of [32] modified the two rings model by using cylinders instead of rings. Scatteres then can have different altitudes thus approximating the three dimensional properties of the channel. The model however, has the same limitations of the two rings model.

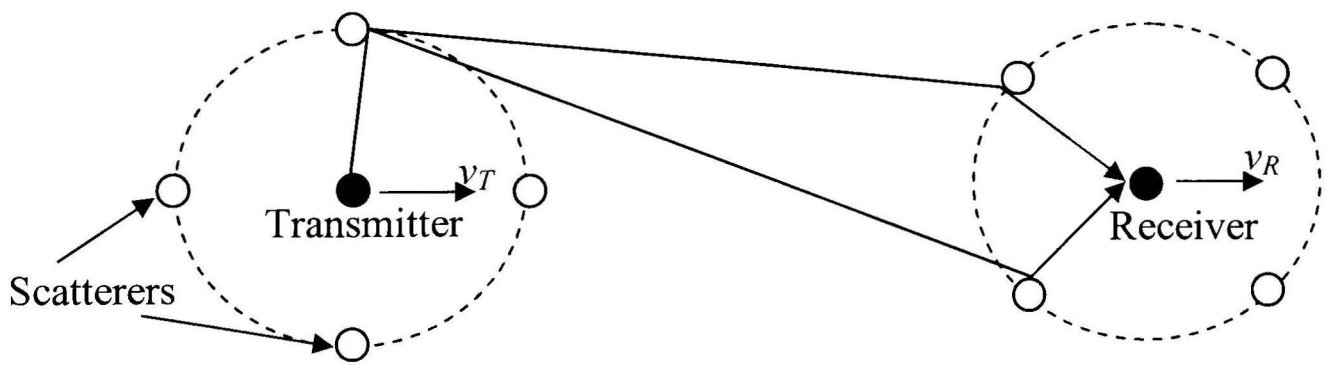

Figure (2.10): Two Rings Model

Ray tracing has been used in [33] to simulate the channel in VANET. Although the model showed good agreement with measurements, ray tracing requires extensive processing and the results are generally specific to the environment under study. Several publications [31, 34-36] attempt to characterise the VANET channel via measurements. Measured parameters include, path loss, delay spread, Doppler spectrum and channel coherence time. The authors use the measured data and adapt exiting channel models to fit the measured statistics. However this usually results in two models one for urban environment and another for suburban areas and highways as each environment has its own characteristics and parameters [34]. In VANET, the channel may range from a simple line of sight channel with little multipath scattering, as in highways and open areas, to rich scattering with complete blockage of line of sight within the city. A good channel model should provide a good approximation for the different conditions. This is difficult to achieve with two different models as the channel changes slowly from the city environment to open areas or vice versa, thus there is no well defined criteria as to when to switch between the models.

2.3.2. Overview of OFDM

The proposed physical layer standard for VANET uses Orthogonal Frequency Division Multiplexing (OFDM) for data transmission [16]. The principle of OFDM is to divide the available bandwidth into a large number of narrow band channels, each approximately having a flat fading response, and send the data through these parallel channels [37]. This eliminates the need for a multi-tap equaliser to equalise the response of the frequency selective channel. To divide the available bandwidth into several flat fading channels, the transmitter processes the data using the Inverse Fast Fourier Transform (IFFT) prior to transmission. The receiver then uses the Fast Fourier Transform (FFT) to undo the IFFT processing before decoding. By using a sufficient number of subcarrier (IFFT/FFT sizes), a frequency selective channel becomes a group of flat fading channels; therefore a single-tap equaliser per channel is sufficient to decode the signal. OFDM has proven to achieve high data rates and better Bit Error

Rate (BER) performance in frequency selective channels compared to single carrier schemes which use multi-tap equalisers [37-39]. The hardware complexity of finding the optimum parameters of N single tap equalisers is less than finding the parameters of an N tap equaliser. Moreover with higher order equalisers the effect of noise is increased as each tap is estimated in the existence of noise. Furthermore, decoding errors can lead to error propagation in feedback equalisers. For these reasons OFDM has higher performance compared to multi-tap equalisers. Figure (2.11) shows the theoretical transmitter equivalent to OFDM operation.

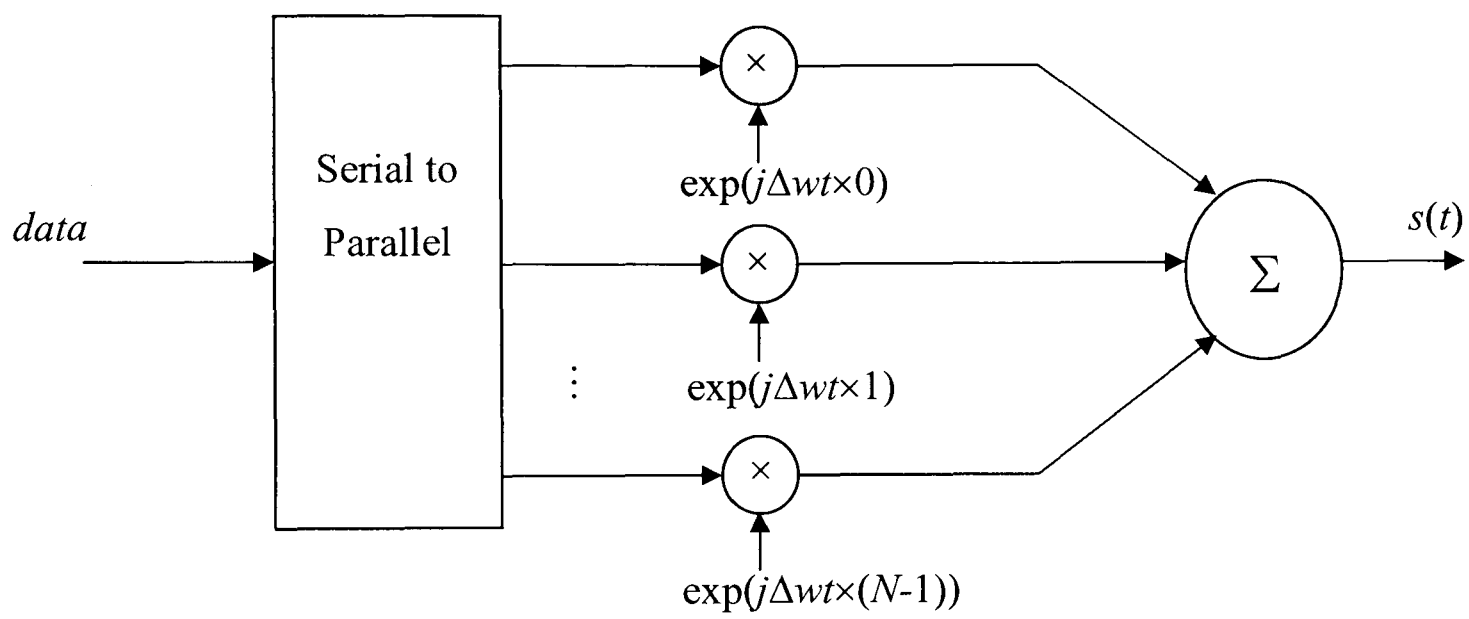

Figure (2.11): Discrete-Component OFDM Transmitter

The minimum frequency shift (Δw) between subcarriers is equal to ($1/NT$) where T is the reciprocal of the symbol rate and N is the number of carriers. The modulator shown in figure (2.11) is not practical since it requires extremely accurate oscillators and is very expensive. The OFDM transmitted signal ($s(t)$) is given by:

$$s(t)=\sum_{i=0}^{N-1} d_i(t) e^{j.i\Delta\omega.t} \qquad (2.11)$$

Where d_i is the modulated data and i is the subcarrier index. For discrete time (n), the signal can be written as:

$$s(n)=\sum_{k=0}^{N-1} d(k) e^{j.k\Delta\omega.nT} = \sum_{k=0}^{N-1} d(k) e^{j\frac{2\pi.}{N}k.n} \qquad (2.12)$$

Except for a scaling factor, equation (2.12) is the Inverse Discrete Fourier Transform (IDFT) which can be computed efficiently using the IFFT algorithm. At the receiver the signal is processed using the FFT algorithm as:

$$d(k)=\sum_{n=0}^{N-1} s(n) e^{-j\frac{2\pi}{N}n.k} \qquad (2.13)$$

However, due to the signal periodicity assumed by FFT algorithms, for the IFFT/FFT system to behave exactly as the system of figure (2.11), the channel impulse response must be circularly convolved with the signal from equation (2.11). The channel response can be approximated by a multi-tap filter of order L, where L depends on the maximum delay and symbol rate. If the OFDM symbol is repeated the signal is then periodic and the IFFT/FFT system can be used indeed. However this repetition is a waste of resources, therefore only part of the signal is repeated, known as cyclic prefix (CP), which should be at least equal to L [37, 39]. A block diagram of the OFDM system is shown in figure (2.12) and the relationship between subcarriers is shown in figure (2.13).

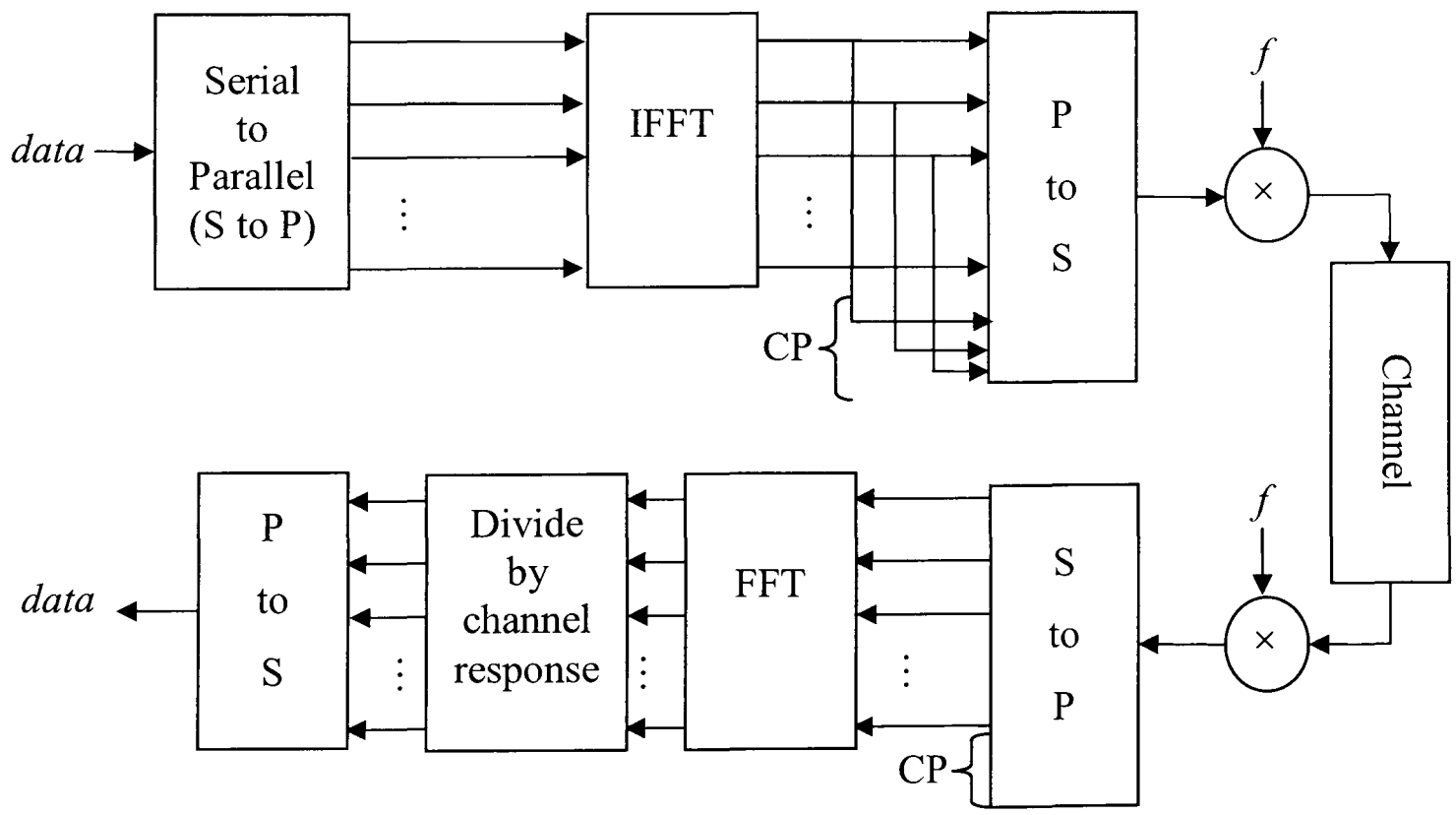

Figure (2.12): OFDM Transmitter and Receiver

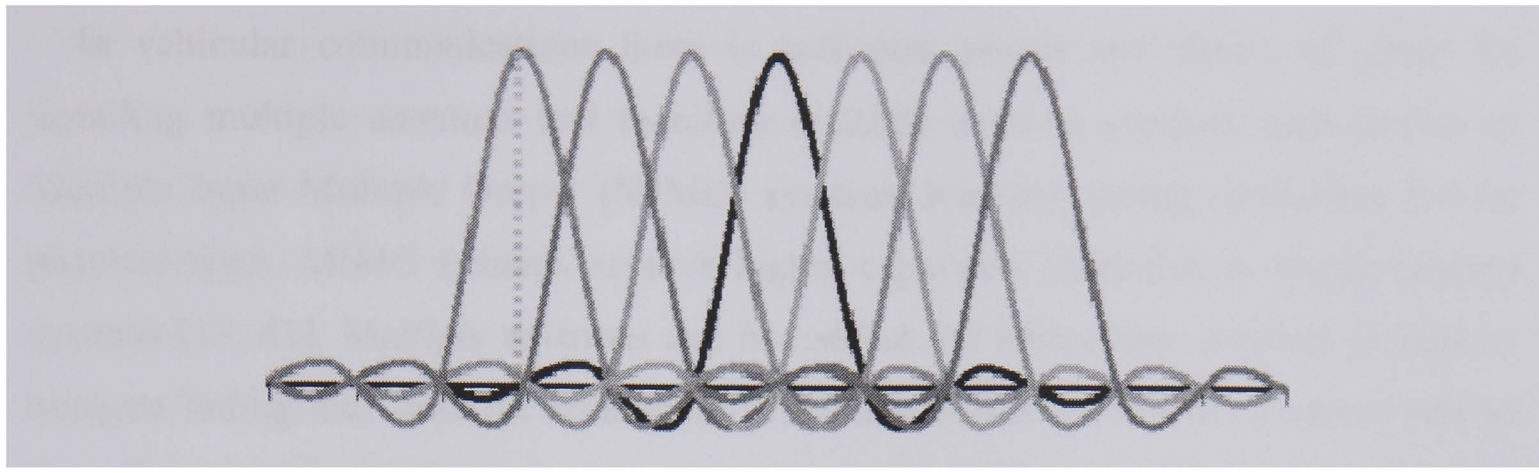

Figure (2.13): Orthogonality of Subcarriers in OFDM Modulation

To achieve best performance, the channel response should be fixed for the duration of the OFDM symbol. This assumption is valid for fixed and slowly varying channels, however in high speed scenarios this is not the case. The variation in channel response destroys the orthogonality between the subcarriers and causes interference between the subcarriers known as inter-carrier-interference (ICI). This interference leads to an error floor in the BER performance of OFDM [40].

2.3.3. Multiple Antenna Systems

The main limiting characteristic of wireless links is the attenuation caused by fast fading [22]. The use of multiple antennas at the receiver can reduce the effects of multipathing since, due to the characteristics of fading, the probability that deep fading occurs simultaneously at two antennas separated by some 'suitable distance' is low [19, 22]. The 'suitable distance' is usually several wavelengths. Using this fact multiple antenna receivers have been studied and constructed and they showed superior performance compared to single antenna receivers. However mobile terminals are usually of limited size and power, therefore it is not possible to use multiple antennas at the terminals. To solve this problem multiple transmit/receive antennas are implemented at the basestation and a single antenna is used at the terminals. The use of two or more antennas for transmitting the signal provides better performance than single antenna systems [19].

In vehicular communications there is sufficient power and plenty of space for installing multiple antennas and therefore multiple antenna systems, also known as Multiple Input Multiple Output (MIMO) systems, are very strong candidates for the physical layer. MIMO systems achieve higher capacities compared to single antenna systems [19, 41]. Multiple antennas can be used at the transmitter, receiver or both to mitigate fading and improve bandwidth efficiency. Although MIMO systems can be treated as separate single antenna (multiuser) systems, higher capacities can be achieved if the encoding and decoding were performed for all the antennas together, hence several encoding and decoding techniques were developed to achieve high capacity [19, 42-44]. Generally there are two methods for improving bandwidth efficiency using MIMO systems. In the first method the reliability of the wireless link is improved using diversity techniques (transmit diversity and/or receive diversity). By improving the reliability of the link, higher modulations and/or more efficient codes can be used to increase the data rate [22, 45]. In the second approach multiple antennas are used at the transmitter and receiver and each transmitting antenna transmits a separate stream of data. The achievable capacity (C) using a MIMO system with N transmit antennas and M receive antennas ($N \leq M$) is given by (2.14) [19]. σ_s^2 is the transmission power per antenna, σ_w^2 is the noise power, $\mathbf{I}_{N\times N}$ is the $N\times N$ identity matrix, $\mathbf{H}$ is the channel response matrix, $\mathbf{E}[.]$ is the expected value and det(.) is the determinant.

$$C = \mathbf{E}\left[\log_2\left[\det\left(\mathbf{I}_{N\times N} + \frac{\rho}{M}\mathbf{H}\mathbf{H}^H\right)\right]\right] \qquad (2.14)$$

$$\rho \equiv N\frac{\sigma_s^2}{\sigma_w^2}$$

2.3.3.1. Receive Diversity Systems

There are two types of diversity systems, receive diversity systems and transmit diversity systems. In receive diversity the receiver uses multiple antennas separated by a distance large enough to ensure independent fading. Different methods of employing these received signals have been introduced in the literature [19, 22]. The optimum

method, know as Maximal Ratio Combining (MRC), multiplies each received signal by a weight which depends on the channel response for that signal and then sums all the signals. The method, therefore, requires accurate channel estimation [22]. A simpler combining method, equal gain combining, only corrects the phase change for each branch (antenna) caused by the channel without modifying the amplitude of the signals. However the most practical combining scheme is selection combining which decodes the signal with the highest signal to noise power ratio (SNR) and ignores the other signals [19].

2.3.3.2. Transmit Diversity Systems

Space-Time Codes (STC) are transmit-diversity systems. There are two types of Space Time Codes, Space Time Block Codes (STBC) and Space Time Trellis Codes (STTC) [19, 43, 46]. STTC use convolutional encoders to encode the signal and then use a serial to parallel converter to create separate streams. Each stream is sent via a separate antenna [43]. The receiver decodes the signal using a Viterbi decoder. Although this scheme has high reliability, the design of the transmission codes is a very difficult process especially for high modulations and/or large number of antennas. Furthermore the complexity of the Viterbi decoder increases exponentially with the data rate and/or number of transmitting antennas [19]. STBC are simpler than STTC and can be decoded using linear decoders. In STBC the data is split into blocks and every block is independently sent from the previous and following blocks. The input data is first converted from serial to parallel and transmitted using the different antennas, then the data is retransmitted, in different formats, for m time slots using different antennas every time slot, i.e. each antenna transmits a different symbol every time slot. The STBC system thus provides time and spatial diversity. The receiver decodes the signals received in the m time slots together. The problem is then reduced to solving a set of m linear equations in which the unknowns are the transmitted data. The rate of a STBC is defined as the ratio of the number of transmitted symbols to time slots (m). The only space time code with a data rate equal to 1 is a two transmit antenna code called Alamouti code after its inventor [19, 45, 46].

In the Alamouti code the transmitter sends the matrix **S** defined in (2.15). The rows represent the symbols sent by each antenna while the columns represent different time intervals. The symbols depend on the type of modulation used. '*' represents complex conjugate.

$$\mathbf{S} = \begin{bmatrix} \tilde{s}_1 & -\tilde{s}_2^{\,*} \\ \tilde{s}_2 & \tilde{s}_1^{\,*} \end{bmatrix} \tag{2.15}$$

All transmission matrices used in space-time codes must be orthogonal in the temporal sense [19], i.e. they must satisfy the relation:

$$\mathbf{S}^H \mathbf{S} = \left(\sum_{j=1}^{N} \left| s_j \right|^2 \right) \mathbf{I} \tag{2.16}$$

Where $(.)^H$ denotes Hermitian transpose and **I** is the identity matrix. The Alamouti transmission matrix satisfies (2.16) and is orthogonal in the spatial sense as well as in the temporal sense, i.e. $\mathbf{SS}^H = \mathbf{S}^H\mathbf{S}$.

The received signal, $x(T)$, can be written as:

$$x(T) = \begin{bmatrix} \tilde{s}_1 & \tilde{s}_2 \end{bmatrix} \begin{bmatrix} h_1(T) \\ h_2(T) \end{bmatrix} + w(T)$$

$$x(2T) = \begin{bmatrix} -\tilde{s}_2^{\,*} & \tilde{s}_1^{\,*} \end{bmatrix} \begin{bmatrix} h_1(2T) \\ h_2(2T) \end{bmatrix} + w(2T) \tag{2.17}$$

where $h_i(T)$ is the channel response between the transmit antenna i and the receive antenna and $w(T)$ is the noise all at time T. If the channel varies slowly we can rewrite equation (2.17) as:

$$\begin{bmatrix} x(T) \\ x(2T) \end{bmatrix} = \begin{bmatrix} \tilde{s}_1 & \tilde{s}_2 \\ -\tilde{s}_2^{\,*} & \tilde{s}_1^{\,*} \end{bmatrix} \begin{bmatrix} h_1(T) \\ h_2(T) \end{bmatrix} + \begin{bmatrix} w(T) \\ w(2T) \end{bmatrix} \tag{2.18}$$

$$\mathbf{x} = \mathbf{S}^T \mathbf{h} + \mathbf{w} \tag{2.19}$$

which can be solved for $\tilde{s}_1$ and $\tilde{s}_2$ since the values of h_i are known (the channel is estimated using a training sequence for example) [45].

Transmit diversity and receive diversity can be combined to further enhance the reliability of the system. Beside diversity systems there exist different architectures

which transmit different streams via each transmit antenna known as Bell Labs Layered Space Time (BLAST) Systems. These will be discussed in the next section.

2.3.4. BLAST Algorithms

BLAST systems employ MIMO systems to provide high data rates and increase bandwidth efficiency. Increasing the number of antennas while keeping everything else fixed results in higher data rates. BLAST systems however operate in rich fading environments since it requires low correlation between the antennas at the receiver [42, 44, 47]. Several BLAST algorithms exist depending on the transmission matrix and decoding process. These include Diagonal BLAST (DBLAST), Horizontal BLAST (HBLAST), Vertical BLAST (VBLAST) and Turbo BLAST (TBLAST).

2.3.4.1. DBLAST

The first type of BLAST systems was the Diagonal BLAST (DBLAST). It is called Diagonal BLAST due to the diagonal form of its transmission matrix. The transmitter for DBLAST is shown in figure (2.14).

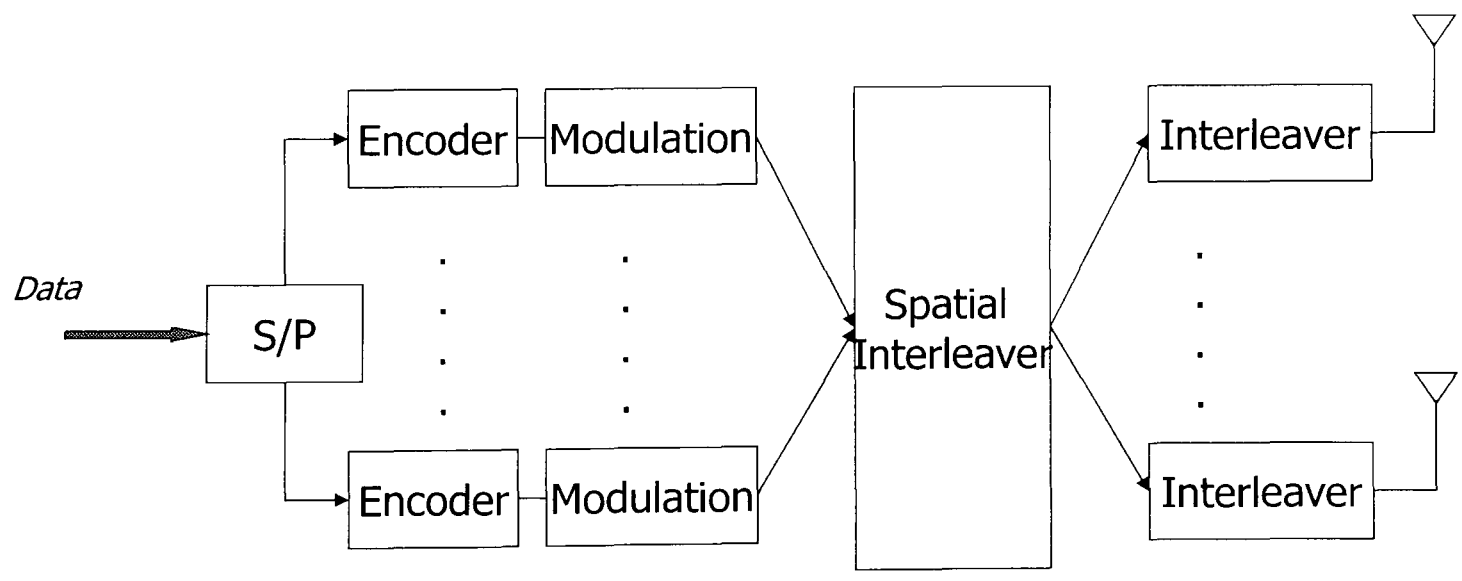

Figure (2.14): DBLAST Transmitter

The input data is split into multiple streams and each stream is then encoded and modulated. The streams are space-time interleaved so that consecutive symbols are transmitted using different antennas and time slots. DBLAST uses a complicated transmission matrix defined for four transmit antennas as [19, 42]:

$$\mathbf{S}=\begin{bmatrix} \tilde{s}_{1,1} & \tilde{s}_{1,2} & \cdots & \tilde{s}_{1,k-1} & \tilde{s}_{1,k} & 0 & 0 & 0 \\ 0 & \tilde{s}_{2,1} & \tilde{s}_{2,2} & \cdots & \tilde{s}_{2,k-1} & \tilde{s}_{2,k} & 0 & 0 \\ 0 & 0 & \tilde{s}_{3,1} & \tilde{s}_{3,2} & \cdots & \tilde{s}_{3,k-1} & \tilde{s}_{3,k} & 0 \\ 0 & 0 & 0 & \tilde{s}_{4,1} & \tilde{s}_{4,2} & \cdots & \tilde{s}_{4,k-1} & \tilde{s}_{4,k} \end{bmatrix} \tag{2.20}$$

where k represents a time delay of k time slots. The symbols on the first diagonal of the **S** matrix are transmitted by antenna 1, the entries on the second diagonal are transmitted by antenna 2 and so on.

Due to the spatial interleaver which provides diversity, DBLAST is capable of achieving higher data rates than other BLAST architectures. However DBLAST suffers from two practical problems. The first problem is the unused antennas at the beginning and end of transmission, which are shown as zeros in equation (2.20). The second limitation of DBLAST is the cost of the spatial interleaver and the use of an independent encoder for each layer [19, 42].

2.3.4.2. HBLAST

The HBLAST transmitter is shown in figure (2.15). It is known as Horizontal BLAST because each layer is encoded independently. As can be seen the difference between HBLAST and DBLAST is the use of time interleavers only without a spatial interleaver. The transmission matrix of HBLAST is given by equation (2.21). $(.)^T$ denotes transpose.

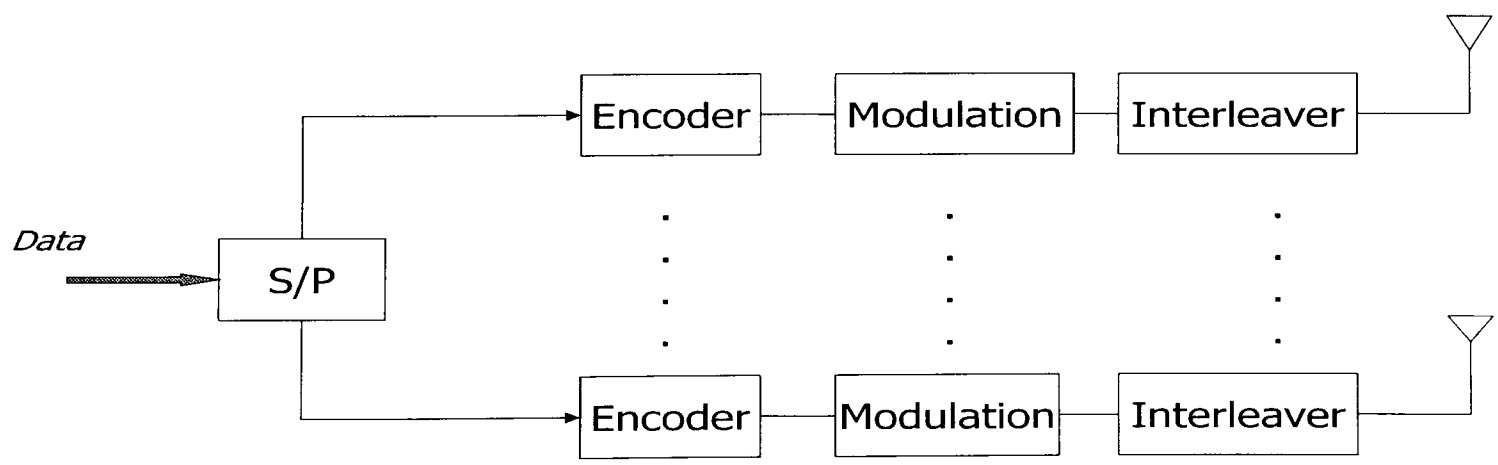

Figure (2.15): HBLAST Transmitter

$$\mathbf{s}=\begin{bmatrix}\tilde{s}_1 & \tilde{s}_2 & \tilde{s}_3 & \cdots & \tilde{s}_N\end{bmatrix}^T \tag{2.21}$$

HBLAST solves the inefficiency in the **S** matrix of DBLAST but at the cost of lower diversity. Since HBLAST still requires an independent encoder and interleaver for each stream, the cost is still high.

2.3.4.3. VBLAST

A simpler BLAST system was introduced by Wolniansky *et. al.* in 1998 known as Vertical BLAST (VBLAST) [44]. The transmitter encodes the data for all the antennas using a single encoder and interleaver for all the layers thus the name Vertical BLAST. The transmitter for VBLAST is shown in figure (2.16). The data is encoded and interleaved prior to the serial to parallel conversion. This way time and space diversity are provided and since only one interleaver and encoder are required, the cost of VBLAST is lower than DBLAST and HBLAST. The transmission matrix of VBLAST is identical to that of HBLAST.

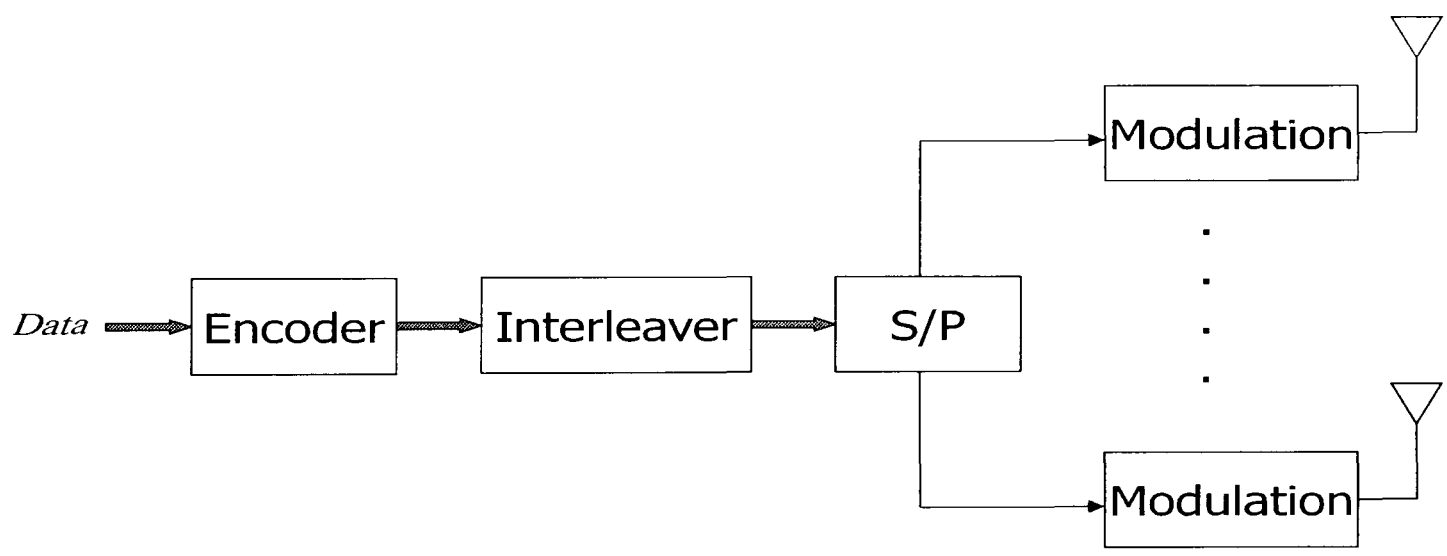

Figure (2.16): VBLAST Transmitter

2.3.4.4. Capacity of BLAST systems

The capacities of DBLAST and VBLAST were studied in [48]. The authors optimised the number of antennas transmitting for a given signal to noise power ratio (SNR) per receive antenna to provide the highest possible capacity. For DBLAST the capacity in bits/s/Hz/dimension is given by equation (2.22) while for VBLAST the capacity is given by equation (2.23). Dimension represents receive antenna, α is the ratio of the number of transmitting antennas to receiving antennas while ρ is the SNR.

$$C_D \approx Max_{\{0<\alpha<1\}}\left\{\alpha \int_0^1 \left[1+\rho\left(\alpha^{-1}-x\right)\right]dx\right\} \approx Max_{\{0<\alpha<1\}}\left\{\alpha+\rho-\frac{\alpha\rho}{2}\right\} \quad (2.22)$$

$$C_V \approx Max_{\{0<\alpha<1\}}\left\{\alpha.\log_2\left[1+\rho\left(\alpha^{-1}-1\right)\right]\right\} \quad (2.23)$$

The number of antennas transmitting gives a trade off between diversity and data rate. It is always kept lower than the number of receive antennas to maintain some spatial diversity. For low SNR values the number of transmitting antennas is reduced to provide more diversity at the receiver and less interference. As the SNR increases, the system is no more limited by noise and the number of antennas transmitting can be increased.

Figure (2.17) is a comparison between the normalised achievable capacity with Additive White Gaussian Noise (AWGN) channel, calculated by equation (2.24) [19], DBLAST and VBLAST with 100 antennas at the transmitter and 100 antennas at the receiver. We used a large number of antennas so that α can take several values. The optimum values of α for various SNR are shown in figure (2.18).

$$C_{AWGN} = \log_2(1+\rho) \quad (2.24)$$

As can be seen from figure (2.17), the performance of DBLAST is superior to VBLAST. This is mainly due to the spatiotemporal interleaver which provides more diversity than in VBLAST. With this diversity, DBLAST is capable of using more transmitting antennas to achieve higher capacities as shown in figure (2.18). Note that the value of α never exceeds 0.99 so that the number of receive antennas is greater than the number of transmitting antennas to maintain some diversity which is necessary to overcome the fading. The capacity of DBLAST is comparable to that of AWGN channel which is considered the ideal channel in wireless communications. However due to the complexity of DBLAST, most research and implementations are based on the simpler and more practical VBLAST.

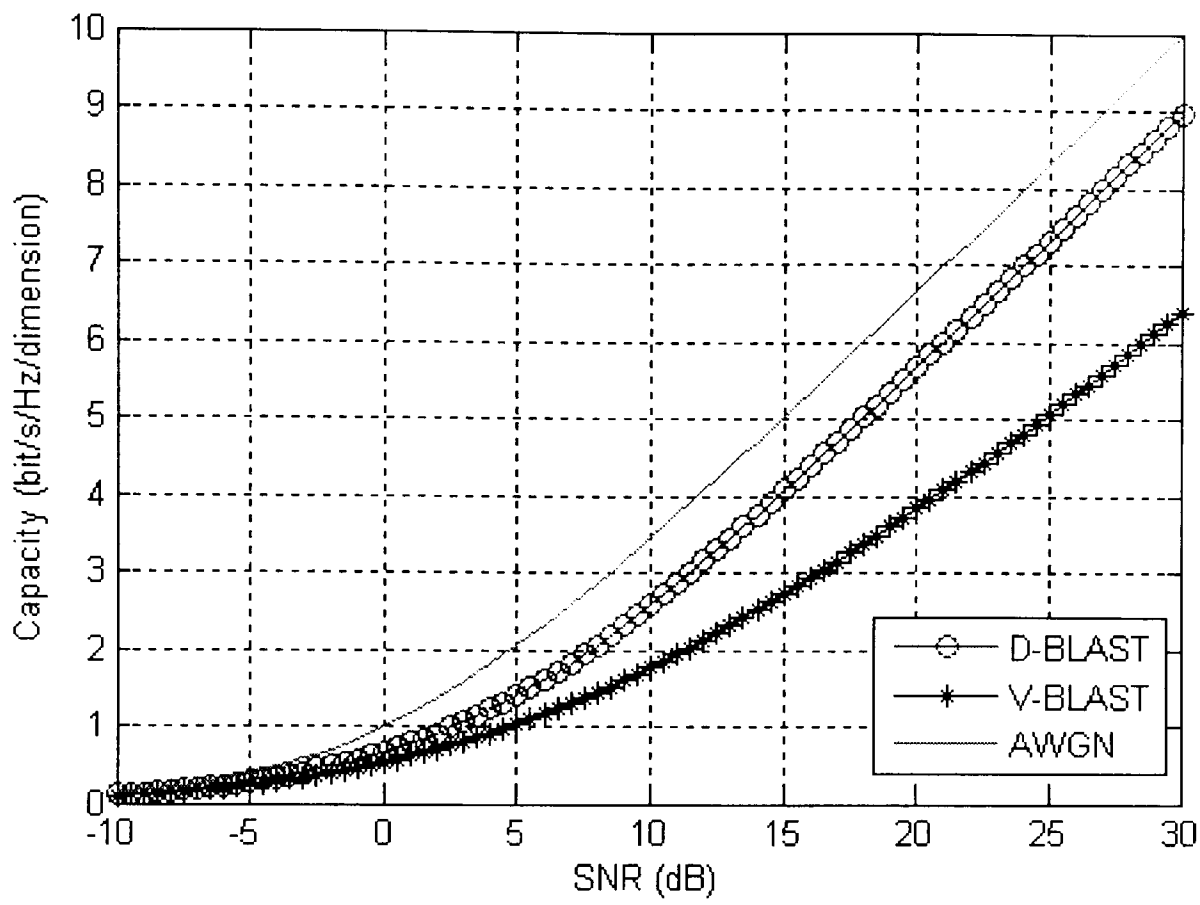

Figure (2.17): Capacity of DBLAST, VBLAST and AWGN Channel

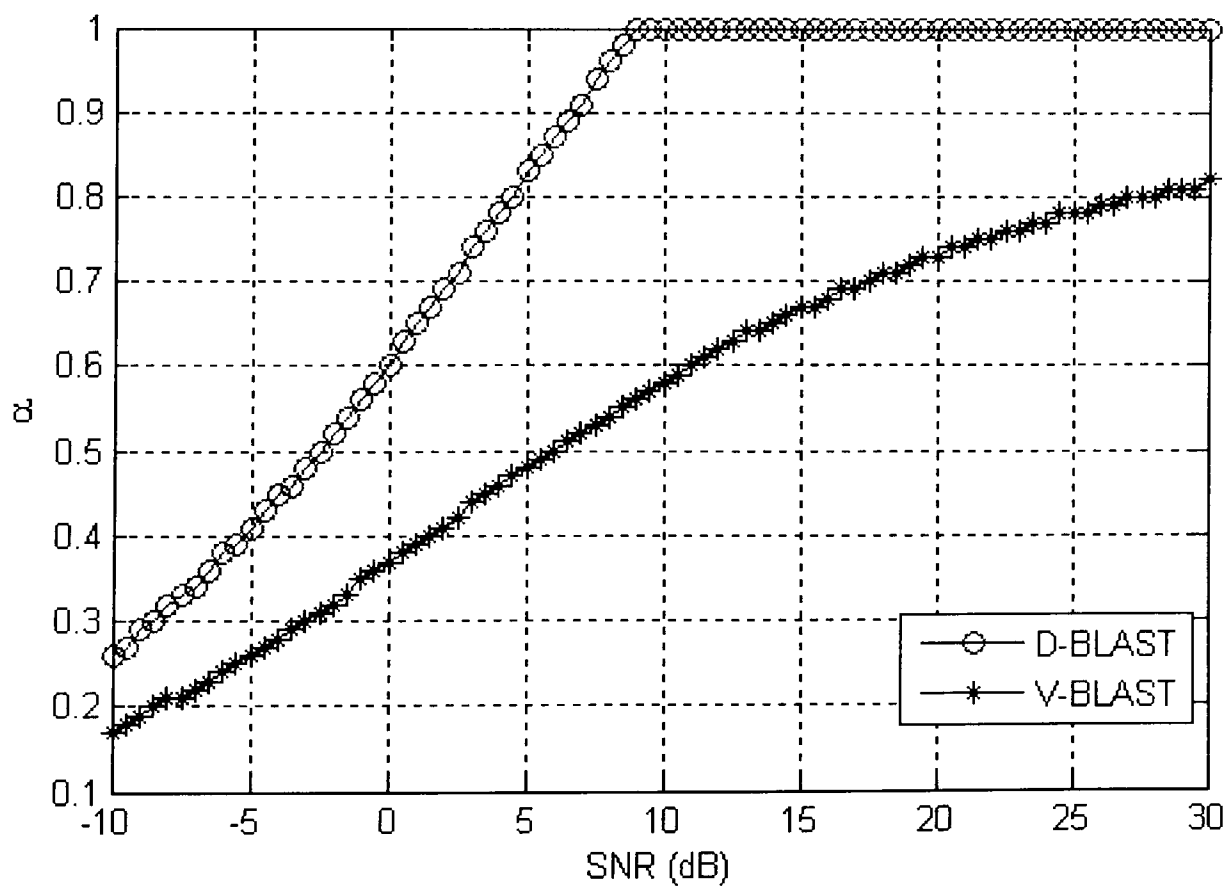

Figure (2.18): Optimum Ratio of Transmit/Receive Antennas vs. SNR

2.3.4.5. VBLAST Decoding

VBLAST systems require the receiver to have a number of antennas (M) equal to or greater than the number of antennas at the transmitter (N). Moreover the receive antennas should have uncorrelated channel responses [44]. This is usually possible in rich Rayleigh scattering conditions, encountered in dense areas, and antenna spacing not less than half a wavelength [19, 47]. The received signal vector (**x**) for VBLAST can be written as:

$$\mathbf{x} = \mathbf{H}\mathbf{s} + \mathbf{w} \tag{2.25}$$

$$\begin{bmatrix} x_1 \\ x_2 \\ \vdots \\ x_M \end{bmatrix} = \begin{bmatrix} h_{11} & h_{12} & \cdots & h_{1N} \\ h_{21} & h_{22} & \cdots & h_{2N} \\ \vdots & \ddots & \ddots & \vdots \\ h_{M1} & h_{M2} & \cdots & h_{MN} \end{bmatrix} \begin{bmatrix} \tilde{s}_1 \\ \tilde{s}_2 \\ \vdots \\ \tilde{s}_N \end{bmatrix} + \begin{bmatrix} w_1 \\ w_2 \\ \vdots \\ w_M \end{bmatrix} \tag{2.26}$$

H is the channel state information matrix, **s** is the vector of transmitted symbols and **w** is the vector of noise samples.

The performance of VBLAST in rich scattering depends on how equation (2.25) is solved for **s** and how the estimation of the **H** matrix is carried out. The simplest way to solve equation (2.25) is to neglect the noise contribution and calculate **s** by multiplying **x** by the inverse (or pseudoinverse) of **H** (i.e. $\mathbf{H}^{\dagger}$). This is known as the Zero Forcing (ZF) algorithm. Clearly this algorithm does not provide good performance especially in low SNR since it ignores the noise, but it is still an attractive algorithm due to its low complexity. The performance of ZF can be improved by detecting the symbols with the highest SNR first since then the decision for this symbol will be more accurate. The interference from this symbol is then subtracted from the received signal before decoding the second symbol. The algorithm, known as VBLAST nulling and cancellation decoding algorithm, works as follows [44]:

For the first step set $i = 1$

$\mathbf{G}^1 = \mathbf{H}^{\dagger}$

In this step G is set to the pseudoinverse ($\mathbf{H}^{\dagger}$) of the **H** matrix, assuming the **H** matrix is known to the receiver. The algorithm now searches for the signal that has the highest

SNR, which is the row with minimum norm in the **G** matrix, to detect it first. This is expressed mathematically as [44]:

$k^1 = argmin_j \, ||(\mathbf{G}^1)_j||^2$

$(G^1)j$ is row j of the matrix G^1. The row with the best SNR is now identified and can be decoded. First this row is stored in a separate variable ($\mathbf{z}_k^i$).

$\mathbf{z}_k^i = (\mathbf{G}^i)_k^i$

Now the transmitted signal (y_k^i) can be estimated from the received signal ($\mathbf{x}^i$) using:

$y_k^i = \mathbf{z}_k^i \times \mathbf{x}^i$

The estimated signal is now compared with the constellation of the transmitted signal to find the point (a_k^i) with the smallest Euclidean distance to y_k^i.

$a_k^i = Quantization(y_k^i)$

The contribution of the decoded symbol can now be cancelled from the received signal vector.

$\mathbf{x}^{i+1} = \mathbf{x}^i - a_k^i[\mathbf{H}]_k^i$

where $[\mathbf{H}]_k^i$ is the kth column of **H** at step i. This column is now set to zero in the **H** matrix since the contribution of this signal has been cancelled and the **G** matrix is updated for the next symbol as:

$\mathbf{G}^{i+1} = \mathbf{H}_k^{i\dagger}$

The algorithm now searches for the signal with the second best SNR to decode it, isolates the corresponding row of **G** and the decoding steps repeat till all the signals are detected.

$k^{i+1} = argmin||(G^{i+1})_j||^2_{j \notin (k1 \ldots ki)}$

$i = i + 1$

The VBLAST decoding algorithm works fine as long as the rank of **H** is greater than the number of transmitting antennas (N). If two or more rows are equal, the nulling and cancellation process will cause these similar rows to become zero. This is the reason why the channel is usually assumed to be rich Rayleigh scattering when studying VBLAST. If the rank of **H** becomes less than N, the algorithm will fail to decode correctly. The rank of **H** is reduced either when there is a correlation between the

receive antennas, when there is a strong line of sight path or when there are fewer receive than transmit antennas. In extreme cases, it can even collapse to 1 in what is known as a keyhole channel [49-51].

To solve the rank(**H**) equations, rank(**H**) < N, for the N unknowns more complicated algorithms are required. The optimum algorithm for solving equation (2.25) is the Maximum Likelihood (ML) algorithm which searches all the possible combinations and finds the one that has the highest probability (smallest Euclidean distance to the received signal). This algorithm, however, is very complicated and its complexity increases exponentially with the number of antennas and/or constellation size. A simpler algorithm that can be used is the Minimum Mean Square Error (MMSE) algorithm which searches for a solution $\mathbf{x}'$ that minimizes the cost function $|\mathbf{x}-\mathbf{x}'|^2$. The performance of MMSE is better than ZF but not as good as the ML algorithm. The **G** algorithm for MMSE is $(E_s\mathbf{H}(\mathbf{I}+E_s\mathbf{H}^H\mathbf{H}))^H$ where E_s is the average SNR per antenna [52]. A number of papers studied decoding algorithms for VBLAST and suggested improved algorithms [53-55]; however these papers generally don't provide details of the hardware complexity or processing time requirements for comparison with the zero forcing algorithm. One of the interesting solutions is to combine the MMSE algorithm with a turbo decoder in what is known as Turbo BLAST (TBLAST) [55]. The transmitter in turbo codes uses convolutional codes with puncturing and interleaving to randomise the data. The turbo receiver uses two decoders and each decoder detects the symbol and provides an estimation of the reliability of the detection (soft output). The soft output of each decoder is fed to the other decoder for a second decoding step (iteration). This process is repeated for a number of iterations to yield more reliable estimations [55, 56]. Turbo codes were first introduced by Berrou *et al.* [57].

Although it is possible to decode the signal when the rank of **H** is less than N, the decoding algorithms are quite complex and their complexity increases with the number of antennas used thus limiting their practicality to a small number of antennas. The rank of **H** can be less than N for different reasons but the most important and most common cause is the correlation between the receive antennas.

2.3.4.6. Challenges facing VBLAST

The signal from the transmitter is scattered and reflected from the surroundings near the transmitter, near the receiver and in the propagation path between the transmitter and the receiver. These reflected signals add up constructively or destructively causing fading variation with respect to time and position. If a large number of scatterers are available around the receiver, the fading changes considerably for short distances (typically > 0.5λ). This means if two antennas are placed at a distance greater than 0.5λ, they will receive two independent versions of the transmitted signal. However if a small number of surroundings is available around the receiver, large distances between the antennas are required to receive independent signals at the antennas. This is why antennas at basestations are usually placed at least 10λ apart because they are located at high positions far from surroundings, while for mobile terminals spaces of 0.5λ are sufficient. The received signals at the antennas can also be correlated if a strong line of sight component exists [49, 50].

The effect of correlation on the performance of VBLAST has been studied in [47]. As the correlation increases more errors occur in the decoding process. To illustrate the relationship between the correlation coefficient and system performance (BER), the authors calculated a curve, figure (2.19), showing the equivalent loss in SNR as the correlation increases. As can be seen from the figure a correlation up to 0.5 is generally acceptable. Any further increase in correlation leads to a large loss in SNR and, therefore, increases the BER.

In VANET a car can be in densely traffic with a large number of surroundings and it can also move to open areas with a small number of surroundings and line of sight conditions. The correlation between the antennas in the later case can cause severe degradation in the performance of VBLAST and lead to very poor BER performance.

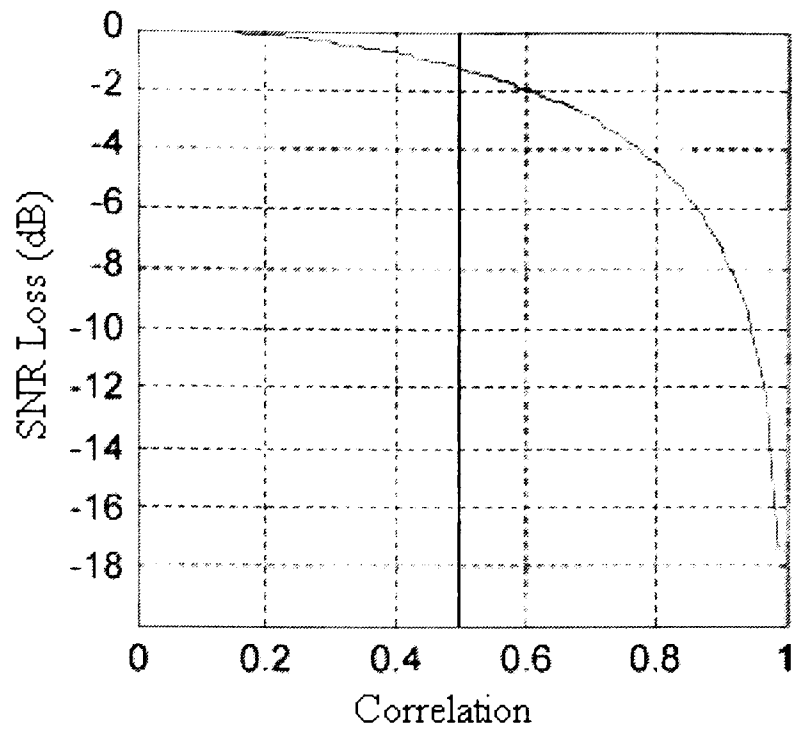

Figure (2.19): SNR Loss vs. Correlation [47]

Beside low correlation, VBLAST requires accurate knowledge of the channel state information matrix (**H**) to decode the signal correctly. In the literature this is usually obtained via a training sequence and assumed to remain constant for the duration of a packet (a quasi-stationary channel). However in VANET speeds of 100 km/h or more are quite common and thus this assumption is not valid. The effects of the change in channel response can be reduced by sending training sequences more frequently. This reduces the bandwidth efficiency since more time is wasted transmitting known training sequences instead of data. The general practice is the training interval should not exceed 10% of the transmission time.

The optimum training sequence for MIMO systems was investigated in [58-61]. It was shown that an orthonormal training matrix is the optimum set. In [61] the number of training pilots was optimised for a given Doppler shift in single carrier systems. It was shown that at high Doppler shifts the optimum number of pilots is equal to the number of transmitting antennas. Several orthonormal training matrices can be used but the most common is the FFT matrix which, for a system with N transmitting antennas and L_t pilot symbols, has element at row m and column n as given by (2.27) [61].

$$s_{m,n} = \frac{1}{\sqrt{N}} e^{-j2\pi(m-1)(n-1)/L_t} \qquad (2.27)$$

The receiver uses the received signal and the known training matrix to obtain an estimate of the channel matrix. Several estimation techniques exist including Least Square Error (LSE), Minimum Mean Square Error (MMSE) and maximum likelihood algorithms but the least square error is the most common due to its simplicity and ease of implementation. In [62-65] the authors investigated the optimum training set for MIMO OFDM via a single OFDM symbol as well as multiple OFDM training symbols. These training sets were generalised in [59]. According to [59], for single OFDM training symbols two methods are possible. In the first method, called Code Division Multiplexing (CDM), all antennas transmit in all the pilot subcarriers. The training sequence for each antenna should be orthogonal to all the training sequences of the other antennas. In the second method, called Frequency Division Multiplexing (FDM), each antenna transmits in a unique set of subcarriers. A combination of CDM and FDM can also be used [59, 65]. The authors derived the optimum allocation of subcarriers to antennas. The number of pilot symbols per antenna should be at least equal to the number of paths (taps) of the channel. When multiple OFDM symbols are used Time Division Multiplexing (TDM) can be combined with CDM and/or FDM to provide several OFDM training symbols for the channel estimation. As with single OFDM training symbol, the optimum training set over multiple symbols should be orthogonal between the different transmitting antennas. The receiver estimates the time domain response of the channel for a particular transmitting antenna (A) by multiplying the received signal by the conjugate of the training set of A and calculating the IFFT of the product. This has the effect of eliminating the interference from the other antennas. The results presented in [59] show that all methods achieve identical results in slowly fading channels. Obtaining channel estimation using one symbol is more suitable to VANET since the channel coherence time is very short.

The training sequence is sufficient to estimate the channel in slowly varying channels, but with high Doppler shifts, the performance drops considerably. This is

particularly true in multi-transmit systems since the channel coherence time in MIMO systems is less than the channel coherence time of single antenna systems [66]. Several methods of channel tracking have been introduced in the literature. In [67] the authors considered the use of Kalman filtering to track the channel for orthogonal Space Time Block Coding (STBC) MIMO. They exploited the orthogonality of the transmission matrix to reduce the complexity of the filter. In [68] a maximum likelihood channel tracking algorithm has been proposed. The authors modelled the channel as an auto regressive (AR) process using Jake's power spectral density. A combination of a Kalman filter and a minimum mean square error decision feedback equaliser (MMSE-DFE) was used in [69] for detection and channel tracking. The DFE is used to estimate the transmitted symbols and its output is fed to the Kalman filter for channel estimation. A polynomial fitting is then employed to further enhance the channel prediction. In [70] an autoregressive moving average (ARMA) filter was developed to model the channel response based on Jake's channel power spectral density. The filter was then used to design a Kalman filter for channel tracking. The method of [67] is applicable only to STBC and therefore cannot be used with VBLAST. The other tracking methods have high complexity since they use high order filters and/or complicated algorithms.

Inter-carrier-interference (ICI) in OFDM also limits the performance of MIMO-OFDM systems. In ordinary OFDM systems it is usually assumed that the channel does not vary within an OFDM symbol. In a fast fading environment, such as in VANET, the channel coherence time is very short and hence the assumption becomes invalid. The variation of the channel within the OFDM symbol destroys the orthogonality between OFDM subcarriers causing interference between them. This interference results in an error floor at high SNR. To reduce the effects of ICI in single antenna systems an equalisation technique was introduced in [71]. An estimate of the change/slope of the channel response at subcarrier k ($a(k)$) is estimated from an impulse sent after the OFDM symbol and then used to formulate a channel matrix that includes the ICI contribution of adjacent subcarriers. The signal is then decoded using the inverse of this matrix. In [72] a two steps receiver was proposed. First an initial estimate of the

transmitted symbols is obtained by a conventional one tap equaliser. A decision feedback filter is then used to cancel the ICI from the subcarriers before decoding the signal again. The authors of [73] used a different technique. They divided the subcarriers into groups of adjacent subcarriers. Within a group, each subcarrier carries the same data multiplied by a certain weight. The weights were designed so that the ICI from the subcarriers within the same group cancel each other. This technique was extended to Space Time Block Coding (STBC) in [74]. A sequential decision feedback sequence estimator (SDFSE) receiver for Alamouti-OFDM systems that takes into account ICI was also introduced in [75]. The method of [73] and [74] shows good bit error rate (BER) performance but the data rate is reduced at least by half since two, or more, subcarriers carry the same data implying a reduction in spectral efficiency. In [71] and [72] the slopes ($a(k)$) are estimated by sending an impulse at the end of the OFDM symbol and calculating the change in channel response during the OFDM symbol. Sending an impulse after the OFDM symbol wastes resources and is not suitable for MIMO systems since each transmit antenna will need a separate impulse. The two steps receiver of [72] becomes very complicated when employed with MIMO systems as the decoding is performed twice.

2.4. Medium Access Control Layer

The medium access control (MAC) layer controls when, where and which terminal accesses the medium. It also resolves and/or avoids collisions when two or more terminals transmit at the same time. The operations and tasks performed by the MAC layer depend on whether a central node to organise access to the channel exists or not. Existing MAC schemes can be classified as central based MAC protocols and non central or ad hoc MAC protocols although some combine both. Central based protocols are used in networks which have a basestation. The basestation provides synchronization for the terminals and controls which terminal accesses the medium. In most protocols all the traffic is relayed through the basestation, which is generally inefficient especially in small area networks. The basestation is usually connected to

other basestations so that terminals associated with different basestations can communicate with each other. Vehicular communications can use these MAC protocols only if the whole road network is covered by basestations. Since this requires a large number of RSUs and, therefore, results in considerable costs, it is not possible to use 'pure' central based MAC protocols in VANET.

Ad hoc MAC protocols do not rely on a central basestation. They are used for communications between peer distributed terminals. MAC protocols rely on one or several multiple access techniques to organise the channel access. Each access mechanism has its benefits and limitations. In the next section we discuss multiple access techniques proposed in the literature.

2.4.1. Multiple Access Techniques

Several access mechanisms to share the medium are available. These can be divided into five categories namely Frequency Division Multiple Access/Orthogonal Frequency Division Multiple Access (FDMA/OFDMA), Time Division Multiple Access (TDMA), Code Division Multiple Access (CDMA), Space Division Multiple Access (SDMA) and random access techniques [19, 22].

2.4.1.1. FDMA/OFDMA

Frequency Division Multiple Access is one of the oldest multiple access techniques. In FDMA the available bandwidth is divided into a number of channels and each terminal is allocated a channel. Channel allocation to terminals is typically handled by a basestation whereas channel allocation for basestations is usually static. Since each channel is dedicated to a single terminal, collisions do not occur. FDMA is a simple and reliable protocol but it has a number of limitations. Bandwidth is a valuable resource and must be used efficiently. If a node is allocated a channel, the channel is used only if the node has traffic. If the node has light traffic, the channel will be idle most of the time. Another limitation of FDMA is the limited number of channels. A terminal is either allocated a channel or denied service, i.e. guaranteed quality of service (QoS) or no service. Furthermore channels typically have a fixed bandwidth, whereas different

terminals usually have different requirements, thus a channel may be larger or smaller than the terminal requirements. Allocating multiple channels for a terminal in FDMA requires multiple transceivers at the terminal, one for each channel [19, 22]. Another problem with FDMA is fading. FDMA channels usually have narrow bandwidth. If the channel experiences deep fading, the link will fail. Figure (2.20) shows channel allocation in FDMA.

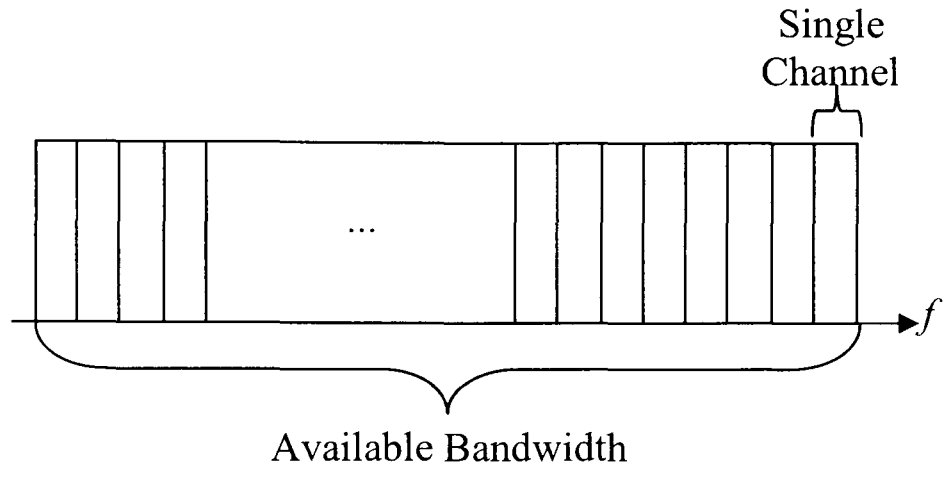

Figure (2.20): FDMA Scheme

OFDMA is a modern implementation of FDMA based on OFDM techniques. In OFDMA all terminals use the whole bandwidth for transmission but the transmitted signal is pre-processed using IFFT. Each terminal is allocated a unique set of subcarriers for its transmission. Since subcarriers in fixed links are orthogonal, the signals from the terminals do not interfere with each other. The receiver processes the received signal, which is the superposition of all transmitted signals, to separate the transmitted signals (regain the subcarriers) and decode the signal. Subcarriers are usually allocated to terminals by a basestation. OFDMA overcomes several FDMA limitations. Unlike FDMA, in OFDMA terminals can be allocated different numbers of subcarriers depending on their traffic requirements using a single transceiver, thus improving the efficiency of the protocol and supporting several data rates [37, 76]. To support a large number of users in OFDMA, large IFFT/FFT sizes can be used. OFDMA with large FFT/IFFT is ideal for fixed or slowly varying channels and has been adopted for WiMax [76] but, with high speed nodes, OFDMA suffers from inter-

carrier-interference (ICI) which increases with the number of subcarriers and speed [40].

2.4.1.2. TDMA

In TDMA terminals share the available channel bandwidth in time. Time is divided into frames and each frame is divided into time slots. Typically the slot duration is fixed and each frame contains a fixed number of slots. Each terminal is allocated one, or more, of these slots and is allowed to transmit only in its slot(s). Since each slot is allocated to a single node, collisions do not occur. TDMA is the most popular access mechanism for wired and wireless networks due to its efficiency and ease of implementation. A large number of voice standards use TDMA, including the Global System for Mobile Communications (GSM) standard, and it has also been adopted for data communications, e.g. Token Ring protocol. With TDMA terminals can be allocated a different number of slots depending on their traffic requirements thus providing various classes of QoS. TDMA achieves high performance in networks with high loads but incorporates unnecessary delays in networks with light traffic and/or small number of nodes since a node can only transmit in its own slot. Another limitation of TDMA is the need for all nodes to be synchronised as timing errors can cause collisions between slots. Typically a basestation handles synchronisation and slot assignment. TDMA systems usually use high data rates thus multi-tap equalisers are employed to eliminate inter symbol interference (ISI) [19]. TDMA provides guaranteed QoS but can support a maximum number of users equal to the total number of slots. Ad hoc versions of TDMA are also available but assume either the nodes are synchronised and/or no hidden terminals exist [77-81]. The hidden terminal problem will be discussed in section (2.4.1.5). Figure (2.21) shows the TDMA frame structure.

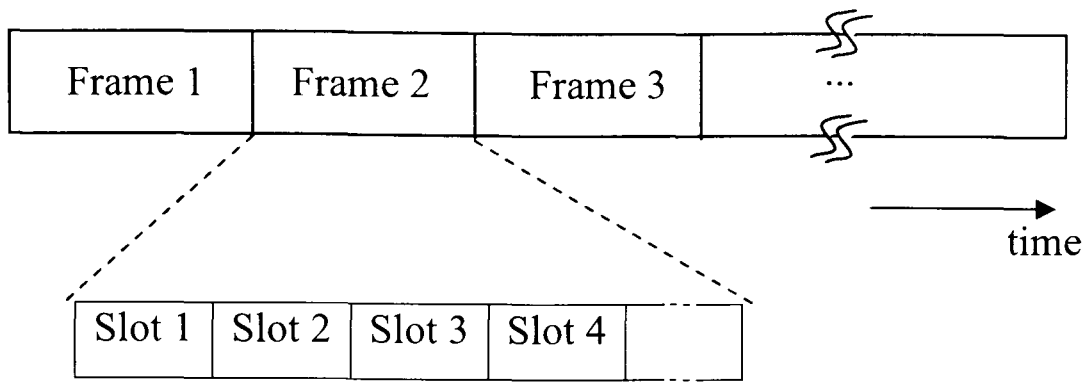

Figure (2.21): TDMA Frame Structure

2.4.1.3. CDMA

In code division multiple access (CDMA) each terminal multiplies its data with a unique spreading signal (code). The product is then transmitted at a symbol rate several times greater than the data rate. This has the effect of spreading the signal to a bandwidth much greater than its original bandwidth. The spreading procedure makes the signal immune to frequency selective fading as well as to interference. Ideally the codes should be orthogonal to eliminate interference between users. The receiver multiplies the received signal by the code of the desired user to retrieve the desired signal to its original bandwidth (de-spreading) while spreading the signals from other users, which can be treated as noise. One of the main limitations of CDMA is the near far problem. If nodes near a basestation transmit at the same power as another very far terminal, the power of the signal from the node nearby after the de-spreading can be comparable to the power of the desired signal. This is usually solved by using power control techniques at the basestation to ensure the signal received from all users have the same power level. Such a solution however is very difficult to implement in peer networks as each pair of nodes will have different power constraints. The performance of CDMA drops gradually as more users use the channel since the signals from the users after de-spreading form a noise floor [19].

2.4.1.4. SDMA

SDMA is an attempt to improve the bandwidth efficiency by reusing the same bandwidth in a different area. Wireless systems experience attenuation with distance. If

the reuse distance is long enough, the frequency can be reused without causing collisions. This, however, causes some interference. Using a short distance increases the efficiency of the wireless system but also increases the interference power while using a long reuse distance reduces the interference but also reduces the efficiency of the system. The efficiency of SDMA can be further improved by using directional antennas. Figure (2.22) shows a sample frequency reuse for a cellular system with seven frequency bands (F1 … F7). As nodes move between cells they use the bandwidth allocated to that cell. In systems with basestations, the basestation is responsible for providing seamless handoff for terminals moving between cells. SDMA is usually combined with another access technique (FDMA, TDMA or CDMA) [19].

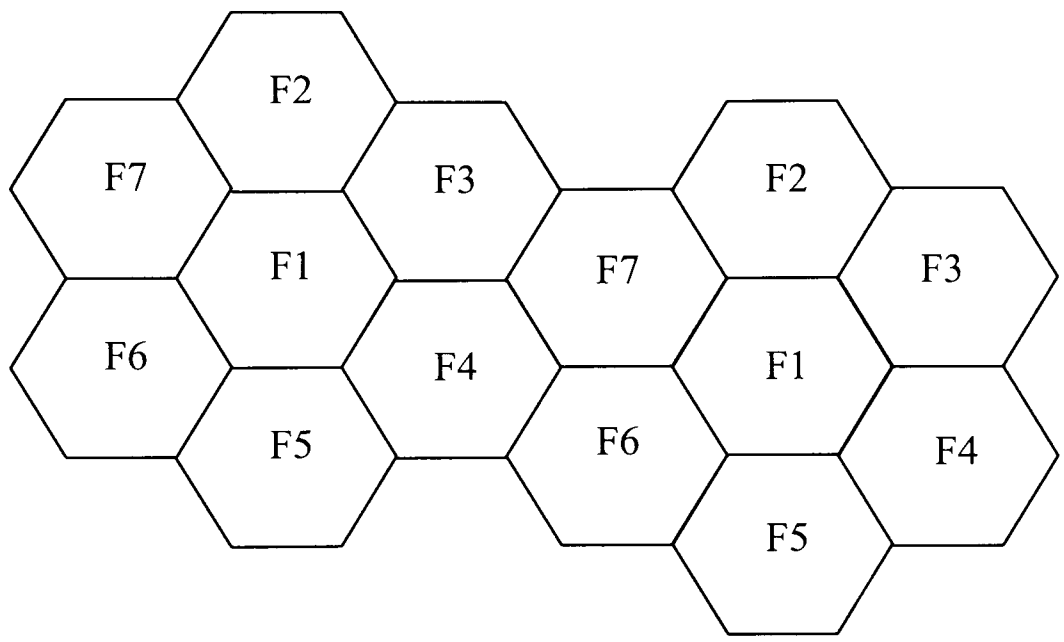

Figure (2.22): Frequency Reuse in SDMA

2.4.1.5. Random Access Techniques

Random access techniques are used in central-based MAC protocols to request the allocation of channels and are also used in peer networks to transmit data. Several random access techniques exist. ALOHA is considered the first ad hoc MAC. In ALOHA, the node simply transmits its data and hopes it reaches the receiver. Obviously the performance of ALOHA is quite poor especially under heavy load conditions. The division of time into transmission slots in slotted ALOHA was an attempt to improve the performance of ALOHA. Here terminals can start transmitting only at the beginning

of a slot therefore whole packets either collide or reach their destination. The use of slots, however, requires some sort of synchronisation technique between all the nodes [82, 83].

To achieve better performance Carrier Sense Multiple Access (CSMA) was introduced. In CSMA prior to transmission a node senses the channel. If no transmission exists, the node sends its packet; otherwise it waits for a random duration before trying again. This is known as non-persistent CSMA. In 1-persistent CSMA, if the node senses an ongoing transmission, it keeps monitoring the channel and transmits once the channel becomes idle. There is also a *p*-persistent CSMA in which the node keeps monitoring the busy channel and when it becomes idle transmits with probability *p*. A slotted version of CSMA can be used in which time is divided into slots and nodes only transmit at the beginning of a slot. Although CSMA can perform better than ALOHA, collisions still occur especially under heavy load conditions. CSMA does not provide fair access to all the terminals and does not solve the hidden terminal problem [82, 84].

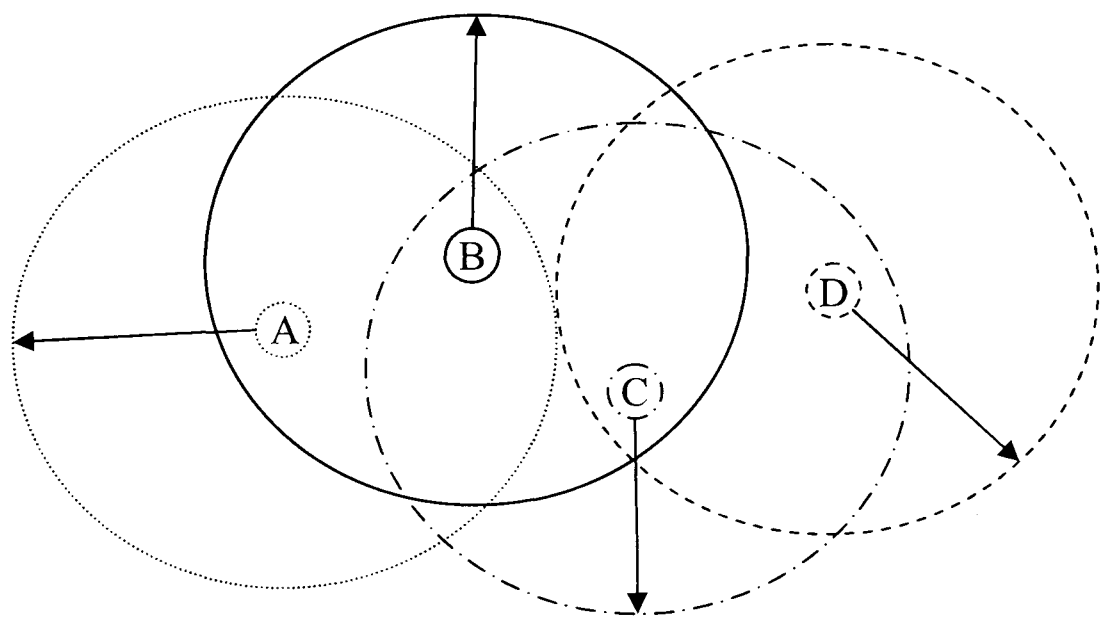

Figure (2.23): Hidden and Exposed Terminal Problems

The hidden terminal problem appears in wireless networks due to the fact that not all terminals can sense each others' transmissions. In figure (2.23) each large circle represents the transmission range of the node at its centre, represented by the small circle. Terminal C, for instance, can sense transmissions from B and D but not from A,

terminal A can sense transmissions from B but not from C or D while B can sense from A and C but not D. Now if, while A is sending to B, C has some data to send to B, C cannot sense the carrier of A's transmission and therefore transmits to B resulting in a collision at B.

To solve this hidden terminal problem, a Request-To-Send/Clear-To-Send (RTS/CTS) scheme was devised [85-87]. Using the same scenario of figure (2.23), before terminal A transmits to B it sends the short RTS packet. If this is received correctly at B, it replies with the short CTS. C cannot sense the RTS sent from A but it can sense the CTS sent from B and therefore C defers its transmission for the duration of the data transmission between A and B (specified in the RTS and CTS packets). Although the use of RTS/CTS packets improves performance, it does not completely solve the hidden terminal problem and it introduces another problem. Considering figure (2.23) again, if A sends RTS to B, B replies with CTS, however if at the same time D sent an RTS to C, it will collide with B's CTS at C. Now C is unaware of A's transmission. D after a timeout will send another RTS for C which replies with a CTS that will collide with A's data at B. Even if B's CTS does not collide with D's RTS there is still a problem. In this case A and B are communicating, however because C sensed B's CTS it cannot reply to D's RTS although C cannot sense any transmission and D's transmission does not affect the A-B link. This is known as the exposed terminal problem [84].

In Busy Tone Multiple Access (BTMA) a separate narrow band channel is checked prior to transmission. If the node detects a sinusoidal signal in the channel then there is an ongoing transmission in the data channel otherwise the data channel is idle. Originally a basestation was responsible of transmitting the busy tone to notify the nodes of an ongoing transmission [88]. A Receiver Initiated BTMA (RI-BTMA) was proposed in [88]. In RI-BTMA the source sends a packet similar to RTS to the destination. If the packet was received successfully, the receiver transmits a busy tone in the tone channel. Any node sensing the busy tone ceases from transmitting RTS packets. The node that sent the RTS sends its data to the destination. This scheme was

enhanced in Dual Busy Tone Multiple Access (DBTMA) by using two channels. A sinusoidal signal is transmitted by the source of transmission in the first channel and in the second channel the destination transmits a similar signal [89]. This scheme solves both the hidden and exposed terminals problems. BTMA and DBTMA, however, require the use of separate narrow band busy tone channel(s), which wastes the scarce bandwidth resource, and separate transmitters for the data and busy tone channel(s), thus increasing the cost of the system. RTS/CTS handshakes and busy tone algorithms provide solutions in unicast transmission and are not applicable to broadcast data.

Random access techniques are the most common in ad hoc MAC protocols since typically a basestation is required for the other schemes. However methods for using SDMA, TDMA, CDMA and FDMA have been considered in the literature [90-94] either by electing a node to play the role of a basestation or in a distributed manner. In random access techniques terminals have the same right to access the medium therefore collisions can occur unless some sort of coordination between the nodes is used.

2.4.2. IEEE 802.11 MAC Protocol

The IEEE 802.11 MAC standard uses an access method based on CSMA known as Carrier Sense Multiple Access with Collision Avoidance (CSMA/CA). It describes two access mechanisms, Point Coordination Function (PCF) in which a basestation polls the terminals for data, and Distributed Coordination Function (DCF) where terminals communicate in an ad hoc manner. In the ad hoc mode the MAC applies CSMA with a Binary Exponential Back-off (BEB) algorithm, to avoid collisions, and the option of using RTS/CTS packets. DCF manages the access to the medium and handles collisions. It uses a variable size Contention Window (CW) and waiting periods denoted by Short, Priority, Distributed and Extended Inter-Frame Spaces (SIFS, PIFS, DIFS and EIFS respectively) as well as counters to manage the access to the medium in a distributed manner. Figure (2.24) shows the 802.11 general frame format [95].

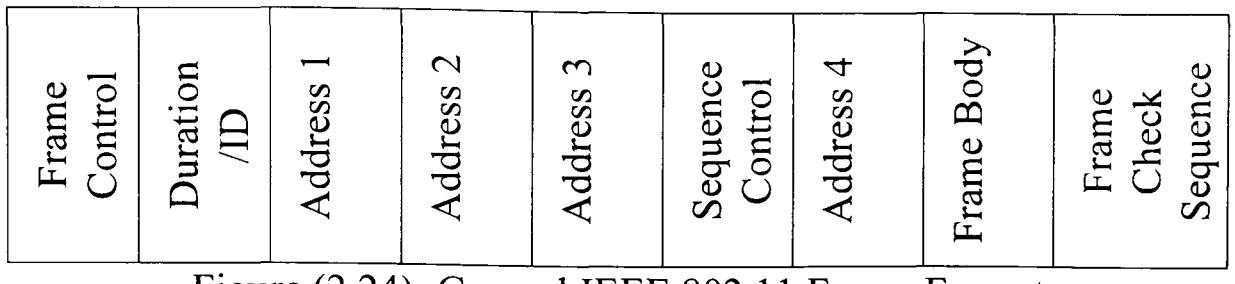

Figure (2.24): General IEEE 802.11 Frame Format

In DCF when a node receives a packet from the upper layer it checks a counter known as Network Allocation Vector (NAV) and if it is zero senses the channel. If the channel is idle for a DIFS duration, the node sets its backoff counter to a random value in the range 0 to CW. Initially CW is set to a minimum value CW_{min}. If the channel becomes busy during backoff, the backoff counter is frozen and the counter is resumed after the channel remains idle for s DIFS. When the backoff counter expires, the node either transmits an RTS packet, if the data is unicast and exceeds a predefined threshold, or transmits the data packet. If the destination decodes the packet correctly, it replies after an SIFS duration by a CTS, if an RTS was received, or an Acknowledgment (ACK), if a data packet was received. If the source does not receive a CTS or ACK, it assumes a collision occurred, doubles the value of CW, up to a maximum value CW_{max}, and repeats the process again. RTS, CTS and data packets contain the remaining time required to complete the transmission (including ACK transmission). Nodes not participating in the data exchange set their NAV to this value and do not attempt to transmit while NAV is greater than 0. Broadcast messages do not use the RTS/CTS handshake or ACK [95-97].

In the PCF mode the basestation/access point waits for the channel to be idle for a PIFS duration (SIFS < PIFS < DIFS) before sending a beacon packet. The beacon announces the start of a Contention Free Period (CFP) and its duration. Each node sets its NAV to the value announced in the beacon and does not access the channel unless the NAV expires, the access point polls it for data or it receives a beacon terminating the CFP period. A node must register itself with the access point in order to enter the polling list. The PCF mode is optional but the standard specifies that all nodes must be

able to co-operate with access points using PCF even if they do not support the polling service of the access point [95-98].

An improved version of DCF, known as the Enhanced Distributed Coordination Function (EDCF), has been developed for the IEEE 802.11e standard. DCF provides equal access to all the nodes in the network. It does not support priority or QoS. EDCF is an attempt to support QoS using DCF. In EDCF up to four QoS classes, known as Access Categories (AC), are used. Each class has a separate queue, uses a different Arbitrary Inter Frame Space (AIFS) instead of DIFS and has different contention window sizes for the backoff counter. High priority traffic uses smaller AIFS, CW_{min} and CW_{max} values than traffic with lower priority to gain access the channel before lower priority traffic. Therefore traffic within the node contends for the channel in a similar fashion as nodes contend for the channel. If the backoff timers of two ACs expire at the same time an internal collision within the node occurs. Although this scheme gives high priority traffic a better opportunity to access the channel, packets of the same priority from different node still contend for the channel and may collide with each other. Hence the performance of 802.11e remains a best effort performance with no guaranteed quality of service [98, 99].

2.4.3. Proposed MAC Protocols for VANET

Several MAC protocols have been developed specifically for VANET. In this section we review some of these protocols and discuss their operation and limitations.

2.4.3.1. IEEE 802.11p

A standard, known as standard IEEE 802.11p, for vehicle to vehicle/roadside communications is being developed by an IEEE committee. It is still a draft but is expected to be released soon for trial use. The draft adopts OFDM for the physical medium and specifies data rates from 3 to 27 Mbps for 10 MHz channels, 6 to 54 Mbps for 20 MHz channels, distances up to 1 km and maximum packet error rate of 10% for a protocol service data unit (PSDU) of 1000 octets. Nodes normally operate in the ad hoc WAVE mode and can optionally join and synchronise with a Wave Basic Service Set

(WBSS) if they receive a WBSS announcement frame from a basestation. Authentication and association are not used in WBSS but can be implemented in higher layers. The frames used for IEEE 802.11p are action frames, RTS, CTS, and ACK (acknowledgement) control frames as well as data frames. Other 802.11 frame types require authentication and association and are therefore not used. The draft also uses the Enhanced Distributed Channel Access (EDCA) specified in IEEE 802.11e to provide priority. PCF in not supported in this standard as beacons are not transmitted in WAVE mode [11, 14].

The RTS/CTS and contention windows used in 802.11 do not solve the hidden/exposed terminals. Due to the high mobility of the terminals in vehicular communications, a packet between two stationary, or slowly moving, cars passing all the DCF constraints can still collide with another packet sent from a fast moving (or in the opposite lane) car not aware of the CTS/RTS handshake. This scenario can occur rapidly in V2V networks causing very low throughput. Moreover RTS/CTS is applicable only in point to point transmission whilst several VANET application are broadcasting by nature (e.g. safety, traffic and weather information).

2.4.3.2. TDMA Protocols

The FleetNet project [10] studied the extension of the UTRA-TDD standard for decentralised vehicular networks. An ad-hoc mode of UTRA-TDD known as Opportunity Driven Multiple Access (ODMA) can provide access to approximately five nodes within coverage range but relies on a basestation for synchronisation. Since a basestation is not always available to provide synchronisation, a new ad-hoc proposal based on UTRA-TDD was introduced in [100]. The new modified UTRA-TDD achieves synchronisation in two steps, first using GPS to achieve coarse synchronisation between nodes, then using a midample (synchronisation bits) to achieve fine synchronisation [101, 102]. The standard uses TDMA slots with 16 CDMA codes for each slot. The frame has a number of high priority slots, used for transmitting urgent messages, followed by regular slots. Each node must first reserve a minimum amount of bandwidth, using Reservation ALOHA (R-ALOHA), even if it has no traffic. This is

then used by the node to request additional bandwidth if required [103]. Simulations showed that the modified UTRA-TDD outperformed the IEEE 802.11b [78]. A frequency hopping technique was later introduced to extend the protocol to multiple channels [104]. Each group of nodes has its hopping sequence or pattern. The patterns were designed such that every two patterns will, at some time, switch together to a specific control band, known as the co-ordination band, to exchange messages. During the rest of the time, the nodes using the pattern can switch to any of the other channels. Although the scheme is a promising solution, the maximum data rate for UTRA-TDD is only 2Mbps which is less than the minimum data rate supported in the ASTM standard. Moreover the proposal is designed to work at 2GHz. Figure (2.25) shows the UTRA-TDD frame.

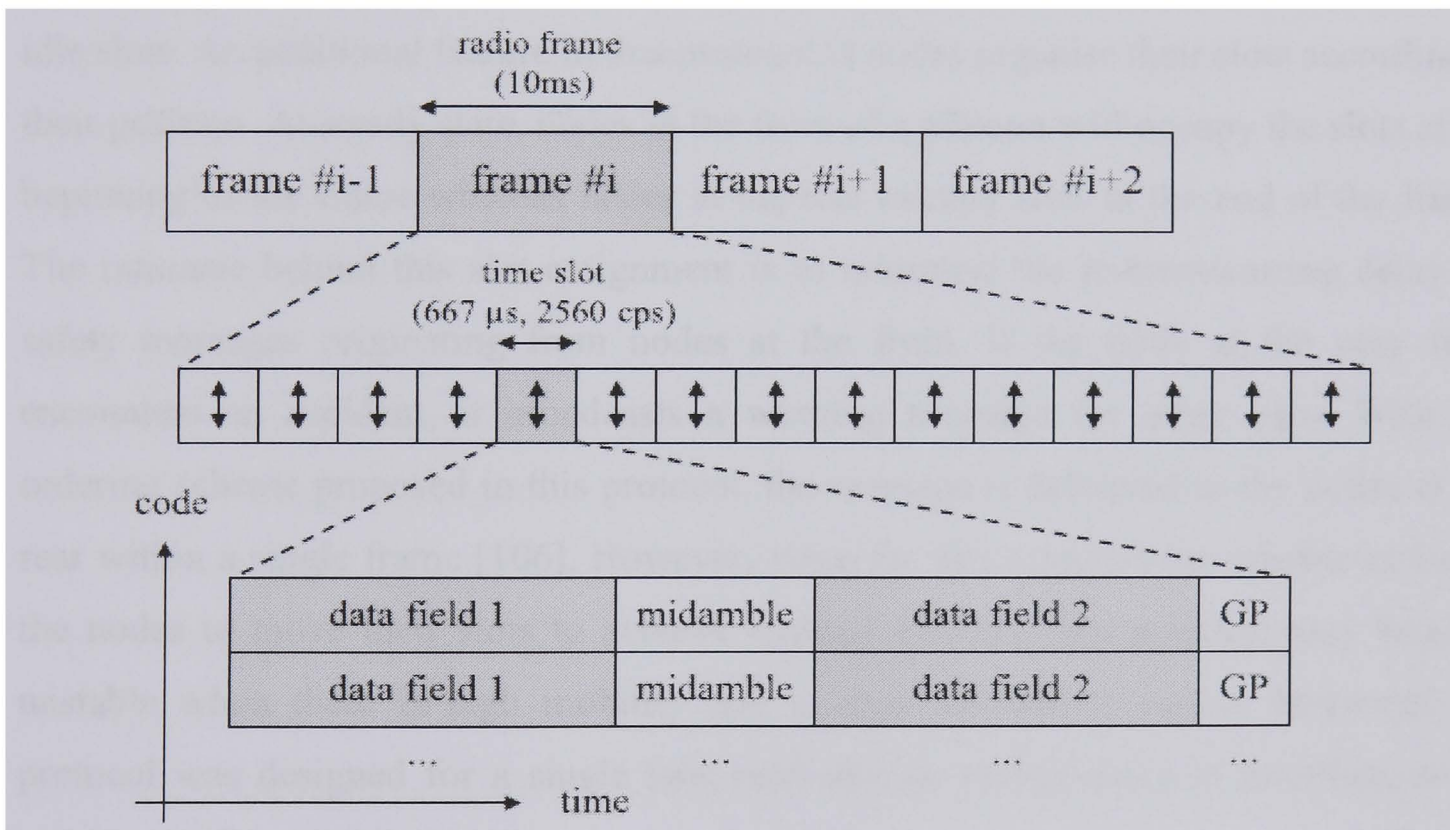

Figure (2.25): UTRA-TDD Frame Structure [101]

Another distributed TDMA protocol for VANET is ADHOC MAC [77, 92]. ADHOC MAC is an improvement of Reservation-ALOHA (R-ALOHA). In R-ALOHA time is divided into frames and each frame contains a number of slots. A node wishing to transmit, attempts to send at a random time slot. If the transmission was successful, the node continues sending in the same slot. If the transmission failed, the node chooses

a random slot for transmission. R-ALOHA is a very simple protocol and has been adopted in several MAC protocols, including the FleetNet MAC, but collisions reduce it performance especially when hidden terminals exist. In ADHOC MAC nodes exchange information about the state of each slot (BUSY/IDLE) as each node senses it. With this information, the nodes are aware of which slots are free even if hidden terminals exist, and attempt to reserve only free slots. The main drawback of ADHOC MAC is the large overhead. The state of each slot in the frame must be transmitted along with the ID of the node transmitting in the slot. Under high traffic this overhead is justifiable but under low traffic densities the performance of TDMA systems is worse than that of DCF [105]. A protocol similar to ADHOC MAC was presented in [81, 106]. The statuses of the time slots are broadcasted by each node and new nodes attempt to reserve one of the idle slots. An additional feature in this protocol is nodes organise their slots according to their position. At steady state, nodes in the front of a platoon will occupy the slots at the beginning of the frame whereas nodes at the rear occupy slots at the end of the frame. The rationale behind this slot assignment is to minimise the re-broadcasting delay for safety messages originating from nodes at the front. If the node at the very front encounters an accident, it broadcasts a warning message for other cars. With the ordering scheme proposed in this protocol, the message is delivered to the nodes at the rear within a single frame [106]. However, since the slot organisation scheme enforces the nodes to move their slots to achieve optimal ordering, the protocol may become unstable when there is high mobility and a large number of nodes. Moreover the protocol was designed for a single lane road and its performance in multilane roads requires further investigation.

The Wireless Token Ring Protocol (WTRP) is another distributed implementation of TDMA [79]. This is a wireless variant of the Token Ring LAN. A node may start transmitting only after it receives a token and continues transmission up to a certain period of time. After the transmission, it sends the token to the next node in the ring as specified in its access table. The protocol defines the algorithms to handle a node joining a ring as well as merging/emerging of rings. It is a fair protocol with guaranteed

Quality of Service (QoS) for all nodes within the ring. WTRP however assumes a maximum number of nodes in a ring and any new nodes beyond this number cannot join the ring but it can form another ring at a different channel. Such assumption is not suitable for broadcasting messages as the nodes will be using different channels.

2.4.3.3. SDMA Protocols

The SDMA scheme was addressed in [90, 91, 107]. The basic principle is to divide the area into small cells (picocells), each big enough to occupy only one node (car) and assign a channel(s) (time slots, frequency bands or codes) for each of these cells. Nodes consult pre-installed channel allocation maps to determine the channel(s) assigned to their positions. The scheme is very reliable and simple but it has poor efficiency since most of the time a large percentage of these cells will be unoccupied and therefore the allocated channels are not used. The authors of [91] proposed a scheme to improve the performance of SDMA. According to their algorithm, each car first determines its position and the position of the car ahead of it. It then has the option of using the channels allocated to cells between its position and the car ahead of it up to a certain limit. The limit is designed to avoid collisions with a car using the same slot ahead as the slots are reused after some distance. The authors assume each node knows the position of the car ahead either via message exchange or using radar. Using periodic messages to determine the location of nodes adds a considerable amount of load to the network. Although radar eliminates this overhead, it cannot find the accurate position of the car ahead in the same lane particularly in curved and multi-lane roads. Another limitation common to all SDMA schemes is that location errors can cause collisions.

2.4.3.4. Cluster-Based Protocols

In Cluster-Based protocols a chosen node takes the role of a basestation to assign channels and may relay data between nodes. Among cluster based protocols, Cluster Based MAC (CBMAC) was introduced in [93] specifically for VANET. In this protocol nodes form a cluster and a cluster head is elected. The Cluster Head (CH) is responsible of assigning time slots to the nodes within the cluster. A frame is constructed to

organise the access. At the beginning of the frame the CH sends a HELLO message followed by the slot assignment. The nodes then start transmitting each at its assigned slot. A random access period then follows in which new nodes compete to declare their presence. A node able to receive information from two or more cluster heads becomes a gateway and it relays information about slot assignments from one CH to the other(s) to avoid collisions. When two cluster heads get within communication range of each other, the clusters are merged and one of the cluster heads is chosen as the new CH based on a cost function. The cost function takes into account the connectivity, relative speed and number of neighbours. The CH with the smallest cost remains as the cluster head.

In [108] the authors proposed the use of two transceivers. Nodes form clusters to exchange safety and non-safety messages. The control channel of the DSRC spectrum is used in the proposed MAC to exchange control messages between clusters. A separate channel is dedicated for exchanging data between clusters. One of the other five channels is used for control messages within the cluster while the rest of the spectrum is for data messages within the cluster. A cluster head (CH) organises the access to the channels within the cluster and relays safety messages between clusters. One of the transceivers in the CH is tuned to the safety and control channel within the cluster and is used to exchange safety and data channel reservation requests from cluster members and organise channel access using TDMA while the other transceiver is used to communicate with other cluster heads and exchange safety messages using 802.11 MAC. For cluster members, one of the transceivers is used to communicate with the CH while the other is used to transmit non-safety data in the channels assigned by the CH. To reduce interference between clusters each cluster uses a different CDMA code which is randomly selected by the CH and announced to cluster members as well as nearby cluster heads. This system has a high cost due to the use of two transceivers. Moreover CDMA has the near-far problem and power control is difficult to implement in ad hoc networks since different destinations experience different path losses. Even if all the traffic is relayed by the CH, the mobility of the CH and the nodes complicates the power control requirements. Issues of cluster head election, cluster merging and loss of

connection to cluster head are usually of concern in all cluster-based protocols. The election of a cluster head typically requires a considerable amount of time and in VANET the topology changes quickly due to the high speeds encountered. Furthermore clusters can merge or lose connection to the cluster head particularly at junctions and exits. This may increase the signalling overhead considerably.

2.4.3.5. Multi-Channel MAC Protocols

In architectural networks, the basestation is responsible for managing the available channels and organising channel assignment. Most ad hoc MAC protocols, including 802.11 standards, were designed for a single channel and assume, in case of multiple channels, that each channel is independent from the other. However in multi-channel systems, some conditions arise which are not encountered in single channel communications. For instance in the RTS/CTS handshake with single channel, if a CTS is not received, this is either due to an ongoing communication or collision of RTS packets. However in multichannel systems the destination may be on a different channel hence missing the RTS packet. This has even a worse impact on the network layer since it may falsely cause an unnecessary search for a new route. A more serious problem is a missed CTS as this can cause collisions [109]. A protocol, known as Dynamic Channel Assignment (DCA), to organise access to channels in a multi-channel system was proposed in [110]. DCA requires two transceivers per node. In DCA a control channel is used for reserving one of the data channels prior to transmission. The source sends an RTS packet with a list of free channels as sensed by the source. The destination replies with a CTS indicating which channel, if any, it can use from the list sent by the source. The source then sends a reserve (RES) packet indicating the channel used and transmission duration and transmits, using the other transceiver, the data in the specified channel. The analysis of the protocol shows that its performance depends on the control channel. If the control channel is not large enough, the reservation handshake will fail leading to idle data channels [110]. Moreover the protocol requires two transceivers, one tuned for the control channel and the other for transmitting data.

The Multi-Channel MAC (MMAC) protocol was designed to enhance the performance of 802.11 when several channels are available [110]. The available traffic is distributed over the available channels by exchanging, prior to transmission, messages known as Ad hoc Traffic Indication Messages (ATIM). In MMAC all nodes tune to a default channel for a fixed duration. During this duration, known as ATIM window, nodes exchange ATIM and ATIM-ACK messages to negotiate the channels that will be used for transmission. The selection algorithm for the channels aims at distributing the load over the channels. Assuming all channels are idle, if an ATIM handshake indicates a channel (c1) will be used for transmission, the next ATIM handshake for another pair will use one of the other available channels but not c1. If a node agrees to use a channel for transmission/reception, it will select the same channel for each ATIM handshake until the next ATIM window starts. Unlike DCA, the default channel can be used for transmitting data after the ATIM window elapses and is not dedicated for control messages. After the ATIM window, nodes switch to the channel they negotiated. The nodes in each channel contend for the channel with any other nodes that agreed to use the channel, i.e. using RTS/CTS or basic access. Since MMAC distributes the nodes over several channels, this improves the performance since fewer nodes compete for channel access. However nodes still contend for access in the negotiated channel and therefore the performance drops as the number of nodes increase. Moreover multicast and broadcast transmissions are very difficult to achieve in MMAC as the nodes will be in different channels [110].

The WAVE standard P1609.4 divides time into segments of 100ms. Each segment is further divided into two time periods each of duration 50ms. Within each segment, all nodes tune to the control channel in one period and may switch to another channel in the other [111].

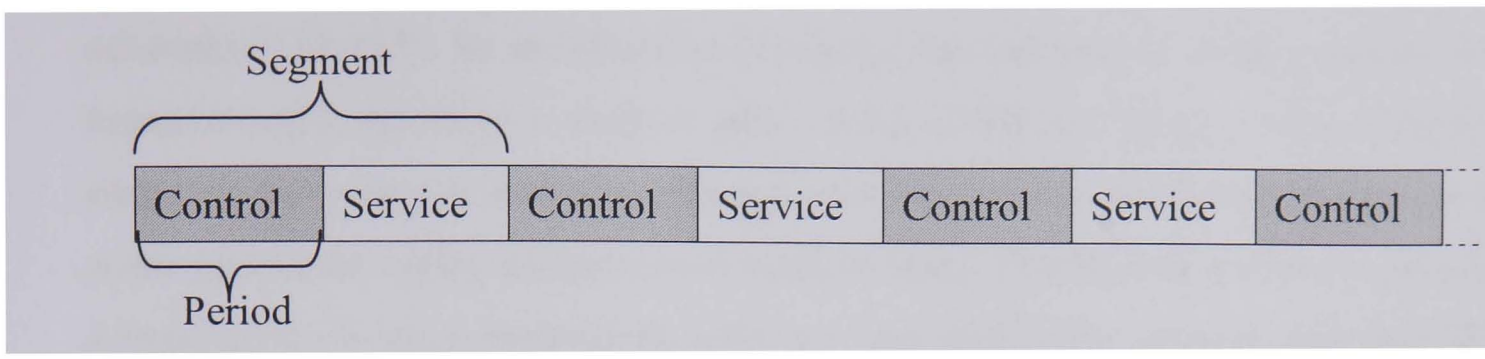

Figure (2.26): Multichannel Operation in WAVE

Vehicular Mesh (VMESH) was proposed in [111, 112]. In VMESH time is divided into frames of two time slots each with duration of 50ms. All nodes switch to the control channel for one slot every frame and may switch to another channel in the other slot as specified in the P1609.4 standard [111, 112]. The control slot is divided into two periods, a beacon period and a safety period. In the beacon period nodes access the channel using R-ALOHA and negotiate reservation of a slot in one of the other six channels. In the safety period nodes access the channel using 802.11p EDCA. The theoretical saturation throughput of VMESH is superior to 802.11p since it eliminates the channel contention in service channels. However the reservation process puts a large load on the control channel which becomes the bottle neck of the protocol since collisions in the reservation process lead to idle slot(s) in the service channel(s) [109, 110].

2.5. Connectivity and Upper Layers

2.5.1. Connectivity

Connectivity is a measure of whether all nodes in the network can communicate with each other or not. A network is defined to be fully connected, i.e. having a connectivity of 1 (or 100%), if any two nodes in the network can communicate with each other either directly or via intermediate hops regardless of their number. Generally, a connectivity of 100% is very difficult and expensive to achieve all the time for all mobile nodes especially in large networks, therefore a target of 90-95% connectivity is usually considered in the design of networks. The problem of connectivity is an old one that has been studied thoroughly for architectural (basestation based) and ad hoc

networks [113-115]. In architectural networks, the basestation usually relays the data between users, therefore a node is either fully connected, when within a basestation range, or has zero connectivity. Basestations are usually connected to each other via some permanent cables, microwave or satellite links. Therefore if a node is connected to a basestation, it can communicate with any user within the network coverage. Hence, the issue of connectivity in architectural networks is reduced to finding the optimum position and characteristics of the basestation, e.g. range, number of channels, etc, which achieve the highest connectivity and satisfy any constraints, e.g. maximum transmit power. The decision is usually based on a survey of the geographical features of the area and the population/node density, and this is one of the reasons why there are different types of cells in cellular phone systems (microcells, picocells). Therefore, the main factors affecting connectivity in architectural networks are the distance and the existence of any obstacles between the node and the basestation.

2.5.1.1. Connectivity in Mobile Ad hoc Networks (MANET)

In ad hoc networks the issue of connectivity is different from architectural networks. As there are no basestations in MANET and the nodes are usually assumed identical in their capabilities, the connectivity will depend on the inter-spacing between the nodes. This is because the network relies on the contribution and co-ordination of the nodes to deliver messages. If the destination is not within the communication range of the source, intermediate nodes must relay the message till it reaches its destination. Connectivity gives a measure of how many nodes within the network can communicate with each other. Since each node can communicate only with a subset of the nodes within the network, the connectivity can take any value from 0 to 1 and is not restricted to 0 or 1 as in architectural networks. MANET is considered a two dimensional network as typically nodes are distributed over a two dimensional space. Connectivity of two dimensional networks was the main concern in several papers such as [113-115]. In these networks each dimension is assumed large enough to accommodate several nodes. It was found that as the density increases, the connectivity approaches 100%. As the node density increases, the probability that a path exists between each source and

destination increases and, therefore, the connectivity is improved. The connectivity depends not only on the node density, but also on the distribution of the nodes in the area and the communication range (R). Assuming omnidirectional radiation and the nodes are uniformly distributed in space, we can estimate the number of neighbouring nodes for a node not at the edge as:

$$No\ of\ Neighbours = \frac{No\ of\ Nodes}{Total\ Area}.\pi R^2 \qquad (2.28)$$

The number of neighbouring nodes is also essential for estimating the performance of the physical and link layers. It was shown in [116] that the performance of CSMA link layer depends on the available load. The performance of the link layer becomes quite poor as the load increases. As the node density increases the load increases causing serious deterioration for CSMA link access. Similar conclusions can be reached for CDMA since more nodes mean more interference and therefore smaller signal to interference plus noise power ratio (SINR) which is the figure of merit for CDMA [22]. For TDMA and FDMA there is a limited amount of channels available and it is important to have an estimate of the number of available nodes to allocate enough channels to serve the nodes or, otherwise, all the channels might become occupied and some nodes will not be able to access the channel.

For the network layer the number of neighbouring nodes is important as each node becomes a potential next hop in a path towards the destination. Having more paths considerably improves the performance of the network layer since it becomes possible to switch to a new path if the current path fails. However it then becomes the responsibility of the routing algorithm to choose the 'best' path based on some cost function.

2.5.1.2. Connectivity in VANET

For vehicular networks the nodes (cars) are distributed in a linear space (road) rather than a two dimensional area. This simplifies the analysis of the system considerably. The single dimensional network was analysed in [114, 117, 118] for fixed nodes and [119] considered the case of nodes with random walk mobility model. In [117] the

probability of achieving full connectivity ($P_n(d)$) in a network with n nodes in a road of length d, normalised to the communication range, was shown to be given by:

$$P_n(d)=\begin{cases} 0, & n<d-1 \\ \left(1-\left(1-\frac{1}{d}\right)^n\right)^{n+1}, & n\geq d-1 \end{cases} \quad (2.29)$$

The expression assumes uniform distribution of the distance between nodes. However the distance between the nodes is usually approximated by the exponential distribution [114, 117] given by:

$$p(x)=\frac{1}{\mu}.e^{\frac{-x}{\mu}} \quad (2.30)$$

μ is the mean value. The speed model affects the distribution of the inter-spacing between the nodes and, hence, the connectivity. A simulation comparison between random walk and vehicular mobility showed that the random walk model is not a valid approximation of vehicular mobility [120].

2.5.2. Network Layer

The network layer is responsible for delivering the packet from the source node to the destination node in a multihop connection via a routing algorithm operating within the network layer. The traditional classifications of routing algorithms are static routing and dynamic routing. With static routing, a fixed routing table is provided and never changes, while dynamic routing updates the routing table depending on the network conditions. Since the topology of the cars in the road is initially unknown and changes rapidly, static routing is not applicable to VANET. Dynamic routing on the other hand requires some overhead which can become enormous in a rapidly changing network as is the case with vehicular communications.

Dynamic routing protocols can be further subdivided into proactive protocols and reactive protocols. In proactive protocols, each node maintains a table of the next hop towards a certain destination or group of destinations. Messages are exchanged between nodes whenever the topology changes to update the routing tables. With proactive

routing, when a connection to a destination is required, the node consults the routing table to determine the next hop and then immediately sends the message to that hop. Proactive protocols perform well in networks with fixed or slowly changing topology. However if the topology changes rapidly, as in VANET, a large amount of routing update packets will be required to update the routing tables. This increases the routing overhead considerably and, hence, reduces the efficiency of the protocol. Reactive protocols do not store routing information for each destination but search for the best next hop whenever a connection is required therefore any overhead used to update the routing table is justified. There is a trend to use position based routing algorithms in vehicular communications as these help in providing multicasting and broadcasting services which are required for safety applications and existing GPS technology can provide the position with reasonable accuracy [121].

Broadcasting and routing algorithms for VANET were studied in FleetNet project [10]. Three reactive routing protocols were considered, Position Based Forwarding (PBF), Contention Based Forwarding (CBF) and Ad hoc On-Demand Distance Vector (AODV). PBF and CBF use location service algorithms to find the position of the destination. Based on this position a node using PBF selects one of the surrounding nodes to forward the message to the next hop. This process is repeated till the message reaches its destination. In CBF the source transmits the message with the position of the destination. Every node receiving the message sets a timer proportional to the difference between its position and the destination. If the timer expires and no other node has broadcasted the message, the node forwards the message to the destination. In AODV the source floods the network with a route request for the destination. Nodes receiving the request calculate a distance vector and forward the message. This process is repeated till the destination is reached which sends a route reply. Once the reply reaches the source, the route is ready for sending the data. To reduce the flooding effects maximum hop count and Time To Live (TTL) fields are used in route messages. The simulation results from FleetNet show that CBF performs better than the other algorithms and it adapts to changes in the topology which interrupt routes in the other two protocols.

CBF, however, requires the assistance of maps in cities when multiple roads intersect and run in parallel. Its performance in congested areas also requires more investigation since several cars might have the same distance to the destination which can lead to collisions [122, 123].

A broadcasting algorithm based on CBF has also been suggested for safety applications [124]. A car encountering an accident broadcasts a safety message and its current position. Other cars receiving this message set a retransmission timer inversely proportional to their distance from the source and re-broadcast the message, if no other node broadcasts first, and keeps re-broadcasting till it receives the same message from another node or the message is no longer relevant [124].

Another routing algorithm known as Greedy Traffic Aware Routing (GyTAR) has also been proposed in [125]. The algorithm targets the routing problem in cities. It works with the aid of maps and traffic density information to calculate the best direction in junctions the packet should take to reach its destination. The calculation is based on the distance, number of cars within that distance, their movement and speed. The paper also proposed a system for collecting and distributing information about the road and traffic conditions which can be used with GyTAR as well as other algorithms.

Although these algorithms, and many others, provide a solution to the routing problem in VANET, still more research is required to examine their performance, applicability and overhead. A major issue of concern is the achievable throughput of the system. This has been examined in [126]. According to their results the throughput decreases considerably as the number of hops increases and can be as low as 20kbps in 2Mbps links with 6 hops.

2.5.3. Transport and Application Layers

As shown in figure (2.1), the transport protocol chosen for the IEEE architecture is the User Datagram Protocol (UDP). UDP is a best effort protocol and does not employ any congestion control mechanisms as in Transmission Control Protocol (TCP). TCP provides a reliable transmission mechanism by using ACK and a retransmit algorithm

and it controls the flow of data via congestion windows to resolve congestions. These mechanisms, however, were mainly designed for wired networks and do not cope well when the network topology changes very frequently as in VANET [127].

A large number of applications have been specified by governments for DSRC applications, we cover here a few of them. Traffic control is a major factor for efficient use of the road network. Currently traffic lights organize the flow of traffic at junctions. With DSRC traffic lights become adaptive to the traffic and can provide priority to emergency cars as well as safety to pedestrians and cyclists. Moreover information about the state of the road can be distributed to cars to warn them of problems ahead such as ice or maintenance work on the road. This system will also be very efficient in the case of accidents, automatically notifying the nearest ambulance and other emergency vehicles to approach the accident if needed and even provide telemedicine services if the patient requires immediate attention, especially when there are no nearby hospitals. Crash prevention is the main motive behind vehicular communications, therefore a number of applications have been specified. Crash prevention applications that rely on an infrastructure include road geometry warning to help drivers at steep or curved roads and warn overweight or over-height vehicles, highway-rail crossing and intersection collision systems to help drivers cross safely, pedestrian, cyclist and animal warning systems to inform drivers of possible collisions, these systems become of vital importance at night or in low visibility conditions [128].

Safety applications which do not rely on an infrastructure include an emergency brake announcement which is the most important application for crash prevention. The first two cars might not benefit from the emergency brake system but farther cars can avoid the crash. Lane change assistance, road obstacle detection, road departure warning as well as forward and rear collision warning are all examples of safety vehicle to vehicle (V2V) applications. Cars can also automatically send help requests in case of an accident which can be vital when no other cars are around [128]. An ongoing European project, Emergency Call (eCall), aims at providing this automatic call service by 2009 using existing cellular infrastructure [129]. The On Board Unit (OBU) can also help the

driver in other different ways such as vision enhancement via image processing techniques, lane keeping assistance and monitoring of onboard systems as well as any cargo or trailers connected to the vehicle. Such systems are generalised as Advanced Driver Assistance Systems (ADAS) [129].

The commercial applications of the system cover a wide range of innovative ideas aiding individuals and tourists such as booking a parking space, downloading tourism information and maps for restaurants and gas stations, navigation and route guidance, payment at toll plazas, Internet access and connection to home computers. Other devices within the car can also be connected to the On Board Units (OBU) to access any services provided by the network or through the Internet. These applications are not required by the government but they encourage people to install the system.

A Japanese project called P-DRGS (Dynamic Route Guidance System) is one possible implementation of the navigation and route service. This project is developing a system known as PRONAVI that currently consists of a server accessible through the Internet. Users enter their start position, destination and time to start their journey and the server responds with the best two routes. The routes are compiled from a 9 months survey as well as simulations. In its final version the system should be able to collect data from the sensors installed in cars and provide the routes to the OBU [130].

The Vehicle Information and Communication System (VICS) is another Japanese implementation of roadside to vehicle communications. Subscribers to the system get an onboard navigation system that receives information about the weather, road conditions, traffic and any other related data from road side units and displays it to the user [131].

In Europe several ongoing projects are studying the impact and implementation of VANET [132-134]. The eSafety initiative was launched in April 2002. Currently it has 14 workgroups working in the areas of accident causation analysis, communications, digital maps, eCall, heavy duty vehicles, Human-Machine Interaction (HMI), information and communication technologies for clean mobility, implementation road map, international cooperation, Real-time Traffic and Travel Information (RTTI), research and development, security, service-oriented architectures and user outreach.

The eSafety forum aims to accelerate the development, deployment and use of eSafety systems to reduce by 2010 the number of fatalities in Europe by 50% [129].

The CARLINK project was launched in 2006 by CELTIC EUREKA [135, 136] with real-time local weather information, the urban transport traffic management and the urban information broadcasting as the primary applications. It aims at integrating WLAN, WiMAX as well as cellular technology to provide the information to cars on the road as well as to PDAs and mobile phones [137].

2.6. Summary

In this chapter we reviewed some related work on vehicular communications. Several challenges exist for each layer in the VANET architecture. The focus of this thesis is to study and analyse the performance of the physical and link layers and develop algorithms to enhance the bandwidth efficiency of VANET. Since there are no space or power restrictions in VANET, we focus on employing VBLAST systems in the physical layer of VANET. VBLAST offers higher spectral efficiency than single antenna systems and it has the lowest computational complexity among existing BLAST algorithms. However correlations and inaccurate channel information can degrade the performance of BLAST considerably. An accurate channel model is essential to study the performance of any physical layer solutions for VANET. Existing VANET models define two zones, an urban zone with rich Rayleigh fading and a suburban zone for open areas with high line of sight probability. These models do not consider the correlation between the antennas and, hence, will not accurately simulate the channel for MIMO systems. For the MAC layer, the IEEE 802.11p standard is been developed. IEEE 802.11 standards are random access, best effort protocols and their performance becomes quite poor in highly congested networks. The RTS/CTS handshake can be used to improve the performance but it only applies to unicast transmissions. In subsequent chapters, we study the performance of 802.11 standards and develop a MAC layer protocol that achieves higher performance than 802.11 and is suitable for unicast as well as broadcast transmissions.

Chapter 3

VANET Channel Model and Analysis

3.1. Overview

VBLAST provides higher bandwidth efficiency compared to single antenna systems [19]. However the correlation between the signals received by the antennas reduces the bit error performance and, hence, this correlation should be low for the VBLAST decoding algorithm to decode the signal correctly [47]. The correlation between the antennas becomes high due to several reasons but the most common are the existence of a strong line of sight, inadequate antenna spacing and inadequate multipathing, small number of surroundings [47, 138]. In this chapter we introduce and analyse our channel model for VANET which provides an accurate representation of the VANET channel. We then compare our model with measurement results from the literature and use the model to simulate the performance of VBLAST systems in VANET. Our model can be used to study the correlation and performance of antenna arrays with and without line of sight components in various scattering environments thus overcoming the limitations of the two rings model which assumes a rich scattering environment. We use the model to study the received signal correlation for broadside as well as endfire antenna arrays. In broadside arrays the elements of the antenna array are aligned perpendicular to the line of sight whereas in endfire arrays the elements are aligned parallel to the line of sight. Based on the results, we design an antenna array configuration to employ VBLAST in VANET. The capacity and bit error rate (BER) of VBLAST in VANET are then analysed both theoretically and via simulations with perfect channel knowledge at the receiver. Afterwards, the effects of line of sight, channel estimation and speed on BER are investigated. The chapter is partially based on the publication [5].

3.2. VANET Channel Model

As discussed in section (2.3.1), most existing wireless channel models assume a fixed basestation and a mobile terminal. Although the two rings model is designed to simulate the vehicular channel within the city, it assumes rich fading and no line of sight. These conditions are encountered only in dense environments and lead to low correlation between the antennas. However cars in highways and open areas typically experience line of sight communications with a small number of surroundings. Moreover, even within the city a line of sight may exist particularly when the distance between the nodes is small. Models extracted from measurements classify the environment into categories. City environments will have a model different from suburban and rural areas. However there are no well defined criteria as to when to switch between the models. In this section we introduce and analyse our channel model and compare its statistical characteristics with measurement results from the literature. Our model is suitable for line of sight and non-line of sight conditions and the number of surroundings is controlled to simulate the channel in city as well as open environments. It is also suitable to study the performance of antenna arrays since the number of surroundings control the severity of the fading and the correlation between the elements.

3.2.1. Model Description

Our model, shown in figure (3.1), is based on the Geometrical Based Single Bounce (GBSB) statistical channel model [29] where scatterers are placed within an ellipse surrounding the transmitter and receiver as shown in figure (2.9). The original model simulates the link between a mobile terminal and a fixed station (basestation) at the height of lamp posts with possible higher buildings around. Mobile terminals are assumed to be on the road with possible line of sight communications or within buildings without line of sight. The basestation and the scatterers are all fixed and the transmitter and receiver are placed at the foci of the ellipse. The primary (a_m) and

secondary (b_m) radii of the ellipse are calculated from the maximum delay spread of interest as follows [27]:

$$a_m = \frac{c\tau_m}{2}$$
$$b_m = \frac{1}{2}\sqrt{c^2\tau_m{}^2 - D^2} \qquad (3.1)$$
$$\tau_m = 3.244\sigma_t + \tau_0$$

Where τ_m is the maximum delay to be considered, σ_t is the delay spread, τ_0 is the minimum delay (line of sight delay), D is the distance between the transmitter and receiver and c is the speed of light. The delay spread of VANET has been measured for various roads and traffic conditions in [34] and [36]. The minimum mean delay spread measured was 103ns. According to [19] the signals reflected from the scatterers towards the receive antennas are clustered around the direct path. As the number of scatterers or ellipse radius increase, the angle of arrival increases causing less correlation between the antennas. Unless mentioned otherwise, we adopt the value 103ns for the delay spread in our model since a larger delay spread leads to larger radii and, hence, smaller antenna correlation which improves the BER of VBLAST [47].

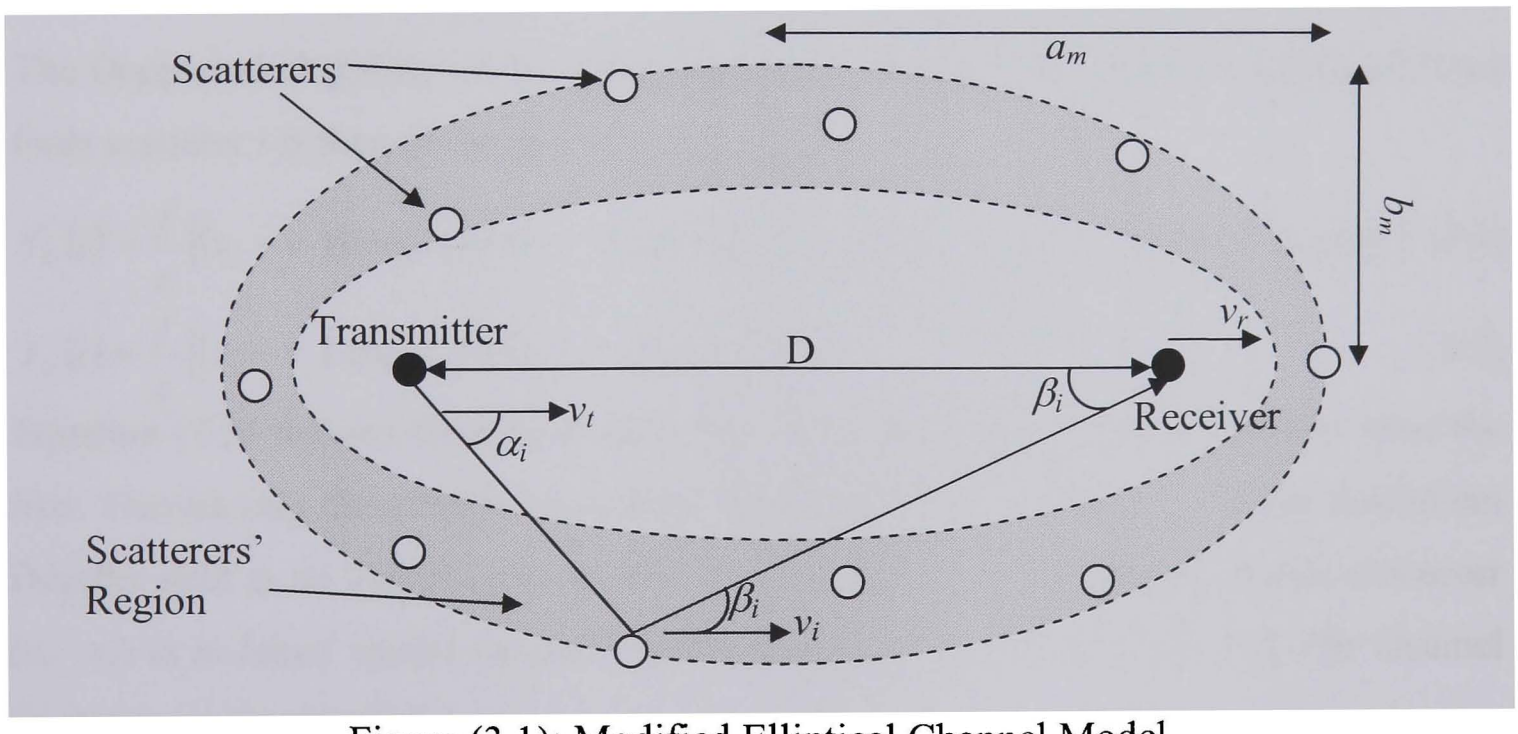

Figure (3.1): Modified Elliptical Channel Model

In our model the scatterers are constrained between two ellipses, as shown in figure (3.1). We use the additional inner ellipse since if no obstacle blocks the line of sight, the

scatterers will be at the edges of the lane/road. Therefore the dimensions of the inner ellipse are extracted from the width of the road and the distance between the source and destination. If obstacles (cars) exist between the transmitter and receiver, we assume the line of sight is blocked. We also add mobility to the transmitter and the scatterers which were assumed fixed in the original model. This will affect the Doppler shift at the receiver. The frequency (f_i) of the signal at scatterer i due to the speed of the transmitter (v_t) and the speed of the scatterer (v_i) is given by [23]:

$$f_i = f\left(1+\frac{v_t - v_i}{c}.\cos(\alpha_i)\right) \tag{3.2}$$

Where the speed is positive if the car is moving towards the right hand side of figure (3.1) and negative otherwise, α_i is as shown in figure (3.1), f is the frequency and c is the speed of light. Similarly the frequency at the receiver (f_{ri}) of the signal reflected from scatterer i is given by:

$$\begin{aligned} f_{ri} &= f_i\left(1+\frac{v_i - v_r}{c}.\cos(\beta_i)\right) = f\left(1+\frac{v_t - v_i}{c}.\cos(\alpha_i)\right).\left(1+\frac{v_i - v_r}{c}.\cos(\beta_i)\right) \\ &= f + f.\left(\frac{v_i - v_r}{c}\right).\cos(\beta_i) + f.\frac{v_t - v_i}{c}.\cos(\alpha_i) + f.\frac{v_t - v_i}{c}\frac{v_i - v_r}{c}.\cos(\alpha_i)\cos(\beta_i) \end{aligned} \tag{3.3}$$

The Doppler shift ($f_D(i)$), which is the difference between f_{ri} and f, of the signal reflected from scatterer i is then given by:

$$f_D(i) = \frac{f}{c}[(v_t - v_i).\cos(\alpha_i) + (v_i - v_R).\cos(\beta_i)] + \frac{f}{c^2}(v_t - v_i)(v_i - v_r)\cos(\alpha_i)\cos(\beta_i) \tag{3.4}$$

$$f_D(i) \approx \frac{f}{c}[(v_t - v_i).\cos(\alpha_i) + (v_i - v_r).\cos(\beta_i)] \tag{3.5}$$

Equation (3.5) follows from (3.4) since the last term in (3.4) is much smaller than the first. Considering the elliptical model in figure (3.1) and equation (3.5), the maximum Doppler shift is no longer defined only by the relative speed of the transmitter-receiver ($v_t - v_r$) as in Jakes' model because the surroundings are not fixed [23, 26]. The channel response can be calculated as:

$$h(t) = \sum_{i=0}^{M} g_i \times \exp\left(j\left\{\frac{2\pi.f_D(i).t}{c} + \phi_i\right\}\right).u(t - t_i) \tag{3.6}$$

where g_i is a parameter that combines the reflection coefficient and extra attenuation for path i relative to the line of sight, t_i is the excess distance delay, ϕ_i is a random phase, M is the number of paths and $u(t)$ is the unit step function. The line of sight is represented by the case $i = 0$. We assume the existence of objects (cars) between the transmitter and receiver leads to blockage of line of sight. When a line of sight exists, a ground reflection is added if the distance between the transmitter and the receiver satisfies equation (3.7).

$$D \geq \frac{4\pi . h_t . h_r}{\lambda} \tag{3.7}$$

h_t and h_r are the heights of the transmit and receive antennas respectively and λ is the wavelength. The right hand side of (3.7) is the minimum distance for the first Fresnel zone to touch the ground, hence a ground reflection may exist only if equation (3.7) is satisfied [20, 21].

The surroundings in our model move at random speeds assumed to be uniformly distributed between 0 and the maximum speed limit. For simplicity we set the speed of the transmitter and surroundings relative to the speed of the receiver. Surroundings above the transmitter in figure (3.1) are either fixed or moving in a direction opposite to the transmitter (negative speed) while those below the transmitter are either fixed or moving in the same direction as the transmitter (positive speed). Using this model we simulate the channel response in VANET to calculate the received signal in each antenna and find the correlation between the elements of antenna arrays.

3.2.2. Model Statistics

For our simulations we use 10 scatterers. The maximum speed for the scatterers was set to 120 km/h with the transmitter moving at 90 km/h and fixed receiver. The ratio of the amplitude of the line of sight component to the amplitude of the signal reflected from any of the scatterers is equal to k. The delay spread is 103ns as measured in [34]. The distance between the transmitter and receiver is 1 km which is the maximum transmission range specified for IEEE 802.11p [11] and the heights of the antennas

were set to 1.5m. The carrier frequency is 5.9GHz as specified by ASTM [16]. Figures (3.2) and (3.3) show the amplitude distribution of the received signal with and without line of sight. As can be seen the distribution of the received signal amplitude follows a Rayleigh distribution for no line of sight and Rician distribution when a line of sight component exists which agrees with the measurements [20, 35]. For strong line of sight, the Rician distribution approaches the Gaussian distribution [139].

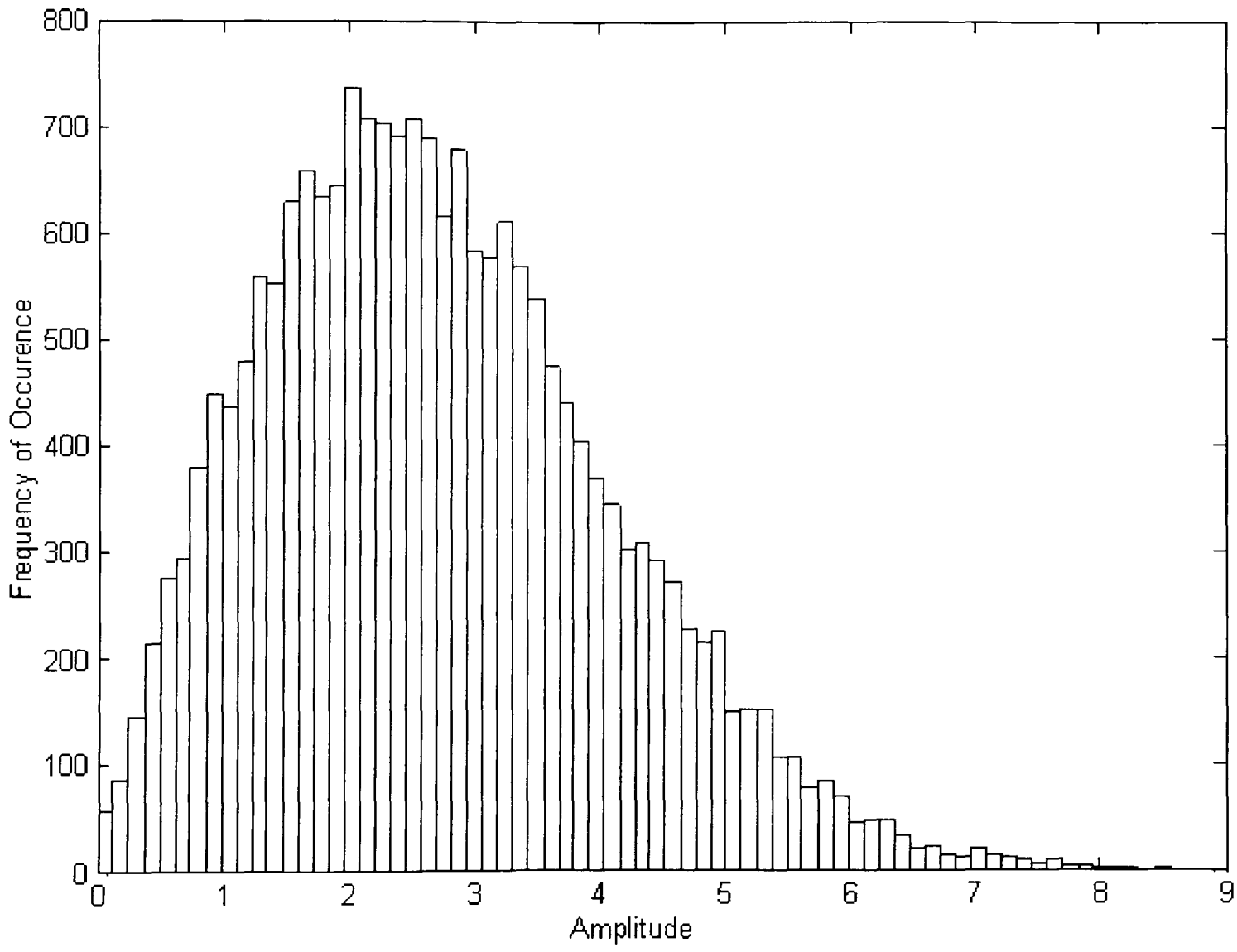

Figure (3.2): Distribution of Received Signal Amplitude for k = 0

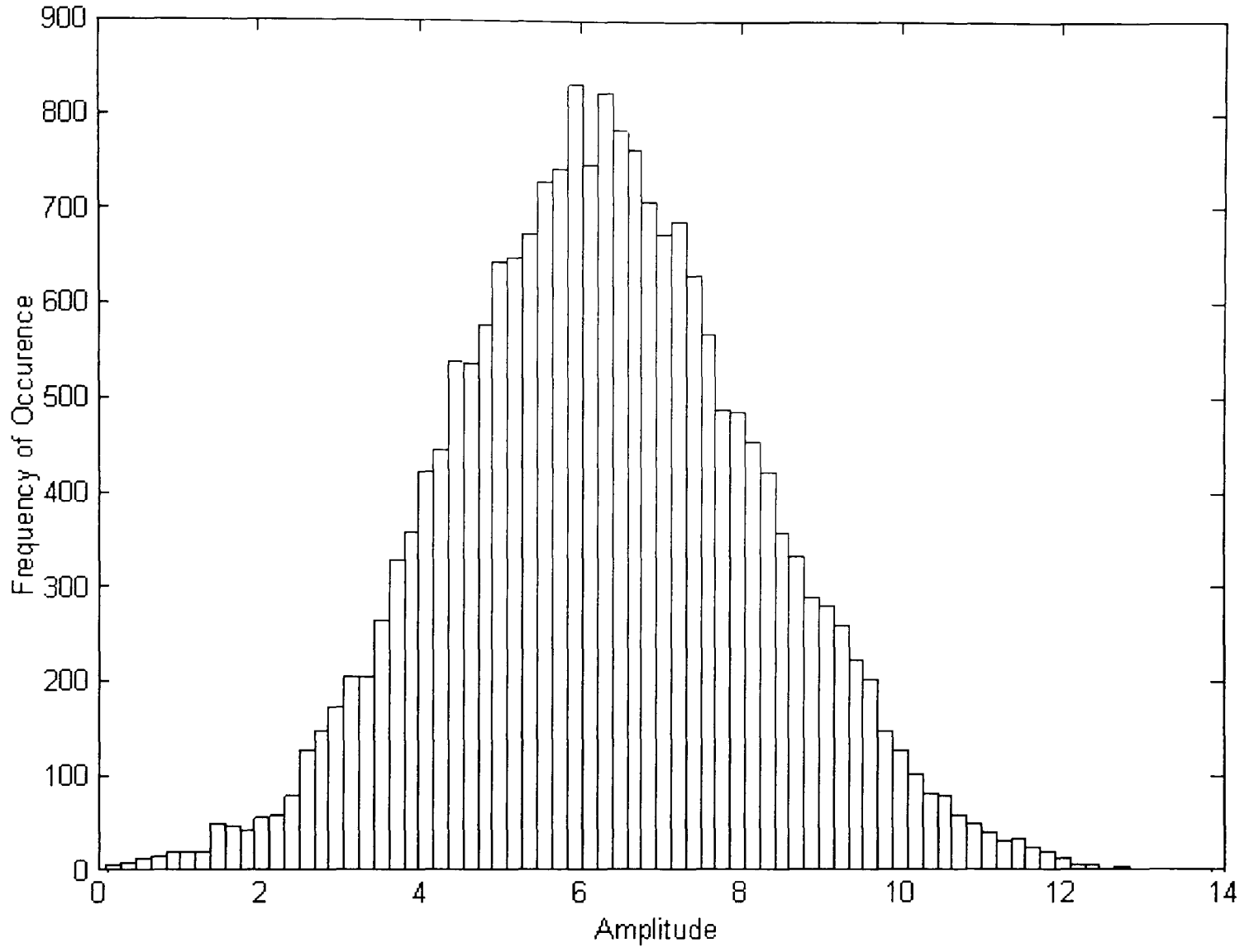

Figure (3.3): Distribution of Received Signal Amplitude for k = 10

The autocorrelation function of the channel impulse is shown in figure (3.4) along with that of Jakes' model. The Doppler spectrum is shown in figure (3.5). Comparing figure (3.5) with the classical Jakes' spectrum [26], figure (2.7), we observe that the maximum Doppler shift exceeds that suggested by Jakes due to the movement of the scatterers. In Jakes' model, the Doppler spectrum is bounded by f_D given by equation (2.7), whereas in VANET the spectrum extends beyond this value as observed from figure (3.5). This effect appears in the autocorrelation function as faster variation compared to that of Jakes' model. Both models give identical results if the speeds of the scatterers are set to zero. Similar conclusions were reached in [31] via measurements.

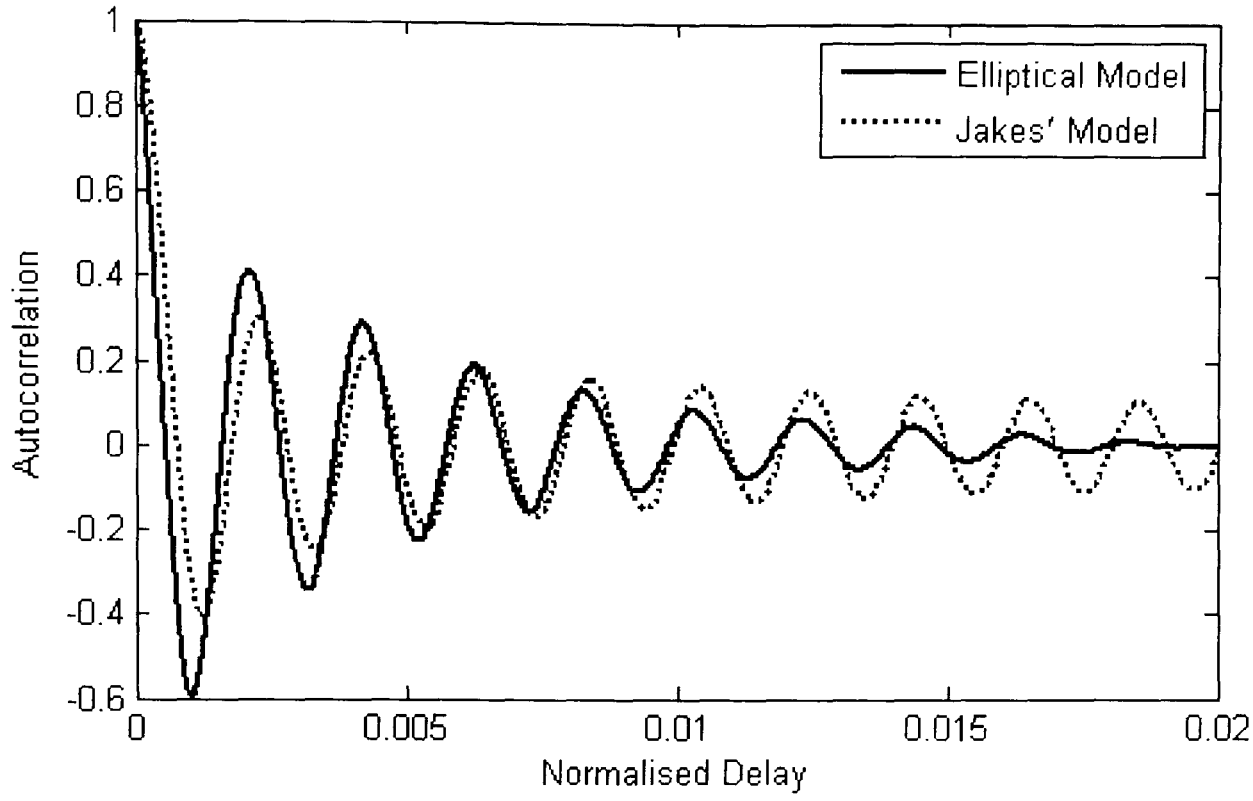

Figure (3.4): Channel Autocorrelation Function for Proposed and Jakes' Models

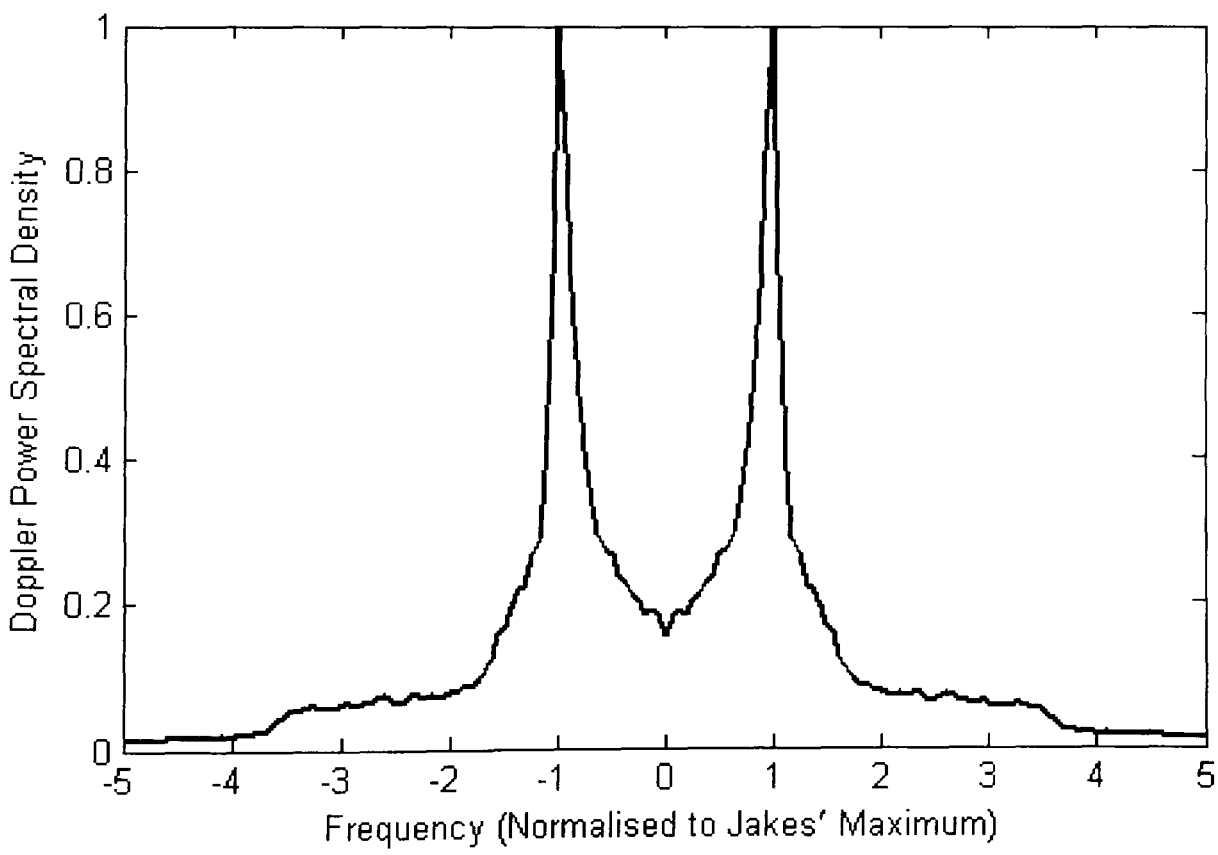

Figure (3.5): Doppler Spectrum of Proposed Model

3.3. Antenna Correlation

The capacity of MIMO systems is reduced as the correlation between the antennas is increased since it reduces the degree of freedom of the system [47, 138]. In this section we investigate the correlation between receive antennas in vehicular environment. Following the discussion of section (2.3.4.6), we aim to achieve a correlation less than 0.5 to minimise the effects of correlation on BER.

3.3.1. Mathematical Models

The correlation (ρ_i) between the signal at the output of two antennas can be calculated theoretically from the probability distribution ($p(\alpha)$) of the angle of arrival (AOA) using the equation [50]:

$$\rho_i = \int_0^{2\pi} e^{j\frac{2\pi}{\lambda}d\cos(\phi-\psi)}.p(\phi).d\phi \tag{3.8}$$

where d is the spacing between the antennas and ψ is the angle of orientation of the array (set to $\pi/2$ for broadside arrays and 0 for end-fire arrays). Several AOA distributions are available in the literature we use here the most common uniform distribution, equation (3.9), and the cosine distribution derived by Aulin in [139], equation (3.10).

$$p(\phi) = \begin{cases} \dfrac{1}{\phi_{\max}}; & 0 \le \phi \le \phi_{\max} \\ 0; & otherwise \end{cases} \tag{3.9}$$

$$p(\phi) = \begin{cases} \dfrac{\pi}{4|\phi_{\max}|}\cos\left(\dfrac{\pi}{2}\dfrac{\phi}{\phi_{\max}}\right); & |\phi| \le |\phi_{\max}| \le \dfrac{\pi}{2} \\ 0; & otherwise \end{cases} \tag{3.10}$$

As can be seen from the equations the maximum value the AOA can reach has to be set before finding the correlation coefficient. Large maximum values occur when the receiver is surrounded by a large number of scatteres and, thus, receives signals from different directions whereas small values correspond to a limited number of scatteres and smaller delay spread [19]. For microcells, where a basestation is placed at a high

position and surrounded by a small number of scatterers, the standard deviation of AOA is approximately 2° [50].

Figure (3.6) shows the correlation between the antennas in a broadside array for AOA with standard deviation of 2°, equivalent to approximately 6° maximum AOA [22, 140]. While the uniform distribution predicts an antenna spacing of 7λ is sufficient to achieve a correlation of 0.3 between the antennas, the cosine distribution suggests a value of 15λ is necessary to achieve the same correlation. Practical implementations usually use 10λ spacing for basestations. Figure (3.7) shows the correlation for a maximum AOA of 45°. In this case small antenna separations are sufficient to provide low correlation as the large value of AOA imply a denser environment than the 2° case and, hence, smaller separations are sufficient to ensure low correlation.

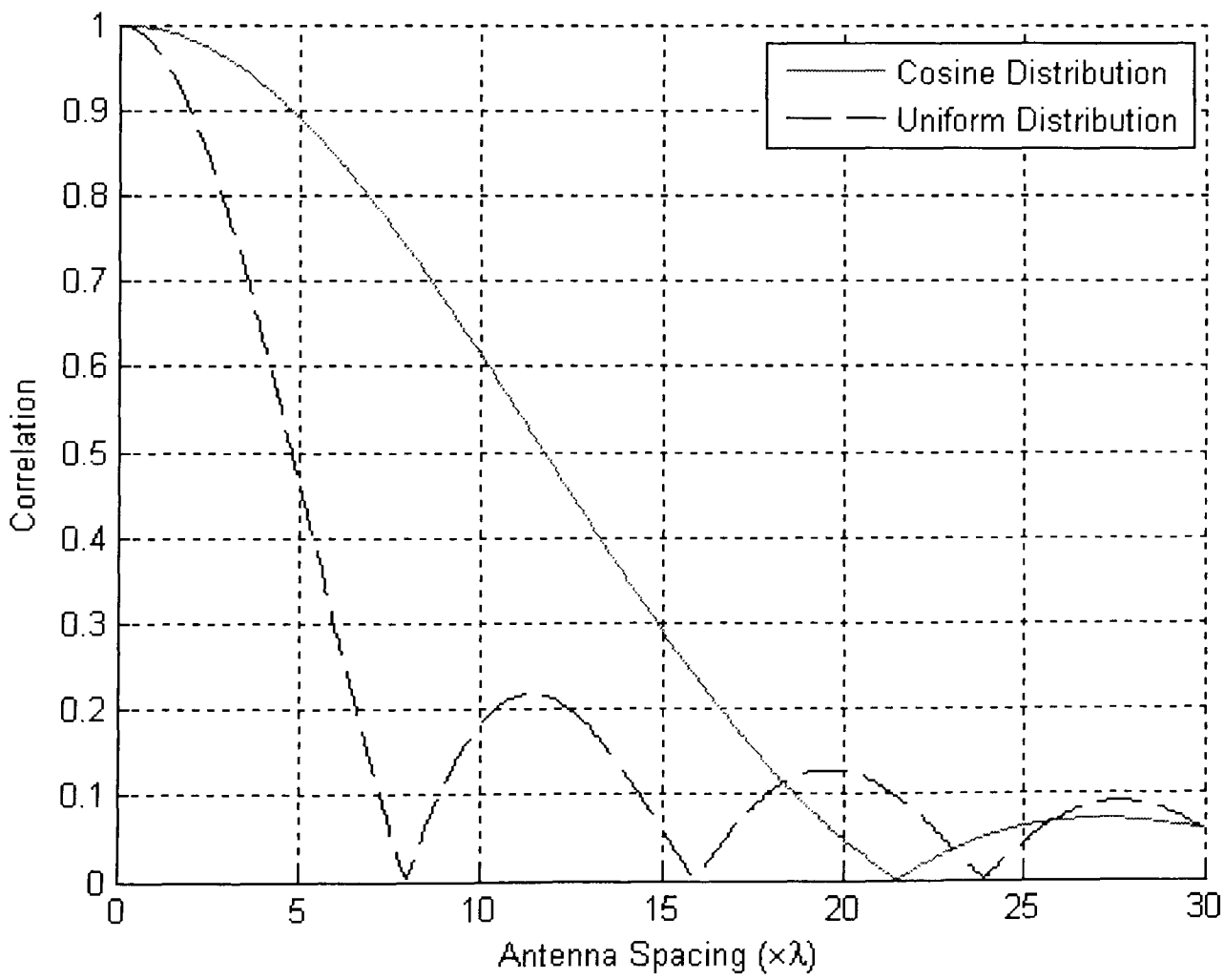

Figure (3.6): Correlation vs. Antenna Spacing (Broadside Array, 2° AOA)

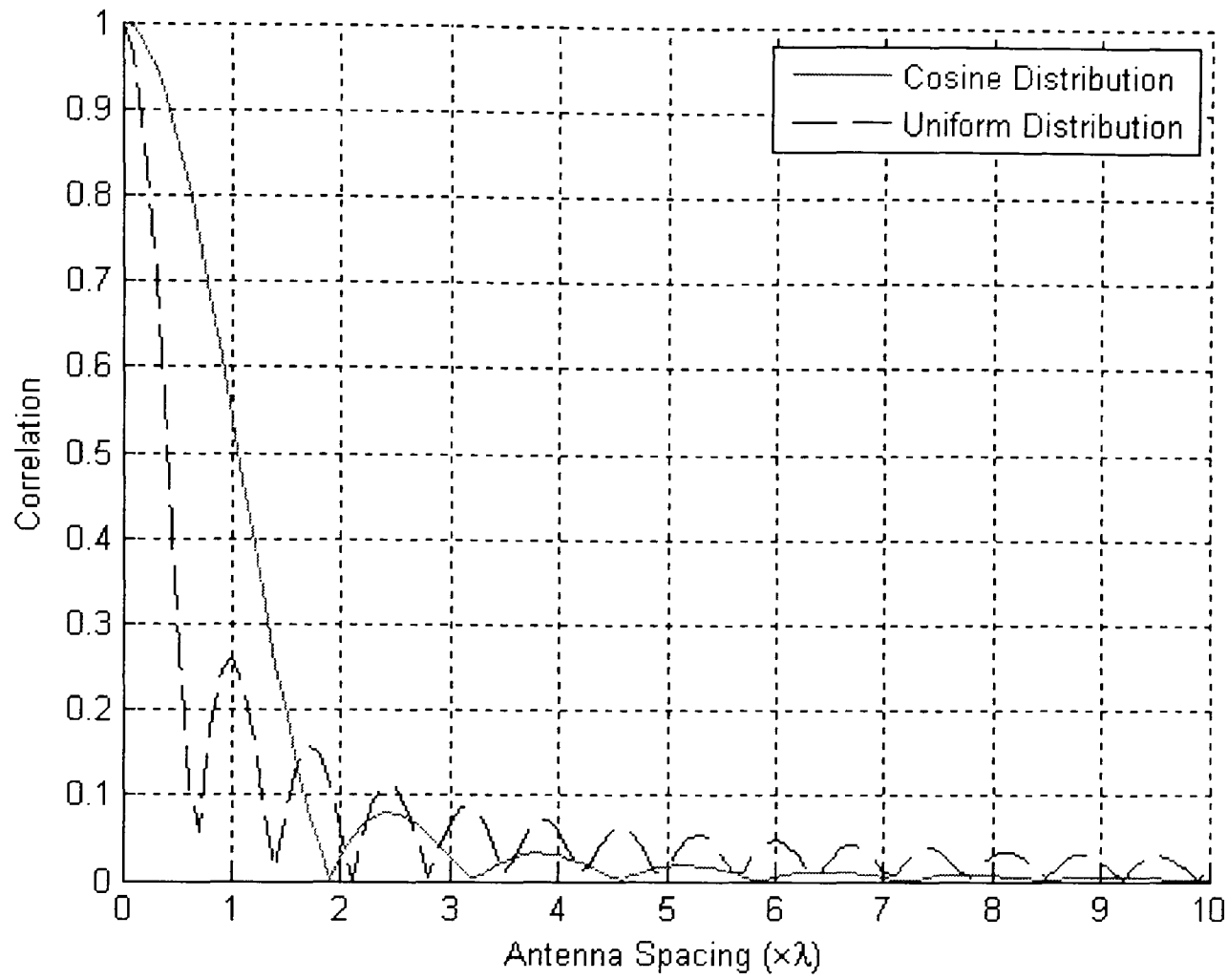

Figure (3.7): Correlation vs. Antenna Spacing (Broadside Array, 45° AOA)

For endfire arrays the correlation with AOA standard deviation of 2° is shown in figure (3.8). The correlation reduces to zero when the spacing between the antennas is an odd multiple of 0.25λ, equivalent to a phase shift of ±90° between the signals received by the antennas. For spacings which are multiples of 0.5λ the correlation is high as these correspond to phase shifts of 0° or 180° between the received signals. The cosine and uniform distributions give identical results. For a maximum AOA of 45° the correlation is shown in figure (3.9). As the spacing increases the signal received from individual scatterers experience different delays and channel responses, hence the received signals become independent for each antenna. As observed with broadside arrays, the correlation between the antennas predicted using the cosine distribution is higher than that from the uniform distribution.

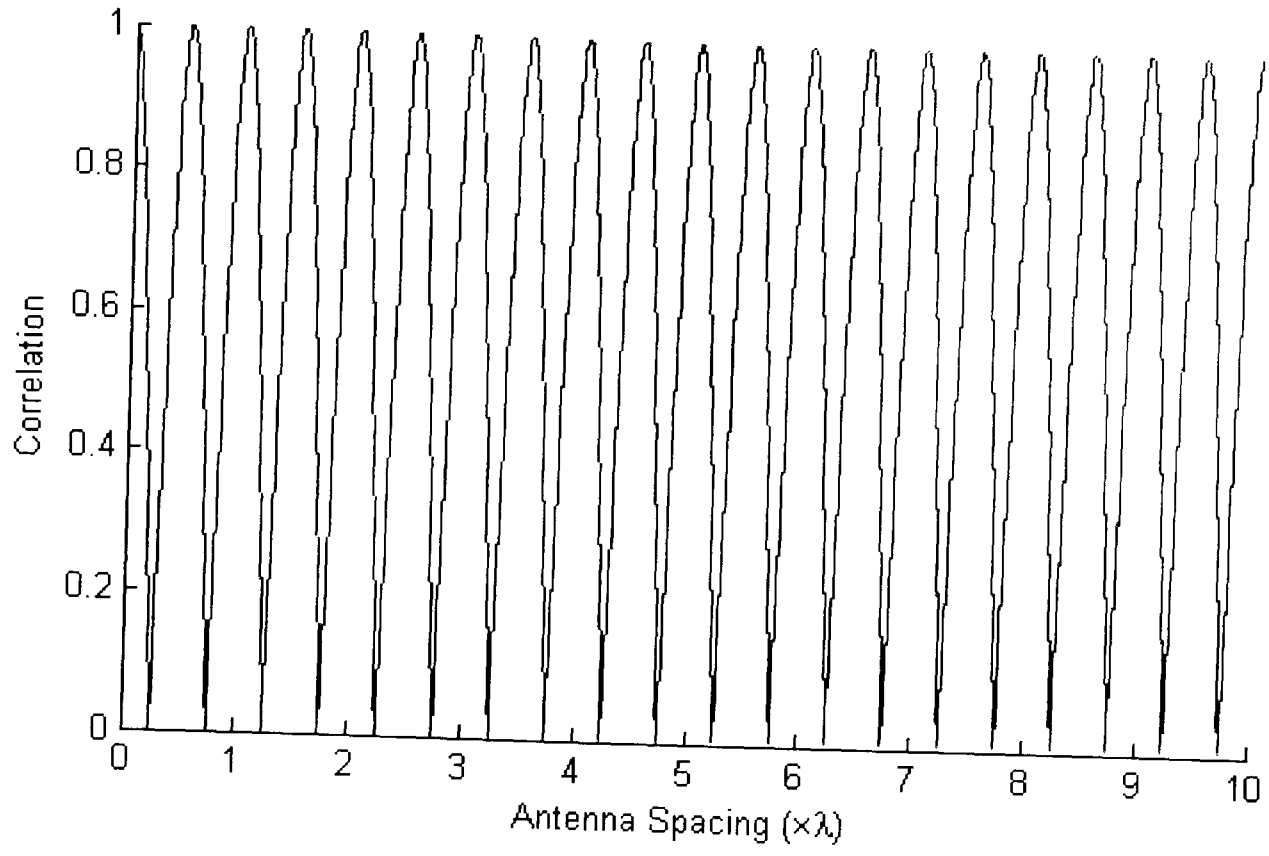

Figure (3.8): Correlation vs. Antenna Spacing (Endfire array, 2° AOA)

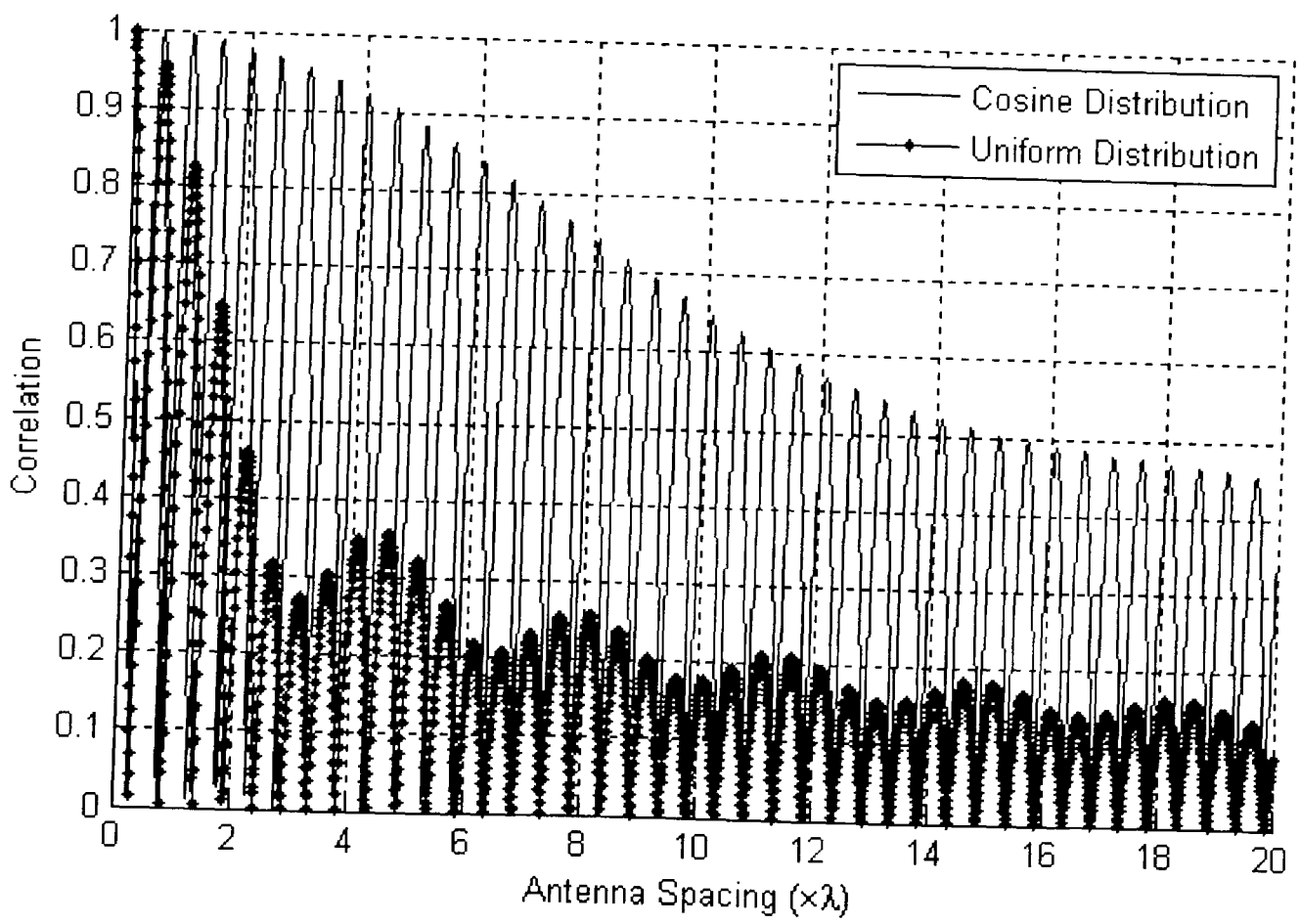

Figure (3.9): Correlation vs. Antenna Spacing (Endfire array, 45° AOA)

3.3.2. Simulation Model

To study the correlation between the receive antennas in VANET the elliptical channel model was programmed in Matlab. The distance between the transmitter and receiver was set to 1 km, which is the maximum range for VANET communication [11]. The number of scatterers used was limited to 10. Initially, the height of the ellipse was constraint to the width of the road. This causes the angular spread to be of small values leading to high correlation at the receive antennas. The simulation results for the correlation are shown in figure (3.10) along with the theoretical results for AOA standard deviation of 2°. As can be seen from the figure, the results from the simulation model show better agreement with the uniform distribution than with the cosine distribution. We predict from figure (3.10) that 10λ spacings are sufficient to guarantee low correlation. The AOA standard deviation of 2° can be thought of as the worst case scenario. In this case the road acts as a waveguide to the signal causing small angular spread at the receiver. This scenario may occur in special conditions, such as tunnels, but is not a general case [49]. The delay spread of VANET has been measured for various roads and traffic conditions in [34]. Using the minimum mean delay spread measured as 103ns in [34] for the elliptical model, we obtained the correlation coefficient shown in figure (3.11) along with the theoretical models for an AOA spread of 45°. From figure (3.11), we conclude that a spacing of 2.5λ or more is sufficient to ensure correlation less than 0.5 for broadside arrays. Figure (3.12) shows the correlation for an endfire array. As with the theoretical model the correlation drops to zero in distances which are odd multiples of 0.25λ due to the 90° phase shift. From the figure we observe that a distance of 10λ is sufficient to ensure low correlation. For AOA standard deviation of 2° the results from the model are identical to that shown in figure (3.8). In this case it is not possible to guarantee low correlation in a practical system since the correlation varies considerably over short distance (from 0 at 0.25λ to 1 at 0.5λ).

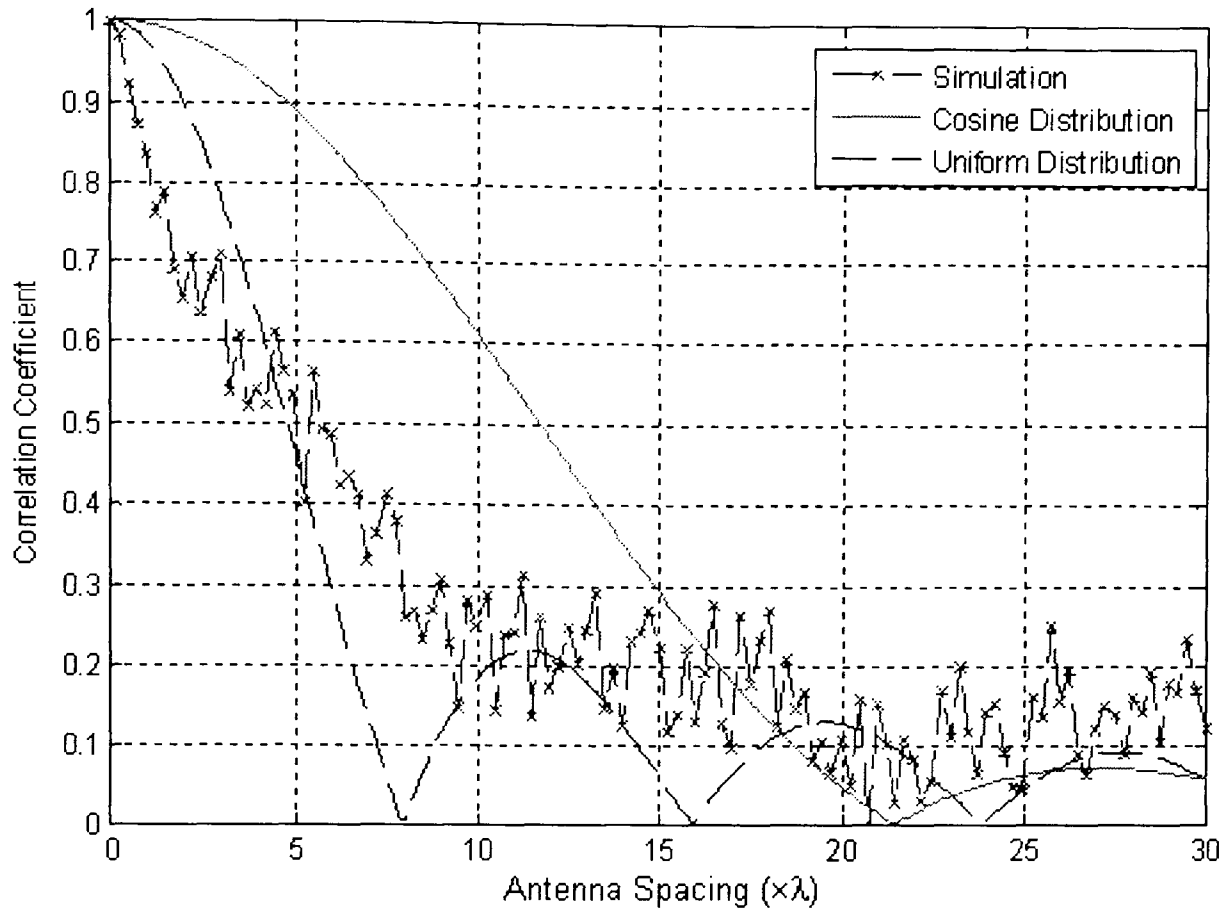

Figure (3.10): Correlation Coefficient for Small AOA Spread

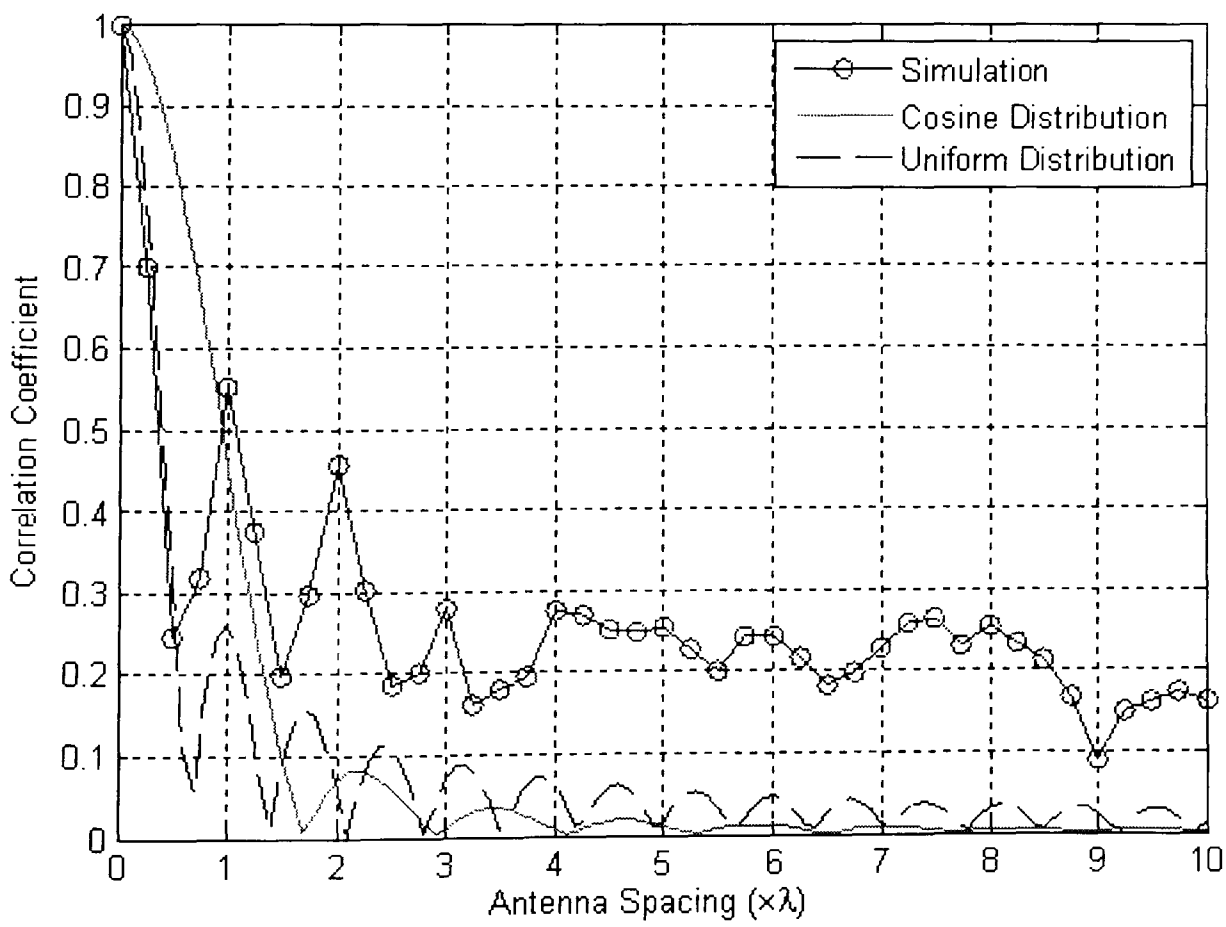

Figure (3.11): Correlation Coefficient for Delay Spread of 103ns

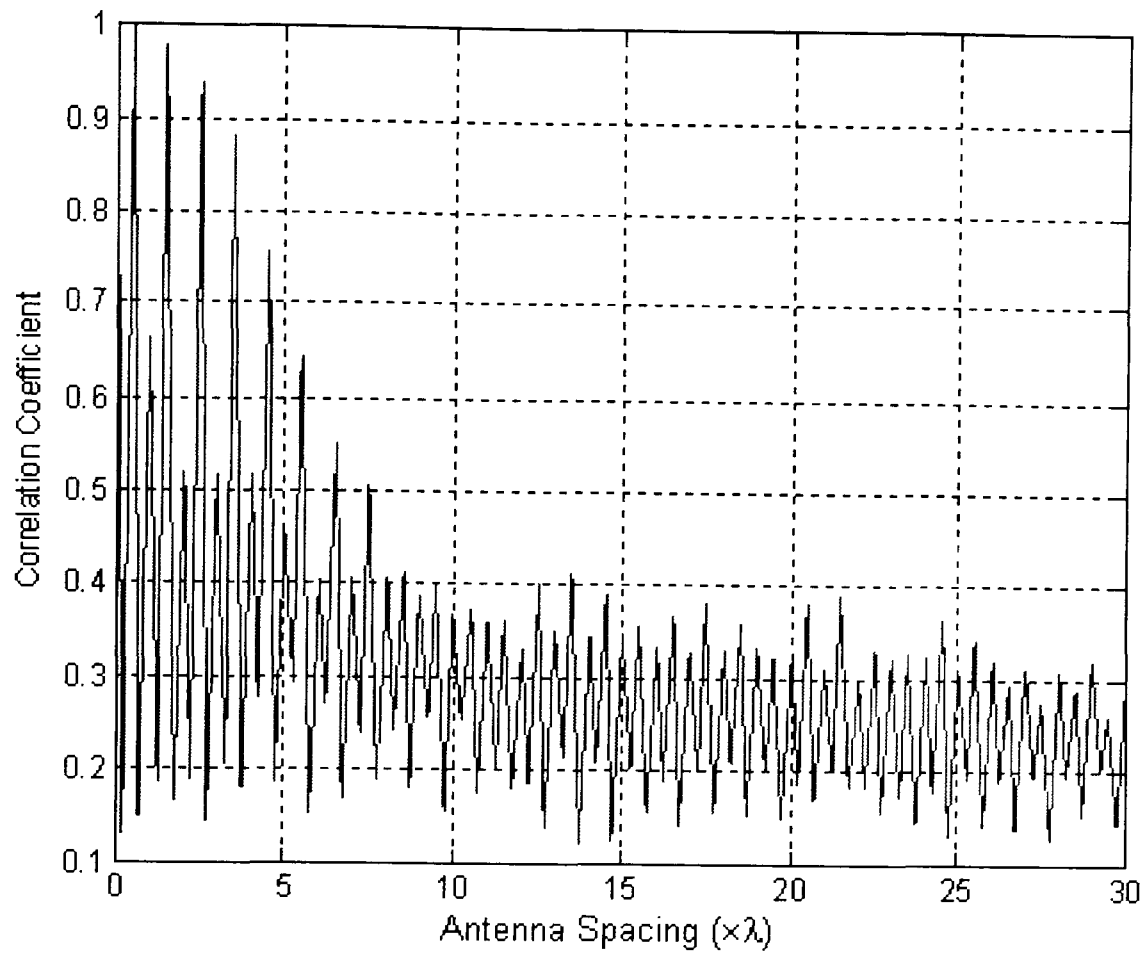

Figure (3.12): Correlation Coefficient for Delay Spread of 103ns (Endfire)

3.3.3. Correlation and Line of Sight

The previous section considered correlation without line of sight. However in VANET, line of sight communications can be encountered occasionally. Figures (3.13) and (3.14) show the correlation between antennas for various line of sight strengths. The parameter k is the ratio of the amplitude of the line of sight electric field to the maximum amplitude of the electric field of the other paths. From the figures we observe that the correlation increases as the line of sight strength increases since the received signal becomes dominated by the line of sight. The ground reflection reduces the correlation since the attenuation for line of sight then varies with $1/D^4$ instead of $1/D^2$, D is the distance between the transmitter and receiver, thus the contribution of line of sight is reduced [19]. Without ground reflection the correlation becomes high and it is not possible to achieve correlation less than 0.5 in strong line of sight conditions unless very large, impractical, antenna spacings are used.

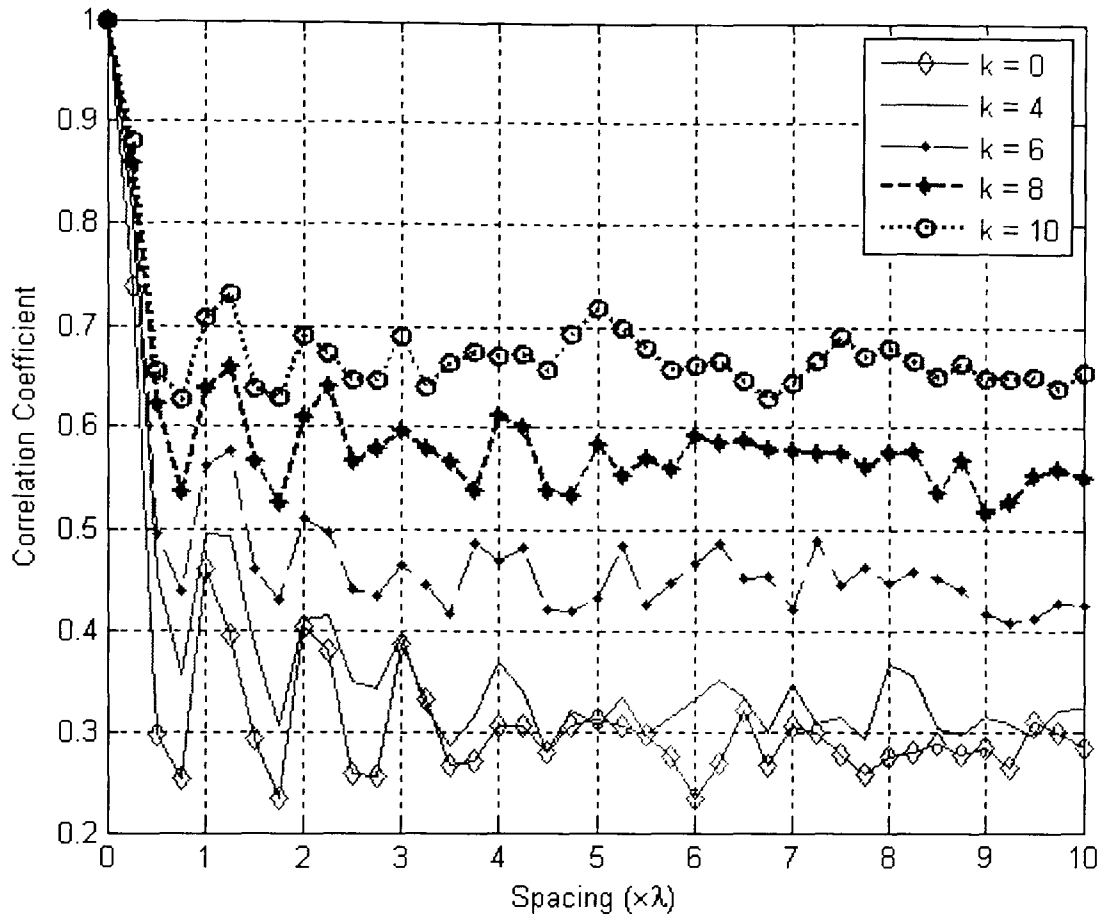

Figure (3.13): Correlation for Various Line of Sight Strengths, with ground reflection

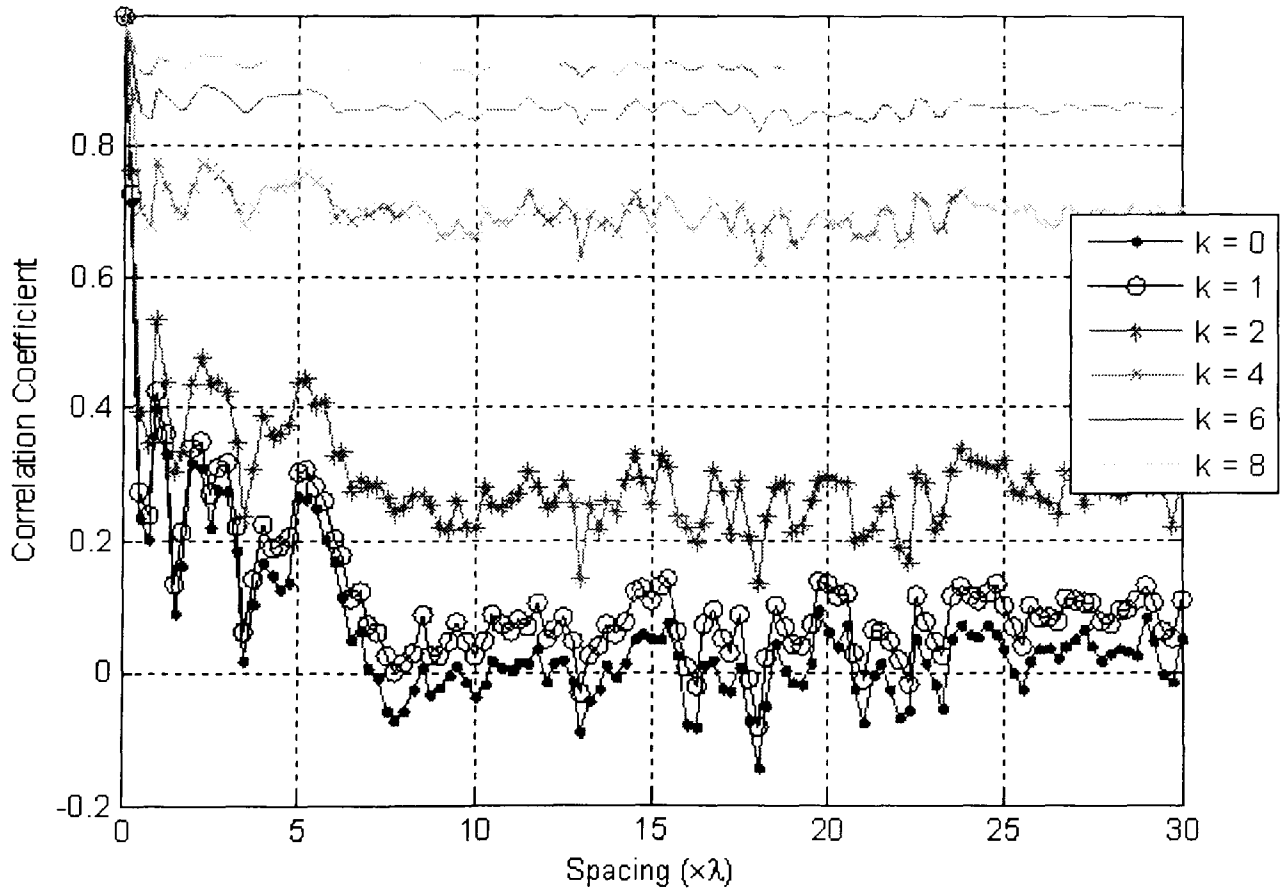

Figure (3.14): Correlation for Various Line of Sight Strengths, no ground reflection

Figure (3.15) is the correlation for an endfire array with line of sight and no ground reflection. As can be seen the correlation increased due to the line of sight component but it is less affected than the broadside case. We believe this is due to the phase shift encountered by the line of sight component due to the antenna spacings. For a two-element broadside with the transmitting antenna placed along the array axis, both elements receive identical line of sight component since the electromagnetic waves of the line of sight component travel equal distances. However in endfire arrays, the antennas are at different distances with respect to the transmitter, hence the signal in the far antenna experience extra attenuation, although it is negligible, and, more importantly, a phase shift which reduces the correlation between the two antennas. Thus the correlation for endfire arrays is less affected by the line of sight.

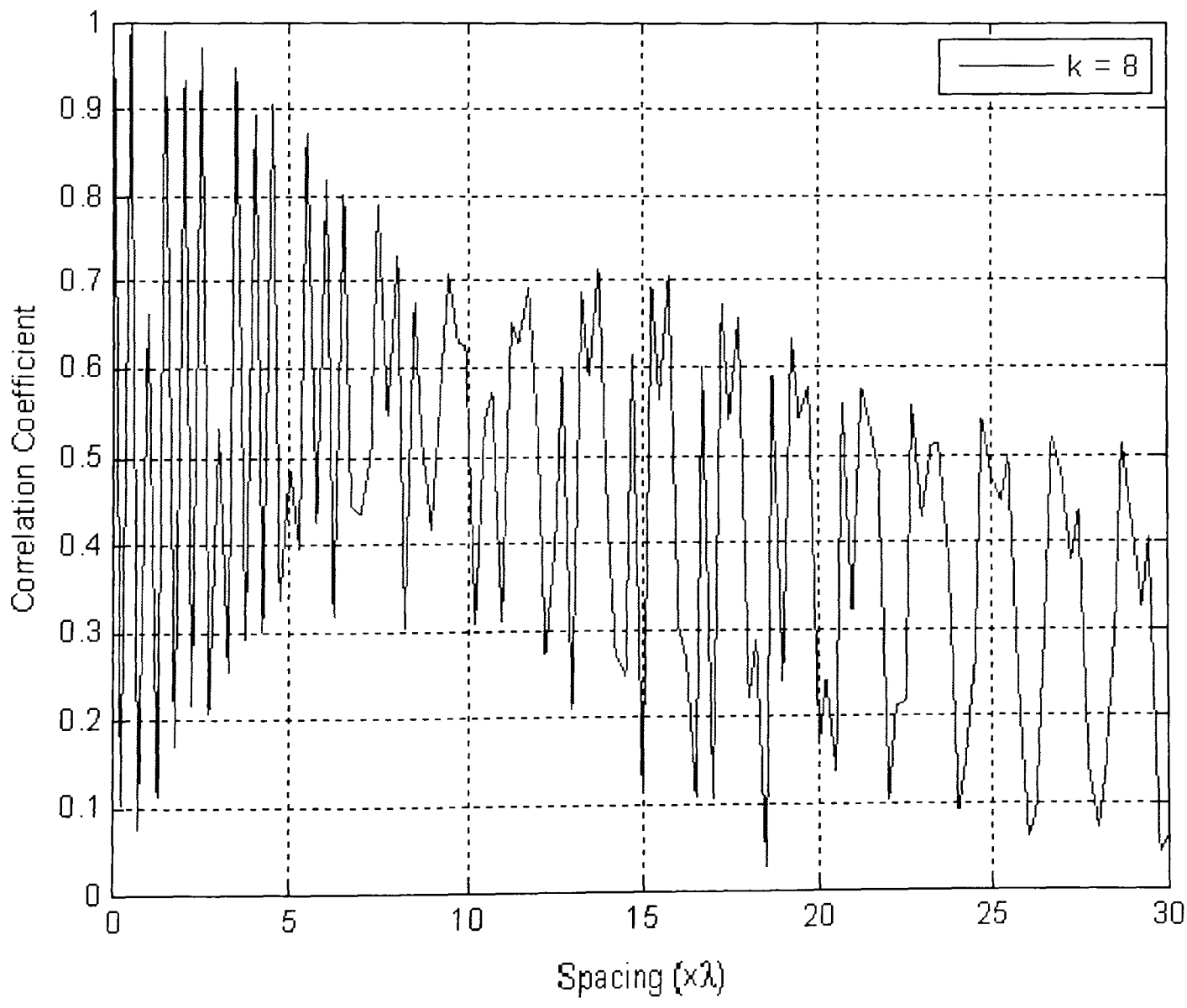

Figure (3.15): Correlation for Delay Spread of 103ns (Endfire), with line of sight

Based on these results we have chosen the antenna array shown in figure (3.16) for VBLAST analysis. The chosen configuration guarantees low correlation for no to moderate line of sight conditions. As the line of sight strength increases the correlation increases leading to an increase in the bit error rate (BER). At 5.9GHz the wavelength is approximately 5.1cm; hence the separation between the antennas will be approximately 98cm.

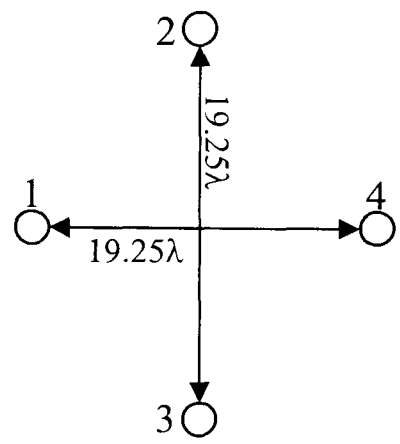

Figure (3.16): VBLAST Antenna Arrangement

3.4. Capacity of VBLAST

We now compare the theoretical capacity of VBLAST with the achievable capacity, via simulations, of the system shown in figure (3.16). Figure (3.17) is a comparison between the approximate theoretical VBLAST capacity, equation (2.23), and the capacity obtained from simulations. In our simulations we assume a 1MHz bandwidth with flat fading and 4×4 VBLAST system using QAM modulation scheme with perfect channel knowledge at the receiver. We optimised the number of transmit antennas, modulation and symbol rate to maximise the data rate while maintaining a maximum bit error rate of 10^{-3} for uncoded data and 10^{-4} when using standard 802.11a rate ½ convolutional code [95]. The code has a constraint length of 7 and its generation polynomials are (171) and (133). The capacity (C) for the optimised values from simulations is calculated as:

$$C = \frac{A \times S \times R_s \times C_r}{B \times BW} \qquad (3.11)$$

Where A is the optimised number of transmitting antennas, B is the number of receive antennas, S is the number of bits per symbol, R_s is the symbol rate, C_r is the code rate and BW is the bandwidth. The highest S, R_s and A that satisfy the BER constraint are found by simulation and then used in (3.11) to calculate the optimum capacity. Figure (3.18) compares the optimum ratio of the number of transmit to receive antennas (α) versus SNR for 100×100 and our 4×4 VBLAST systems calculated from equation (2.23). We note that the optimum number of transmitting antennas never exceeded 3 in our 4×4 system to maintain some receive diversity.

As can be seen from Fig (3.17) it is possible to achieve high capacities by using VBLAST. At 20dB a maximum of 2.4bits/s/Hz/dimension is achievable without coding and 3.6bits/s/Hz/dimension with coding compared to the theoretical value of 3.8bits/s/Hz/dimension from equation (2.23). The results from simulation increase in a staircase manner since the QAM constellation increases in multiples of 2.

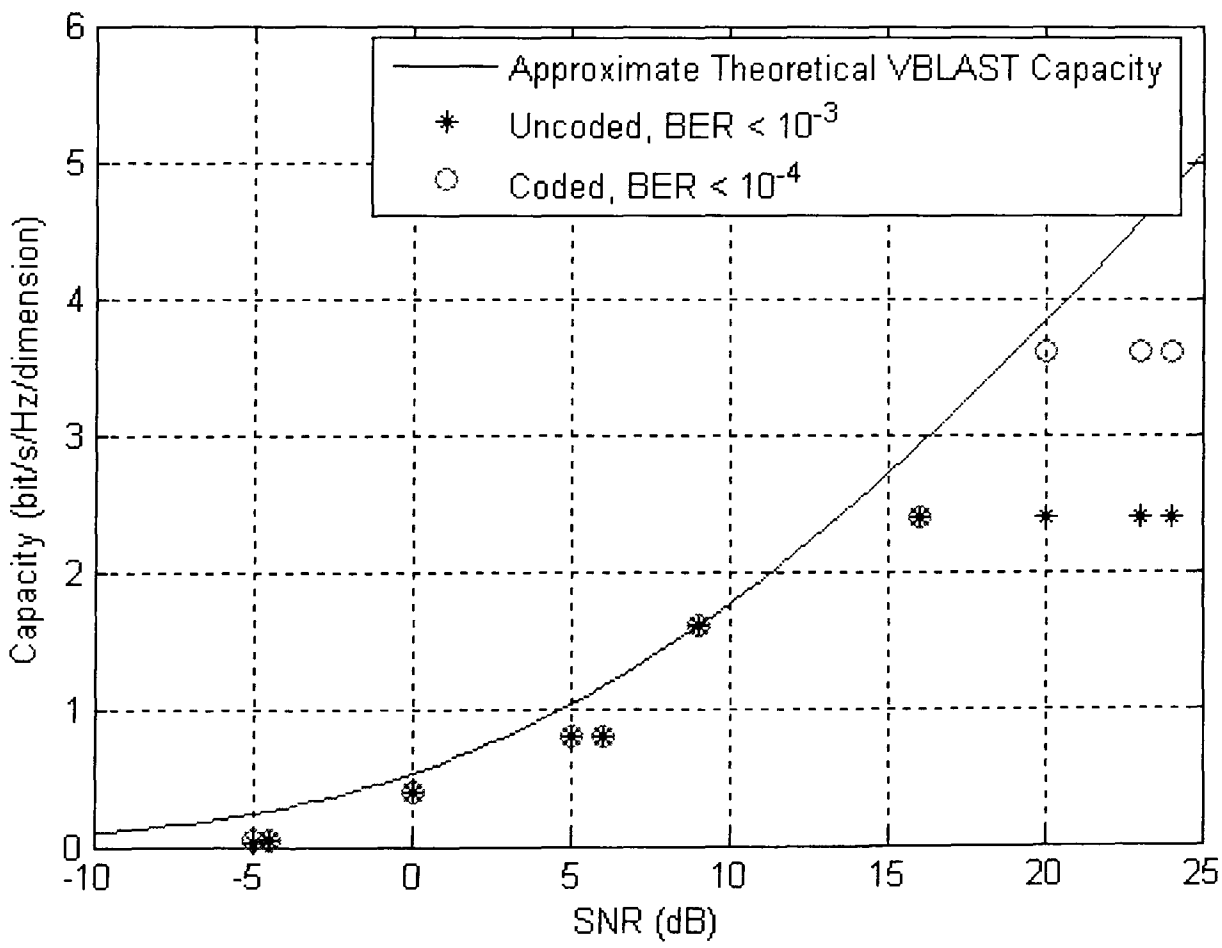

Figure (3.17): Achievable Capacity Using 3×4 VBLAST

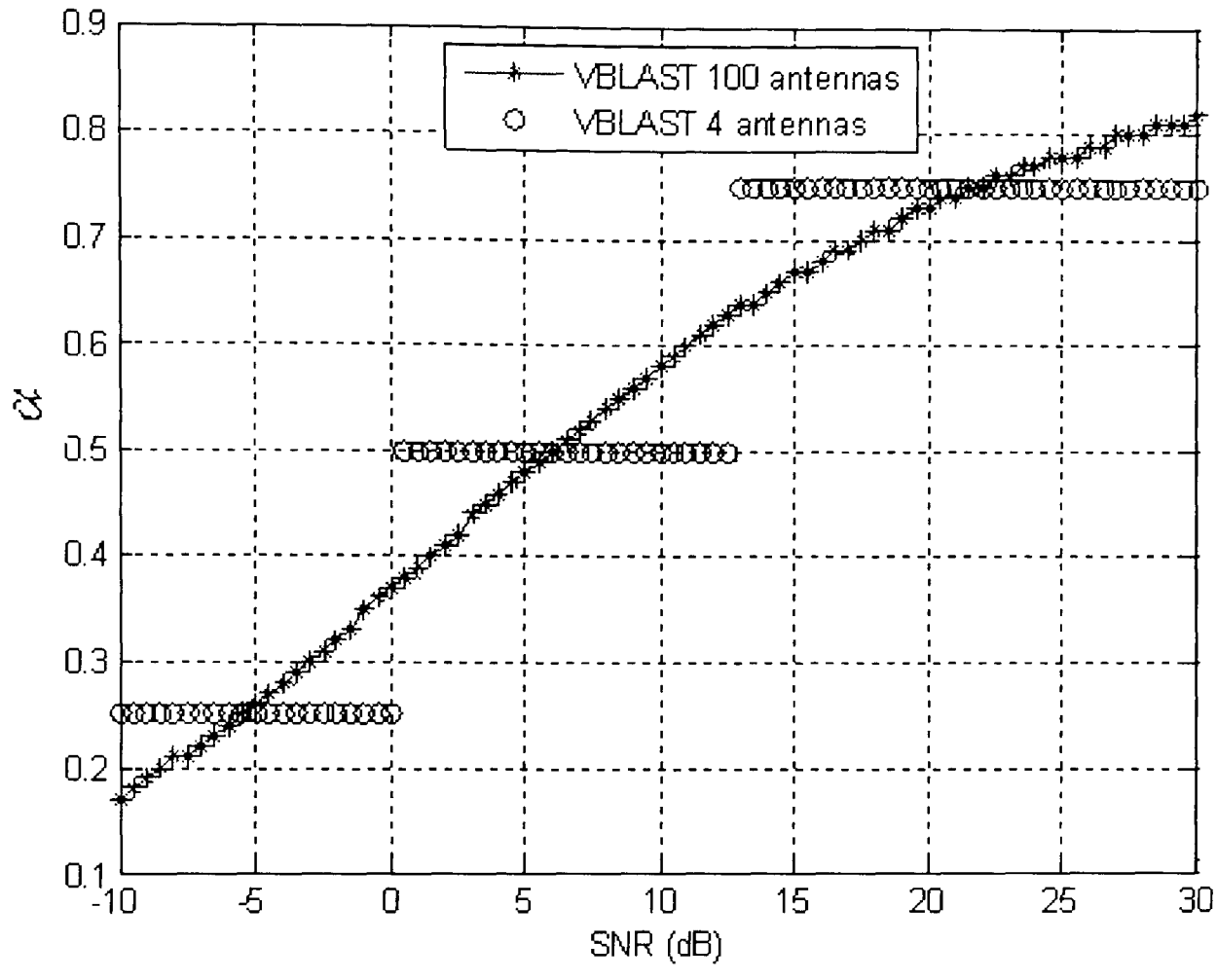

Figure (3.18): Optimum α for VBLAST with 100×100 and 4×4 Systems

3.5. Analysis of VBLAST Bit Error Rate

In this section we study the BER performance of VBLAST. First we derive mathematical expressions for BER performance with Phase Shift Keying (PSK) modulation and perfect channel knowledge. This is then extended to QPSK modulation. We then investigate the effects of line of sight on BER. Finally we consider the effects of speed on BER performance when the channel is estimated only at the begining of the packet.

3.5.1. VBLAST-PSK Bit Error Rate

We derive expressions for the bit error rate (BER) of PSK in an $A \times B$ VBLAST system where the number of transmit antennas (A) is less than or equal to the number of receive antennas (B). According to [141, 142] the error performance of each decoding step in the VBLAST algorithm can be approximated by the performance of a maximal

ratio combiner. However since the diversity order and signal to noise ratio (SNR) change each step, the probability of error varies between the steps [142].

In [142] a 2×2 system was studied and expressions for the BER were derived. The paper determines the total probability of a single error to be:

$$P_{total} = P_1 + P_2(1 - P_1) \tag{3.12}$$

Where P_1 and P_2 are the probabilities of error in the first and second decoding steps respectively. Assuming the decoding steps are independent, equation (3.12) can be generalised for any number of antennas (A) as [22, 142]:

$$\begin{aligned} P_{total} &= P_1 + P_2(1 - P_1) + P_3(1 - P_1)(1 - P_2) + P_4(1 - P_1)(1 - P_2)(1 - P_3) + \ldots \\ &= P_1 + \sum_{i=2}^{A} P_i \times \prod_{j=1}^{i-1}(1 - P_j) \end{aligned} \tag{3.13}$$

For a 3×4 system we get:

$$P_{total} = P_1 + P_2 + P_3 - P_1P_2 - P_1P_3 - P_2P_3 + P_1P_2P_3 \tag{3.14}$$

This is an approximate expression since in reality the SNR between the different decoding steps are not independent and therefore P_1, P_2 and P_3 are not statistically independent as assumed in equations (3.12) to (3.14).

At each decoding step the probability of error can be approximated by the maximal ratio combining BER given by, equations (14.4-15) and (14.4-16) in [22]:

$$P_e = \left[\frac{1}{2}(1 - \mu)\right]^L \sum_{k=0}^{L-1} \left\{ \frac{(L - 1 + k)!}{k! \times (L - 1)!} \left[\frac{1}{2}(1 + \mu)\right]^k \right\} \tag{3.15}$$

$$\mu = \sqrt{\frac{\bar{\gamma}_c}{1 + \bar{\gamma}_c}} \tag{3.16}$$

where L is the diversity order and $\bar{\gamma}_c$ is the SNR per receive antenna.

The diversity order for decoding step i in VBLAST is [142]:

$$L = B - A + i \tag{3.17}$$

The SNR per receive antenna for decoding step i ($\bar{\gamma}_i$) is given by [142]:

$$\bar{\gamma}_i = \frac{\bar{\gamma}_t}{L} \qquad (3.18)$$

$\bar{\gamma}_t$ is the initial SNR per transmit antenna.

For a fair comparison between VBLAST and Single Input Single Output (SISO) systems we define the symbol energy to noise power spectral density ($\frac{E_s}{N_0}$) for VBLAST as the total signal energy to noise power density if all the transmitting antennas transmit the same symbol. When using different data for each antenna, the interference from the different data streams is cancelled in VBLAST by the nulling and cancellation processes in the decoding algorithm which eliminates all the streams except the one to be decoded. However these processes are not capable of eliminating noise [44, 141, 142]. With our definition of $\frac{E_s}{N_0}$, the value $\bar{\gamma}_t$ is then calculated as:

$$\bar{\gamma}_t = \frac{E_s}{N_0 \times A} \qquad (3.19)$$

Using these relations we can now calculate the BER of each decoding step as well as the total BER of VBLAST. Figures (3.19) and (3.20) show the BER performance of 2×4 and 3×4 VBLAST. We observe that the BER is dominated by the error in the first decoding step. The reason for this is that the first step has the lowest diversity order. As the decoding proceeds, higher diversities are achieved, as observed from equation (3.17), and therefore it is possible to decode the signal even if the stream has a low SNR. Moreover as the decoding proceeds, the interference is reduced by the cancellation process of VBLAST decoding algorithm. The simulation results, with no line of sight, show reasonable agreement with the theoretical results particularly at high SNR since the approximation of equation (3.13) becomes more valid.

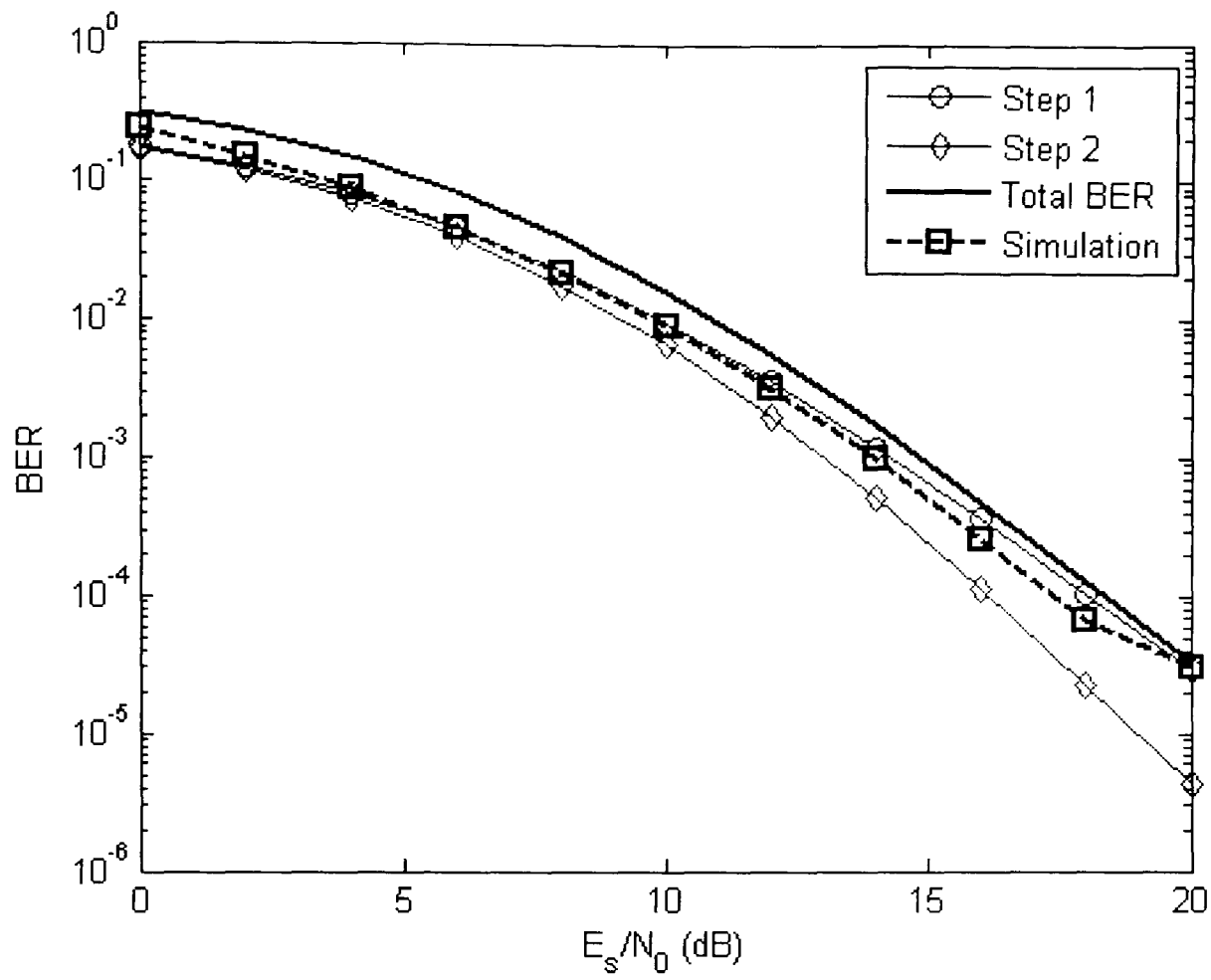

Figure (3.19): PSK BER from Theory and Simulations for 2×4 VBLAST

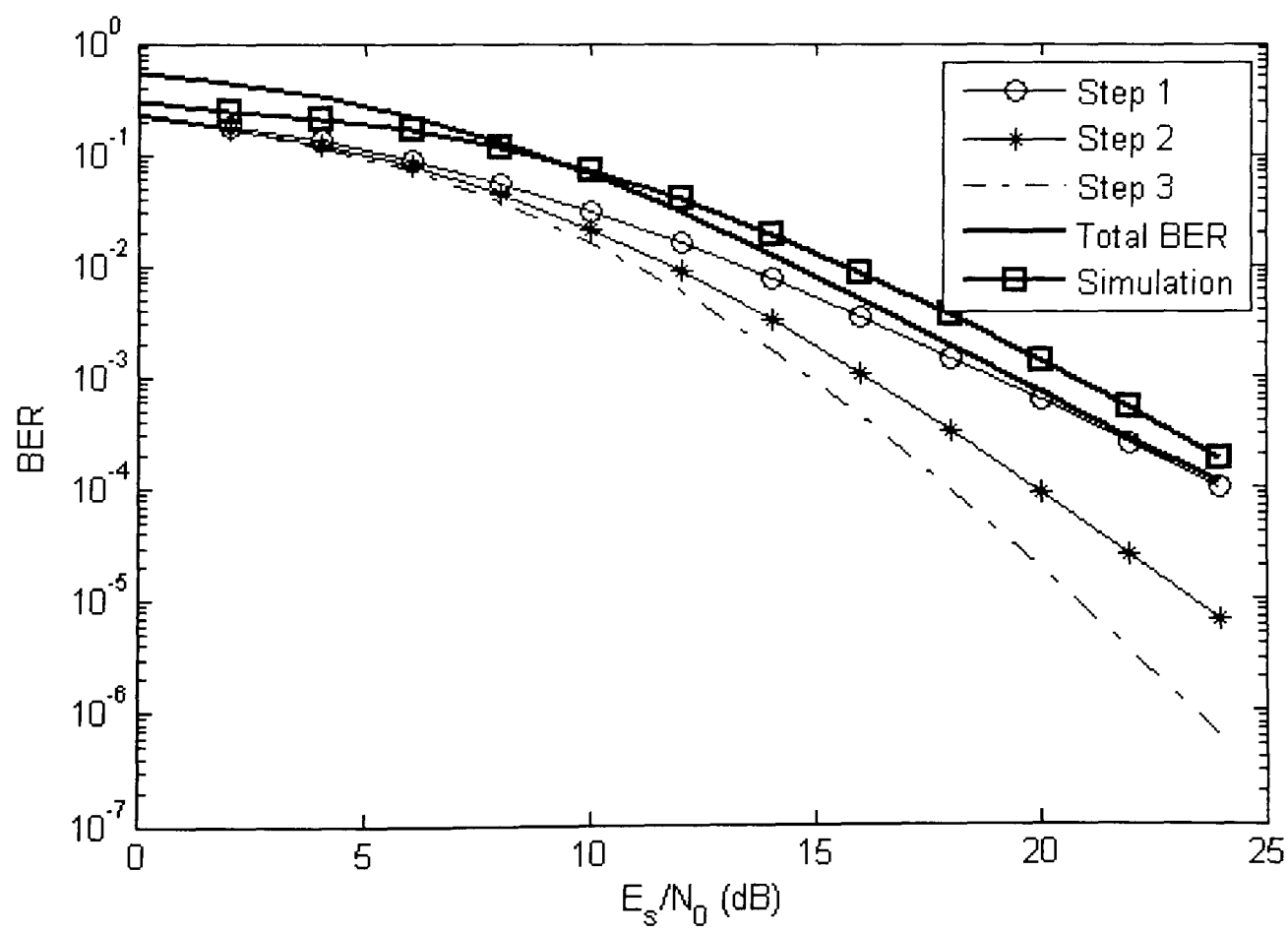

Figure (3.20): PSK BER from Theory and Simulations for 3×4 VBLAST

3.5.2. VBLAST-QPSK Bit Error

Following the same analysis of BER for PSK we can find expressions for the BER of QPSK, or any other modulation, provided that BER expressions for maximal ratio combining diversity exist. The probability of error for a maximal ratio combining system with L diversity order and QPSK modulation is given by, equation (14.4-41) in [22]:

$$P_e = \frac{1}{2}\left[1 - \frac{\mu}{\sqrt{2-\mu^2}} \sum_{k=0}^{L-1} \left\{ \frac{(2k)!}{k! \times k!} \left[\frac{1-\mu^2}{4-2\mu^2} \right]^k \right\} \right] \qquad (3.20)$$

Where μ is given by equation (3.16). All the other equations, (3.13) and (3.17) to (3.19), remain unaltered. Figures (3.21) and (3.22) show the theoretical BER performance and compare it with the results from simulations. As with PSK the results show reasonable agreement and the BER is dominated by the error in the decoding of the first step.

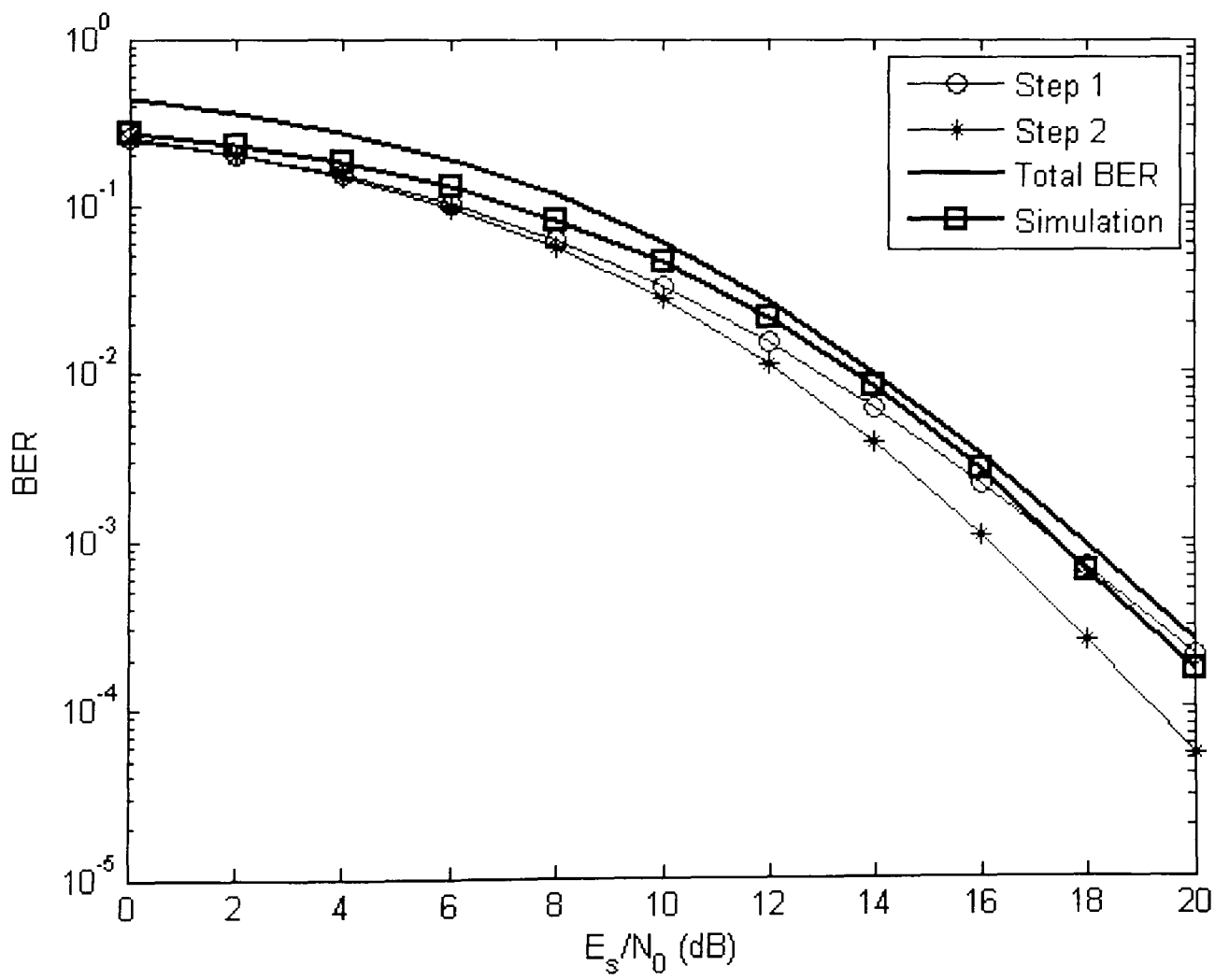

Figure (3.21): QPSK BER from Theory and Simulations for 2×4 VBLAST

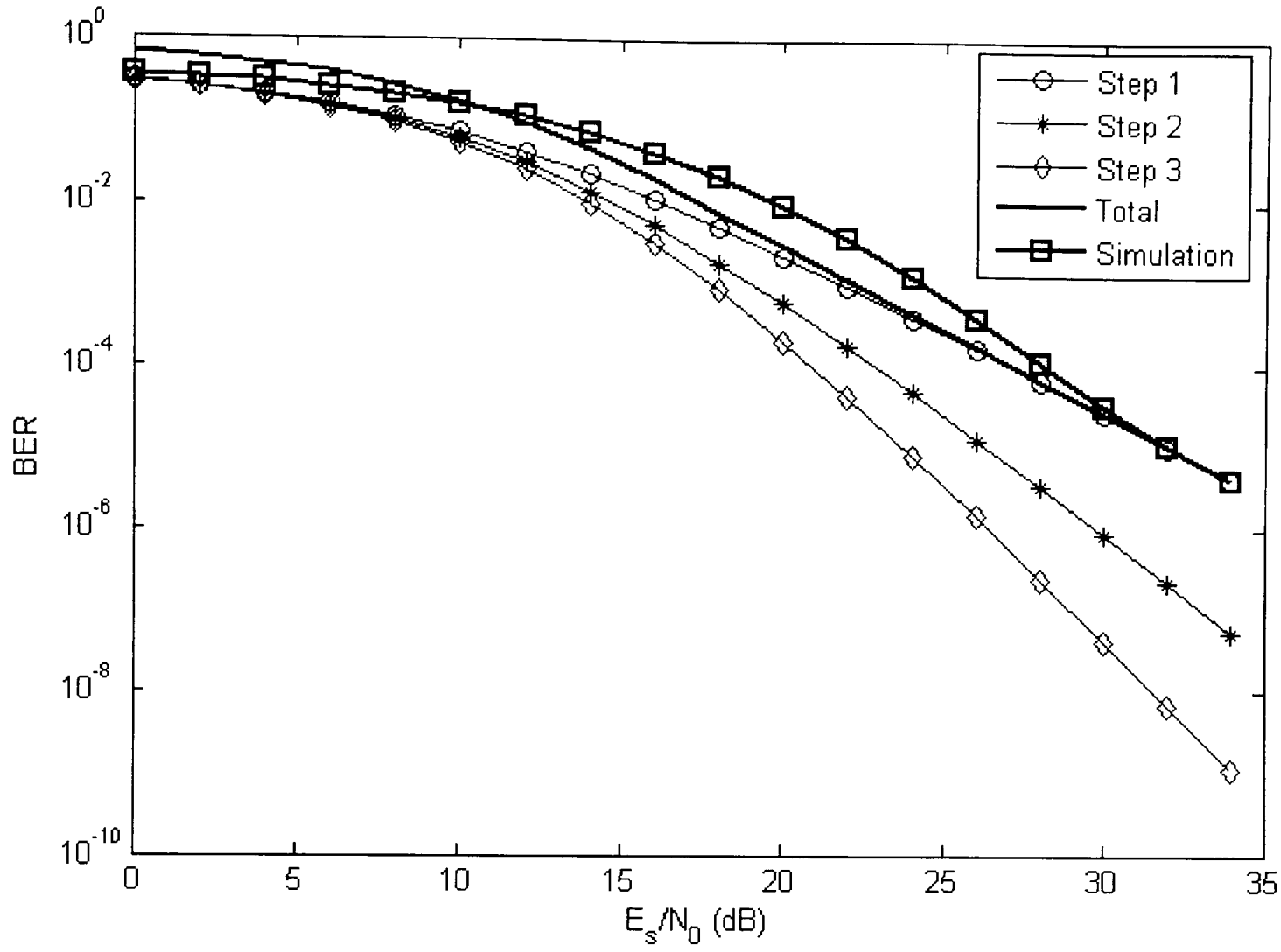

Figure (3.22): QPSK BER from Theory and Simulations for 3×4 VBLAST

3.5.3. VBLAST Bit Error Rate with Antenna Correlation

The BER expressions and simulations of the previous sections assume rich Rayleigh fading with no correlation between the antennas. As discussed in section (2.3.4.6), the correlation increases the probability of error. Figure (3.23) shows the BER performance of VBLAST, using simulations, with various line of sight strengths. The antenna array used in the simulations was a broadside linear array with 7λ antenna spacing. Two antennas were transmitting using PSK modulation with four antennas at the receiver. As can be seen, the performance degrades as the line of sight becomes stronger due to the increased correlation between the antennas. With strong line of sight it may become better to use a single transmitter with higher modulations than using VBLAST as the performance of SISO improves with line of sight [22]. The results agree with the conclusions obtained in [47].

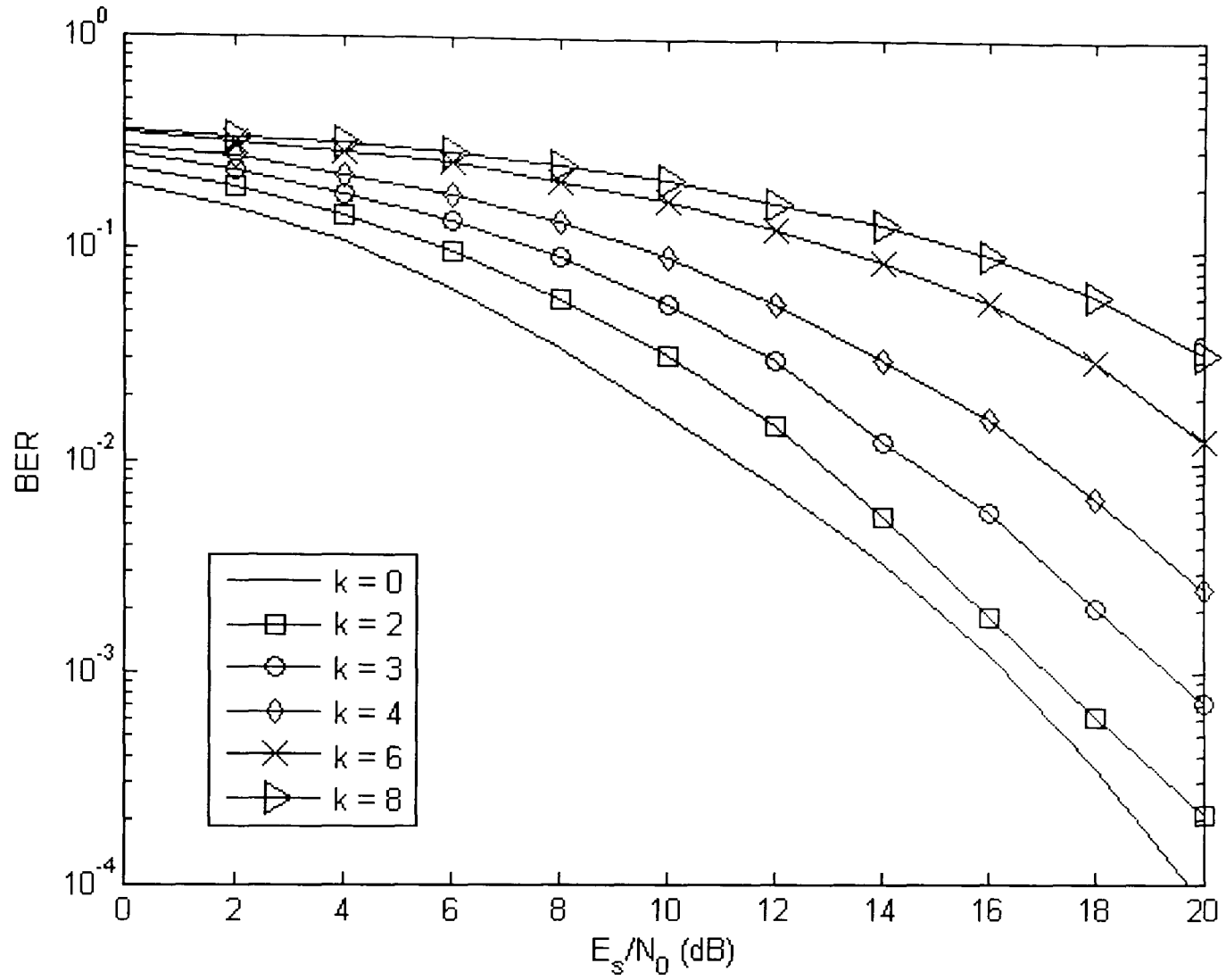

Figure (3.23): Effect of Line of Sight on the BER Performance of 2×4 VBLAST

3.5.4. Effects of Outdated Channel Estimates on VBLAST BER

In most MIMO systems the channel is assumed to be quasi-stationary. Under this condition, the receiver estimates the channel response using a known training sequence and assumes the response remains fixed until the next training interval. In VANET nodes move at high speeds leading to high Doppler shifts and small channel coherence time. Hence the quasi-stationary channel assumption becomes a poor one in VANET. In [66] the authors analysed the effects of outdated channel estimation on MIMO systems. The difference between the real and estimated channel leads to decoding errors. The authors expressed the effect of the outdated channel estimation by a loss in signal to interference power ratio (SIR) calculated as [66]:

$$SIR = -10\log_{10}\left(2^m\left[1-\mathrm{sinc}\left(2\pi f_D T_{tr}\right)\right]\right) \quad (3.21)$$

Where m is the number of bits per symbol, T_{tr} is the time between training intervals, f_D is the Doppler shift and sinc(x) = sin(x)/x. This can be used with (3.19) to approximate the performance of VBLAST with an outdated channel estimate. For 60 km/h speed, 1MSymbol/s, 256 symbols between training intervals and 2×4 VBLAST system with PSK modulation, the BER performance is as shown in figure (3.24). We observe that the BER experiences an error floor due to the inaccurate channel estimation. This can be reduced by sending the training sequence more frequently thus enhancing the estimate but reducing the spectral efficiency. Another method is to employ channel tracking techniques between training intervals. This maintains the spectral efficiency but increases the hardware complexity of the receiver. The performance drops even further with higher speeds since higher Doppler shifts lead to lower SIR. The performance also drops if the time between training intervals increases. In the next chapter we develop and evaluate a simple channel tracking algorithm for VBLAST systems.

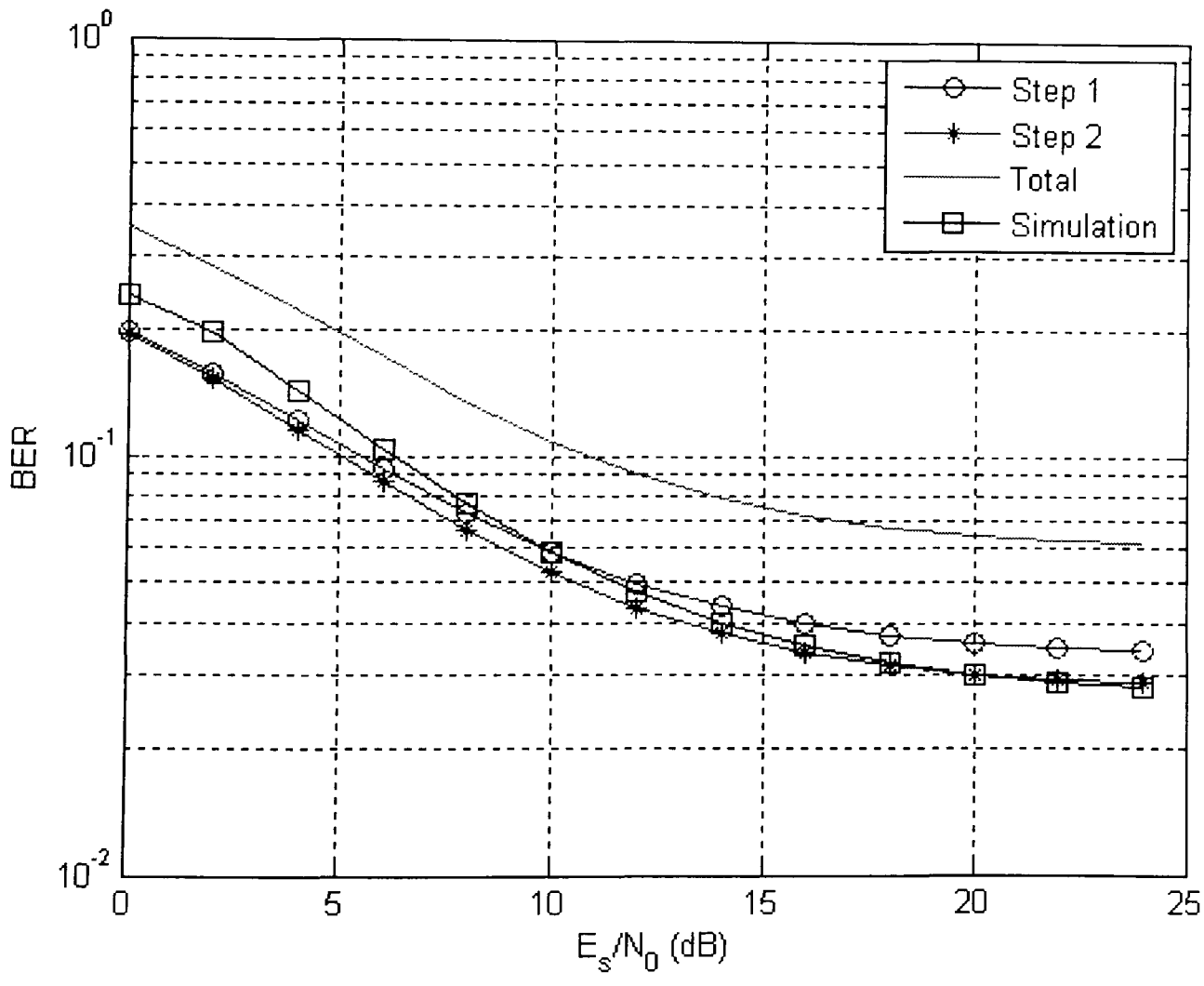

Figure (3.24): Effect of Outdated Channel Estimate on BER, speed is 60 km/h

3.6. Concluding Remarks

In this chapter we introduced our VANET channel model. The model expands to VANET the elliptical geometrical channel model originally designed to simulate mobile-basestation links in microcells. The scatterers in our model are not stationary causing the Doppler spectrum to expand beyond Jakes' spectrum. These conclusions agree with the findings in the literature obtained via measurements. We studied the correlation between receive antennas for different array configurations and designed a 4 elements antenna array for VANET. The correlation increases for small delay spreads and/or under strong line of sight conditions leading to higher bit error rates. The bit error rate for rich Rayleigh fading and perfect channel knowledge was analysed theoretically and via simulations and the results from both methods showed reasonable agreement. VBLAST requires accurate channel information to decode the signal correctly. As the nodes in VANET move at high speeds, the channel coherence time is very short. This leads to an error floor in the BER performance of VBLAST since the estimated channel response losses its significance after a very short duration. Channel tracking techniques are required to update the channel matrix at the receiver and maintain high performance.

Chapter 4

Channel Tracking for VBLAST

4.1. Overview

In the previous chapter it was shown that VBLAST can provide high bandwidth efficiency in channels with no to moderate line of sight provided the channel is known at the receiver. In this chapter we consider the performance of VBLAST when perfect channel knowledge is not available at the receiver. Since cars in VANET move at high speeds, the channel response changes rapidly thus affecting the decoding process and degrading system performance. We develop in this chapter channel tracking algorithms for VBLAST in flat fading channels and articulate the performance of VBLAST-OFDM systems in frequency selective channels. We first investigate VBLAST channel tracking in flat fading channels and develop and evaluate a simple algorithm to update the channel matrix and enhance performance. Afterwards, we study the performance of VBLAST-OFDM and analyse the inter-carrier-interference (ICI) problem. Finally, we extend our channel tracking algorithm to OFDM and propose an algorithm to reduce ICI. The chapter is partially based on the publications [2, 6, 7].

4.2. Channel Tracking in a Flat Fading Channel

In this section we develop a channel tracking algorithm for a single carrier VBLAST system in a flat fading channel. We assume an initial estimate of the channel matrix is available at the receiver via a training sequence. The algorithm tracks the changes in the channel response and updates the channel matrix.

4.2.1. Algorithm Derivation

First we develop a mathematical model of the problem. Let **r** be the received signal vector, **s** the transmitted signal vector, $\hat{\mathbf{H}}$ the estimated channel matrix, **H** the exact channel matrix and **w** the noise vector. We have:

$$\mathbf{r} = \mathbf{H}\mathbf{s} + \mathbf{w} \tag{4.1}$$

and

$$\mathbf{H} = \hat{\mathbf{H}} + \mathbf{H}_e \tag{4.2}$$

where $\mathbf{H}_e$ is the error in the estimated channel matrix. Now considering a simple receiver without noise, from (4.1) we have:

$$\hat{\mathbf{s}} = \hat{\mathbf{H}}^{-1} \times \mathbf{r} \tag{4.3}$$

where $\hat{\mathbf{s}}$ is an estimate of the transmitted symbols and $\hat{\mathbf{H}}^{-1}$ is the pseudoinverse of the estimated matrix $\hat{\mathbf{H}}$. Equation (4.1) can be expanded as:

$$\mathbf{r} = \left(\hat{\mathbf{H}} + \mathbf{H}_e\right)\mathbf{s} + \mathbf{w} = \hat{\mathbf{H}}\mathbf{s} + \mathbf{H}_e\mathbf{s} + \mathbf{w} \tag{4.4}$$

Assuming correct symbol decoding, we can regenerate the transmitted symbols vector (**s**). Since $\hat{\mathbf{H}}$ is also known it is straight forward to calculate:

$$\mathbf{r} - \hat{\mathbf{H}}\mathbf{s} = \mathbf{H}_e\mathbf{s} + \mathbf{w} \tag{4.5}$$

Define $\Delta\mathbf{H}$ as:

$$\Delta\mathbf{H} = \left(\mathbf{r} - \hat{\mathbf{H}}\mathbf{s}\right)\mathbf{s}^{-1} \tag{4.6}$$

The update algorithm can be implemented in a recursive manner to produce more accurate channel estimations as follows:

$$\hat{\mathbf{H}}_{new} = \hat{\mathbf{H}}_{old} + \Gamma.\Delta\mathbf{H} \tag{4.7}$$

Γ is a matrix of positive, real-valued update parameters and the dot multiplication ($\Gamma.\Delta\mathbf{H}$) is element by element multiplication. An interesting point about this algorithm is that the VBLAST decoding algorithm automatically produces the value ($\mathbf{r}$ - $\hat{\mathbf{H}}\mathbf{s}$) from the cancellation step [44], see section (2.3.4.5):

$$\mathbf{r}^{i+1} = \mathbf{r}^{i} - a_k^i \left[\mathbf{H}\right]_k^i \tag{4.8}$$

Where $\mathbf{r}^i$ is the received signal vector after decoding i symbols, k is the column index, a_k^i is the decoded symbol, and $[\mathbf{H}]_k$ is the kth column in the matrix $\mathbf{H}$. So after the detection of all the symbols, the value of $\mathbf{r}^{i+1}$ needs to be multiplied by the pseudoinverse of $\mathbf{s}$ to give $\Delta\mathbf{H}$. The optimum value of Γ is the one that minimises the expression:

$$E\left[\left|\mathbf{H}-\hat{\mathbf{H}}_{new}\right|^2\right] \tag{4.9}$$

4.2.2. Optimum Value of the Update Parameter Γ

To find the optimum value of Γ we first start with the simple case of $1\times B$ VBLAST, our simulations use B = 4, and extend it to the general case of multiple transmit antennas. Table (4.1) lists the variable that will be used in the derivation of optimum Γ.

T_s	Symbol duration
n	Symbol index (time index)
$\mathbf{r}_n$	Received signal vector at time n
$\mathbf{s}_n$	Vector of transmitted symbols at time n
$\mathbf{H}_n$	Exact channel matrix at time index n
$\mathbf{H}_e^n$	Change in exact channel matrix between time n and n-1 ($\mathbf{H}_n - \mathbf{H}_{n-1}$)
$\hat{\mathbf{H}}_n$	Estimated channel matrix at time n
$\hat{\mathbf{s}}_n$	Vector of decoded symbols at time n
$\mathbf{w}_n$	Noise vector at time n
Δ_n	Difference (error) between real and estimated channel matrices at time n
f_D	Maximum Doppler shift

Table (4.1): List of Variables Used

The general MIMO equation for the received signal at time n-1 is:

$$\mathbf{r}_{n-1} = \mathbf{H}_{n-1}\mathbf{s}_{n-1} + \mathbf{w}_{n-1} \tag{4.10}$$

The receiver, with knowledge of $\mathbf{r}_{n-1}$ and $\hat{\mathbf{H}}_{n-1}$, and using the VBLAST algorithm, generates an estimate $\hat{\mathbf{s}}_{n-1}$ of the transmitted symbol. We then have:

$$\mathbf{r}_{n-1} - \hat{\mathbf{H}}_{n-1}\hat{\mathbf{s}}_{n-1} = \mathbf{H}_{n-1}\mathbf{s}_{n-1} - \hat{\mathbf{H}}_{n-1}\hat{\mathbf{s}}_{n-1} + \mathbf{w}_{n-1} \tag{4.11}$$

Assuming the data was decoded correctly (i.e. $\hat{\mathbf{s}}_{n-1} = \mathbf{s}_{n-1}$) we get:

$$\mathbf{r}_{n-1} - \hat{\mathbf{H}}_{n-1}\hat{\mathbf{s}}_{n-1} = \left(\mathbf{H}_{n-1} - \hat{\mathbf{H}}_{n-1}\right)\mathbf{s}_{n-1} + \mathbf{w}_{n-1} \tag{4.12}$$

Define the variable $\Delta\mathbf{H}_n$ as:

$$\Delta\mathbf{H}_n = \left(\mathbf{r}_{n-1} - \hat{\mathbf{H}}_{n-1}\hat{\mathbf{s}}_{n-1}\right)\hat{\mathbf{s}}_{n-1}^{-1} = \left(\mathbf{H}_{n-1} - \hat{\mathbf{H}}_{n-1}\right)\mathbf{s}_{n-1}\mathbf{s}^{-1}{}_{n-1} + \mathbf{w}_{n-1}\mathbf{s}_{n-1}^{-1} \tag{4.13}$$

$\Delta\mathbf{H}_n$ is then used to predict the channel matrix for the next time index (n) as:

$$\hat{\mathbf{H}}_n = \hat{\mathbf{H}}_{n-1} + \mathbf{\Gamma}.\Delta\mathbf{H}_n \tag{4.14}$$

Γ here will be a column vector since only one antenna is transmitting. From the definition of $\Delta\mathbf{H}_n$, the elements of Γ should be less than or equal to 1. Assuming the receive antennas have independent and identically distributed channels with equal average signal to noise ratio (SNR), the elements of Γ will be equal and thus Γ can be replaced by a scalar γ as will be shown. The difference between the estimated and actual channel matrix is given by:

$$\begin{aligned}\mathbf{\Delta}_n &= \mathbf{H}_n - \hat{\mathbf{H}}_n = \mathbf{H}_n - \mathbf{H}_{n-1} + \mathbf{H}_{n-1} - \hat{\mathbf{H}}_{n-1} - \mathbf{\Gamma}.\Delta\mathbf{H}_n \\ &= \mathbf{H}_e^n + \mathbf{\Delta}_{n-1} - \mathbf{\Gamma}\left(\mathbf{H}_{n-1} - \hat{\mathbf{H}}_{n-1} + \mathbf{w}_{n-1}\mathbf{s}_{n-1}^{-1}\right) \\ &= \mathbf{H}_e^n + \mathbf{\Delta}_{n-1} - \mathbf{\Gamma}.\mathbf{\Delta}_{n-1} - \mathbf{\Gamma}.\mathbf{w}_{n-1}\mathbf{s}_{n-1}^{-1} \\ &= \left(\mathbf{1}_B - \mathbf{\Gamma}\right).\mathbf{\Delta}_{n-1} + \mathbf{H}_e^n - \mathbf{\Gamma}.\mathbf{w}_{n-1}\mathbf{s}_{n-1}^{-1}\end{aligned} \tag{4.15}$$

$\mathbf{1}_B$ is a B elements vector with all elements = 1. Let $\mathbf{m}_n = \mathbf{w}_n\,\mathbf{s}_n^{-1}$. Following the line of analysis used in [143], we split the error (Δ_n) into two uncorrelated parts, one due to the change in the channel response ($\Delta_n^{(L)}$) and the other due to the noise ($\Delta_n^{(N)}$).

$$\mathbf{\Delta}_n = \mathbf{\Delta}_n^{(L)} + \mathbf{\Delta}_n^{(N)} \tag{4.16}$$

$$\mathbf{\Delta}_n^{(L)} = \left(\mathbf{1}_B - \mathbf{\Gamma}\right).\mathbf{\Delta}_{n-1}^{(L)} + \mathbf{H}_e^n = \sum_{i=0}^{n}\left[\mathbf{1}_B - \mathbf{\Gamma}\right]^i.\mathbf{H}_e^{n-i} \tag{4.17}$$

$$\mathbf{\Delta}_n^{(N)} = \left(\mathbf{1}_B - \mathbf{\Gamma}\right)\mathbf{\Delta}_{n-1}^{(N)} - \mathbf{\Gamma}.\mathbf{m}_{n-1} = -\mathbf{\Gamma}.\sum_{i=0}^{n-1}\left[\mathbf{1}_B - \mathbf{\Gamma}\right]^i.\mathbf{m}_{n-i-1} \tag{4.18}$$

$[\Gamma]^i$ is the dot product of Γ i times. The optimum value of Γ is the one that minimises the value $E[|\Delta_n|^2]$, where E denotes expectation. For the error due to the change in channel response, the expectation is given by:

$$E\left[\left|\mathbf{\Delta}_n^{(L)}\right|^2\right] = \sum_{i=0}^{n}\sum_{j=0}^{n}\left[\mathbf{1}_B - \mathbf{\Gamma}\right]^i \times \left(\left[\mathbf{1}_B - \mathbf{\Gamma}\right]^j\right)^H.E\left(\mathbf{H}_e^{n-i} \times \left(\mathbf{H}_e^{n-j}\right)^H\right) \tag{4.19}$$

$(.)^H$ represents conjugate transpose. The value $E\left(\mathbf{H}_e^p \times \left(\mathbf{H}_e^q\right)^H\right)$ is the correlation matrix of the change in channel response between the receive antennas at time indexes p and q. Considering Rayleigh fading with correlation function ($C^{a,b}(p,q)$) of the change in channel between antennas a and b we get for a 1×4 system:

$$E\left(\mathbf{H}_e^p \times \left(\mathbf{H}_e^q\right)^H\right) = \begin{bmatrix} C^{1,1}(p,q) & C^{1,2}(p,q) & C^{1,3}(p,q) & C^{1,4}(p,q) \\ C^{2,1}(p,q) & C^{2,2}(p,q) & C^{2,3}(p,q) & C^{2,4}(p,q) \\ C^{3,1}(p,q) & C^{3,2}(p,q) & C^{3,3}(p,q) & C^{3,4}(p,q) \\ C^{4,1}(p,q) & C^{4,2}(p,q) & C^{4,3}(p,q) & C^{4,4}(p,q) \end{bmatrix} \quad (4.20)$$

However since we assume independent and identically distributed Rayleigh fading for the receive antennas, the channel correlation ($C^{a,b}(p,q)$) between different antennas ($a \neq b$) is assumed equal to zero leading to:

$$E\left(\mathbf{H}_e^p \times \left(\mathbf{H}_e^q\right)^H\right) = C^{a,a}(p,q) \begin{bmatrix} 1 & 0 & 0 & 0 \\ 0 & 1 & 0 & 0 \\ 0 & 0 & 1 & 0 \\ 0 & 0 & 0 & 1 \end{bmatrix} = C(p,q)\mathbf{I} \quad (4.21)$$

$\mathbf{I}$ is the identity matrix and $C(p,q) = C^{a,a}(p,q)$. Since the noise at the antennas is also assumed independent and identically distributed with equal average power, the elements of Γ will be equal, hence we replace it with a scalar (γ). Substituting (4.21) in (4.19):

$$E\left[\left|\Delta_n^{(L)}\right|^2\right] = \mathbf{I}\sum_{i=0}^{n}\sum_{j=0}^{n}(1-\gamma)^i(1-\gamma)^j \times C(n-i,n-j) \quad (4.22)$$

The autocorrelation function of Rayleigh fading channels is given by the zeroth order Bessel function ($J_0(2\pi f_D \tau)$) [26] which, for discrete time and $f_D T_s < 0.1$, can be approximated by [26, 40, 143]:

$$J_0(2b\pi f_D T_s) \approx 1 - (b\pi f_D T_s)^2 \quad (4.23)$$

The function $C(p,q)$ is then given by [26, 40, 143]:

$$C(p,q) = C(0,p-q) = C(0,b) = \frac{-\partial^2\left(J_0(2b\pi f_D T_s)\right)}{\partial b^2} \approx 2(\pi f_D T_s)^2 \quad (4.24)$$

Substituting in (4.22), the summation for large n reduces to [143]:

$$E\left[\left|\mathbf{\Delta}_n^{(L)}\right|^2\right] \approx 2\left(\frac{\pi f_D T_s}{\gamma}\right)^2 \times \mathbf{I} \tag{4.25}$$

We now turn our attention to equation (4.18) and calculate the term $E[|\Delta_n^{(N)}|^2]$:

$$E\left[\left|\mathbf{\Delta}_n^{(N)}\right|^2\right] = \gamma^2 \sum_{i=0}^{n-1}\sum_{j=0}^{n-1}(1-\gamma)^i(1-\gamma)^j \times E\left(\mathbf{m}_{n-i-1} \times \left(\mathbf{m}_{n-j-1}\right)^H\right) \tag{4.26}$$

Assuming independent, identically distributed (i.i.d) white Gaussian noise with equal average power (N_0) for the receive antennas we get [143]:

$$E\left(\mathbf{m}_{n-i-1} \times \left(\mathbf{m}_{n-j-1}\right)^H\right) = N_0 \times \delta(n-i-1, n-j-1) \times \mathbf{I} \tag{4.27}$$

Where the Dirac-Delta function ($\delta(i,j)$) is defined as:

$$\delta(i,j) = \begin{cases} 1, & i = j \\ 0, & otherwise \end{cases} \tag{4.28}$$

Therefore (4.26) becomes:

$$E\left[\left|\mathbf{\Delta}_n^{(N)}\right|^2\right] = \gamma^2 \times \mathbf{I} \sum_{i=0}^{n-1}\sum_{j=0}^{n-1}(1-\gamma)^i(1-\gamma)^j N_0 \times \delta(n-i-1, n-j-1) \tag{4.29}$$

Using (4.28), the summation in (4.29) reduces for large n to [143]:

$$E\left[\left|\mathbf{\Delta}_n^{(N)}\right|^2\right] = \frac{\gamma}{2-\gamma} N_0 \times \mathbf{I} \approx \frac{\gamma}{2} N_0 \times \mathbf{I} \tag{4.30}$$

and therefore:

$$E\left[\left|\Delta_n\right|^2\right] \approx 2\left(\frac{\pi f_D T_s}{\gamma}\right)^2 \times \mathbf{I} + \frac{\gamma}{2} N_0 \times \mathbf{I} \tag{4.31}$$

The optimum value of γ can now be found by differentiating (4.31), setting the result equal to zero and solving for γ leading to:

$$\gamma \approx 2\left(\sqrt[3]{\frac{(\pi f_D T_s)^2}{N_0}}\right) \tag{4.32}$$

We now consider the general case of $A \times B$ VBLAST. However instead of analysing for B receive antennas, we assume rich Rayleigh fading and i.i.d noise, hence we need

only to analyse for a single receive antenna then generalise for all the receive antennas since the optimisation process is independent for each receive antenna as proven by equations (4.21) and (4.27). Equations (4.10) to (4.14) remain the same. To understand the effects of multiple transmitting antennas we need to calculate the elements (Δh_{ij}) of the matrix $\mathbf{\Delta H}$. From equation (4.13), this is given by:

$$\Delta h_{ij}^{n} = \left(r_i^{n-1} - \sum_{l=1}^{A} \hat{h}_{il}^{n-1} \hat{s}_l^{n-1} \right) a_j^{n-1} \tag{4.33}$$

The lower case, regular characters denote elements of the matrix/vector denoted by bold characters. The superscript (n) denotes the time index and the subscripts identify the row (i) and column (j or l). a_j is element j of the row vector ($\mathbf{s}^{-1}$). Equation (4.33) can be expanded as:

$$\Delta h_{ij}^{n} = \left(\sum_{l=1}^{A} h_{il}^{n-1} s_l^{n-1} - \sum_{l=1}^{A} \hat{h}_{il}^{n-1} \hat{s}_l^{n-1} + w_i^{n-1} \right) a_j^{n-1} \tag{4.34}$$

and assuming correct decoding:

$$\Delta h_{ij}^{n} = \left(\sum_{l=1}^{A} \left(h_{il}^{n-1} - \hat{h}_{il}^{n-1} \right) s_l^{n-1} \right) a_j^{n-1} + w_i^{n-1} a_j^{n-1} = \sum_{l=1}^{A} \varepsilon_{il}^{n-1} s_l^{n-1} a_j^{n-1} + w_i^{n-1} a_j^{n-1} \tag{4.35}$$

Where ε_{ij}^{n-1} denotes element (i, j) of the Δ_{n-1} matrix. If the Moore-Penrose pseudoinverse of $\mathbf{s}$ exists, then by definition $\mathbf{s}\mathbf{s}^{-1}\mathbf{s} = \mathbf{s}$. Expanding this relation we get:

$$\begin{bmatrix} s_1 \\ s_2 \\ \vdots \\ s_A \end{bmatrix} \begin{bmatrix} a_1 & a_2 & \cdots & a_A \end{bmatrix} \begin{bmatrix} s_1 \\ s_2 \\ \vdots \\ s_A \end{bmatrix} = \begin{bmatrix} s_1 \\ s_2 \\ \vdots \\ s_A \end{bmatrix} \tag{4.36}$$

$$\begin{bmatrix} a_1 s_1 & a_2 s_1 & \cdots & a_N s_1 \\ a_1 s_2 & a_2 s_2 & \cdots & a_N s_2 \\ \vdots & \vdots & \ddots & \vdots \\ a_1 s_A & a_2 s_A & \cdots & a_A s_A \end{bmatrix} \begin{bmatrix} s_1 \\ s_2 \\ \vdots \\ s_A \end{bmatrix} = \begin{bmatrix} s_1 \left(\sum_{i=1}^{A} a_i s_i \right) \\ s_2 \left(\sum_{i=1}^{A} a_i s_i \right) \\ \vdots \\ s_A \left(\sum_{i=1}^{A} a_i s_i \right) \end{bmatrix} = \begin{bmatrix} s_1 \\ s_2 \\ \vdots \\ s_A \end{bmatrix} \tag{4.37}$$

Therefore

$$\sum_{i=1}^{A} a_i s_i = 1 \tag{4.38}$$

Let $a_j s_j = \beta$ where β is some constant value. Equation (4.35) then becomes:

$$\Delta h_{ij}^{n} = \beta \varepsilon_{ij}^{n-1} + \sum_{\substack{l=1 \\ l \neq j}}^{A} \varepsilon_{il}^{n-1} s_l^{n-1} a_j^{n-1} + w_i^{n-1} a_j^{n-1} \tag{4.39}$$

We use the update equation:

$$\hat{h}_{ij}^{n} = \hat{h}_{ij}^{n-1} + \gamma_j \Delta h_{ij}^{n} \tag{4.40}$$

Expanding Δh_{ij}^{n} we get:

$$\hat{h}_{ij}^{n} = \hat{h}_{ij}^{n-1} + \beta . \gamma_j . \varepsilon_{ij}^{n-1} + \gamma_j \sum_{\substack{l=1 \\ l \neq j}}^{A} \varepsilon_{il}^{n-1} s_l^{n-1} a_j^{n-1} + \gamma_j w_i^{n-1} a_j^{n-1} \tag{4.41}$$

Which is identical to the update equation for a selective fading channel except for the constant β [143]. This is expected since in selective fading we have interference from previously detected symbols, typically with less power than the current symbol, passing through different channels, while here we have interference from different antennas each encountering independent fading. According to [143], if we assume white data, i.e. no correlation between the data from each antenna, we can approximate the last two terms in equation (4.41) by an additive white Gaussian noise with average power:

$$\overline{N}_{0,j} = \frac{N_0}{\rho_j} \left(1 + \sum_{\substack{l=1 \\ l \neq j}}^{N} e_l \right) \tag{4.42}$$

Where N_0 is the original total white noise power for receive antenna (i), e_l is the average error covariance reduction value [143] and ρ_j is a constant that specifies the fraction of power associated with stream j [143]. This result will be verified in the next section.

Using the white data assumption equation (4.41) can be written as:

$$\hat{h}_{ij}^{n} = \hat{h}_{ij}^{n-1} + \beta . \gamma_j . \varepsilon_{ij}^{n-1} + \gamma_j . \tilde{w}_j^{n-1} \tag{4.43}$$

Where $\tilde{w}_j^{n-1}$ is the noise sample plus the interference from other symbols. Let $\mu_j = \beta\,\gamma_j$:

$$\hat{h}_{ij}^{n} = \hat{h}_{ij}^{n-1} + \mu_j.\varepsilon_{ij}^{n-1} + \mu_j \frac{\tilde{w}_j^{n-1}}{\beta} = \hat{h}_{ij}^{n-1} + \mu_j.\varepsilon_{ij}^{n-1} + \mu_j.\overline{\overline{w}}_j^{n-1} \tag{4.44}$$

The average power for the noise $\overline{\overline{w}}_j^{n-1}$, $\overline{\overline{w}}_j^{n-1} = \dfrac{\tilde{w}_j^{n-1}}{\beta}$, will then be:

$$\overline{\overline{N}}_{0,j} = \frac{N_0}{\rho_j.\beta^2}\left(1 + \sum_{\substack{l=1 \\ l\neq j}}^{N} e_l\right) \tag{4.45}$$

The prediction error (ε_{ij}^{n}) can now be calculated as:

$$\begin{aligned}\varepsilon_{ij}^{n} &= h_{ij}^{n} - \hat{h}_{ij}^{n} = h_{ij}^{n} - \hat{h}_{ij}^{n-1} - \mu_j\varepsilon_{ij}^{n-1} - \mu_j\overline{\overline{w}}_j^{n-1} = h_{ij}^{n} - h_{ij}^{n-1} + h_{ij}^{n-1} - \hat{h}_{ij}^{n-1} - \mu_j\varepsilon_{ij}^{n-1} - \mu_j\overline{\overline{w}}_j^{n-1} \\ &= h_e^{n} + \varepsilon_{ij}^{n-1} - \mu_j\varepsilon_{ij}^{n-1} - \mu_j\overline{\overline{w}}_j^{n-1} = (1-\mu_j)\varepsilon_{ij}^{n-1} + h_e^{n} - \mu_j\overline{\overline{w}}_j^{n-1}\end{aligned} \tag{4.46}$$

As with the single transmit antenna and flat fading case, this can be split into two errors, channel error and noise error. The process for finding the optimum value for the update parameter is identical to that of a single transmit antenna leading to the result [143]:

$$\mu_j \approx 2\left(\sqrt[3]{\frac{(\pi f_D T_s)^2}{\overline{\overline{N}}_0}}\right) = \sqrt[3]{\frac{8(\pi f_D T_s)^2}{\dfrac{N_0}{\rho_j.\beta^2}\left(1 + \sum_{\substack{l=1 \\ l\neq j}}^{N} e_l\right)}} \tag{4.47}$$

$$e_j^{(\min)} = \frac{E\left[\left|\varepsilon_{ij}^{n}\right|^2\right]^{(\min)}}{N_0} \approx 0.75\mu_j \tag{4.48}$$

γ_j is then given by:

$$\gamma_j = \frac{\mu_j}{\beta} = \frac{2}{\beta} \times \sqrt[3]{\frac{\rho_j(\pi f_D T_s)^2}{\dfrac{N_0}{\beta^2}\left(1 + \sum_{\substack{l=1 \\ l\neq j}}^{A} e_l\right)}} = \sqrt[3]{\frac{8.\rho_j(\pi f_D T_s)^2}{\dfrac{\beta^3.N_0}{\beta^2}\left(1 + \sum_{\substack{l=1 \\ l\neq j}}^{A} e_l\right)}} \tag{4.49}$$

$$\gamma_j = \sqrt[3]{\frac{8.\rho_j(\pi f_D T_s)^2}{\beta.N_0\left(1+\sum_{\substack{l=1\\l\neq j}}^{A} e_l\right)}} \tag{4.50}$$

The constant β needs to be determined. The actual value of β may vary depending on the transmitted symbols and used constellation. Assuming equal transmitting power for the antennas and a fixed power constellation, $\beta = 1/A$ [144-146]. Moreover since we assume equal transmitting power from each transmit antenna, ρ_j is equal to $1/A$. Equation (4.50) then becomes:

$$\gamma_j = \sqrt[3]{\frac{\frac{8}{A}(\pi f_D T_s)^2}{\frac{N_0}{A}\left(1+\sum_{\substack{l=1\\l\neq j}}^{A} e_l\right)}} = \sqrt[3]{\frac{8(\pi f_D T_s)^2}{N_0\left(1+\sum_{\substack{l=1\\l\neq j}}^{A} e_l\right)}} \tag{4.51}$$

and e_j is given by:

$$e_j^{(\min)} \approx 0.75\beta.k_j = \frac{0.75}{A}\gamma_j \tag{4.52}$$

The γ_j parameters are calculated recursively. First we assume no interference from the other symbols and set all $e_j = 0$. We then calculate γ_1 and update e_1. Next we substitute the new value of e_1 for γ_2 and update e_2. This process is repeated till all the γ_j and e_j parameters are calculated and then we repeat the calculations again with the new e_j values. The process converges very quickly, approximately 3 iterations. The γ_j parameters are then used to update the channel estimate. The algorithm is summarised in tables (4.2) and (4.3).

The optimum update parameters (γ_{opt}) are shown in figures (4.1) and (4.2) for 2 and 3 transmitting antennas respectively and symbol rate of 1MSymbol/s. At low SNR and/or low speeds, the update parameters take small values to reduce the effects of noise. As the SNR and speed increase the parameters increase to provide better channel tracking. As the number of antennas increase, the interference increases thus leading to lower

parameter values. If all streams have equal power, the optimum update parameters (γ_j) will be equal for all j. The update algorithm requires the calculation of A γ_j parameters, one for each transmit antenna using equations (4.51) and (4.52). These can be calculated once at the beginning of the packet and held constant for the duration of the packet. $\Delta\mathbf{H}_n$ requires the pseudoinverse of the ($A\times1$) vector $\mathbf{s}$, which can be pre-computed and stored, and then multiplying it by the term $\left(\mathbf{r}_{n-1} - \hat{\mathbf{H}}_{n-1}\hat{\mathbf{s}}_{n-1}\right)$, equation (4.13), which is calculated in the VBLAST algorithm. This multiplication consists of $A\times B$ complex multiplications. The channel update, equation (4.14), requires $A\times B$ real by complex multiplications and $A\times B$ complex additions.

Calculation of γ_j Parameter Algorithm
1) set $e_j = 0$ for all j
2) iteration = 1
3) j = 1
4) calculate γ_j using equation (4.51)
5) calculate e_j using equation (4.52)
6) $j = j+1$
7) if (j < number of transmit antennas) go to 4
8) iteration = iteration +1
9) if (iteration < max number of iterations) go to 3

Table (4.2): Calculation of γ_j Parameters Algorithm

Channel Update Algorithm
1) calculate the γ_j parameters
2) calculate $\Delta\mathbf{H}$ *using equation* (4.13)
3) update the channel using equation (4.14)

Table (4.3): Channel Update Algorithm

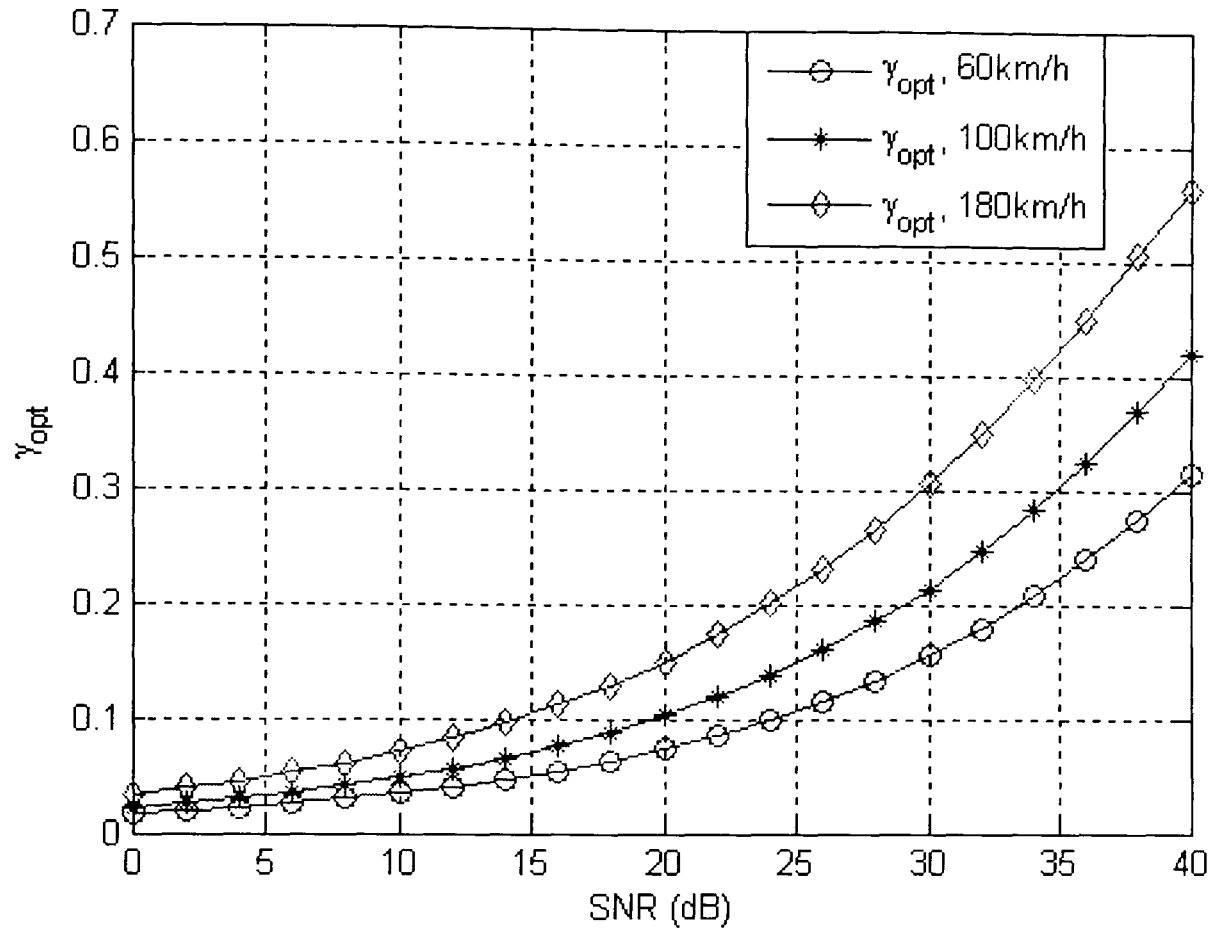

Figure (4.1): γ_{opt} for Two Transmitting Antennas vs. SNR

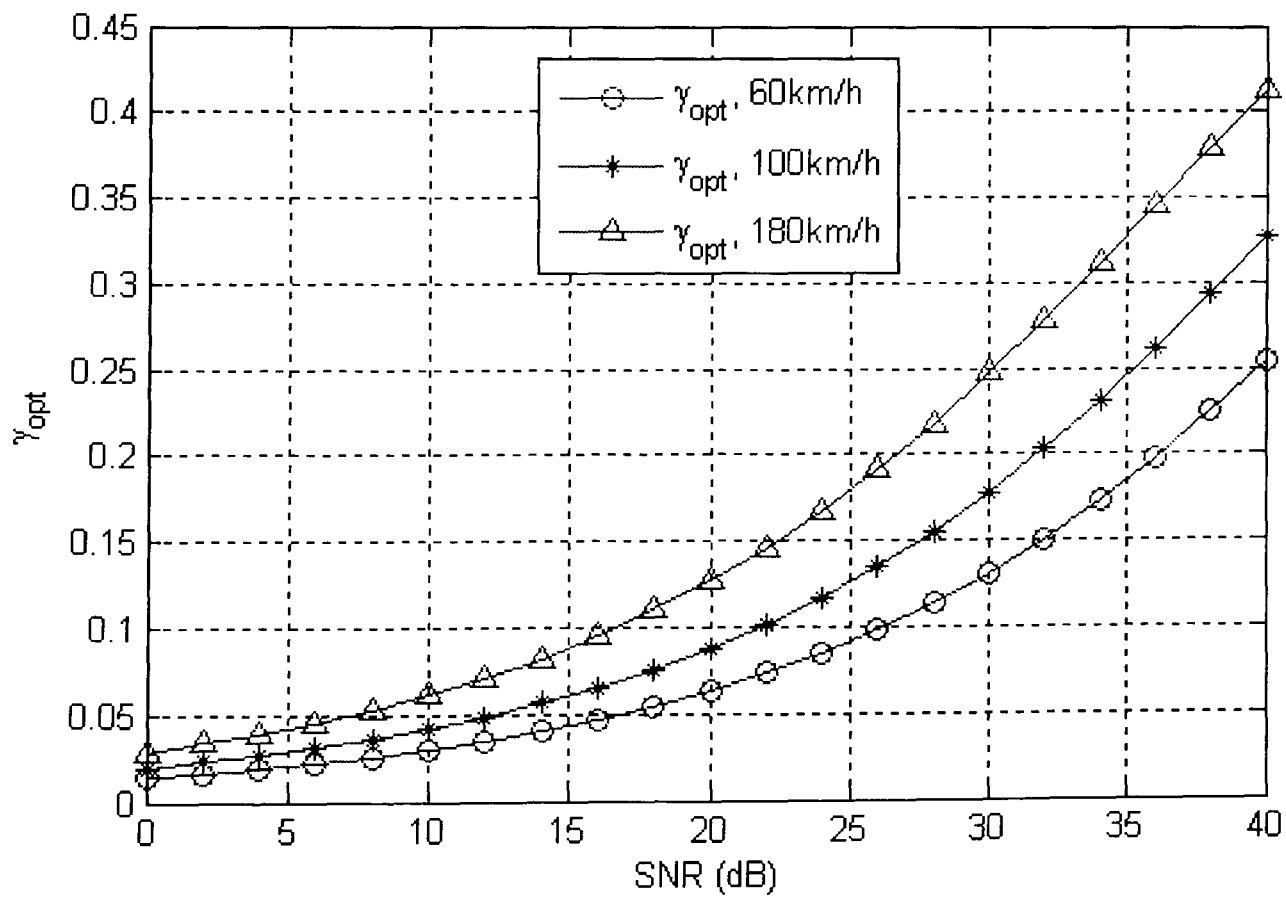

Figure (4.2): γ_{opt} for Three Transmitting Antennas vs. SNR

4.2.3. White data approximation

In this section we examine the approximation of the interference of the symbols from other antennas by white noise, equation (4.42), and prove its validity. We assume a Rician fading channel (Rayleigh fading is a special case of Rician fading) and uniformly distributed data in the interval [-1, 1]. The derivation will be restricted to the real part as the analysis of the imaginary part is identical.

According to [143] the last two terms in equation (4.41), interference from other symbols plus white noise, can be approximated by white Gaussian noise with power calculated using equation (4.42) if the data is assumed white. In other words the interference for symbol j is approximated by a Gaussian noise with power:

$$N_j = N_0 \sum_{\substack{l=1 \\ l \neq j}}^{N} e_l \qquad (4.53)$$

The interference is the product of the channel error (ε_{il}) and the white data s_l and a_j. Hence its probability density function (PDF) is the product of the PDFs of ε_{il}, s_l and a_j. A Rician fading channel consists of real and imaginary parts both having identical Gaussian distribution [19] with mean (μ) and variance (σ^2), defined as:

$$f(x) = \frac{1}{\sqrt{2\pi\sigma^2}} e^{\frac{-(x-\mu)^2}{2\sigma^2}} \qquad (4.54)$$

The term ε_{il} in (4.43) is defined as:

$$\varepsilon_{il} = h_{il} - \hat{h}_{il} \qquad (4.55)$$

Since the algorithm will track the channel, it is reasonable to assume both the channel and the estimate will have identical distributions, hence from (4.55) and [147], the random variable ε_{il} will have zero mean and variance $2\sigma^2$. The interfering symbols (s_l) and decoded data (a_j) are assumed independent and identically distributed white data, hence their PDF is:

$$f(x) = \begin{cases} 0.5, & |x| < 1 \\ 0, & otherwise \end{cases} \qquad (4.56)$$

Although a_j and s_l are not independent, since typically they are generated from the same convolutional error correcting code, the use of interleavers in wireless communication systems randomises the data sequence and, therefore, the assumption of independent a_j and s_l remains a valid approximation. The distribution of the product (Z) of two random variables (X and Y) is calculated as [147]:

$$f_Z(z)=\int_{-\infty}^{\infty}\frac{1}{|x|}f_X(x)f_Y\left(\frac{z}{x}\right)dx \tag{4.57}$$

Using (4.57) and from [147], the PDF of the product of s and a is:

$$f(x)=\begin{cases}-0.25\ln(|x|), & |x|<1\\ 0, & otherwise\end{cases} \tag{4.58}$$

Which has a discontinuity at $x = 0$. Substituting (4.58) and the Gaussian distribution function (equation (4.54)) in (4.57) we get [148]:

$$\begin{aligned}f(z)=&\frac{-\ln(z)}{4\sqrt{2\pi b^2}}\left[E_1\left(\frac{z^2}{2b^2}\right)\right]-\frac{1}{2\sqrt{2\pi b^2}}\left[\frac{\ln^2(z)}{2}-\frac{\ln(z)}{2}\left(\Gamma\left(0,\frac{z^2}{2b^2}\right)+\ln\left(\frac{z^2}{2b^2}\right)+\alpha\right)\right]\\&-\frac{1}{16\sqrt{2\pi b^2}}\frac{z^2}{b^2}F_3^3\left(1,1,1;2,2,2;\frac{z^2}{2b^2}\right)\end{aligned} \tag{4.59}$$

Where b^2 is the variance of ε_{il}, E_1(x) is the exponential integral, Γ(a, x) is the incomplete gamma function, α is Euler's constant (α = 0.577216) and $F_p^q(a,b,x)$ is the generalised hyper-geometric function [148]. Figure (4.3) Compares the PDF from (4.59) with the Gaussian PDF. The Gaussian PDF has zero mean and variance calculated using (4.53) for 10dB SNR. As can be seen the approximation is indeed reasonable. For large noise power the variance increases causing the Gaussian PDF to become wider and the peak at 0 becomes smaller therefore the approximation becomes a poor one. However the noise then is the dominant component in (4.41). As the SNR increases the Gaussian distribution approaches a delta function approximating the peak at 0.

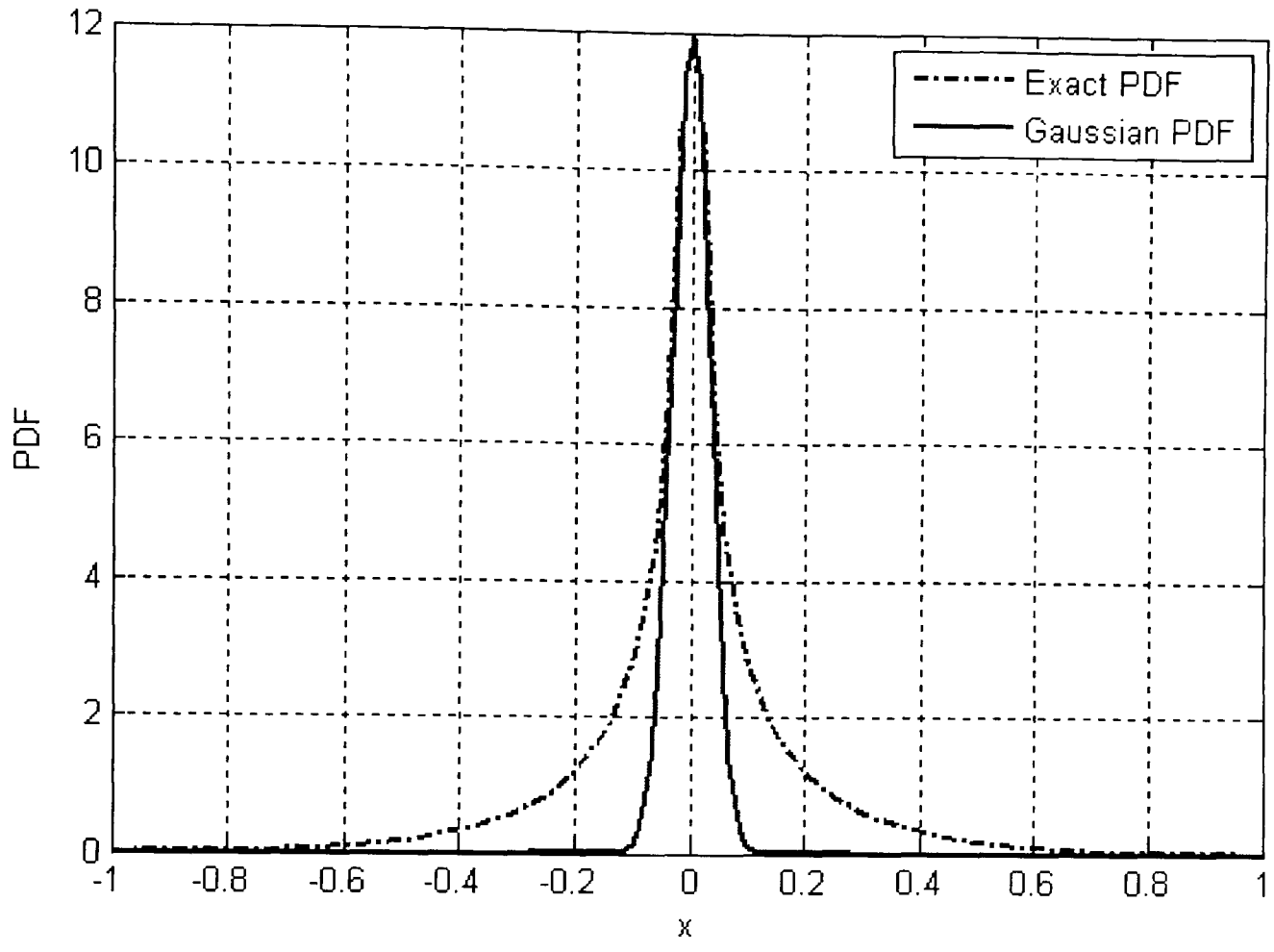

Figure (4.3): Comparison between Exact and Approximate PDFs

4.2.4. Simulation Results

We ran a number of simulations using Matlab to study the performance of the channel tracking algorithm. In our simulations we use VBLAST systems with 2×4 and 3×4 antenna arrays, the channel model introduced in chapter 3 and QPSK data modulation with a symbol rate of 1MSymbol/s transmitted at radio frequency 5.9GHz. In the simulations, initially the receiver will have perfect channel knowledge rather than estimating from a training sequence to isolate any errors that might arise from the use of training sequence estimation. The performance with a training sequence is examined afterwards. The receiver decodes the signal then uses the outcome of the decoding process in the channel update, therefore the algorithm will be affected by decoding errors. Figure (4.4) shows the mean square error (MSE) of the channel estimation for the cases of 256, 512 and 1024 symbols per packet per antenna using 2×4 VBLAST with the channel update algorithm compared to 256 symbols per packet without channel

update. As can be seen from figure (4.4) the update algorithm reduces the MSE by 50% at 12dB E_s/N_0. The MSE in figure (4.4) without update does not depend on the SNR because the receiver is assumed to have perfect, noise free, estimate of the channel at the beginning of the packet and this is held constant for the duration of the packet. From equation (4.16), the MSE is affected by two components, the first is the change in the channel response and the second component is the noise. At low SNR the noise is the dominant component, hence the performance with the channel update is worse than the performance without channel update as observed from figure (4.4). As the SNR increases, the effect of noise is reduced and, at high SNR, the noise effects become negligible and the MSE becomes dominated by the change in the channel response. The update algorithm tracks the channel to minimise the difference between the real and estimated channel response. Each update step is affected by an irreducible error due to the noise. As the update proceeds, this error accumulates leading to higher MSE for larger packet sizes as observed from figure (4.4). At high SNR, the contribution of the noise is small and hence the differences in MSE for different packet sizes become small as noted for 26dB SNR in figure (4.4).

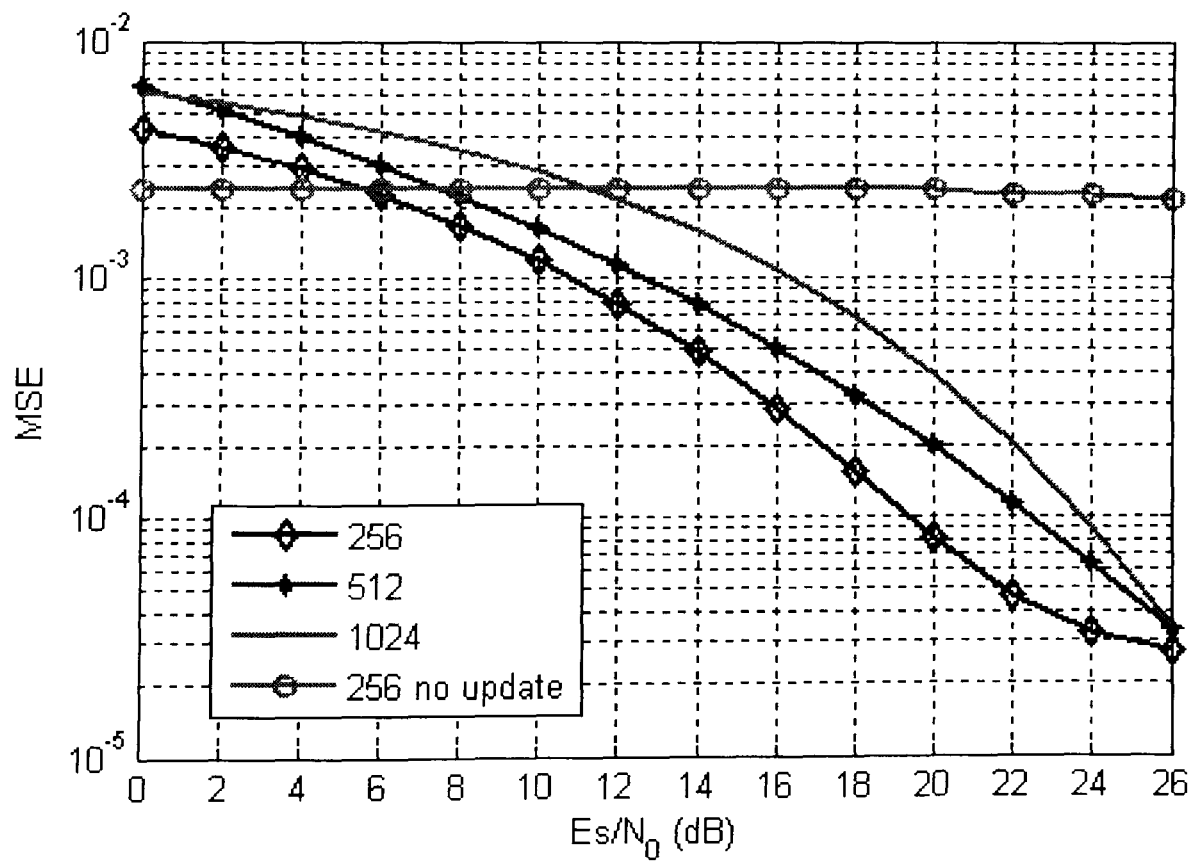

Figure (4.4): MSE of Channel Estimation for 180 km/h

Figure (4.5) shows the MSE of 2×4 VBLAST vs. the symbol number for 26dB E_s/N_0. Initially the receiver will have perfect channel knowledge (MSE ≈ 0) but with time this estimate becomes invalid due to the high Doppler shift. We observe that the channel update algorithm reduces the MSE by approximately 10^{-2}. The performance at 180 km/h is slightly worse than the performance at 100 km/h. This is expected since the higher the speed the faster is the variation in the channel and the higher the MSE. For no update both speeds seem to give similar results after 200 symbols. This means the channel varies very quickly that, after 200 symbols, the estimated matrix becomes a poor representation of the actual channel matrix. We note from the figure that with the channel update algorithm the MSE remains approximately independent of the packet size. The reason behind this is the channel update algorithm minimises the error between the real and estimated channel response on a symbol by symbol basis. For high SNR the outcome of the algorithm at each update is accurate and hence leads to small MSE. However at low SNR, the estimate is affected by noise leading to errors in the estimation. These errors accumulate as the update progresses thus degrading the performance for large packets at low SNR.

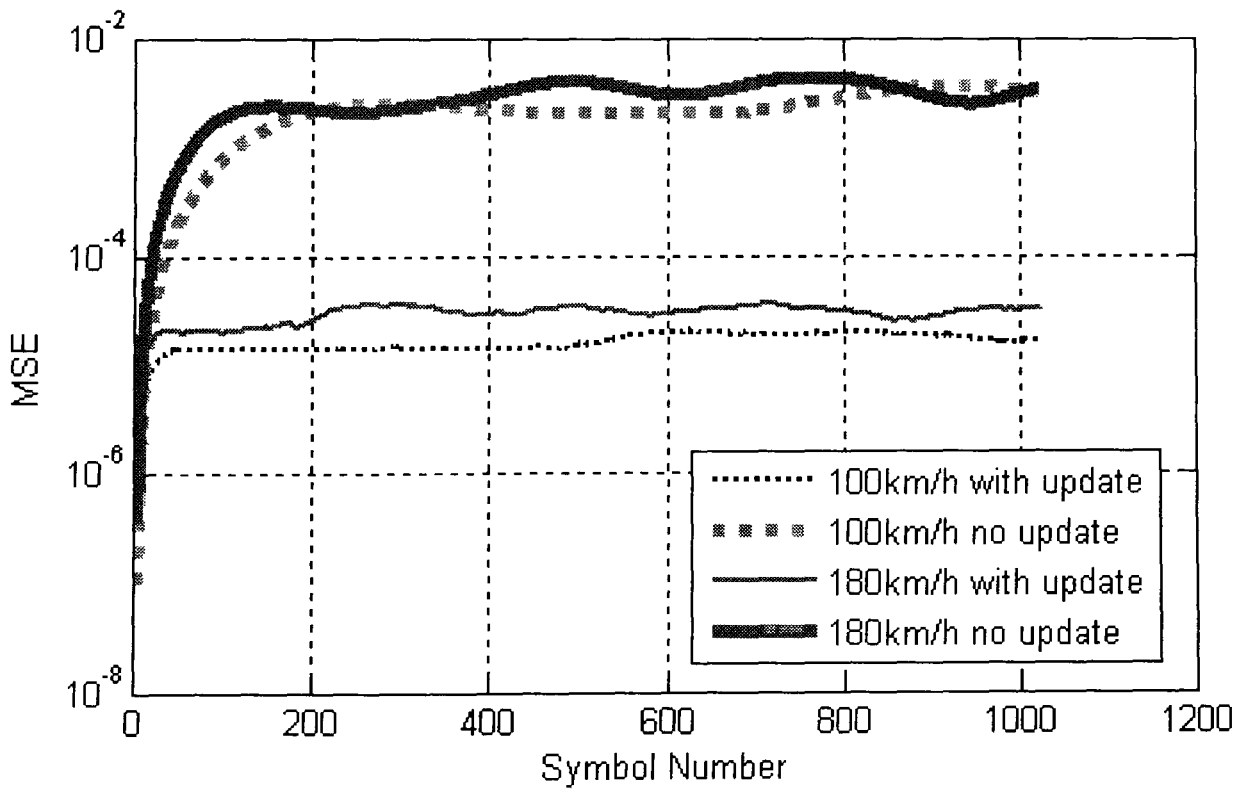

Figure (4.5): MSE of Channel Estimation vs. Symbol No. (26dB SNR)

Figure (4.6) shows the BER performance of the 2×4 system for various relative car speeds. As can be seen the performance improves when the algorithm is used and is 2dB from that of perfect channel knowledge at 60 km/h. To maintain figure clarity the performance without update was shown only for a speed of 60 km/h. The performance without update drops as the speed increases and hence the performance with 100 km/h and 180km/h is worse than 60 km/h as expected from equation (3.21). We note from figure (4.6) that the performance with the update is superior to the performance without update at high SNR. In fact for SNR greater than 12dB, the update algorithm gives better performance at 180 km/h than the training sequence at only 60 km/h.

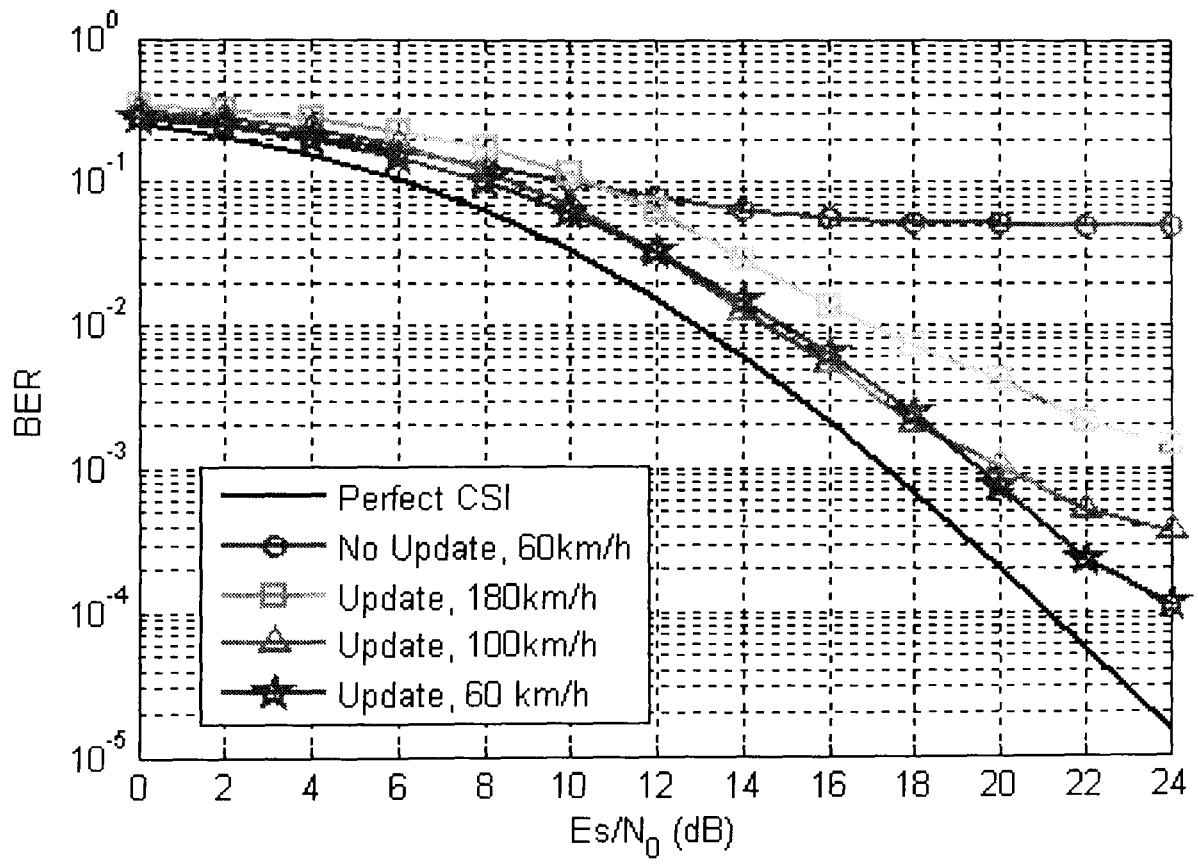

Figure (4.6): 2×4 VBLAST BER with and without Channel Update

Figure (4.7) shows the BER performance of 2×4 VBLAST with various packet lengths and a speed of 60 km/h. We observe that the performance degrades as the packet length increases; this is due to two reasons. The first reason is estimation error. As the estimation process proceeds, the error in the estimation accumulates and for long packets this leads to erroneous estimation near the end of the packet. The second reason is detection errors since the probability of incorrect symbol detection within a packet

increases as the packet length increases. The estimation algorithm assumes correct decoding; therefore decoding errors will degrade its performance.

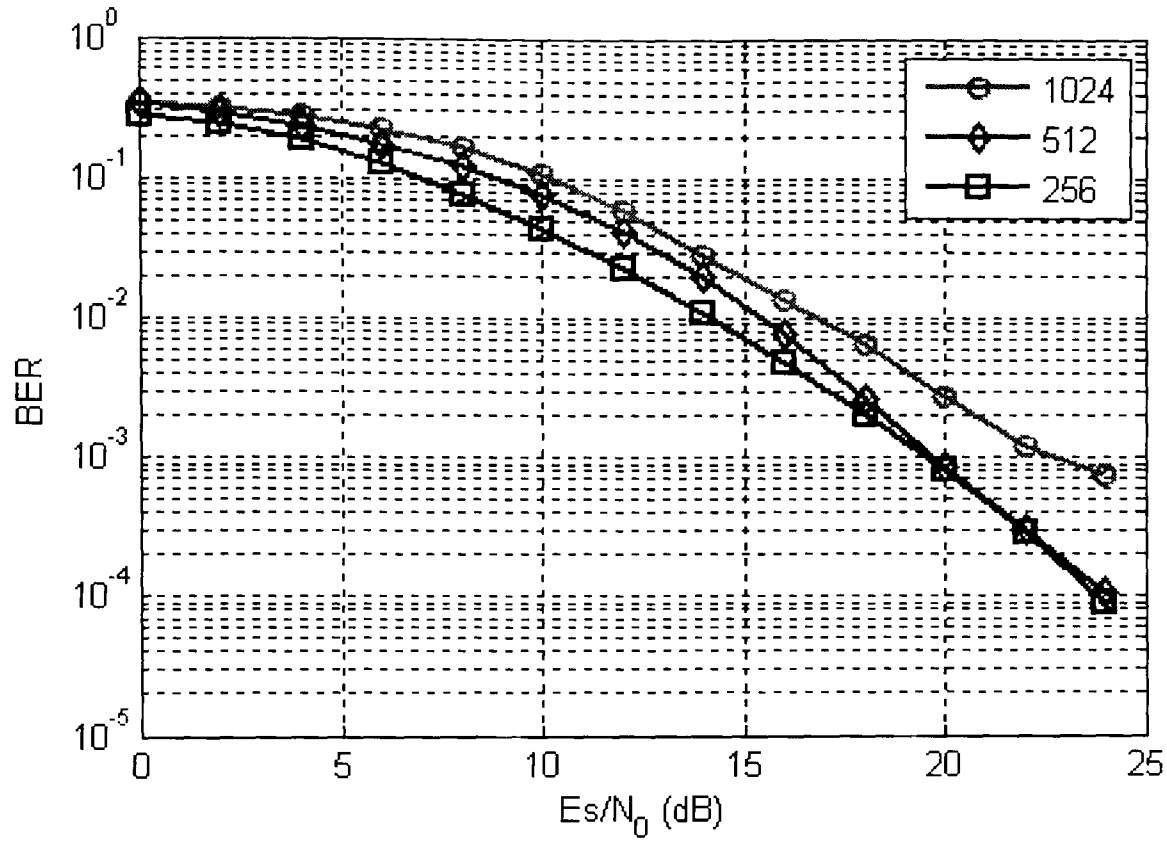

Figure (4.7): 2×4 VBLAST BER for Different Packet Sizes, 60 km/h

Figure (4.8) is a comparison between BER performance with the initial Channel State Information (CSI) matrix obtained via a training sequence and BER with perfect initial CSI for 256 symbols per transmit antenna. The optimum training sequence for B transmit antennas at high speeds is a $B \times B$ orthogonal matrix as proven in [61]. The element ($s_{m,n}$) at position (m, n) of the optimum training matrix ($\mathbf{S}_{tr}$) is calculated by (4.60) as proposed in [61] yielding the training matrices shown in (4.61) for $B = 2$ and (4.62) for $B = 3$. As can be seen from figure (4.8), the use of a training sequence for initial channel estimation degrades the performance compared to the performance using perfect initial CSI. However the channel update algorithm still provides superior performance compared to the training only case which experiences an error floor, see figure (4.6).

$$s_{m,n} = \frac{1}{\sqrt{B}} e^{-j\frac{2\pi}{B}(m-1)(n-1)} \qquad (4.60)$$

$$\mathbf{S}_{tr} = \frac{1}{\sqrt{2}}\begin{bmatrix} 1 & 1 \\ 1 & -1 \end{bmatrix} \tag{4.61}$$

$$\mathbf{S}_{tr} = \frac{1}{\sqrt{3}}\begin{bmatrix} 1 & 1 & 1 \\ 1 & -\frac{1}{2}-\frac{\sqrt{3}}{2}j & -\frac{1}{2}+\frac{\sqrt{3}}{2}j \\ 1 & -\frac{1}{2}+\frac{\sqrt{3}}{2}j & -\frac{1}{2}-\frac{\sqrt{3}}{2}j \end{bmatrix} \tag{4.62}$$

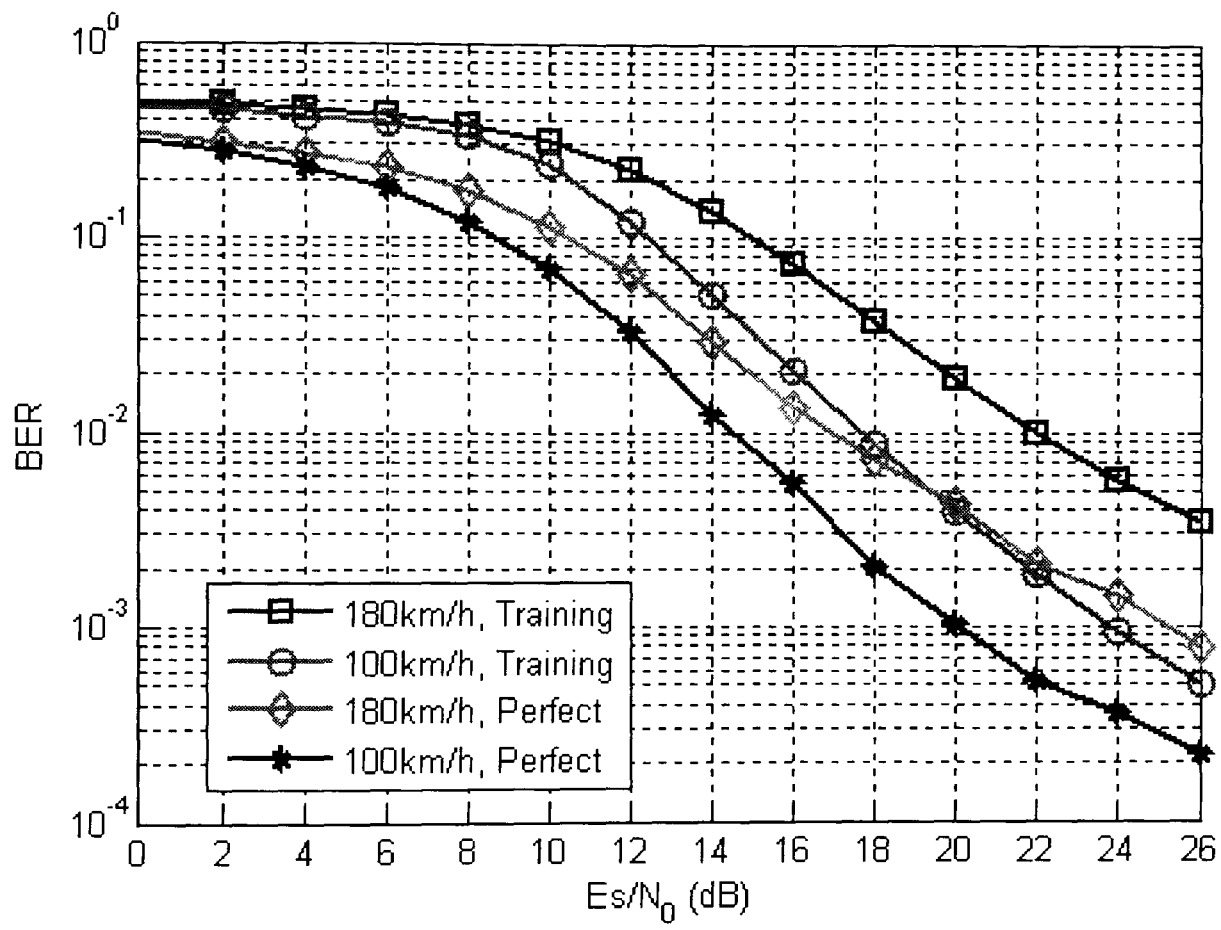

Figure (4.8): BER Comparison Using Perfect and Training-Based Initial CSI

Finally figure (4.9) shows the performance of 3×4 VBLAST with the training sequence of (4.62). From the figure we observe the performance of VBLAST with the channel update algorithm at high SNR is superior to channel estimation using only a training sequence (with perfect initial CSI) which experiences an error floor.

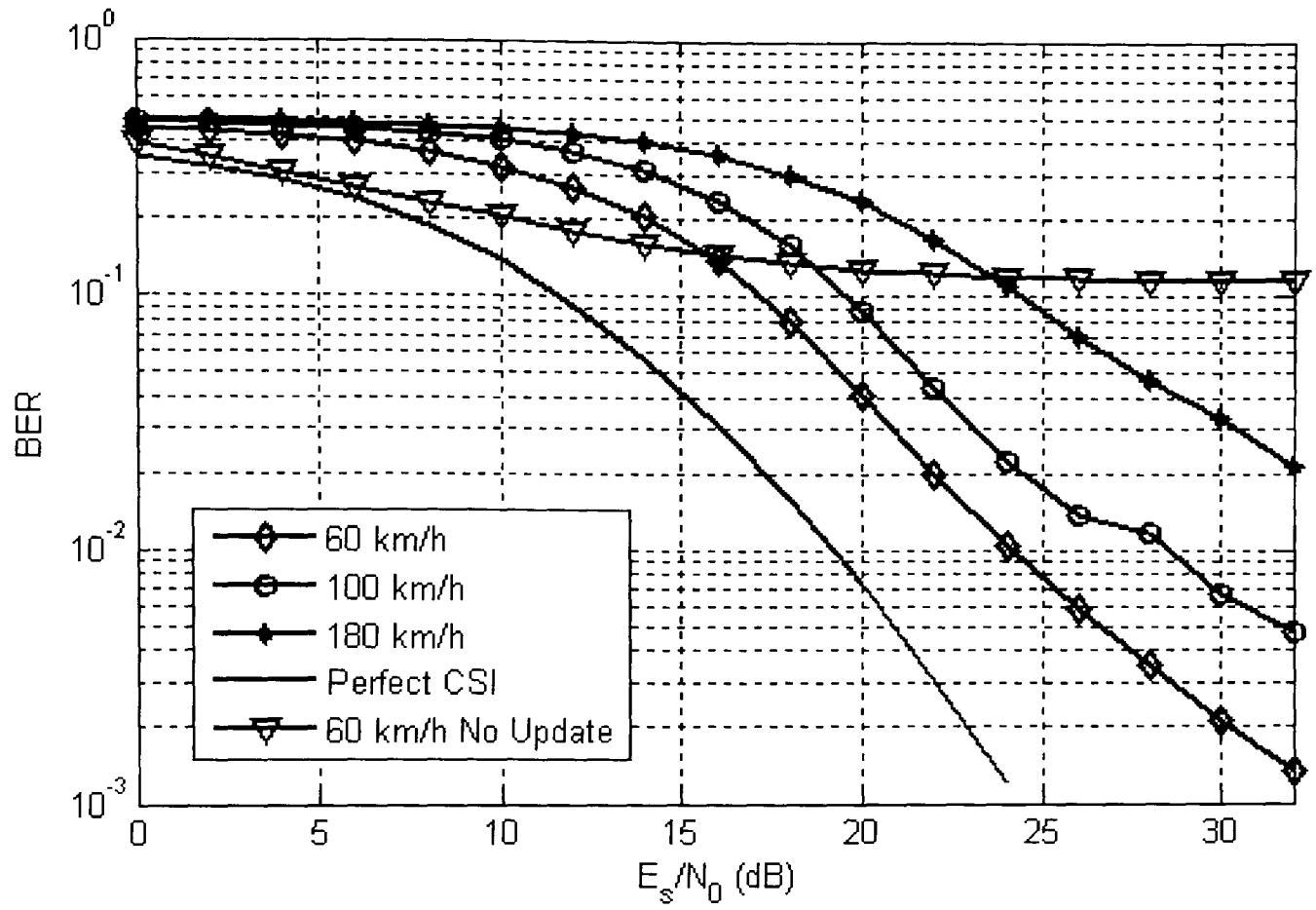

Figure (4.9): BER Performance of 3×4 VBLAST with and without Channel Update

4.3. ICI Analysis of VBLAST-OFDM

In this section we develop the mathematical analysis for VBLAST-OFDM and ICI. The results obtained in this section will be used to extend the channel update algorithm introduced in the previous section to OFDM and develop an ICI equalisation algorithm. Starting with a SISO-OFDM system, the transmitted signal ($s(n)$) is given by [37, 39]:

$$s(n)=\frac{1}{N}\sum_{p=0}^{N-1}d(p)e^{j\frac{2\pi}{N}p.n} \qquad (4.63)$$

Where N is the IFFT size, $d(p)$ is the data at subcarrier p and n is the time index. Throughout the rest of this chapter matrices and vectors are represented by bold upper and bold lower case characters respectively. The transmitted signal is convolved with the channel response to yield the received signal ($y(n)$):

$$y(n)=\sum_{l=0}^{M-1}s(n-l)z_l(n)+w(n) \qquad (4.64)$$

Here $z_l(n)$ is the channel response of path (tap) l at time index n, M is the number of channel paths, $M <$ Cyclic Prefix $< N$, and $w(n)$ is the noise sample. After the FFT, the received signal ($x(k)$) at subcarrier k is given by:

$$x(k)=\sum_{n=0}^{N-1} y(n).e^{-j\frac{2\pi}{N}k.n} = \sum_{n=0}^{N-1}\sum_{l=0}^{M-1} s(n-l)z_l(n).e^{-j\frac{2\pi}{N}k.n} + \sum_{n=0}^{N-1} w(n).e^{-j\frac{2\pi}{N}k.n}$$

$$=\frac{1}{N}\sum_{n=0}^{N-1}\sum_{l=0}^{M-1}\left(z_l(n).e^{-j\frac{2\pi}{N}k.n} \sum_{p=0}^{N-1} d(p)e^{j\frac{2\pi}{N}p.(n-l)} \right) + \sum_{n=0}^{N-1} w(n).e^{-j\frac{2\pi}{N}k.n}$$

$$=\frac{1}{N}\sum_{n=0}^{N-1}\sum_{p=0}^{N-1}\left(d(p)e^{j\frac{2\pi}{N}p.n} e^{-j\frac{2\pi}{N}k.n} \sum_{l=0}^{M-1} z_l(n).e^{-j\frac{2\pi}{N}p.l} \right) + \sum_{n=0}^{N-1} w(n).e^{-j\frac{2\pi}{N}k.n} \quad (4.65)$$

Let the N point FFT of the channel response $z_l(n)$ be:

$$h(n,p)=\sum_{l=0}^{N-1} z_l(n).e^{-j\frac{2\pi}{N}p.l} = \sum_{l=0}^{M-1} z_l(n).e^{-j\frac{2\pi}{N}p.l} \quad (4.66)$$

Where $z_l(n)$ is equal to 0 for $l \geq M$. Using (4.66) in (4.65), equation (4.65) reduces to:

$$x(k)=\frac{1}{N}\sum_{n=0}^{N-1}\sum_{p=0}^{N-1} d(p).h(n,p).e^{j\frac{2\pi}{N}n.p}.e^{-j\frac{2\pi}{N}n.k} + W(k) \quad (4.67)$$

$W(k)$ is the N point FFT of the noise samples. If the channel does not vary within the OFDM symbol we have:

$$h(n,p)=h(p) \quad (4.68)$$

Equation (4.67) then becomes:

$$x(k)=\frac{1}{N}\sum_{p=0}^{N-1} d(p).h(p)\sum_{n=0}^{N-1} e^{j\frac{2\pi}{N}n.(p-k)} + W(k) = \sum_{p=0}^{N-1} d(p).h(p).\delta(p-k) + W(k) \quad (4.69)$$

$\delta(p\text{-}k)$ is the shifted Dirac-Delta function. Therefore equation (4.69) reduces to:

$$x(k)=d(k)h(k)+W(k) \quad (4.70)$$

However if the channel experiences fast fading, equation (4.68) is not satisfied, we rewrite equation (4.67) as:

$$x(k)=\frac{1}{N}\sum_{n=0}^{N-1}d(k).h(n,k)+\frac{1}{N}\sum_{n=0}^{N-1}\sum_{\substack{p=0\\p\neq k}}^{N-1}d(p).h(n,p).e^{j\frac{2\pi}{N}n.(p-k)}+W(k) \tag{4.71}$$

$$x(k)=\frac{1}{N}d(k)\sum_{n=0}^{N-1}h(n,k)+\frac{1}{N}\sum_{\substack{p=0\\p\neq k}}^{N-1}d(p).\sum_{n=0}^{N-1}h(n,p).e^{j\frac{2\pi}{N}n.(p-k)}+W(k) \tag{4.72}$$

Note that the first term in the right hand side of (4.72) is the desired data multiplied by the channel response at frequency k averaged over the OFDM symbol duration while the second term is the ICI. Since the OFDM duration is usually small compared to the channel coherence time we can approximate the change in the channel with a linear equation as [40, 71]:

$$h(n,k)=h(0,k)+a(k)n \tag{4.73}$$

Where $h(0,k)$ is the channel response at the beginning of the OFDM symbol and $a(k)$ is the change (slope) in channel response at frequency k in one symbol period (T_s) which we assume constant for the duration of an OFDM symbol. This approximation is valid for $f_D \times T_{OFDM} < 0.1$, where T_{OFDM} is the OFDM symbol duration and f_D the Doppler shift [40, 71]. Using (4.73) in (4.72) we get:

$$x(k)=\frac{1}{N}d(k)\sum_{n=0}^{N-1}[h(0,k)+a(k)n]+\frac{1}{N}\sum_{\substack{p=0\\p\neq k}}^{N-1}d(p).\sum_{n=0}^{N-1}[h(0,p)+a(p)n].e^{j\frac{2\pi}{N}n.(p-k)}+W(k) \tag{4.74}$$

$$x(k)=d(k)\left[h(0,k)+\frac{N-1}{2}a(k)\right]+\frac{1}{N}\sum_{\substack{p=0\\p\neq k}}^{N-1}d(p).h(0,p).\delta(p-k)$$
$$+\frac{1}{N}\sum_{\substack{p=0\\p\neq k}}^{N-1}a(p)d(p).\sum_{n=0}^{N-1}ne^{j\frac{2\pi}{N}n.(p-k)}+W(k) \tag{4.75}$$

$$x(k)=d(k)\left[h(0,k)+\frac{N-1}{2}a(k)\right]+\frac{1}{N}\sum_{\substack{p=0\\p\neq k}}^{N-1}a(p)d(p).\sum_{n=0}^{N-1}n.e^{j\frac{2\pi}{N}n.(p-k)}+W(k) \tag{4.76}$$

Equation (4.76) can be generalised for an $A\times B$ MIMO system as:

$$x_r(k)=\sum_{i=1}^{A}\left[d_i(k)\left[h_{ri}(0,k)+\frac{N-1}{2}a_{ri}(k)\right]+\frac{1}{N}\sum_{\substack{p=0\\p\neq k}}^{N-1}a_{ri}(p)d_i(p).\sum_{n=0}^{N-1}n.e^{j\frac{2\pi}{N}n.(p-k)}\right]+W_r(k) \quad (4.77)$$

The subscript i represents the transmit antenna and r the receive antenna. Let

$$C_{pk}=\frac{1}{N}\sum_{n=0}^{N-1}n.e^{j\frac{2\pi}{N}n(p-k)} \quad (4.78)$$

The value of C_{pk} affects the contribution of the subcarriers in ICI. Figure (4.10) and (4.11) show the imaginary and absolute square value of C_{pk} for k = 30 and 64-point FFT. The value of k shifts the curves to the left or right without changing the shape. The real part of C_{pk} was found to be –½ regardless of the subcarrier index except for $p = k$, i.e. the desired subcarrier, where its value is (N-1)/2 as can be seen from equation (4.76). The contribution of ICI mainly comes from the few adjacent subcarriers as can be seen from figures (4.10) and (4.11). By cancelling or equalising the ICI contribution of these subcarriers the interference can be reduced thus improving the performance of the OFDM system.

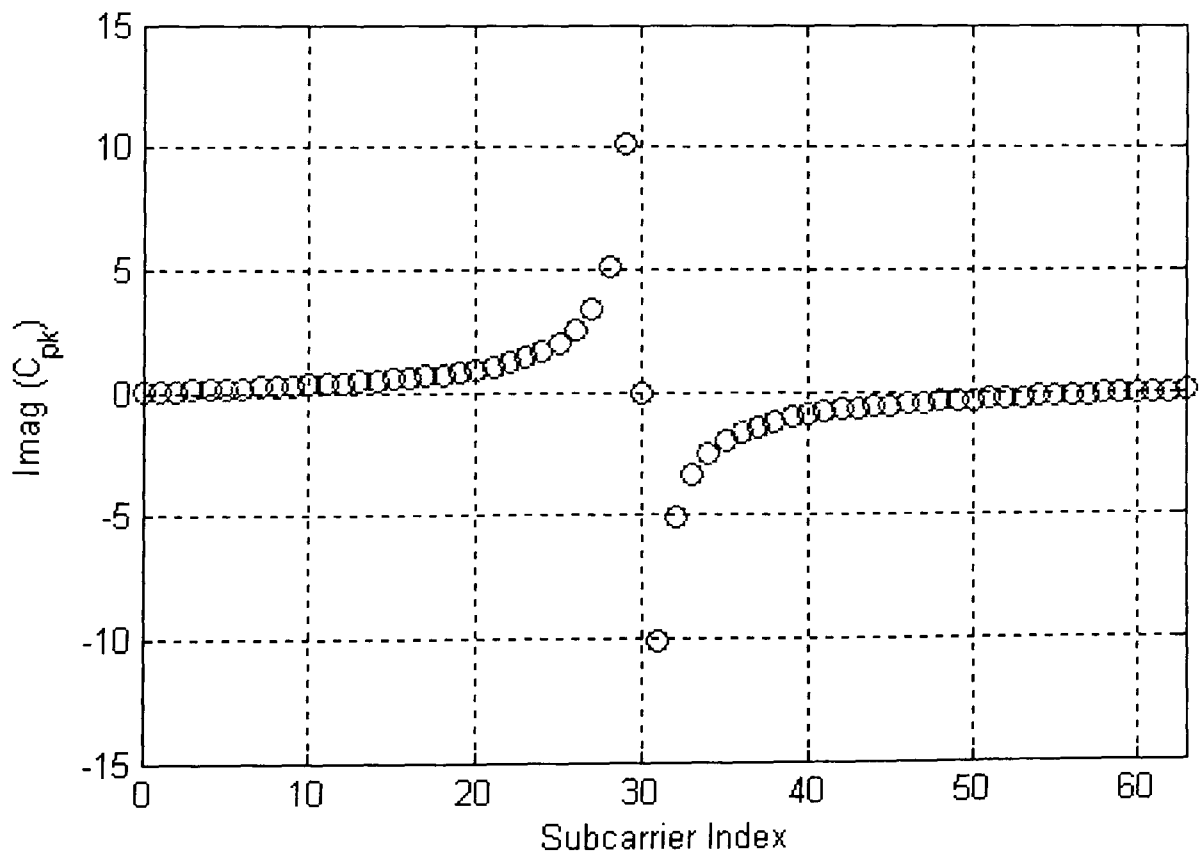

Figure (4.10): Imaginary Part of Subcarrier Contribution (C_{pk}) to ICI

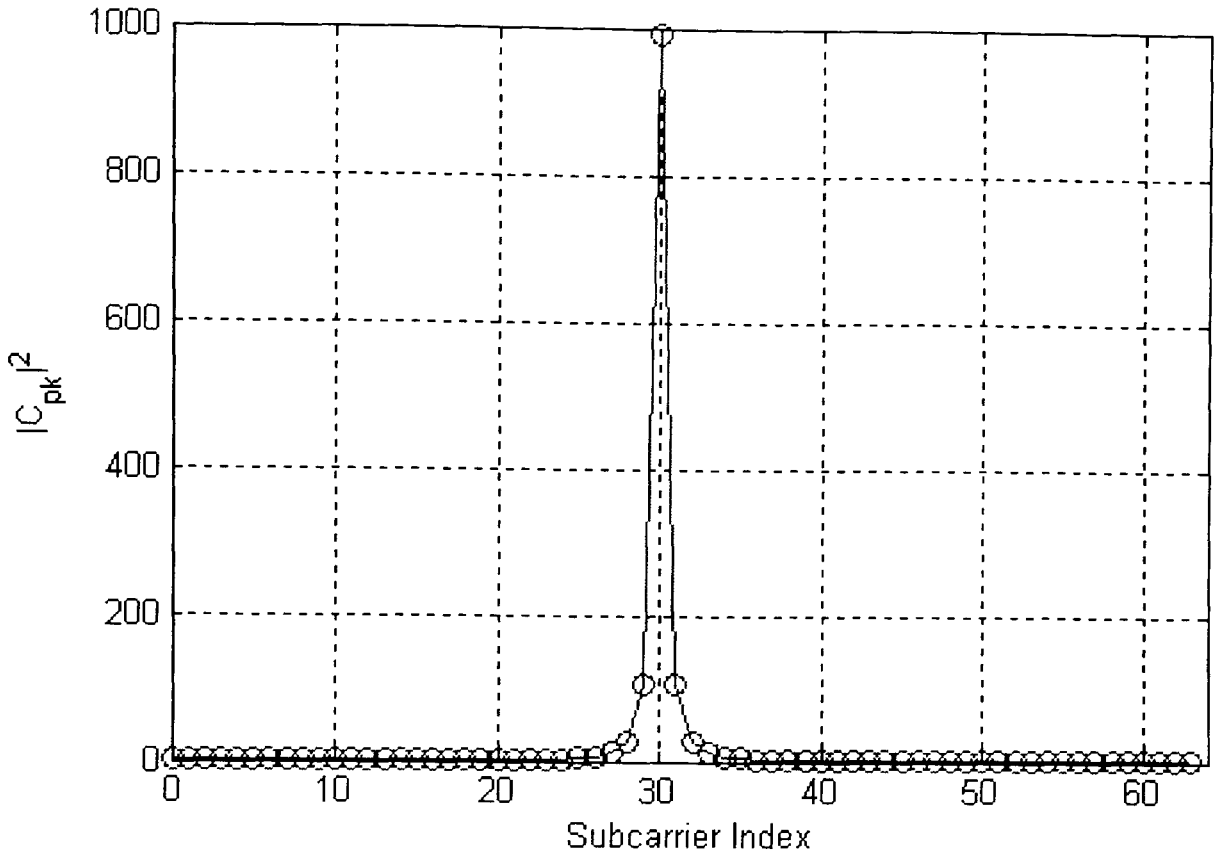

Figure (4.11): $|C_{pk}|^2$ vs. Subcarrier Index for 64 Subcarriers and $k = 30$

The ICI power is plotted in figure (4.12) for a single transmitting antenna, fixed bandwidth and various FFT sizes. As can be seen the size of the FFT has a major impact on performance. At high speeds using a small number of subcarriers gives better performance since the OFDM symbol duration is short, leading to smaller channel variation within the OFDM symbol, and fewer subcarriers generate less interference. Both factors reduce the ICI power. The use of a small FFT size, however, leads to wider bandwidth per subcarrier and, if the coherence bandwidth of the channel is small, the subcarriers may experience frequency selective fading and inter-symbol-inference (ISI) instead of flat fading. For low speeds and fixed links using more subcarriers is feasible to ensure a flat fading channel and possibly to provide Orthogonal Frequency Division Multiple Access (OFDMA) to serve a larger number of users. The number of transmit antennas (A) will also cause an increase in the ICI power by $10\times\log_{10}(A)$ as shown in figure (4.13) since the power in the interfering subcarriers increases.

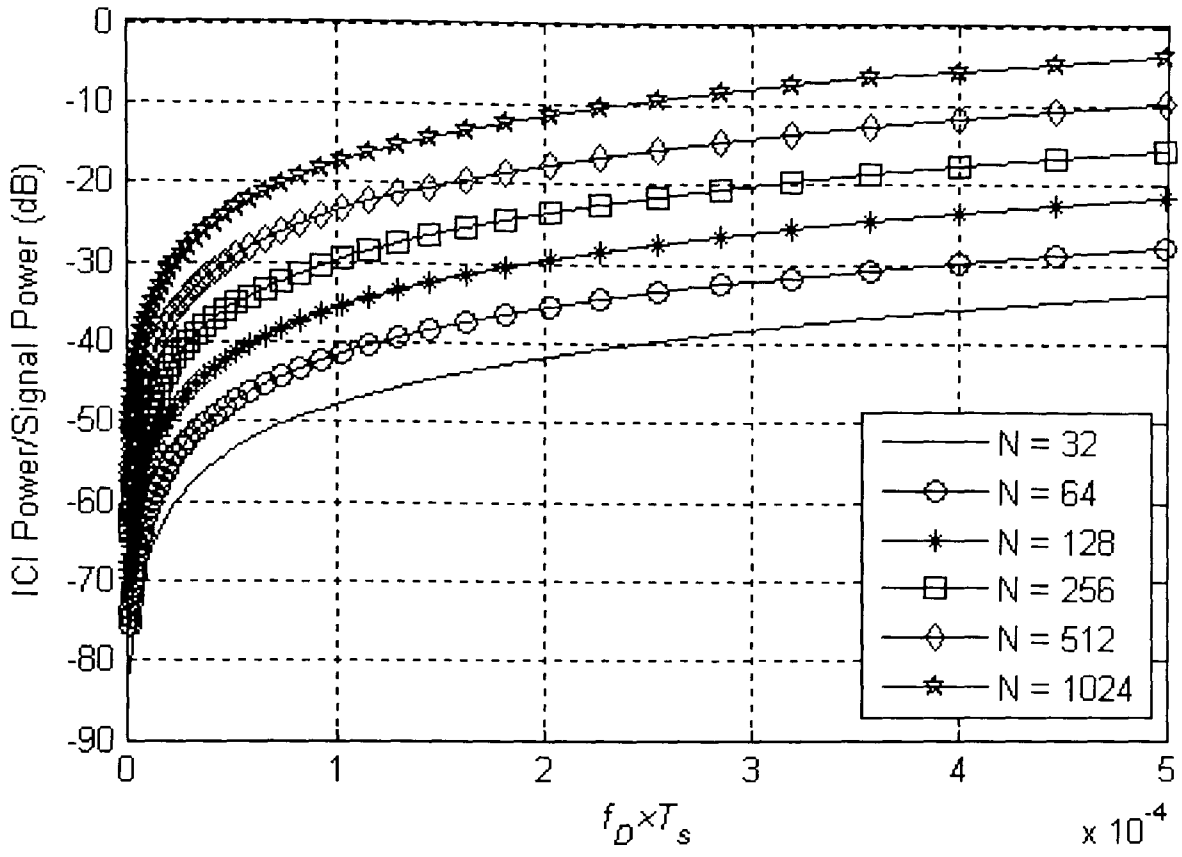

Figure (4.12): SISO ICI to Signal Power Ratio vs. Normalised Doppler Shift

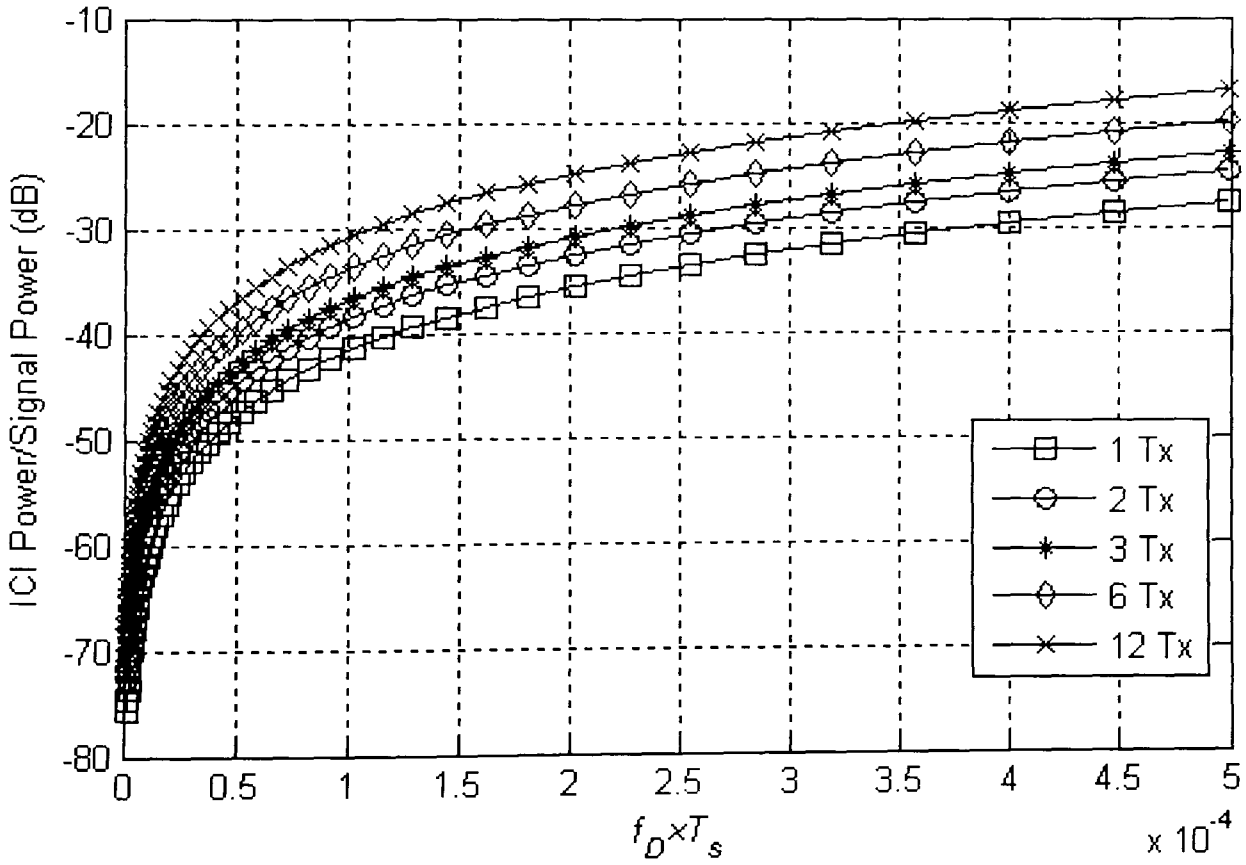

Figure (4.13): MIMO ICI to Signal Power Ratio vs. Normalised Doppler Shift, $N = 64$

ICI becomes dominant at high SNR leading to an error floor for large Doppler shifts even with perfect CSI knowledge. Figure (4.14) shows the BER performance of 2×4 VBLAST-OFDM using QPSK modulation, 10MHz bandwidth, 512 subcarriers and perfect channel knowledge. As can be seen the error floor due to ICI increases with speed and limits the performance of the system. Figure (4.15) compares the performance of the same system with 64, 128, 256 and 512 subcarriers and a speed of 180 km/h. We observe from the figure that using a smaller number of subcarriers improves the BER performance of the system. The analysis of ICI in VBLAST-OFDM shows that it becomes necessary to use ICI equalisation/cancellation at high speeds, with large number of subcarriers and/or large number of transmitting antennas to eliminate the error floor.

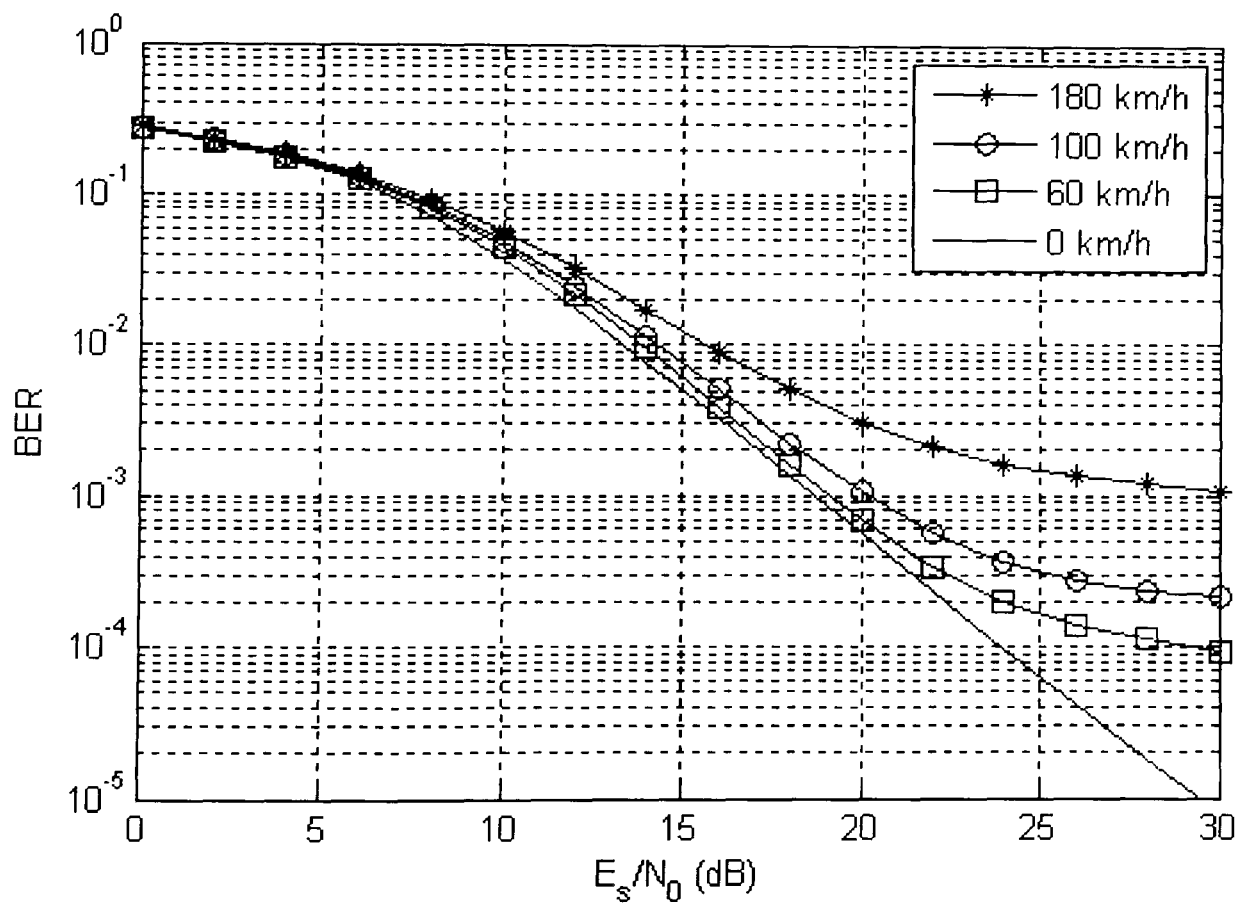

Figure (4.14): BER of 2×4 VBLAST-OFDM with 512 Subcarriers (Perfect CSI)

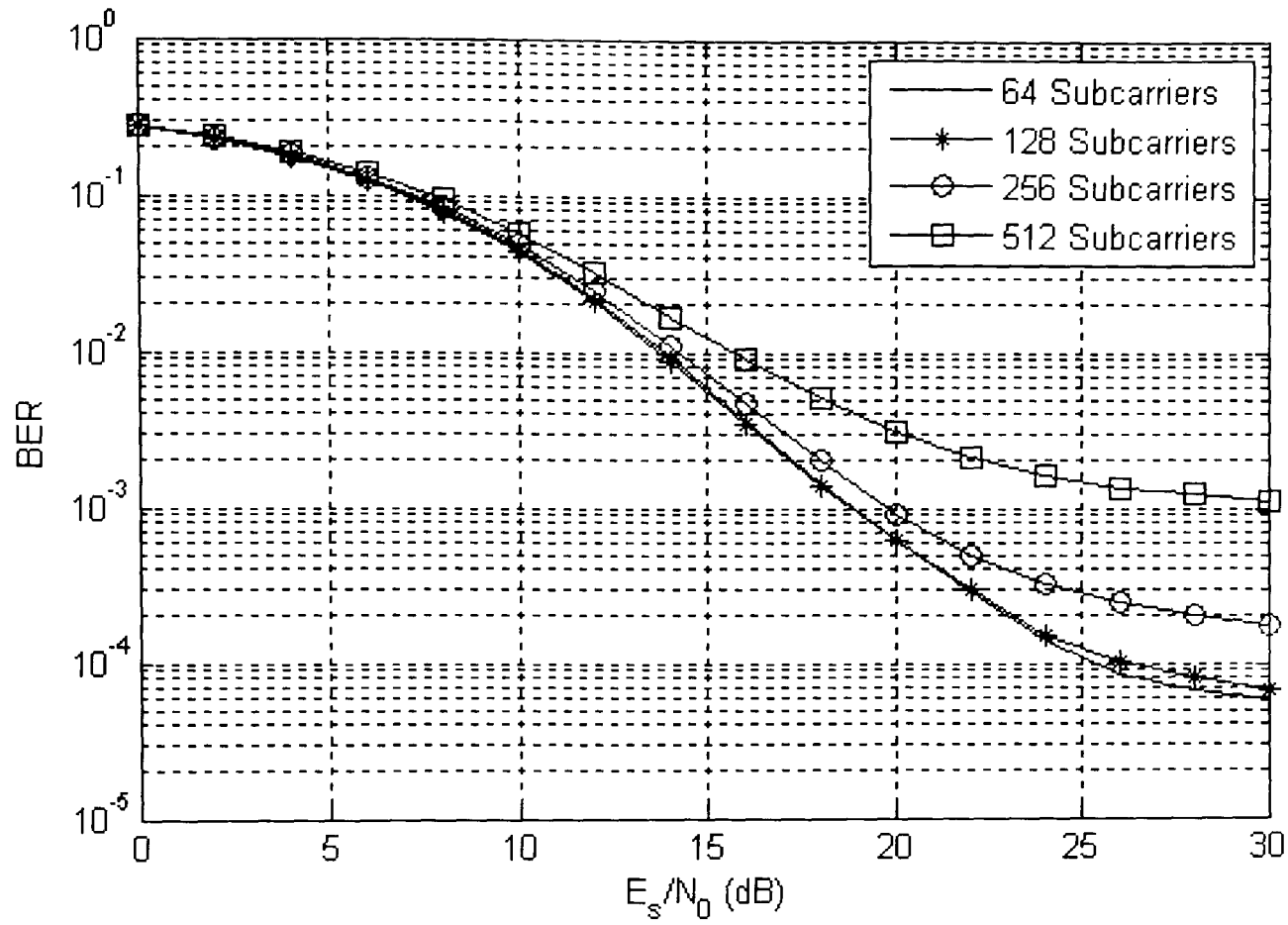

Figure (4.15): BER of 2×4 VBLAST-OFDM for 180 km/h (Perfect CSI)

4.4. Extension of the Update Algorithm to VBLAST-OFDM

In this section we extend the channel update algorithm introduced in section (4.2) to VBLAST-OFDM. Let:

$$h_{ri}(k)=h_{ri}(0,k)+\frac{N-1}{2}a_{ri}(k) \tag{4.79}$$

Substituting equations (4.79) and (4.78) in (4.77) we may express the signal received by antenna r at subcarrier k in VBLAST-OFDM by:

$$x_r(k)=\sum_{i=1}^{A}\left[d_i(k)h_{ri}(k)+\frac{1}{N}\sum_{\substack{p=0\\p\neq k}}^{N-1}a_{ri}(p)d_i(p)C_{pk}\right]+W_r(k) \tag{4.80}$$

The receiver then with knowledge of an estimate ($\hat{h}_{ri}(k)$) of $h_{ri}(k)$ decodes the OFDM symbol using the VBLAST algorithm and, assuming correct decoding, formulates the term:

$$x_r(F,k)-\sum_{i=1}^{A}\hat{h}_{ri}(F,k)d_i(F,k)=\sum_{i=1}^{A}\left[d_i(F,k)\varepsilon_{ri}(F,k)+\frac{1}{N}\sum_{\substack{p=0\\p\neq k}}^{N-1}a_{ri}(F,p)d_i(F,p)C_{pk}\right]+W_r(F,k) \qquad (4.81)$$

Where $\varepsilon_{ri}(F, k)$ is the error between the estimated and exact channel response for transmit antenna i and receive antenna r at subcarrier k. The variable F (OFDM symbol index) was introduced to indicate that these variables change between different OFDM symbols. Define $\Delta\mathbf{H}(F, k)$ as:

$$\Delta\mathbf{H}(F,k)=\left[\mathbf{x}(F,k)-\hat{\mathbf{H}}(F,k)\mathbf{s}(F,k)\right]\times\mathbf{s}^{+}(F,k) \qquad (4.82)$$

Where $\mathbf{x}(F, k)$ is the length B column vector of received signal, $\mathbf{s}(F, k)$ is the length A column vector of transmitted symbols, $\mathbf{s}^{+}(F, k)$ is the length A row vector of the reciprocal of the decoded symbols and $\hat{\mathbf{H}}(F, k)$ is the estimated channel matrix, all at subcarrier k of OFDM symbol F. The element $\Delta h_{ri}(F, k)$ of the matrix $\Delta\mathbf{H}(F, k)$ at any column (transmit antenna) i and row (receive antenna) r is then:

$$\Delta h_{ri}(F,k)=\varepsilon_{ri}(F,k)+\sum_{\substack{b=1\\b\neq i}}^{A}\frac{d_b(F,k)}{d_i(F,k)}\varepsilon_{rb}(k)+\sum_{b=1}^{A}\left(\frac{1}{N}\sum_{\substack{p=0\\p\neq k}}^{N-1}a_{rb}(F,p)\frac{d_b(F,p)}{d_i(F,k)}C_{pk}\right)+\frac{W_r(F,k)}{d_i(F,k)} \qquad (4.83)$$

Assuming i.i.d fading and noise for the antennas, the ith column vector ($\hat{\mathbf{H}}_i(F, k)$) of the estimated channel matrix ($\hat{\mathbf{H}}(F, k)$) is updated to produce the new estimate ($\hat{\mathbf{H}}_i(F+1, k)$) using the equation:

$$\hat{\mathbf{H}}_i(F+1,k)=\hat{\mathbf{H}}_i(F,k)+\gamma_i\times\Delta\mathbf{H}_i(F,k) \qquad (4.84)$$

The parameter γ_i is chosen to minimise the mean square error between the exact and estimated channel response, $|\mathbf{H}_i(F+1,k)-\hat{\mathbf{H}}_i(F+1,k)|^2$. Assuming equal average power for each subcarrier and transmit antenna, the optimum value of γ_i for transmit antenna i (γ_i^{opt}) is obtained by differentiating the mean square error and setting the derivative equal to zero to obtain the minimum mean square error. Using this method, the optimum update parameter (γ_i^{opt}) is calculated as (see Appendix I):

$$\gamma_i^{opt} = \sqrt[3]{\frac{8[\pi f_d T_s (N+CP)]^2}{N_T}} \tag{4.85}$$

$$N_T = \sum_{\substack{b=1 \\ b\neq i}}^{A} \sigma_b^2(k) + 2A(2\pi f_d T_s)^2 \sum_{\substack{p=0 \\ p\neq k}}^{N-1} |C_{pk}|^2 + \frac{N_{oise}}{P} \tag{4.86}$$

$$\sigma_b^2(k) = 2\left[\frac{\pi f_d T_s (N+CP)}{\gamma_b^{opt}}\right]^2 + \frac{\gamma_b^{opt}}{2-\gamma_b^{opt}} N_T \tag{4.87}$$

Where P is the symbol power per antenna, N_{oise} is the noise power, T_s is the symbol rate, f_D is the maximum Doppler shift, and CP is the length of the cyclic prefix.

γ_i^{opt} is calculated recursively by first setting the MSE ($\sigma_b^2(k)$) to zero for all $b \in \{1,...,A\}$ and calculating an initial γ_i^{opt}. This calculated γ_i^{opt} is then used to update $\sigma_i(k)$ and the process is repeated again. The algorithm converges very quickly. Figures (4.16) and (4.17) show the update parameter for 2 and 3 transmitting antennas using 64-OFDM and 10MHz. Note that at high SNR and high speed the update parameter remains fixed due to the ICI.

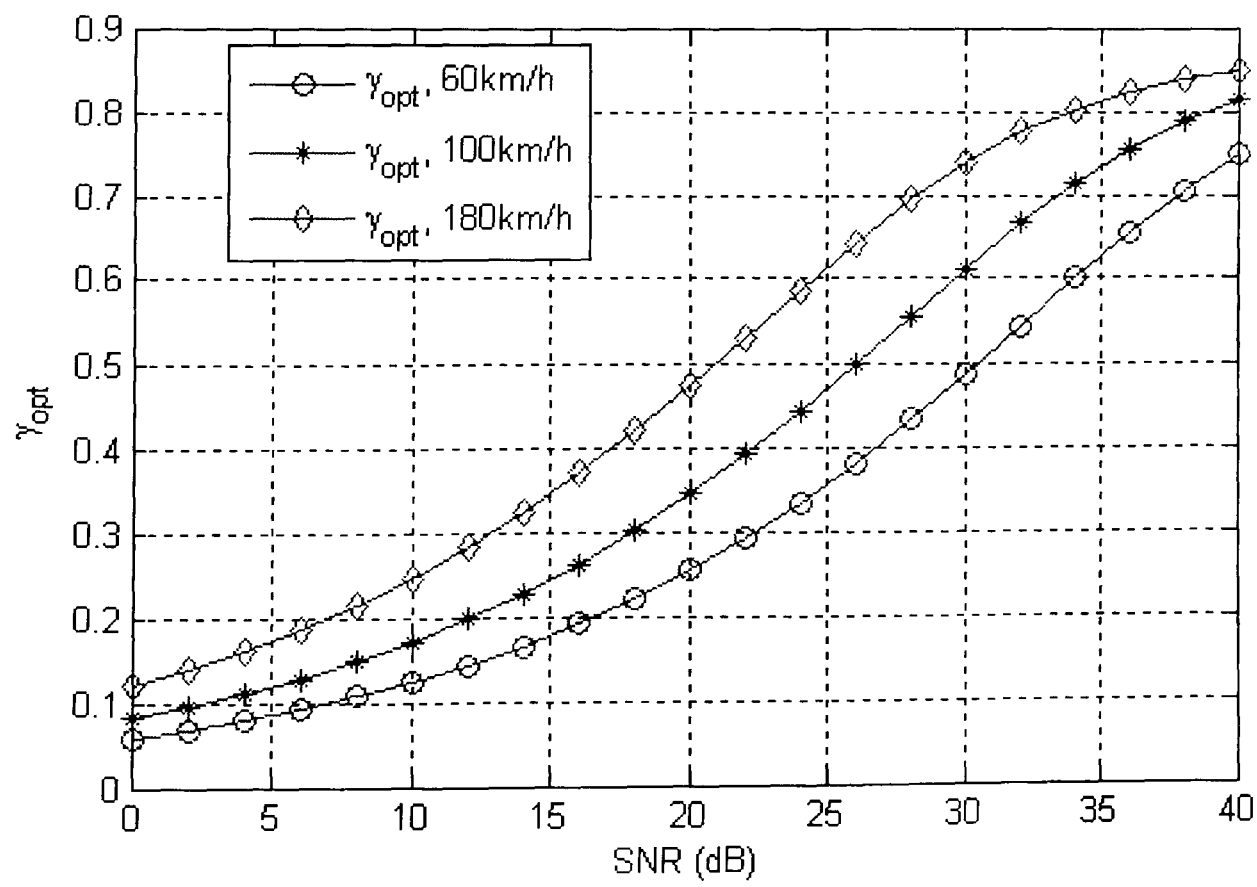

Figure (4.16): γ_{opt} for 2×4 VBLAST-OFDM with 64 Subcarriers

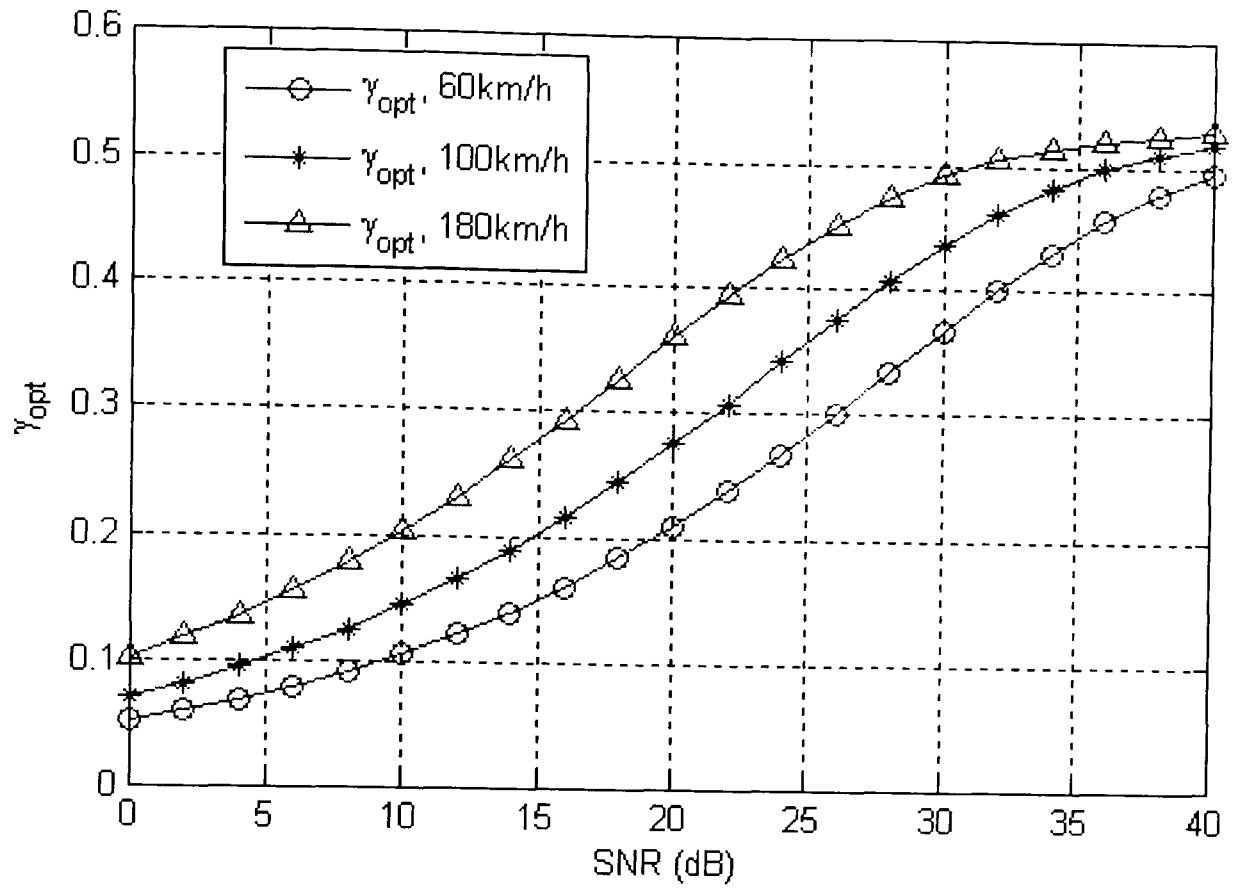

Figure (4.17): γ_{opt} for 3×4 VBLAST-OFDM with 64 Subcarriers

At high SNR and high Doppler shift, VBLAST-OFDM systems become dominated by ICI. Looking at equation (4.80), the interference can be reduced by cancelling the contribution of detected streams and/or by equalisation.

4.5. ICI Equalisation

In [71] an equalisation technique to reduce the effects of ICI in single antenna systems was introduced. An estimate of the change (slope) of the channel is calculated and then used to formulate a channel matrix that includes the ICI contribution of adjacent subcarriers. The signal is then decoded using the inverse of this matrix. In [72] a two steps receiver was proposed. First an initial estimate of the transmitted symbols is obtained by a conventional single tap equaliser. A decision feedback filter is then used to cancel the ICI from the subcarriers before decoding the signal again. The values of $a(F, k)$ are estimated in [71] and [72] by sending an impulse at the end of the OFDM symbol and calculating the difference in channel response before and after the OFDM symbol. Sending an impulse after the OFDM symbol wastes resources and is not

suitable for MIMO systems since each transmit antenna will need a separate impulse. We adapt the equalisation scheme derived in [71] and extend it to VBLAST. However, instead of sending an impulse, we use our proposed channel update algorithm and the linear assumption of the change in channel, equation (4.73), to calculate an estimate of the slope $a_{ri}(F, k)$. This estimate is then used to formulate a channel matrix analogous to that of [71]. By decoding the signal using this matrix, the VBLAST decoding algorithm reduces ICI because the pseudoinverse process eliminates the contribution of the other columns of the matrix [44]. Equation (4.80) can be written in matrix form as:

$$\mathbf{x} = \mathbf{H}' \times \mathbf{d} + \mathbf{w} \tag{4.88}$$

$\mathbf{x}$ is the vector of received signal, $\mathbf{d}$ is the vector of transmitted symbols, $\mathbf{w}$ is the noise vector and $\mathbf{H}'$ is the channel matrix with elements:

$$h'(r + k \times B, i + p \times A) = \begin{cases} h_{ri}(F,k), & if\ p = k \\ a_{ri}(F,p).C_{pk}, & if\ p \neq k \end{cases} \tag{4.89}$$

for receive antenna r ($=\{1,...,B\}$), transmit antenna i ($=\{1,...,A\}$), transmit subcarrier p, receive subcarrier k (p and k $=\{1,...,N-1\}$) and frame index F. An estimate, $\hat{a}_{ri}(F, k)$, of the slope $a_{ri}(F, k)$ is found by:

$$\hat{a}_{ri}(F,k) = \frac{\hat{h}_{ri}(F,k) - \hat{h}_{ri}(F-1,k)}{N + CP} = \frac{\gamma_i^{opt} \times \Delta h_{ri}(F,k)}{N + CP} \tag{4.90}$$

Let k be the subcarrier to be decoded and q the number of subcarrier pairs, one to left and another to the right of k, to be equalised. Our equalisation scheme assumes the ICI contribution from subcarriers beyond q is zero. Define the matrix $\hat{\mathbf{H}}'(k)$ with elements:

$$G(r + v.B, i + p.A) = G_{ri}(k + v - q, k + p - q) = \begin{cases} \hat{h}_{ri}(F, k + v - q), & if\ \ v = p \\ a_{ri}(F,p).C_{k+p-q,k+v-q}, & if\ \ v \neq p \end{cases} \tag{4.91}$$

v, p $=\{0,...,2q\}$, $0 \leq k\text{-}q$, $k\text{+}q \leq N\text{-}1$ and $G(m,n)$ is the element at row m and column n. The matrix $\hat{\mathbf{H}}'(k)$, which is an estimated subset of $\mathbf{H}'$ in (4.88), is built by first fixing r, v and p and varying i. When i reaches its maximum (A), p is incremented and i is reset to 1. After all the possible combinations of i and p are considered, v is increased and i and

p are reset. When all the v, p and i combinations are calculated, r is incremented. This process is repeated until all the r, v, p, i combinations are considered to yield:

$$\hat{\mathbf{H}}'(k)=\begin{bmatrix} G_{11}(k-q,k-q) & \cdots & G_{1A}(k-q,k-q) & G_{11}(k-q,k-q+1) & \cdots & G_{1A}(k-q,k+q) \\ \vdots & \ddots & \vdots & \vdots & \ddots & \vdots \\ G_{B1}(k-q,k-q) & \cdots & G_{BA}(k-q,k-q) & G_{B1}(k-q,k-q+1) & \cdots & G_{BA}(k-q,k+q) \\ \vdots & \ddots & \vdots & \vdots & \ddots & \vdots \\ G_{11}(k,k-q) & \cdots & G_{1A}(k,k-q) & G_{11}(k,k-q+1) & \cdots & G_{1A}(k,k+q) \\ \vdots & \ddots & \vdots & \vdots & \ddots & \vdots \\ G_{B1}(k,k-q) & \cdots & G_{BA}(k,k-q) & G_{B1}(k,k-q+1) & \cdots & G_{BA}(k,k+q) \\ \vdots & \ddots & \vdots & \vdots & \ddots & \vdots \\ G_{B1}(k+q,k-q) & \cdots & G_{BA}(k+q,k-q) & G_{B1}(k+q,k-q+1) & \cdots & G_{BA}(k+q,k+q) \end{bmatrix} \quad (4.92)$$

The vector of received signal ($\mathbf{x}'(k)$) used for decoding is given by:

$$\mathbf{x}'(k)=[x_1(k-q) \;\cdots\; x_B(k-q) \;\; x_1(k-q+1) \;\cdots\; x_1(k) \;\cdots\; x_B(k+q)]^T \quad (4.93)$$

Let $\mathbf{d}'$(k) be the vector of symbols transmitted at subcarriers k-q to k+q:

$$\mathbf{d}'(k)=[d_1(k-q) \;\cdots\; d_A(k-q) \;\; d_1(k-q+1) \;\cdots\; d_1(k) \;\cdots\; d_A(k+q)]^T \quad (4.94)$$

Using equations (4.90) to (4.94) we approximate equation (4.88) by:

$$\mathbf{x}'(k)=\hat{\mathbf{H}}'(k)\mathbf{d}'(k) \quad (4.95)$$

Clearly left multiplying (4.95) by the inverse (or pseudoinverse) of $\hat{\mathbf{H}}'(k)$ provides an estimate of $\mathbf{d}'(k)$ while eliminating the ICI from the adjacent q subcarriers. Another approach is to use VBLAST. VBLAST decodes the symbols recursively [44], therefore we can decode only the symbols at subcarrier k. Separate $\hat{\mathbf{H}}'(k)$ matrices should be formed for different values of k. Using higher values of q reduces ICI by taking more subcarriers into account but also increases the size of the $\hat{\mathbf{H}}'(k)$ matrix, matrix size = $(2q+1)B\times(2q+1)A$, and hence, the complexity of the pseudoinverse.

4.6. Performance Evaluation

We simulated 2×4 and 3×4 VBLAST-OFDM systems with the elliptical channel model, 10MHz bandwidth, 64 subcarriers OFDM and radio frequency 5.9GHz as specified in the ASTM standard for VANET [16]. In the simulations perfect CSI is provided to the receiver every 10 OFDM symbols. This CSI is then either held constant

(no update case) or updated every OFDM symbol using the derived algorithm (with update case). For the perfect CSI case, the perfect channel information at the beginning of the OFDM symbol is provided to the receiver every OFDM symbol.

Figures (4.18) and (4.19) show the BER performance. As can be seen at low SNR the performance without update is better than when using the update algorithm. This is due to the high noise power which affects the algorithm in two ways. First the high noise is directly affecting the channel estimate of the update algorithm, second at low SNR the probability of error is higher, and since the algorithm assumes correct decoding, the estimate of the channel will not be accurate. At high SNR, the update algorithm has higher performance. For 40dB SNR the BER performance of the channel update algorithm is superior by approximately 10^{-1} for 3×4 VBLAST and 10^{-2} for 2×4 VBLAST compared to the no update case. Without update, the BER drops as the speed increases due to the change in the channel and the ICI. The proposed channel update tracks the changes in the channel and takes into account the ICI, thus reducing the error and improving the BER. Both methods (i.e. with and without update) however experience an error floor due to ICI. Similar performance is observed from figures (4.20) and (4.21) which use training sequences to obtain the initial channel estimate. In the optimum training sequence used, each antenna transmits in a unique set of subcarriers as proposed in [59, 63]. This is used at the receiver to estimate the channel using only one OFDM symbol. The channel tracking algorithm is then employed to track the channel for the next 10 OFDM symbols after which another training sequence is sent. The sequences used are periodic and shown in equation (4.96) for 2 antennas and (4.97) for 3 antennas. α_2 and α_3 are normalised to maintain equal total transmitting power, $\sum_{p=0}^{N-1}|\alpha_i|^2 = N$, $i = 2$ or 3.

$$\mathbf{S}_2 = \begin{bmatrix} 0 & \alpha_2 & 0 & 0 & 0 & \alpha_2 & 0 & 0 & 0 & \alpha_2 & 0 & 0 & 0 & \alpha_2 & 0 & 0 & \cdots \\ 0 & 0 & \alpha_2 & 0 & 0 & 0 & \alpha_2 & 0 & 0 & 0 & \alpha_2 & 0 & 0 & 0 & \alpha_2 & 0 & \cdots \end{bmatrix} \quad (4.96)$$

$$\mathbf{S}_3 = \begin{bmatrix} 0 & \alpha_3 & 0 & 0 & \alpha_3 & 0 & 0 & 0 & 0 & \alpha_3 & 0 & 0 & \alpha_3 & 0 & 0 & 0 & \cdots \\ 0 & 0 & \alpha_3 & 0 & 0 & \alpha_3 & 0 & 0 & 0 & 0 & \alpha_3 & 0 & 0 & \alpha_3 & 0 & 0 & \cdots \\ 0 & 0 & 0 & \alpha_3 & 0 & 0 & \alpha_3 & 0 & 0 & 0 & 0 & \alpha_3 & 0 & 0 & \alpha_3 & 0 & \cdots \end{bmatrix} \quad (4.97)$$

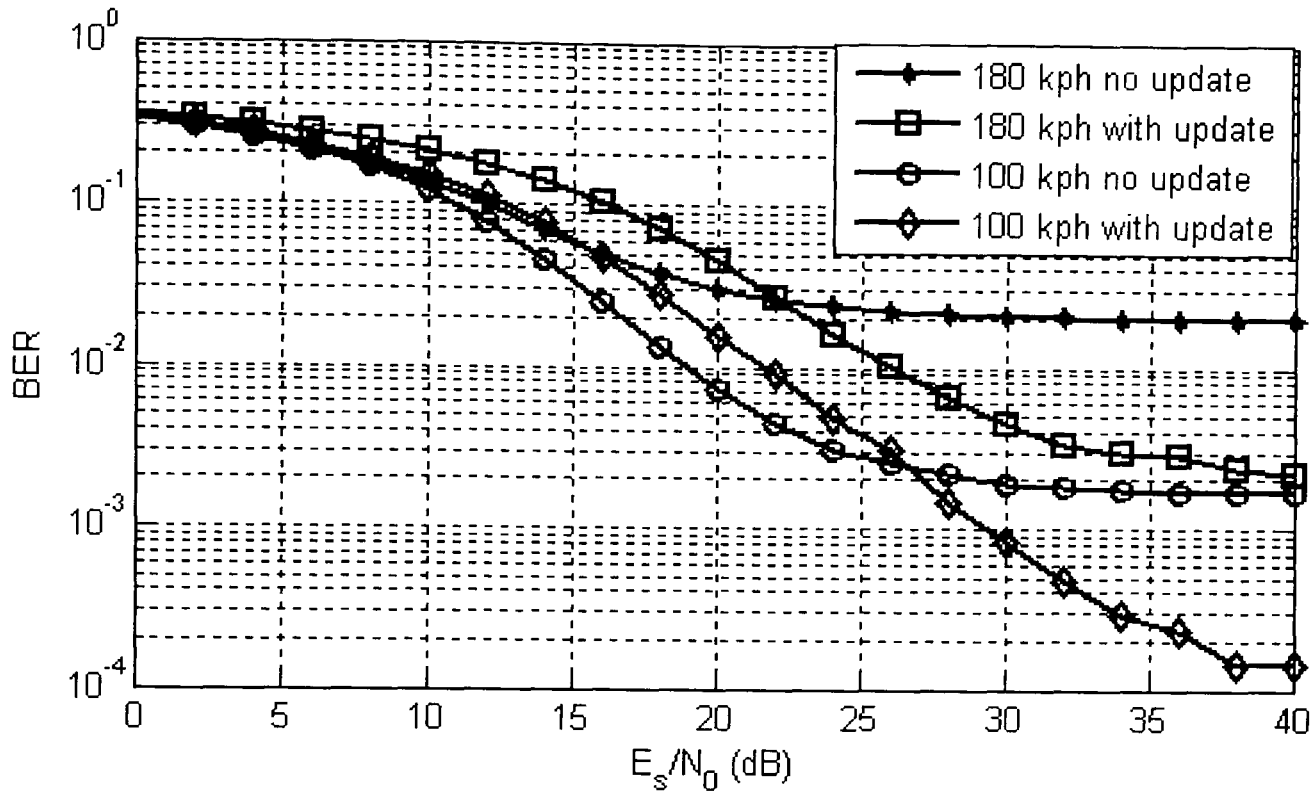

Figure (4.18): BER Performance of 3×4 VBLAST with and without Channel Update

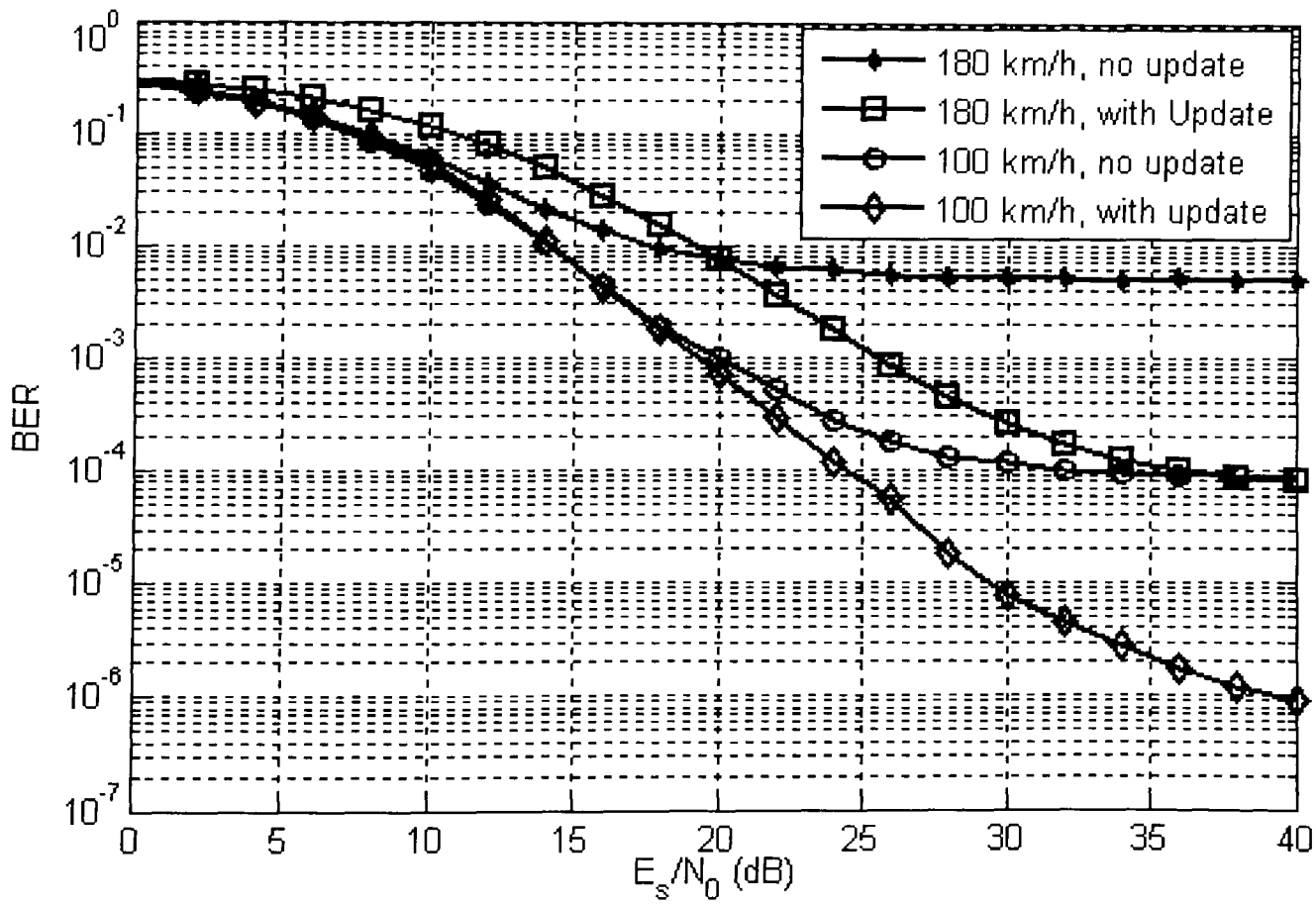

Figure (4.19): BER Performance of 2×4 VBLAST with and without Channel Update

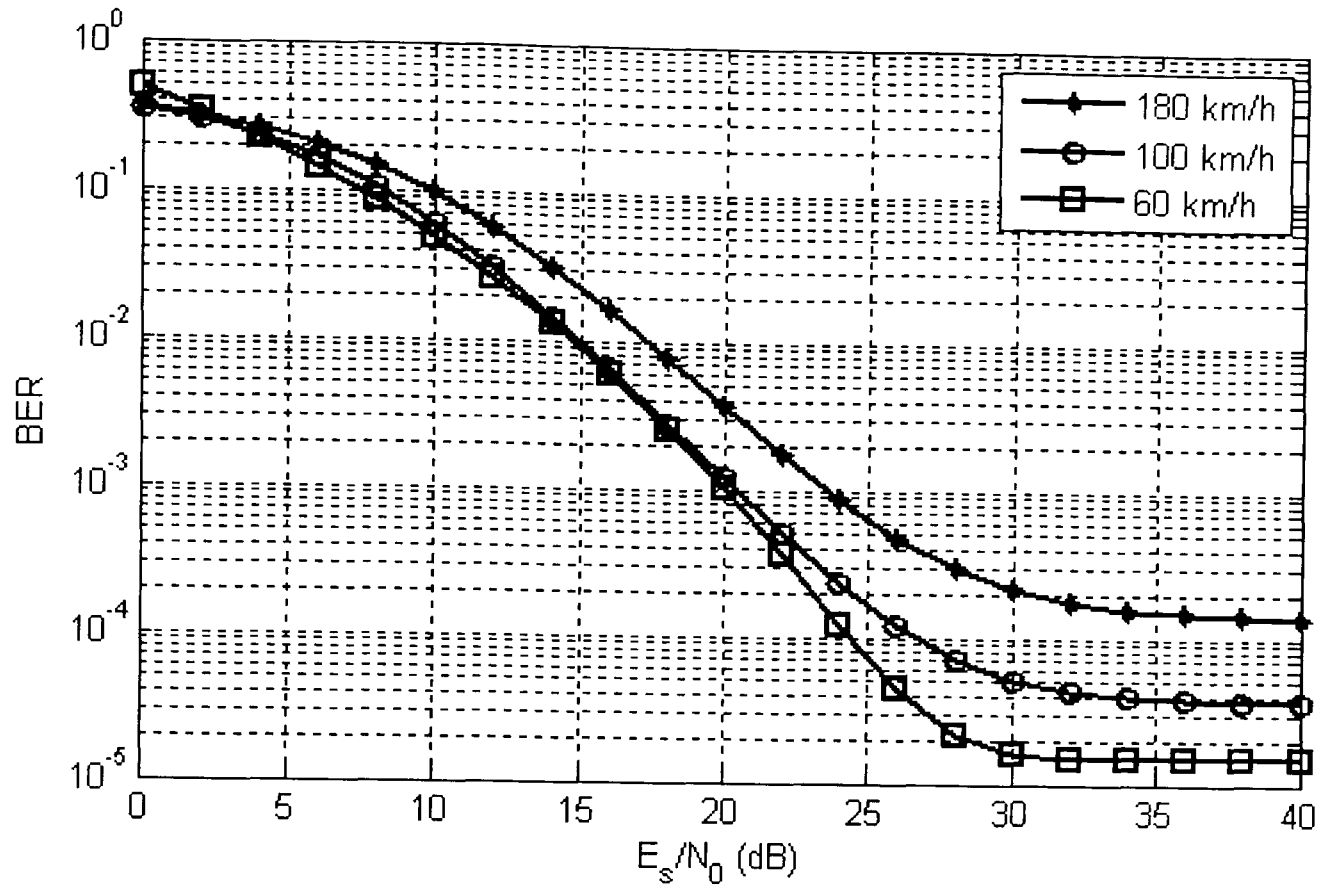

Figure (4.20): BER of 2×4 VBLAST with Channel Update and Training Sequence

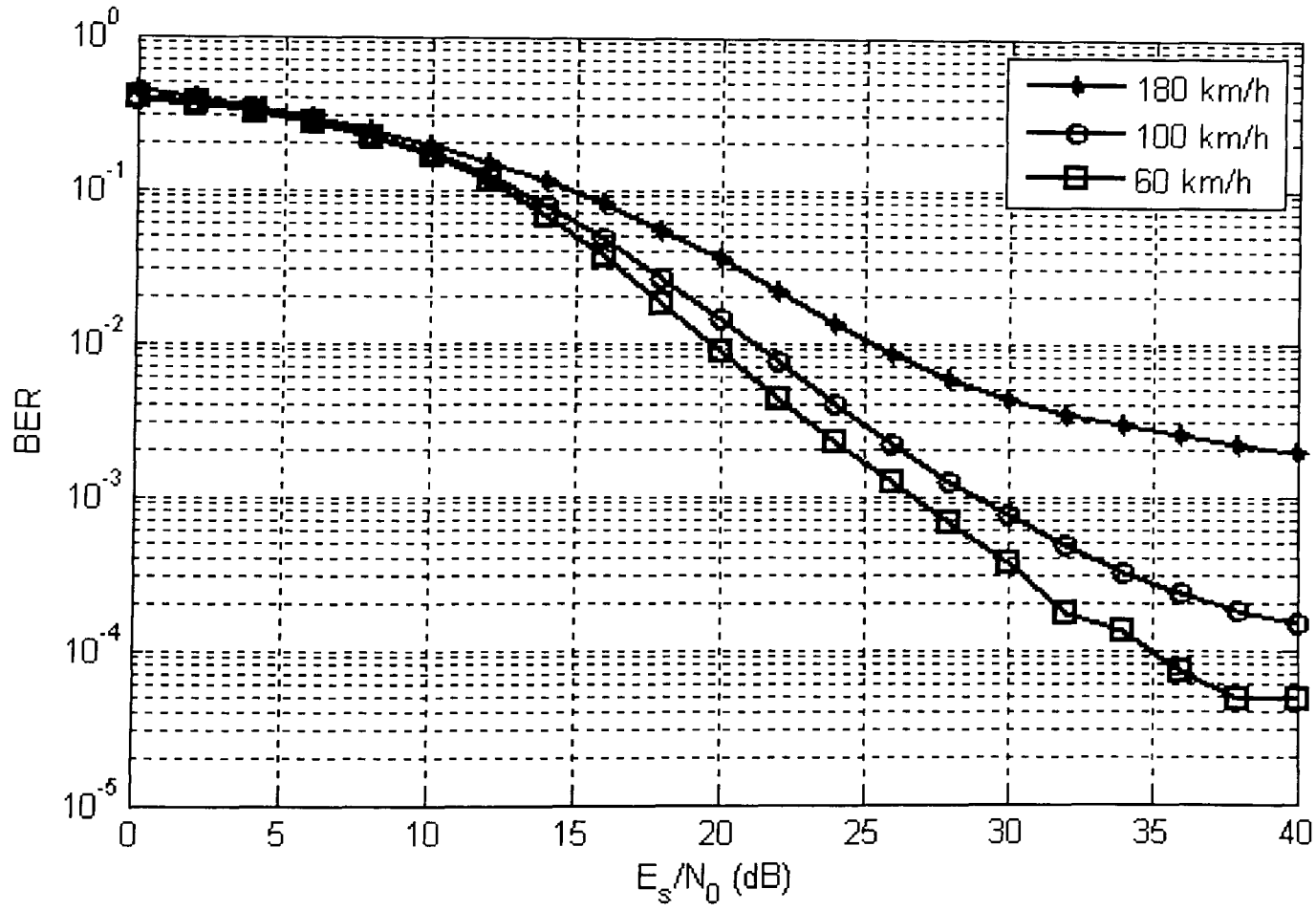

Figure (4.21): BER of 3×4 VBLAST with Channel Update and Training Sequence

Figures (4.22) and (4.23) compare the BER performance with and without the proposed channel update and ICI equalisation. When $q = 0$, the channel update algorithm is employed without ICI equalisation. The No ICI case represents the ideal performance without ICI (speed = 0) and perfect channel knowledge at the receiver. The "No update" curve is the performance without channel tracking or ICI equalisation. As can be seen the performance improves as the number of interfering subcarriers considered in the equaliser increases. As more subcarriers are considered, more ICI power is cancelled in the decoding process thus providing more reliable decisions. This however, comes at the price of increased receiver complexity since the size of the channel matrix becomes larger and, therefore, the pseudoinverse and decoding processes become more complicated [44]. By equalising five pairs we gain approximately 4dB improvement for 2×4 and 3dB improvement for 3×4 systems. Beside the reduction of ICI the algorithm also enhances the signal power since the power leaked to adjacent subcarriers is included in the detection process.

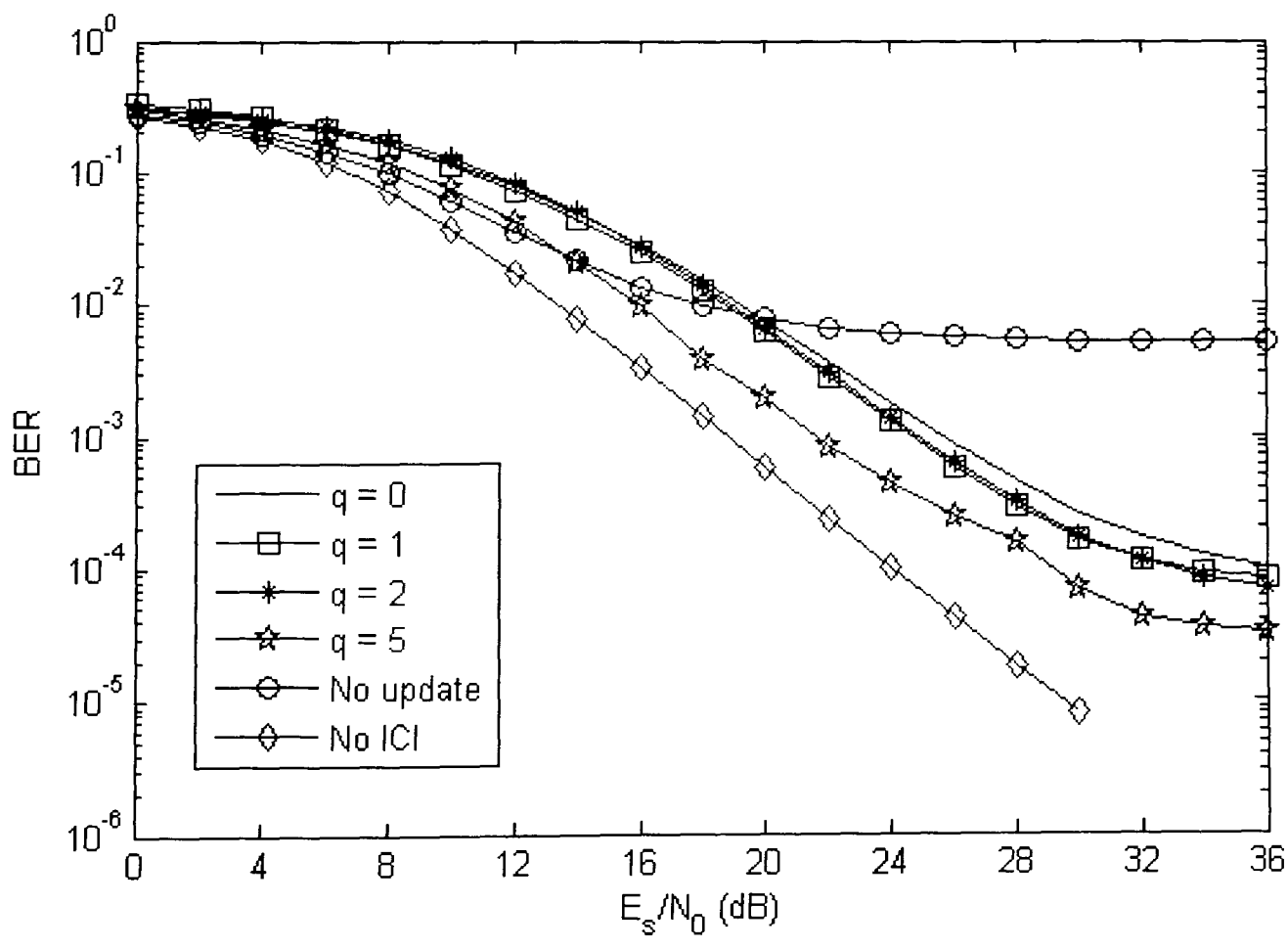

Figure (4.22): BER of 2×4 VBLAST-OFDM with ICI Cancellation, 180 km/h

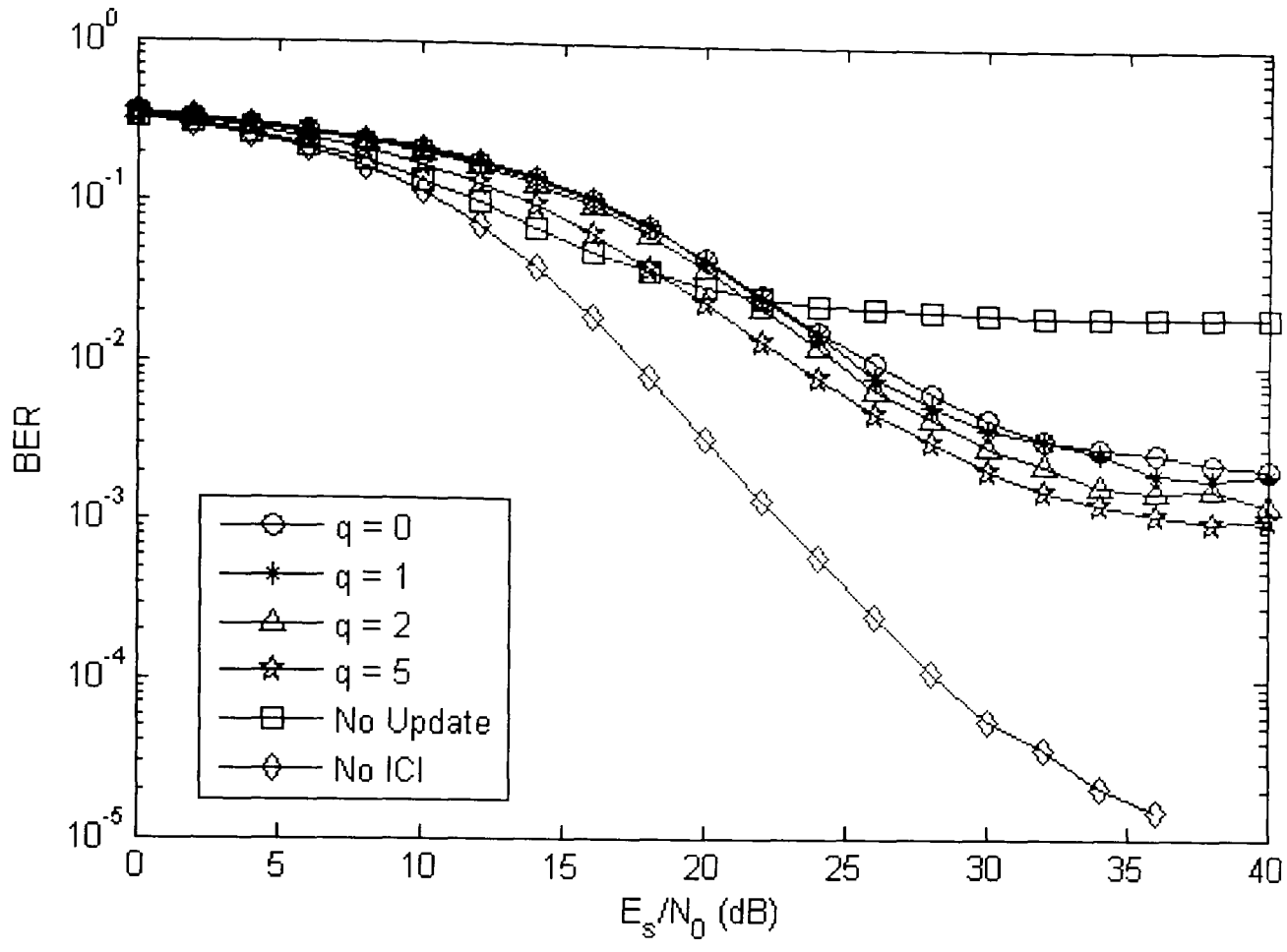

Figure (4.23): BER of 3×4 VBLAST-OFDM with ICI Cancellation, 180 km/h

4.7. Concluding Remarks

In this chapter we developed a simple recursive algorithm to keep track of changes in the channel and update the channel estimation matrix for VBLAST in flat fading channels. The update algorithm enhances the channel estimation on a symbol by symbol basis, but this can be relaxed for high symbol rates and/or slow fading as the channel coherence time will be large compared to the symbol duration. The proposed algorithm improves the system BER and channel estimate MSE via continuous and accurate channel updating and has low computational complexity as a result of using a set of simple single tap filters. Simulation results showed improvements in MSE and BER when using the update algorithm compared to the training only channel estimation. We also analysed the inter-carrier interference (ICI) problem and introduced algorithms for channel tracking and ICI equalisation in VBLAST-OFDM systems. ICI was found to increase with the number of subcarriers used, antennas transmitting and speed. The

analysis showed that ICI causes an error floor at high SNR. The channel update algorithm was extended to OFDM and it showed improvement in BER performance when compared to the conventional training based channel estimation. Both methods, however, experience an error floor at high SNR due to ICI. An equalisation technique to reduce ICI for SISO systems was extended to VBLAST and evaluated. Our channel tracking algorithm updates the channel and estimates the slope of the channel response. This estimate is then fed to an equaliser to reduce the ICI. The equalisation scheme reduces the error floor as the number of subcarriers included in the equaliser increases. This, however, comes at the expense of more receiver complexity.

Chapter 5

VANET Connectivity

5.1. Overview

Connectivity is a measure of how many nodes in the network are able to communicate with each other. A network is declared to be fully connected, i.e. has a connectivity of 100%, if there exists a route between every pair of nodes in the network. Connectivity is particularly important for routing information packets across the network. A network with low connectivity suffers from route discontinuities leading to complications in the network layer to guarantee packet delivery. Low connectivity means the network is divided into isolated clusters or groups. The number of nodes within the cluster affects the performance of the MAC layer. Connectivity is affected by the node density, node distribution and communication range. Two nodes are usually assumed connected if they can correctly exchange information regardless of the quality of the communication link or the bit rate. In the previous chapters we considered the performance of the physical layer and showed it varies with the SNR. Error correcting codes can be used to enhance the BER of links with poor quality. A link between two nodes is assumed to exist only if the error correcting code is capable of correcting the errors. This simplifies the analysis of connectivity considerably as the nodes are either connected, if the errors can be corrected, or not connected, if the BER is too high for the error correcting code. In this chapter we analyse, evaluate and simulate the connectivity and the clustering of the nodes in VANET. We assume nodes within the communication range of a node receive a signal with SNR high enough to decode the signal correctly whereas nodes outside the communication range get very low SNR and hence cannot

communicate with the node. The results derived in this chapter will provide a baseline for the analysis of the MAC layer.

5.2. Connectivity in VANET

Although connectivity has been analysed for MANET and closed form expressions were obtained, VANET is a unique case. In vehicular networks, the nodes (cars) are distributed in a linear road rather than a two dimensional area as in MANET. This simplifies the analysis of the system considerably. The single dimensional network was analysed in [114, 117, 118] for fixed nodes and [119] considered the case of nodes with random walk motion model. In [117] the probability of full connectivity ($P_n(d)$) of a network with n nodes, communication range = 1, in a road of length d was shown to be:

$$P_n(d)=\begin{cases} 0, & n<d-1 \\ \left(1-\left(1-\frac{1}{d}\right)^n\right)^{n+1}, & n\geq d-1 \end{cases} \tag{5.1}$$

The above expression assumes the distance (space) between nodes is uniformly distributed. However the distance between the cars is usually approximated by the exponential distribution [114, 117] defined as:

$$p(x)=\frac{1}{\lambda}.e^{\frac{-x}{\lambda}} \tag{5.2}$$

λ is the mean value. The speed model affects the distribution of the inter-space between the nodes and, therefore, the connectivity. In our analysis we use the exponential distribution to model the interspaces between the nodes.

We now introduce our model to calculate the connectivity in VANET. Two nodes i and j are connected if the distance ($X_{i,j}$) between them is less than or equal to the communication range (R) or there exists a set (m) of nodes between i and j such that:

$$\begin{aligned} &X_{i,a}\leq R, X_{b,j}\leq R, \quad a,b\in m, \\ &X_{m(k),m(k-1)}\leq R, \qquad \forall k \end{aligned} \tag{5.3}$$

Where $m(k)$ is the element at index k in the set m. If there is no set that satisfies these conditions, then the two nodes are not connected. To calculate the connectivity of the

network shown in figure (5.1), assume the distance between nodes i and i-1 is greater than R, then these nodes are not connected. However nodes p to i-1 and i to q have interspaces less than R and are, hence, connected (dotted ellipses correspond to some of the connected sets).

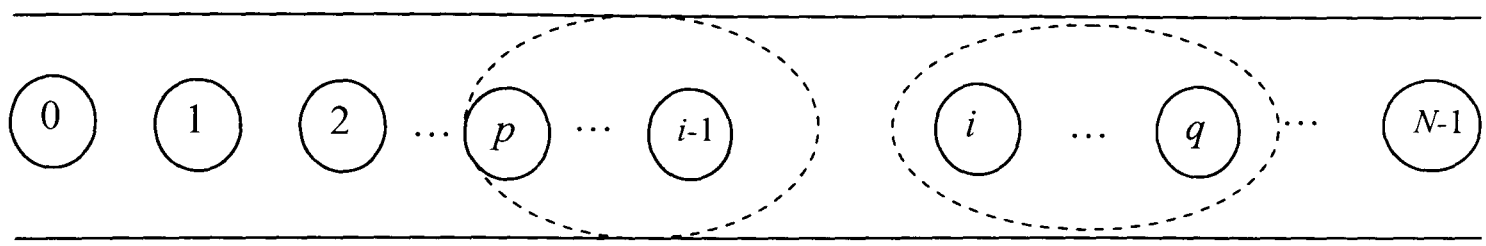

Figure (5.1): Network Layout

Assume the nodes in a connected set (s) are indexed i_s to q_s. Then there are q_s-i_s+1 nodes in this set and each node can connect to $T_s = q_s$-i_s nodes, the difference by 1 is because a node can always connect to itself. Therefore the connectivity of a single node in this set is given by:

$$Connectivity_{node} = \frac{T_s}{N-1} = \frac{q_s - i_s}{N-1} \tag{5.4}$$

Since, at most, a node can connect to N-1 nodes in a network of N nodes. We define the connectivity of the network as the average connectivity of all the nodes in the different sets given by:

$$\begin{aligned} Connectivity_{Network} &= \sum_{s=1}^{n}\sum_{j=i_s}^{q_s}\frac{T_s}{N(N-1)} = \sum_{s=1}^{n}\sum_{j=i_s}^{q_s}\frac{q_s - i_s}{N(N-1)} \\ &= \sum_{s=1}^{n}\frac{(q_s - i_s)(q_s - i_s + 1)}{N(N-1)} \end{aligned} \tag{5.5}$$

The last expression follows since all nodes within a single set (q_s-i_s+1 nodes) have equal connectivity. In (5.5) s corresponds to one of the n sets available in the network.

5.3. Connectivity in Highways

In this section we examine the connectivity in highways via Matlab. Highways are characterised by long distances, high speeds and a small number of intersection. We set the transmission range to 1 km, which is the maximum transmission range defined for the physical layer of VANET [11, 14, 16]. Our program simulates the connectivity in a

road 100 km long. The program generates random exponentially distributed numbers which form the spaces between the cars. The number of nodes in the road is varied to simulate the effect of node density on connectivity. The program calculates the connectivity of the network, averages it over 1000 trials and plots the results. For multilane models we assume equal node density for each lane and the interspaces in the different lanes are independent and identically distributed.

With this model and assumptions we simulated the connectivity of VANET. Figure (5.2) compares the probability of full connectivity from our model with equation (5.1). As can be seen, the results from both models show good agreement despite the different distributions used. We expect this to be due to the long distance of the road which makes the probability less affected by the distribution model used [117]. To achieve full connectivity a density of 12cars/km or more is required. The average space between the cars for this density is approximately 85m.

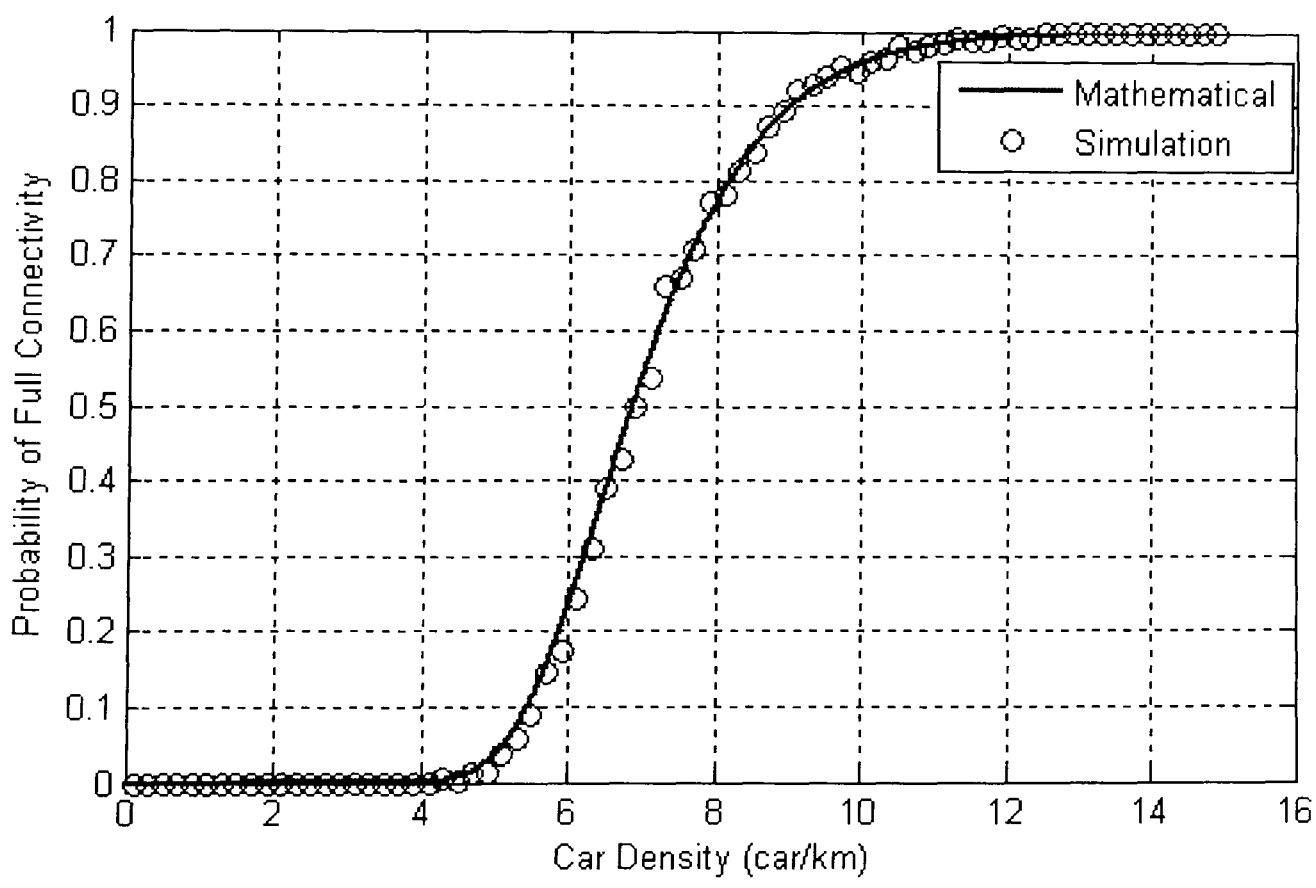

Figure (5.2): Probability of Full Connectivity for 1-Lane Road vs. Car Density

Figure (5.3) shows the average connectivity of the network. From the figure we note that even at low car densities, a node will have some neighbouring cars with which it

can communicate. The network becomes fully connected for densities of 12cars/km or more.

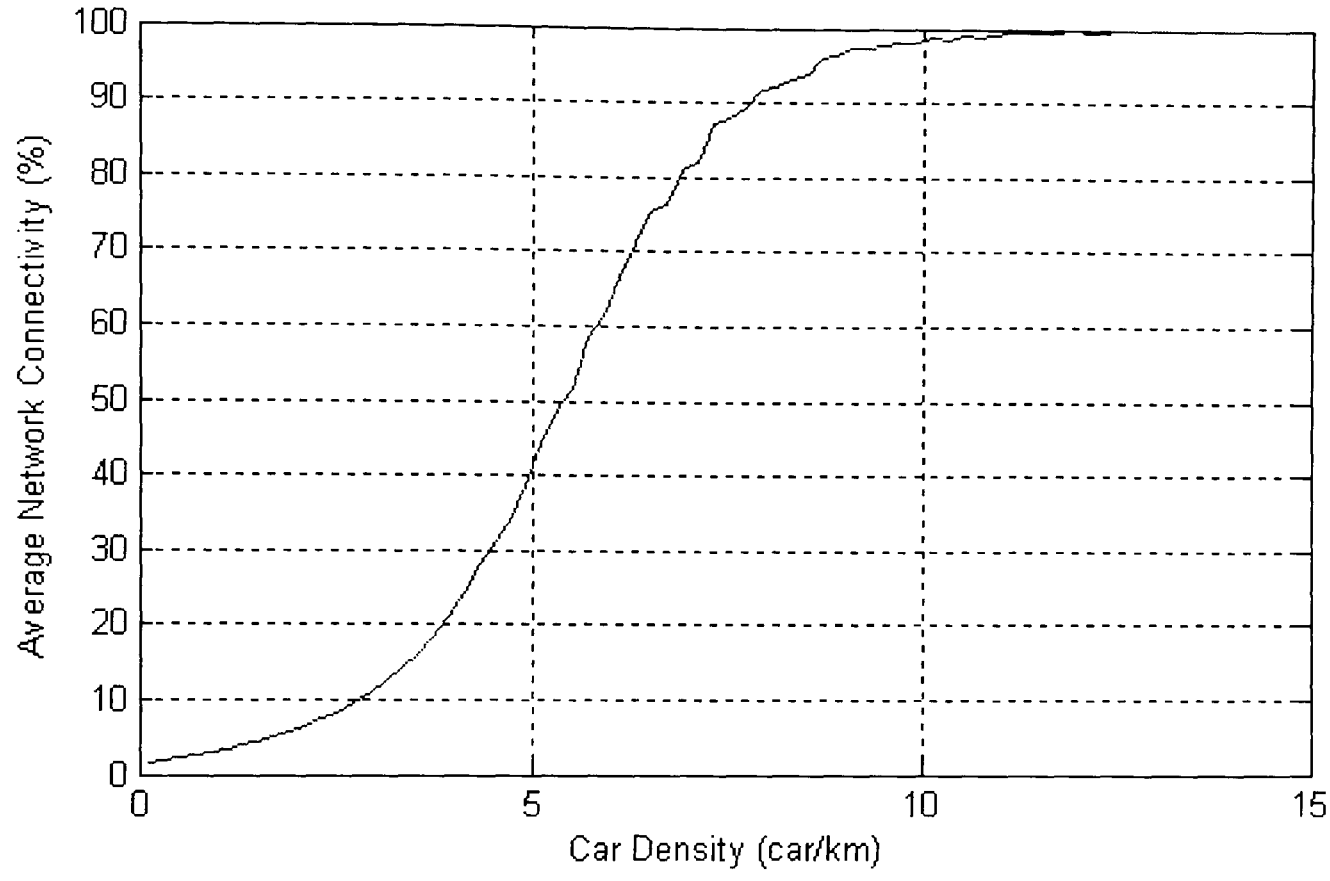

Figure (5.3): Average Network Connectivity vs. Car Density

Figure (5.4) shows the number of groups in the network. A group, or set, is a number of cars which can communicate with each other. If the network is fully connected the number of groups is 1 as all the nodes can communicate with each other. The higher the number of groups the worse is the performance of the network layer as there will be no hop between the different groups, whereas for the link layer more groups means less number of hidden terminals and therefore better chances of accessing the channel without collision. As seen in the figure the number of groups increases initially as the number of nodes is increased. This is because the nodes are so far from each other that even when more nodes are added, the interspaces between the nodes are still larger than the communication range. To illustrate this consider 15 nodes in the 100 km road, the average space is then approximately 6.5 km. If the number of nodes is doubled, the average space reduces to approximately 3 km which is still greater than the communication range. The maximum number of groups that can exist in a 100 km road

is 50 groups since each node has 2 km coverage diameter. From the figure we note that the number of groups reaches a maximum at 1car/km then starts decreasing. This is expected since the range is set to 1 km and therefore we need at least a car every kilometre to relay the packet. For densities more than 1car/km more cars become within the range of each other and, hence, the number of groups decreases.

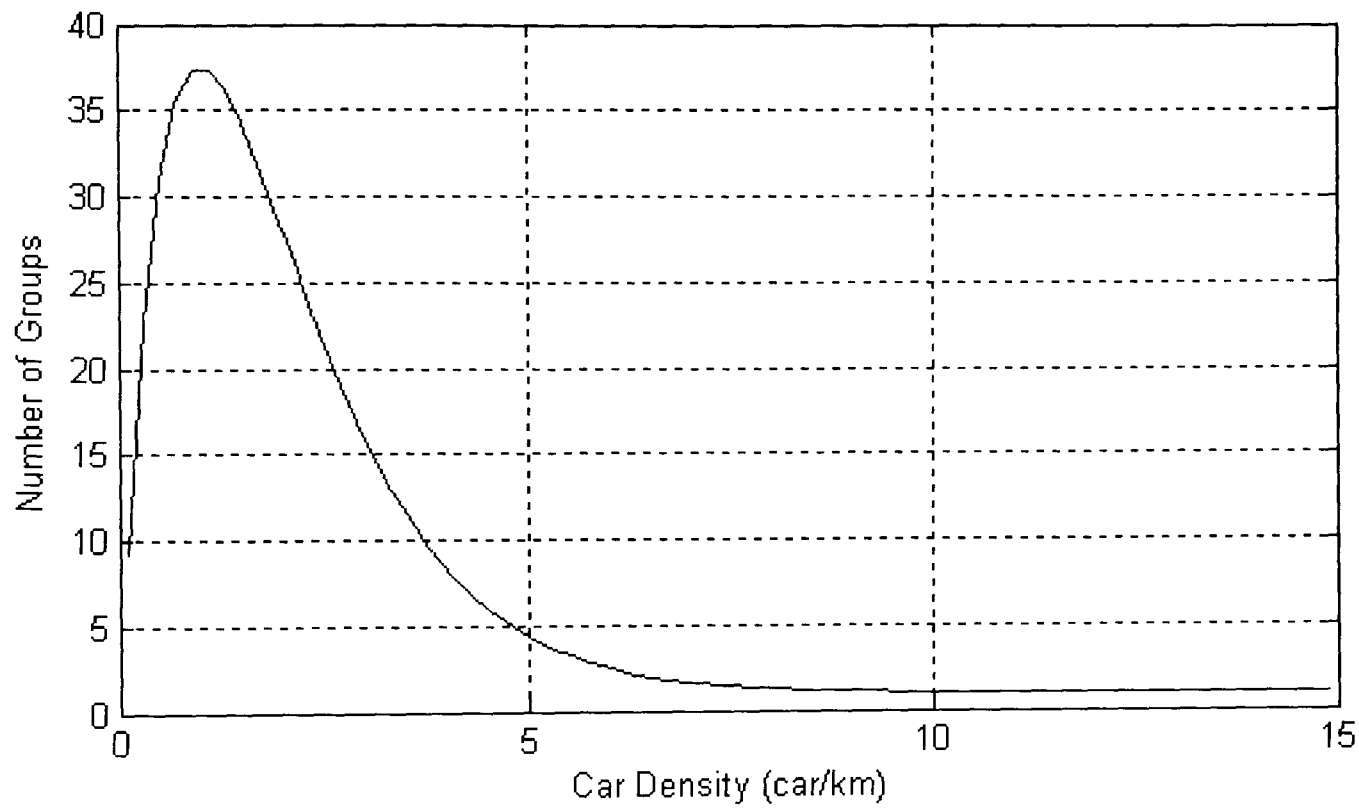

Figure (5.4): Average Number of Groups vs. Car Density

Figure (5.5), obtained via simulation, shows the number of cars within communication range versus car density. Clearly a linear relation exists and the average number of neighbouring nodes can be calculated using the equation:

$$No\ of\ Neighbours = 2 \times \frac{No\ of\ Nodes}{Road\ Length} \times Communication\ Range \qquad (5.6)$$

Where the multiplication by 2 is due to the circular area covered by omnidirectional radiation.

Now we consider roads with more than 1 lane. For multilane roads we assume half the lanes are in each direction, for instance a 4 lane road consists of 4 lanes with 2 lanes in each direction as shown in figure (5.6). The communication ranges we consider are 250m for the city environment and 1 km for highways, hence the road width is assumed

small compared to the communication range. In the analysis of the network layer of VANET, the maximum communication range within the city is usually assumed 250m since a higher range will lead to high interference and collisions in nearby roads [149].

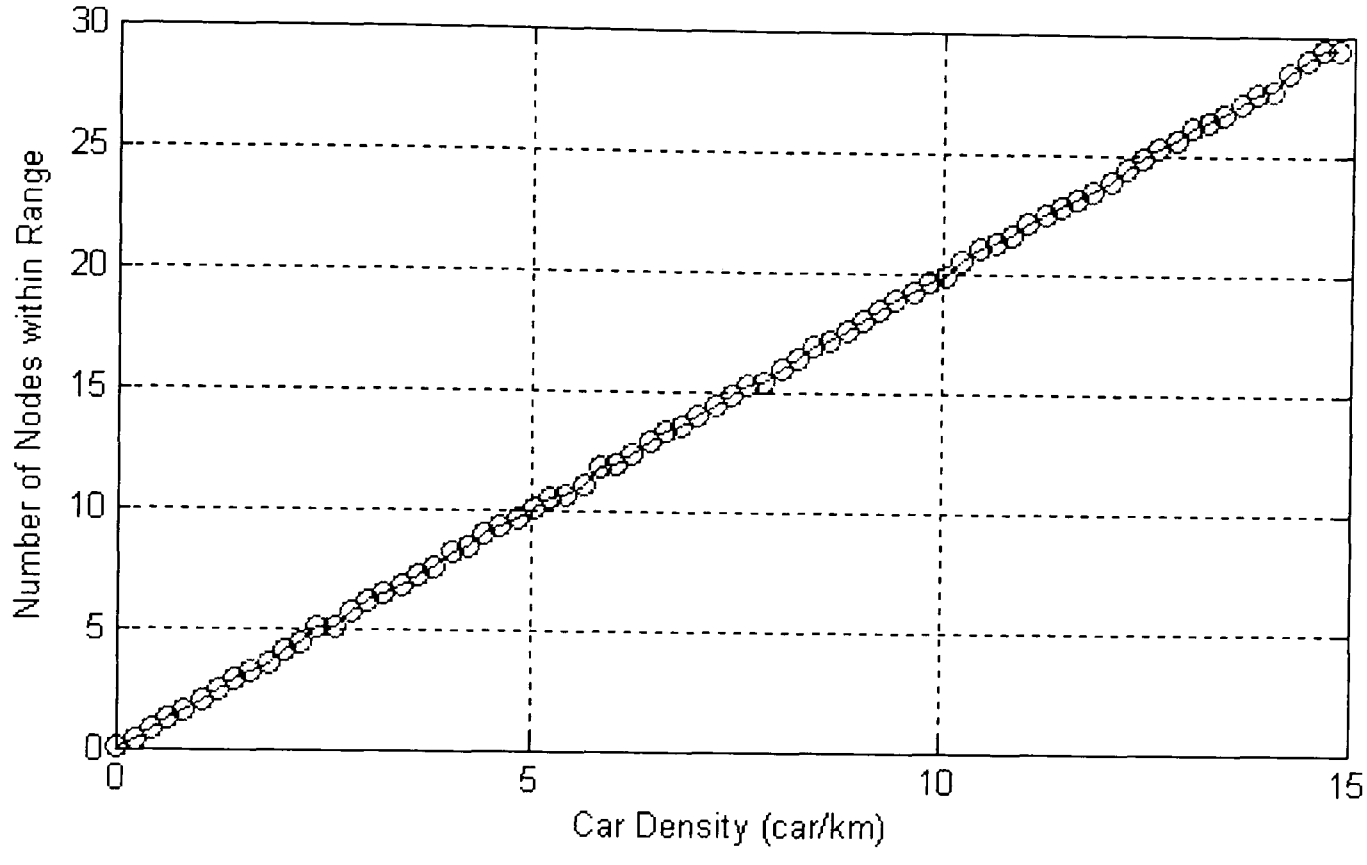

Figure (5.5): Average Number of Nodes within Communication Range vs. Car Density

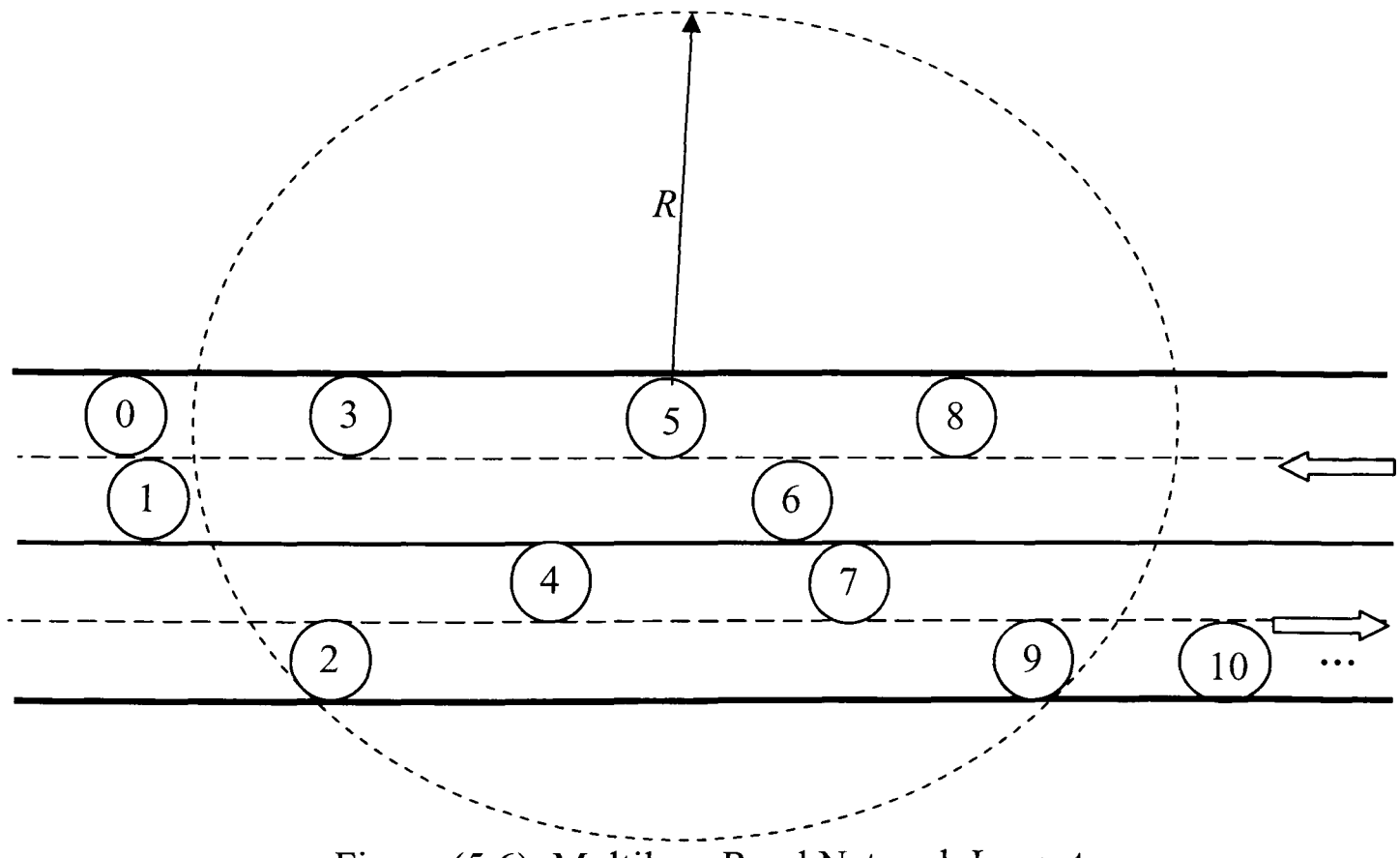

Figure (5.6): Multilane Road Network Layout

Figures (5.7) to (5.10) show the average connectivity, probability of full connectivity, number of groups and average number of neighbours for roads with 1, 2, 4 and 8 lanes. From figure (5.7) we observe that the connectivity slightly improves with the number of lanes because several paths may exist between the communicating nodes. However the probability of achieving full network connectivity is reduced as shown in figure (5.8). The reason for this is the nodes now can be at the same distance along the road if they are in different lanes. This is not possible for single lane roads since it is not possible for two cars to overlap. In other words the cars tend to cluster in fewer groups with larger number of nodes per group compared to single lane roads as can be seen from figures (5.9) and (5.10). Due to this clustering it becomes more likely to have isolated groups or even isolated cars thus having low probability of full connectivity. Although the probability of full connectivity is low the network has high average connectivity because most of the nodes in the network will be able to communicate with each other and the isolated nodes form a small percentage thus having a small effect on the average but a large effect on the probability.

We observe from figure (5.9) that the maximum number of groups is reduced as the number of lanes increases. This is due to the clustering of the nodes as discussed. However a high node density is required for the network to become one group i.e. fully connected. Figure (5.10), obtained via simulation, proves that groups with more nodes are formed in multilane roads since the average number of neighbouring cars has increased compared to single lane roads.

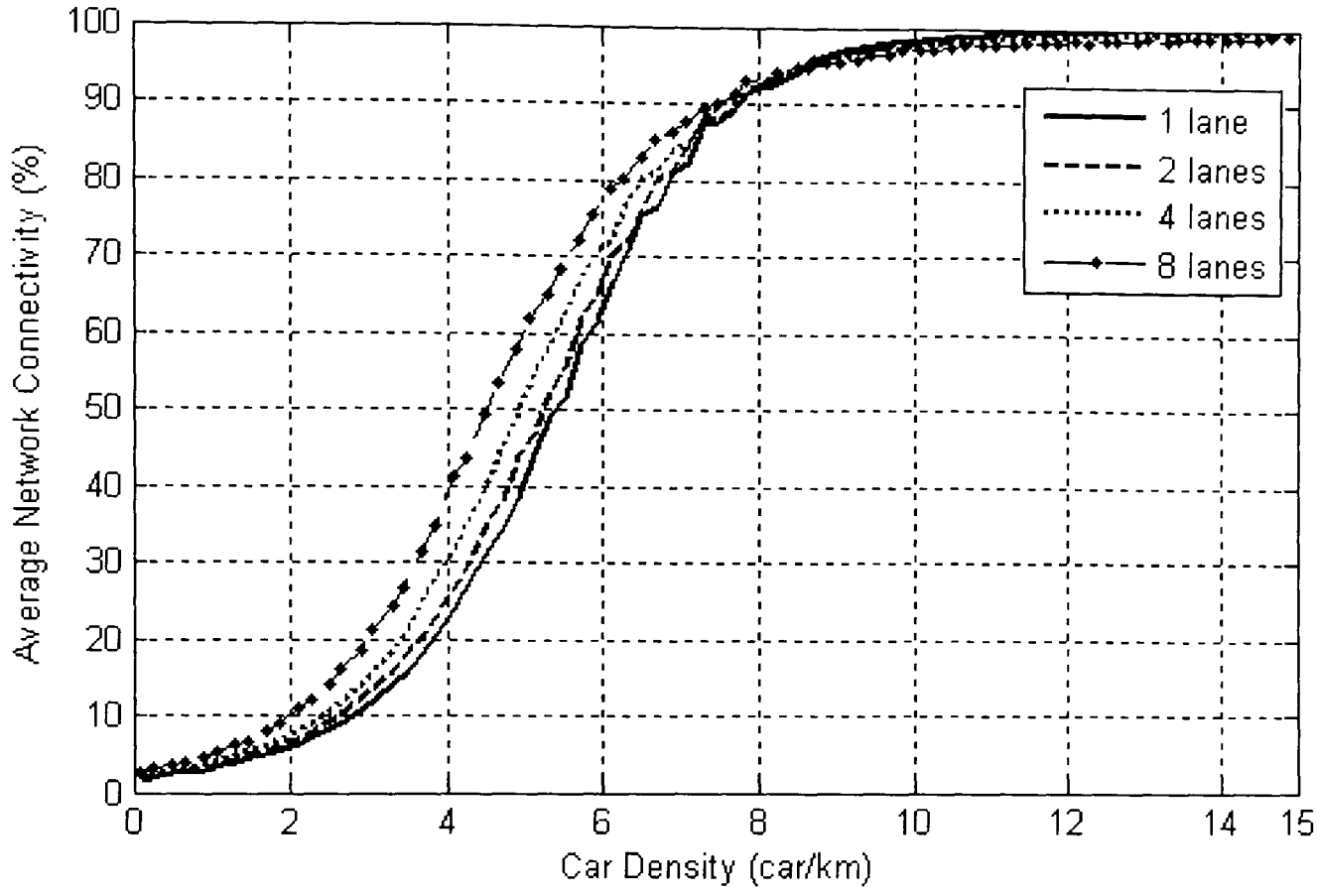

Figure (5.7): Average Network Connectivity vs. Car Density

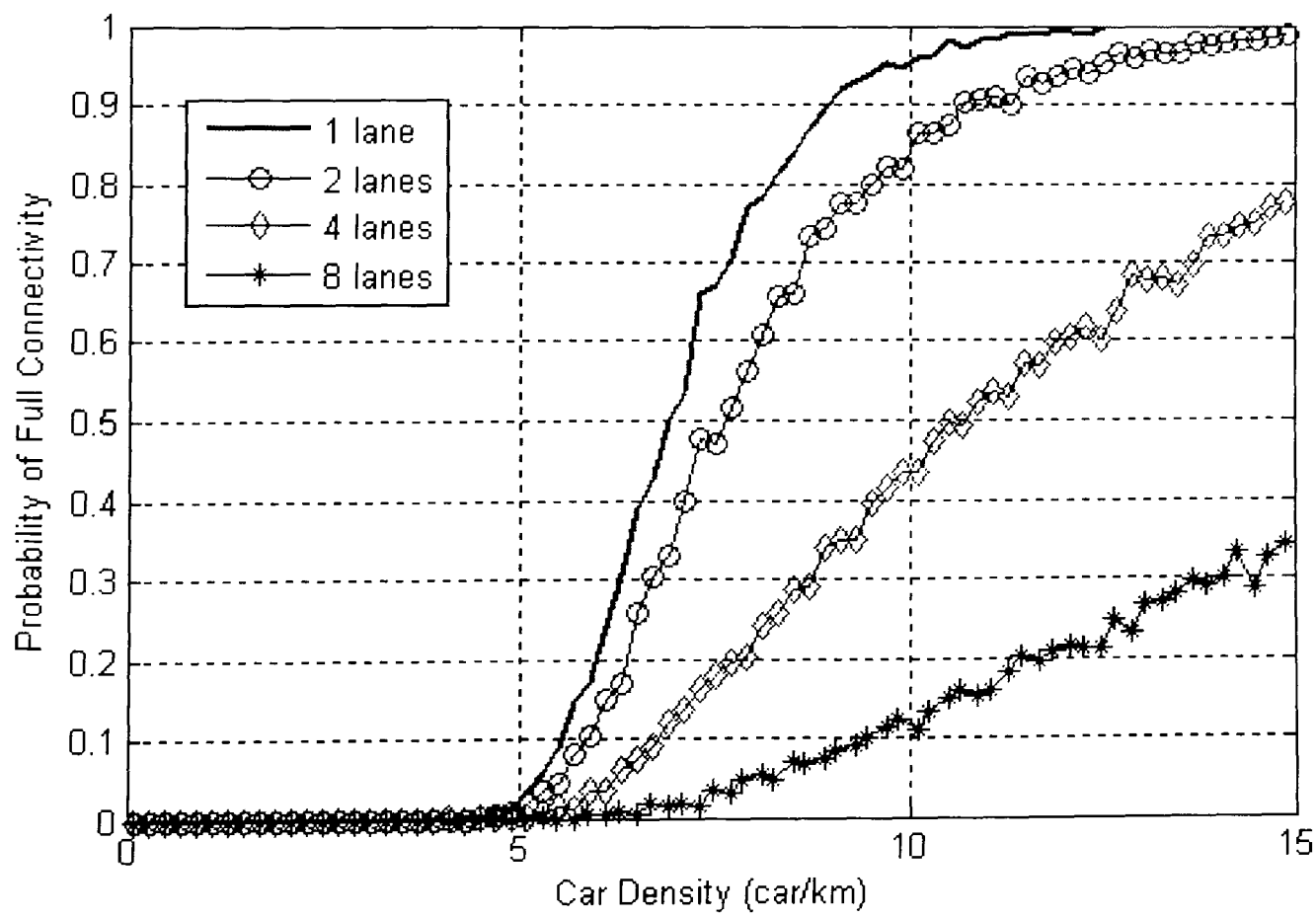

Figure (5.8): Probability of Full Connectivity vs. Car Density

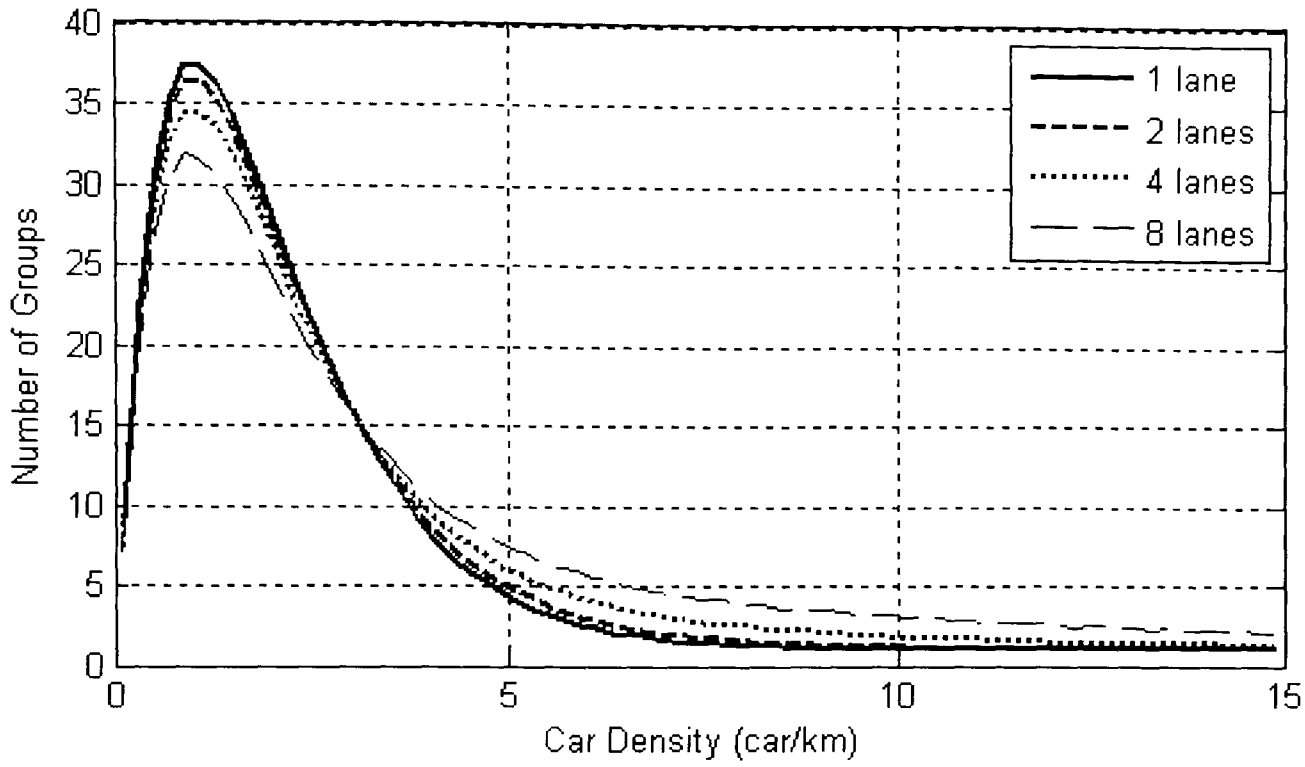

Figure (5.9): Average Number of Groups vs. Car Density

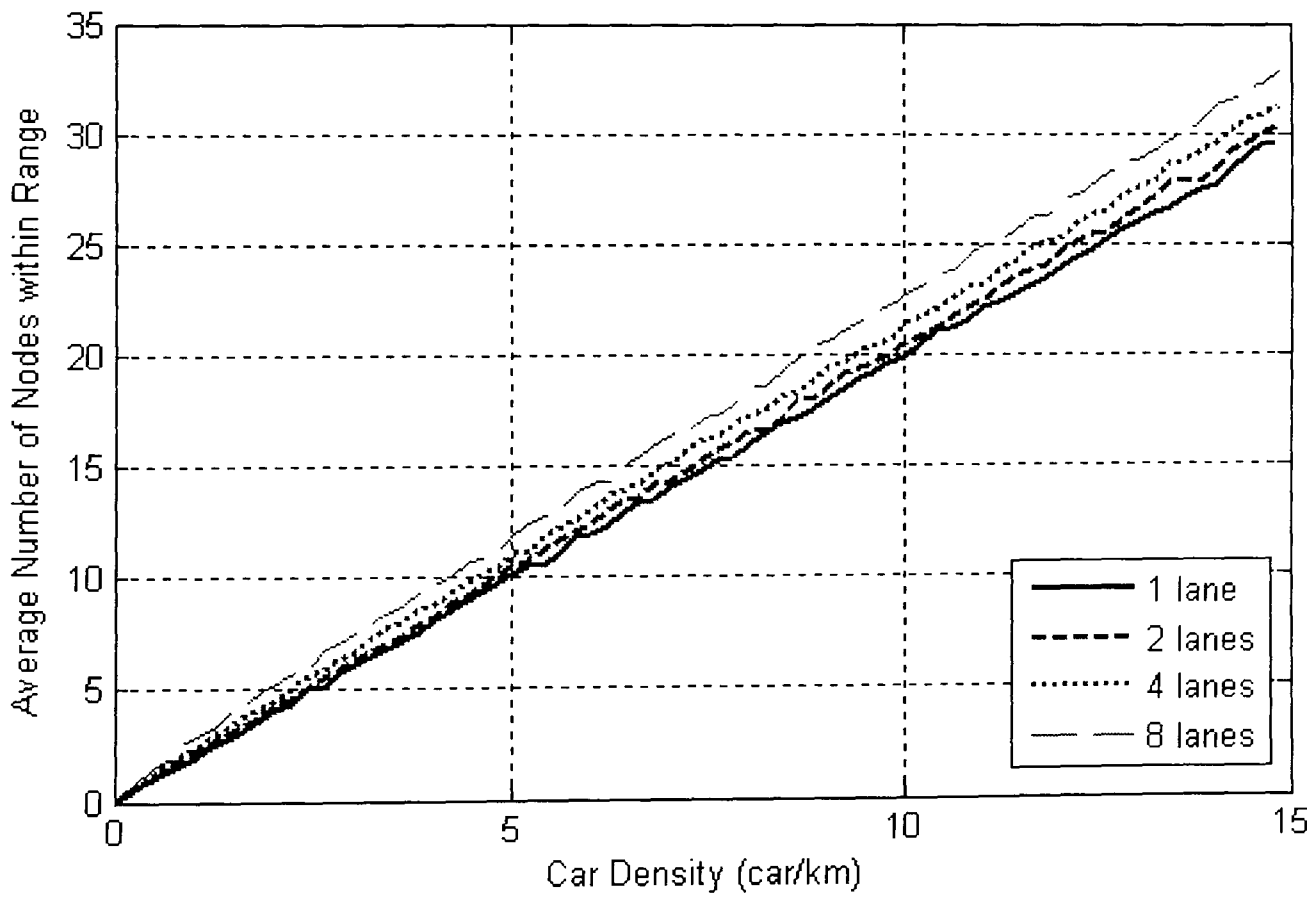

Figure (5.10): Average Number of Neighbours vs. Car Density

5.4. Connectivity in the City

The 100 km road and 1 km transmission range parameters are suitable for cars in highways; however within the city the roads are usually much shorter and the transmission power should be reduced to minimise the interference for other cars. We consider a communication range (R), which is set to 250m in our simulations but the results are normalised to R, and roads of lengths 3R, 5R, 8R and 10R. Typical roads within the city have 1-4 lanes in total and two directions. Considering the single lane case, equation (5.1) can be applied for the different road lengths producing the results shown in figure (5.11).

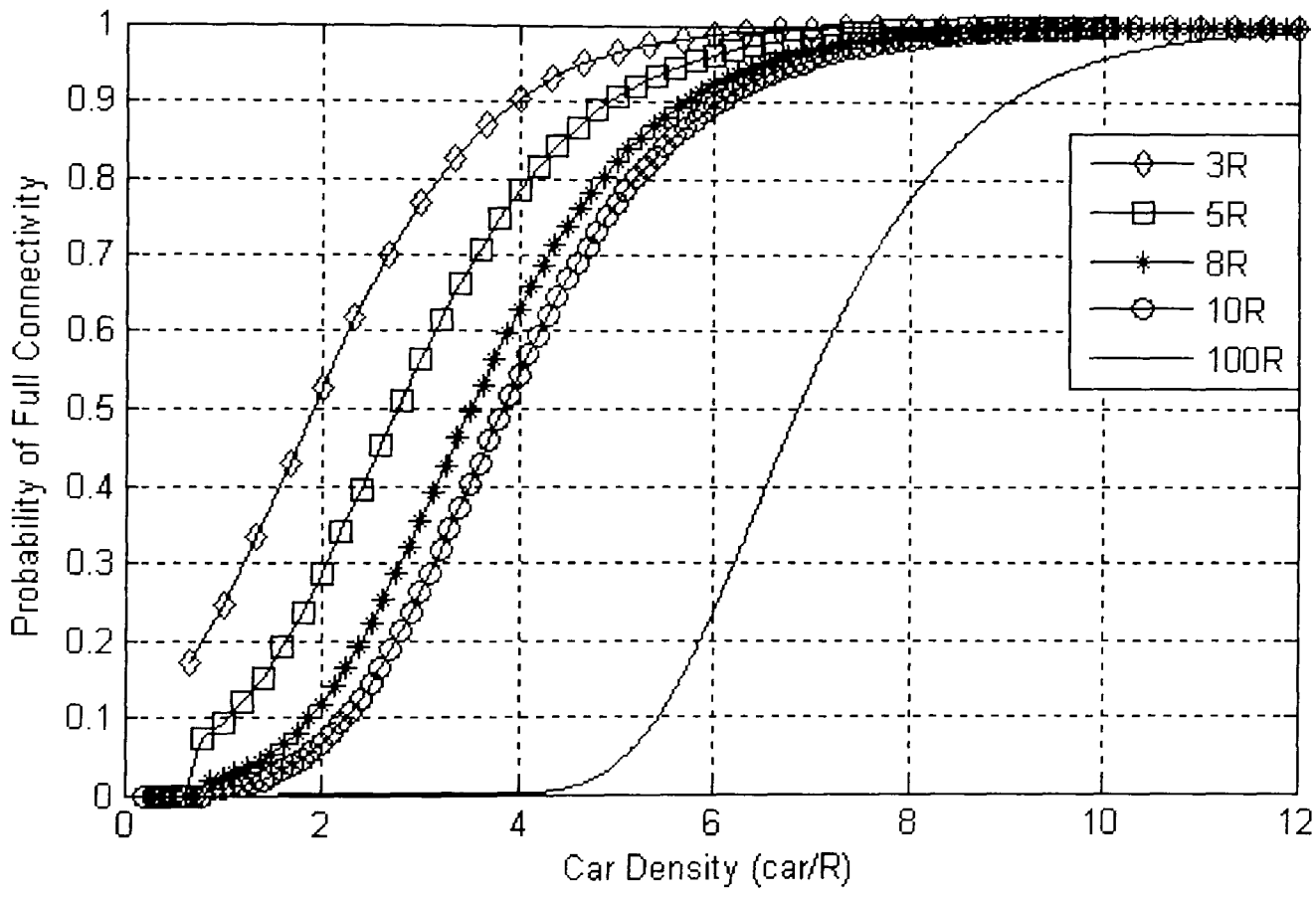

Figure (5.11): Theoretical Probability of Full Connectivity, uniform distribution

As can be seen from figure (5.11) the number of cars required to achieve full connectivity depends on the length of the road. As the road length increases, higher densities are required to achieve full connectivity. This is expected since with larger roads more hops are required to relay the messages and therefore the probability of connectivity is reduced. Equation (5.1) is for uniform distribution, however as discussed in section (5.2), exponential distribution is more accurate to model the interspaces

between the cars. For exponential distribution the probability of full connectivity was approximated in [150] by:

$$P(\rho,R,m)=\left(1-e^{-\rho R}\right)^m \qquad (5.7)$$

Where ρ is the car density, R is the communication range, and m is the ratio of road length to communication range. Using (5.7) to calculate the probability of full connectivity, figure (5.12) was obtained, while figure (5.13) is from simulations.

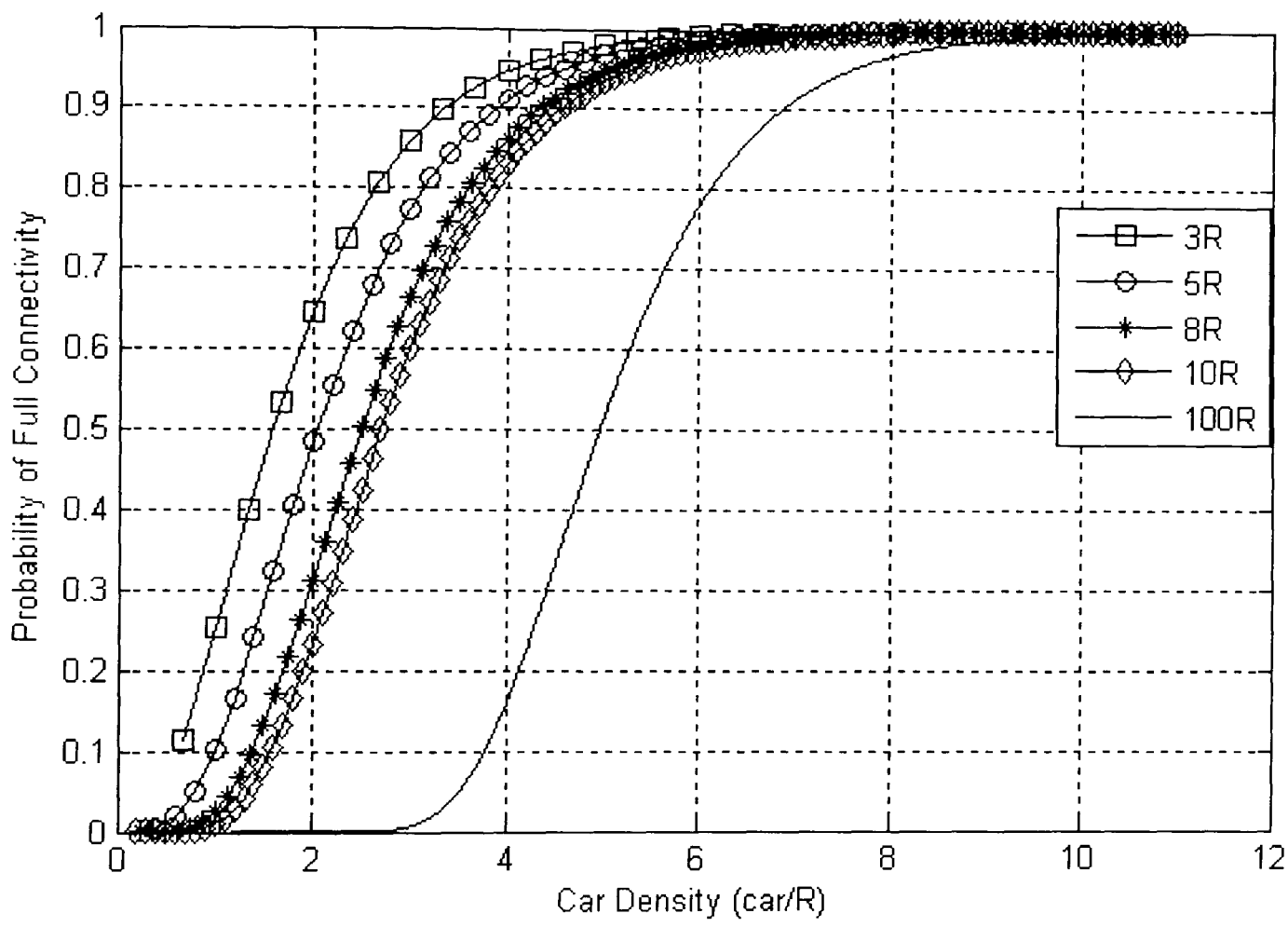

Figure (5.12): Theoretical Probability of Full Connectivity, exponential distribution

Equation (5.7) was originally derived to study connectivity in the city. It assumes the interspaces between the nodes are independent, exponentially distributed random variables. However in reality, the interspaces are not independent and therefore equation (5.7) provides an upper bound of the probability of full connectivity since the dependency between spaces will reduce the probability. This is observed from figure (5.14) which compares the probability calculated from equations (5.1) and (5.7) with the results from simulations. The difference between the exponential and other models

increases as the length of the road increases. For short roads ($3R$) the upper bound is tight but for large networks the upper bound gives a very optimistic prediction.

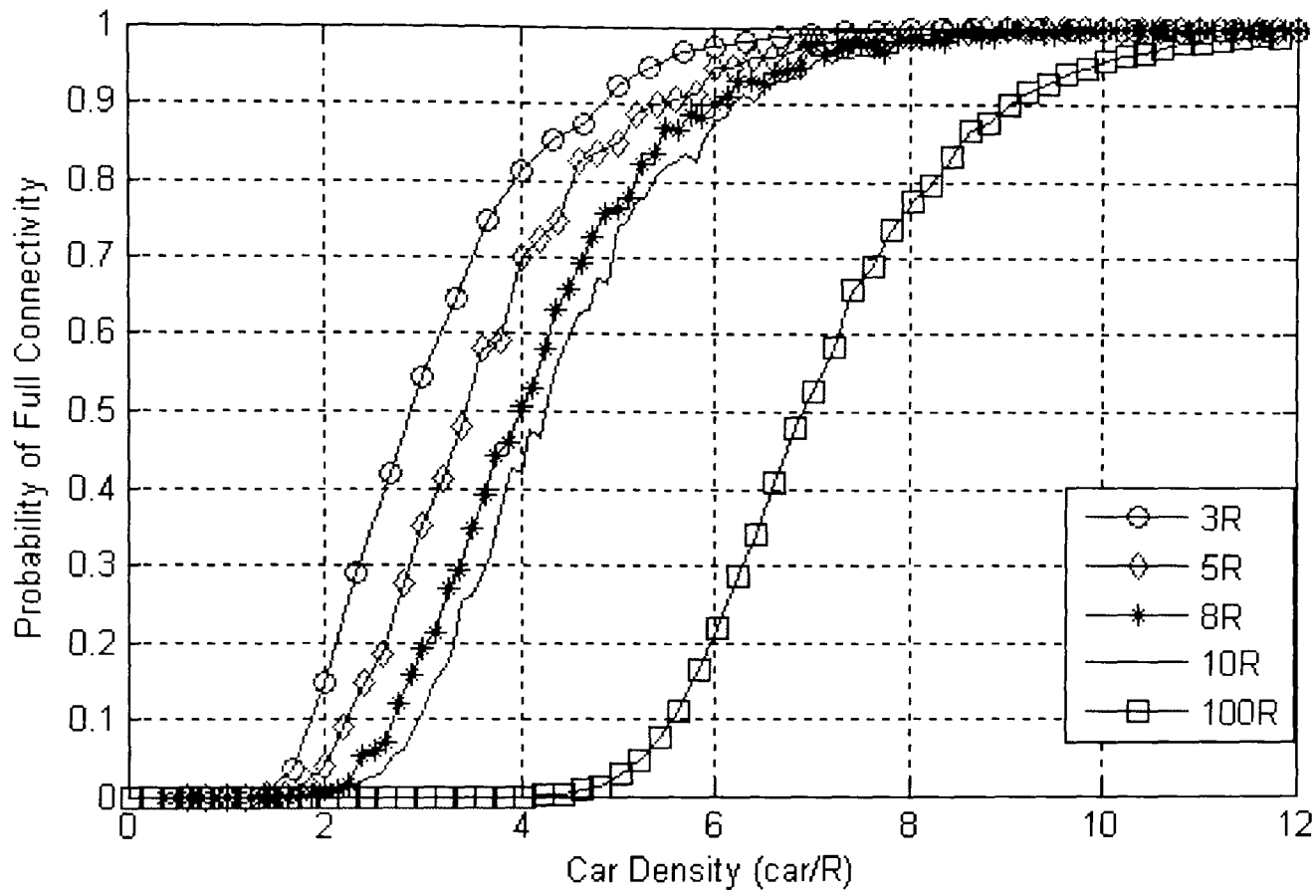

Figure (5.13): Probability of Full Connectivity, simulations

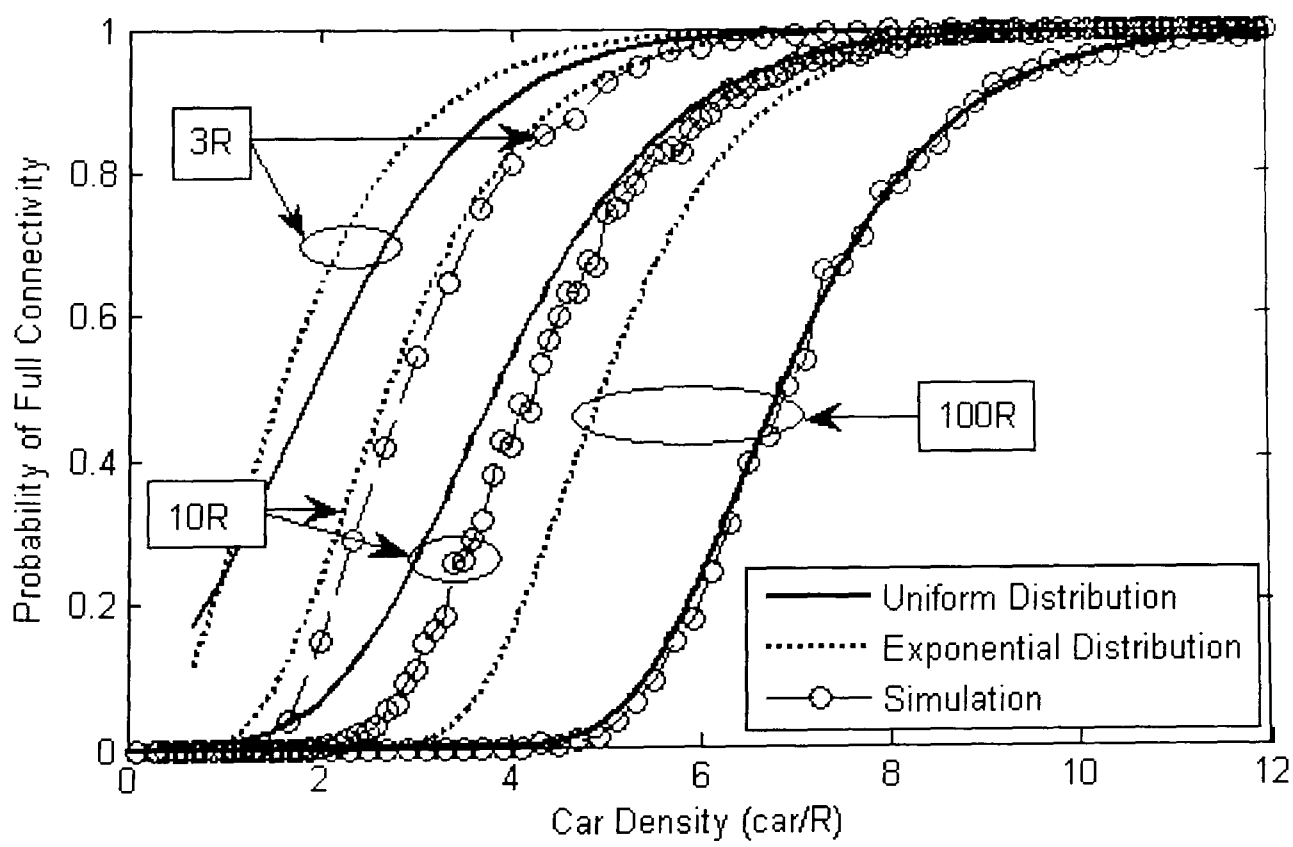

Figure (5.14): Comparison Between Mathematical and Simulation Models

Comparing the probability from simulations and from equation (5.1), figure (5.14), we arrive to a similar conclusion that full connectivity is achievable for shorter roads with lower car densities. However we note a difference for small car densities in the results from the simulation, which uses exponential distribution, and equation (5.1), which assumes uniform distribution. The reason for this difference is that cars tend to cluster in groups when exponential distribution is used whereas the nodes are assumed to be distributed uniformly for equation (5.1). The uniform distribution thus is an idealised case and gives optimistic results. As the node density increases both distributions tend to produce similar results and the network becomes one large group. From figures (5.11) and (5.13) we note that a car density of 7cars/R is sufficient to guarantee 95% probability of full connectivity for cars in city environments compared to 10cars/R for a 100R road.

Figure (5.15) shows the average number of groups for cars in the city for different road lengths. Similar to figure (5.5), the number of groups increases first linearly with the number of nodes since the nodes are distributed throughout the road and isolated, till it reaches a maximum value. The maximum value for uniform distribution is given by:

$$Max\ No\ of\ Groups = \left\lceil \frac{length\ of\ Road}{2 \times Communication\ Range} \right\rceil \qquad (5.8)$$

Where $\lceil x \rceil$ represents the first integer greater than x. For exponential distribution the maximum value will be different since cars tend to cluster but equation (5.8) can be used as an upper bound.

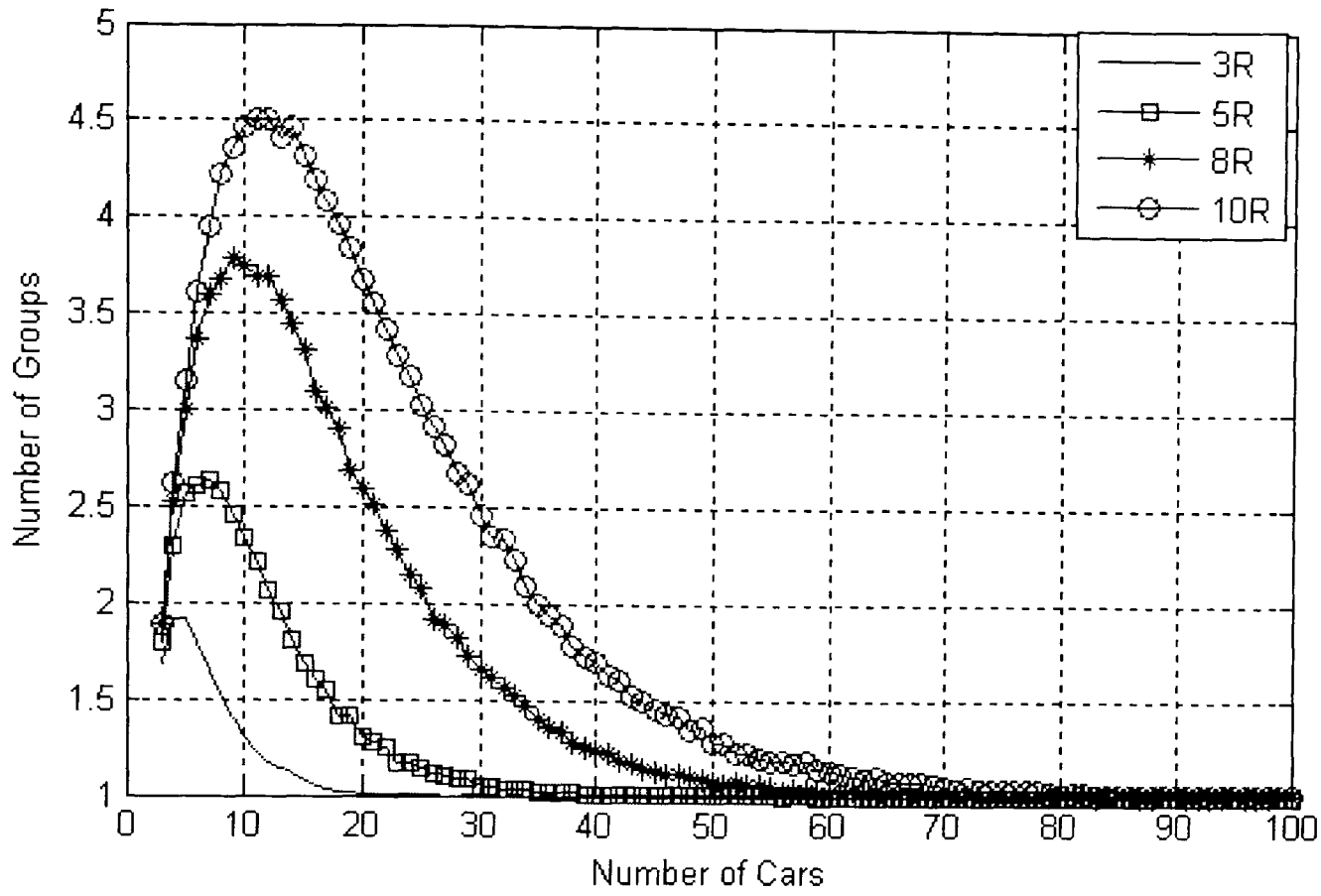

Figure (5.15): Average Number of Groups vs. Number of Cars in Road

For 2 and 4 lane roads the results are shown in figures (5.16) to (5.19). As observed from figures (5.16) and (5.17) the probability of full connectivity is lower in roads with multiple lanes than in single lane roads. For instance a density of 7cars/R was sufficient to achieve 95% probability for single lane roads, 10R long. However with this density, the probability is approximately 88% for 2-lane roads and 65% for 4-lane roads. The reason for this reduction is that cars in multilane roads can be at the same distance from the end of the road but in different lanes. Cars tend to cluster in large groups leading to smaller number of groups compared to single lane roads as observed from figures (5.18) and (5.19). These isolated groups cannot communicate with each other due to the large distances between them thus reducing the probability of full connectivity. From figures (5.15), (5.18) and (5.19) we note that the number of cars required for 10R network to become one group, i.e. fully connected is approximately 80 cars for single lane and 90 cars for 2-lanes whereas 4-lanes require more than 150 cars.

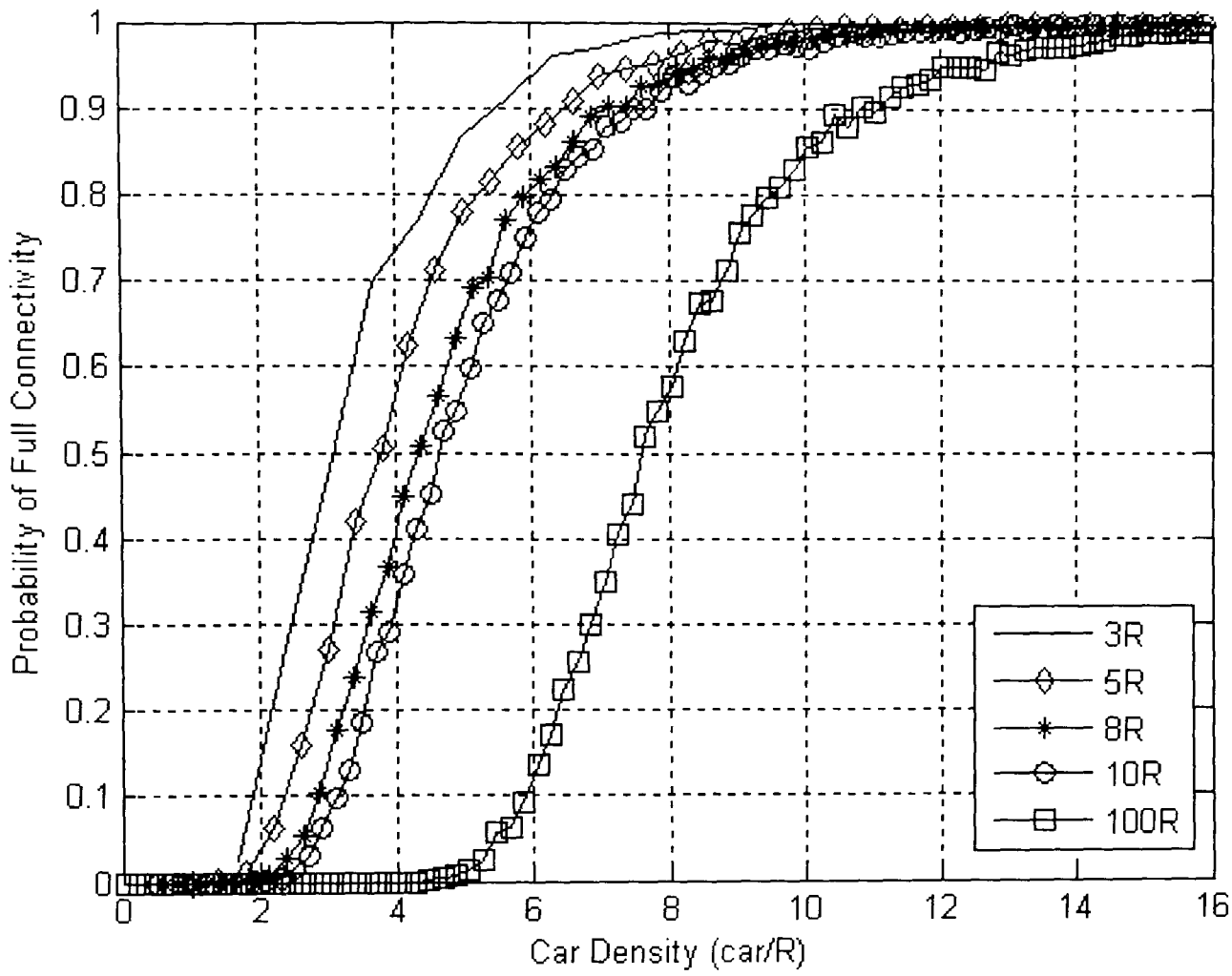

Figure (5.16): Probability of Full Network Connectivity for 2-Lane Roads

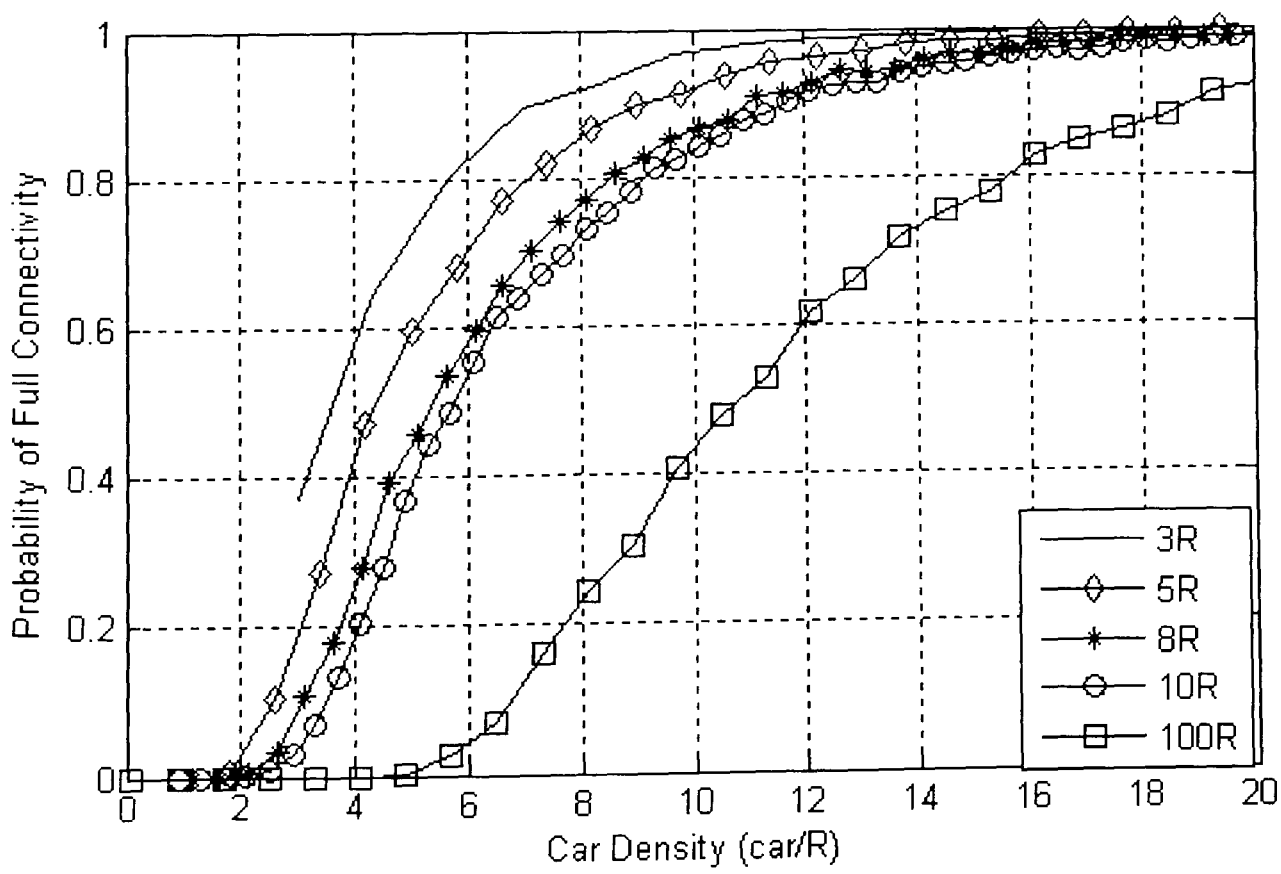

Figure (5.17): Probability of Full Network Connectivity for 4-Lane Roads

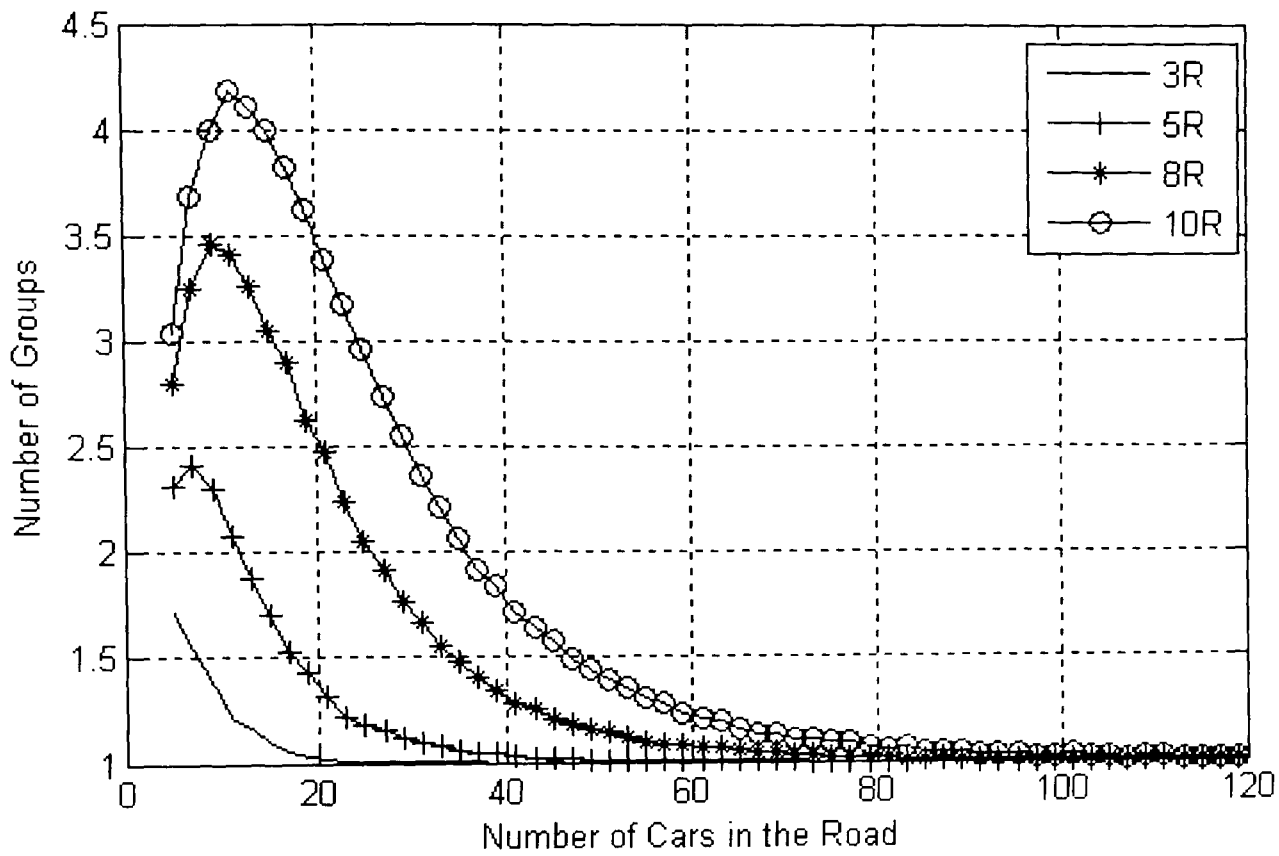

Figure (5.18): Average Number of Groups for 2-Lane Roads

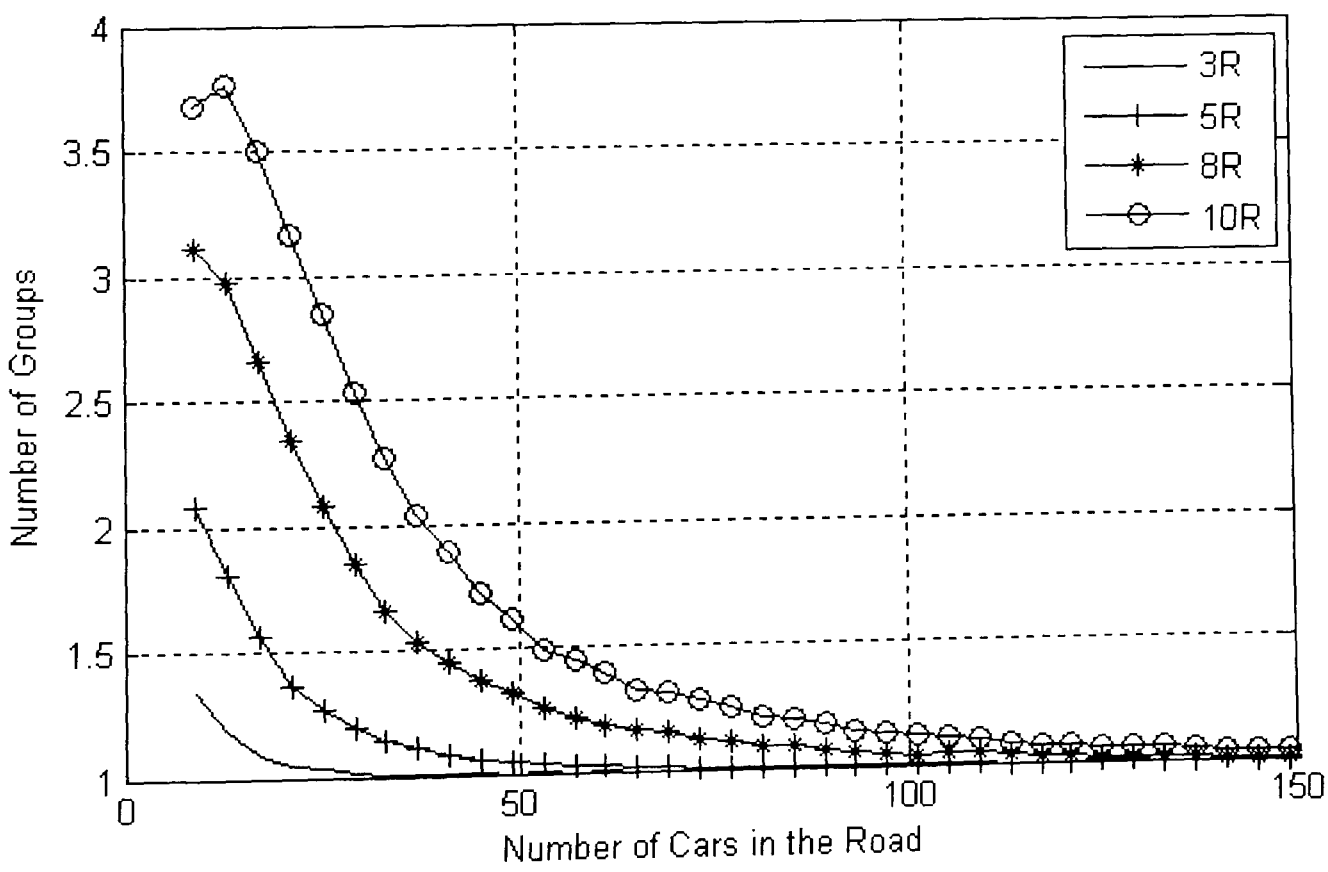

Figure (5.19): Average Number of Groups for 4-Lane Roads

5.5. Connectivity for Junctions and Turns

The previous linear topology approximates VANET in the middle of the road, however junctions, curves and roundabouts are encountered occasionally especially in city environment. In this section we investigate the effects of junctions, roundabouts and curves on connectivity.

5.5.1. Curves and Turns

Consider the topology shown in figure (5.20) which shows a single lane, curved road. ϕ is the angle between the original and new direction of the road and from the figure $\theta = 90 - \phi$. The car (a) is the first car before the turn moving towards the turn. We assume communication is possible only if a line of sight exists. The point (c) represents the maximum distance node (a) can communicate with since, for distances farther than c, the line of sight is blocked. If a car exists within the triangle gmc (Δgmc), then it is connected to node a, otherwise there will be a discontinuity in the network. The existence of scatteres may increase the communication area beyond Δgmc, hence the line of sight case represents the worst case scenario. The line of sight of cars behind a will cover an area smaller than that specified by Δgmc.

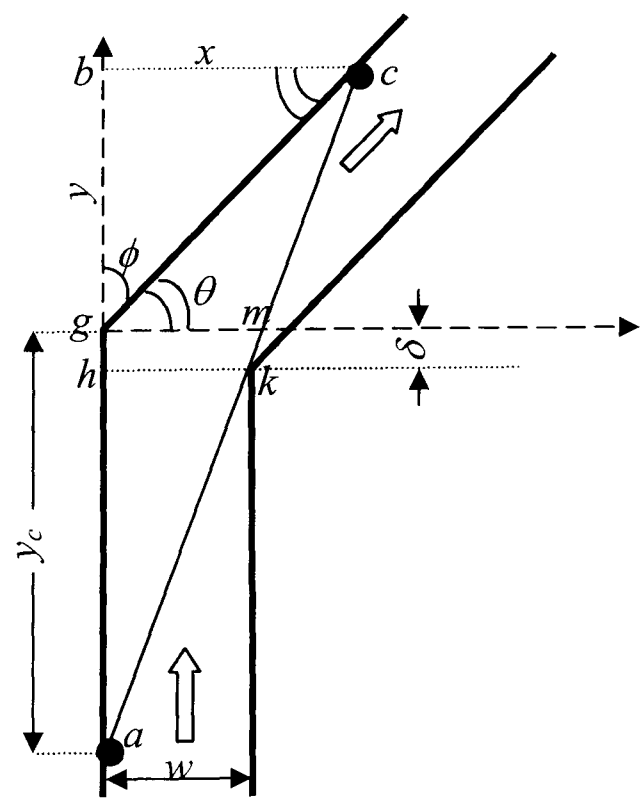

Figure (5.20): Layout for Road Turns

We now find the values x and y for a given car position (y_c), road width (w), and turn angle (ϕ or θ). From Δgbc we have:

$$y = x.\tan(\theta) \tag{5.9}$$

Triangles Δabc and Δahk are similar, hence:

$$\frac{y + y_c}{x} = \frac{y_c - \delta}{w} \tag{5.10}$$

Solving for y we get:

$$y = \left(\frac{y_c - \delta}{w}\right)x - y_c \tag{5.11}$$

Using (5.9) in (5.11) and solving for x we have:

$$x = \frac{w.y_c}{y_c - \delta - w.\tan(\theta)} \tag{5.12}$$

However δ still needs to be determined. Assuming the width of the road after the turn is equal to the width before the turn we can find δ from figure (5.21).

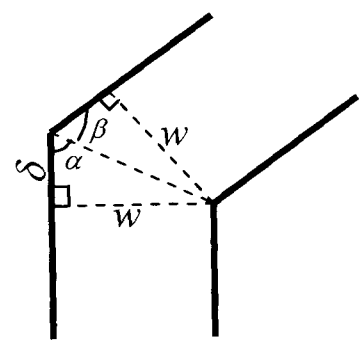

Figure (5.21): Calculation of δ

From figure (5.21), since $\sin(\alpha) = \sin(\beta)$ and, from figure (5.20), $\alpha+\beta = 90°+\theta \leq 180°$, the angles α and β are equal. Hence:

$$\alpha = 45^\circ + \frac{\theta}{2} \tag{5.13}$$

$$\delta = \frac{w}{\tan(\alpha)} = \frac{w}{\tan\left(45^\circ + \frac{\theta}{2}\right)} \tag{5.14}$$

From equations (5.14) and (5.12) we get:

$$x = \frac{w.y_c.\tan\left(45^\circ + \frac{\theta}{2}\right)}{y_c.\tan\left(45^\circ + \frac{\theta}{2}\right) - w - w.\tan(\theta).\tan\left(45^\circ + \frac{\theta}{2}\right)} \qquad (5.15)$$

Using this model we simulated the connectivity of VANET in roads with a curve or turn. In our simulations the communication range (R) was set to 250m, the road was a single lane road 10R long and the turn (or curve) is in the middle of the road. Figure (5.22) shows the probability of full connectivity for a road 10m wide and various turn angles (ϕ). As observed the probability of full connectivity decreases as the angle ϕ increases due to the loss of communication between cars before and after the curve. This is a major issue for safety applications as the driver may not be aware of cars approaching from the opposite direction. Figure (5.23) shows the effect of the road width on connectivity. As shown the connectivity improves as the road width increases. From equation (5.15) we note that x increases as the road width increases. As x increases the area within communication range of cars before the curve, triangle *agc* in figure (5.20), increases and hence more cars are within the communication area. This results in the improvement in connectivity observed from figure (5.23).

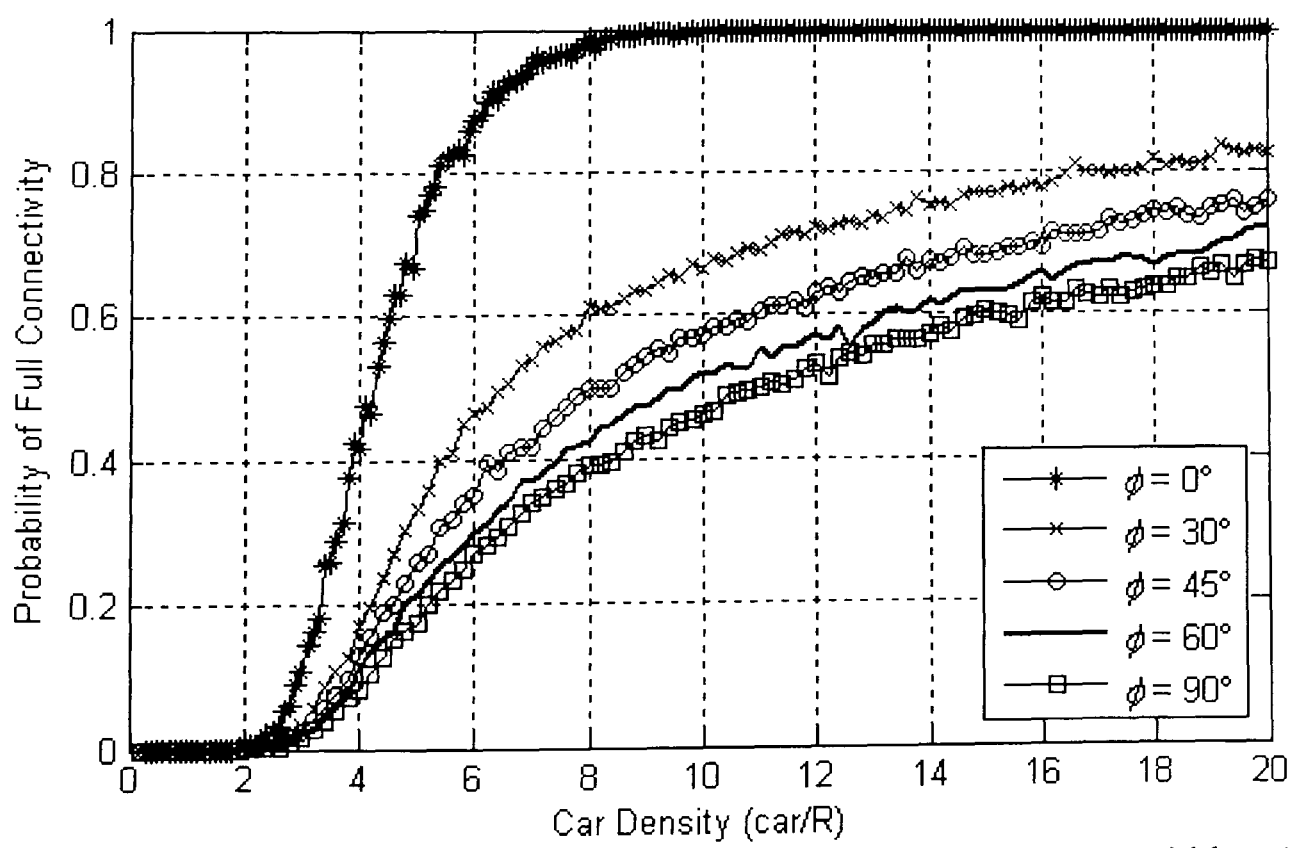

Figure (5.22): Probability of Full Connectivity for Roads with Turns, width = 10m

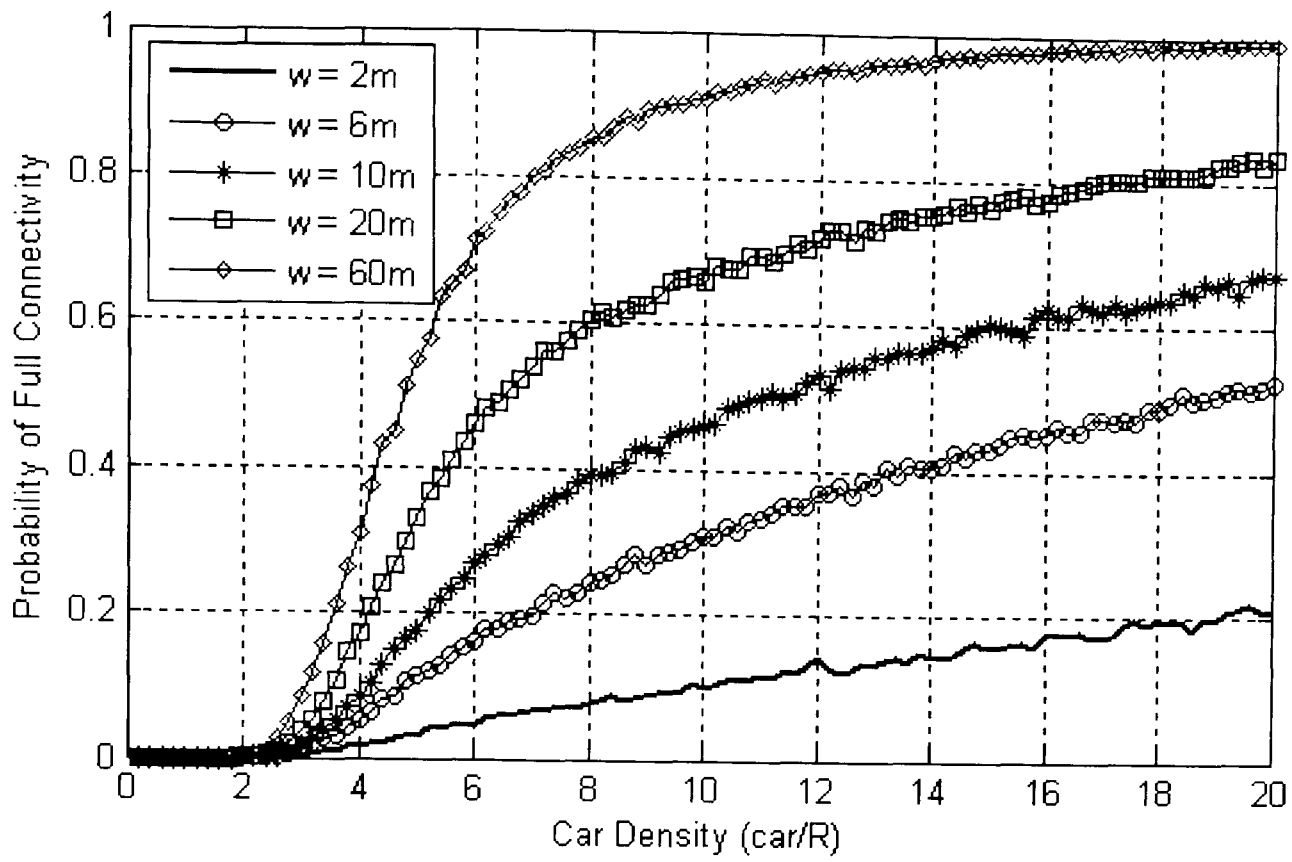

Figure (5.23): Probability of Full Connectivity for Various Road Widths, $\phi = 90°$

5.5.2. Junctions

Figure (5.24) shows the layout for two single-lane roads forming a junction. The two roads form two 90° turns from the prospect of each car, therefore we calculate the communication area for the cars before and after the junction using the equations of section (5.5.1). Due to the symmetry of the communication links we need only to calculate four covering areas, two for the car in road (*a*) before the junction and two for the car after the junction in the same road. In this topology the direct path is not the only possible path. For instance the direct route between the two nodes in road *a* may not exist if the distance between them is large. However a route may exist via one, or both, of the nodes in road *b*. The cars in the two roads are disconnected if any of the conditions listed in table (5.1) are satisfied. The first three conditions represent the cases when two of the four nodes at the junction can communicate with each other but not with the other two whereas the other four conditions are for when one of the nodes is disconnected from the other three.

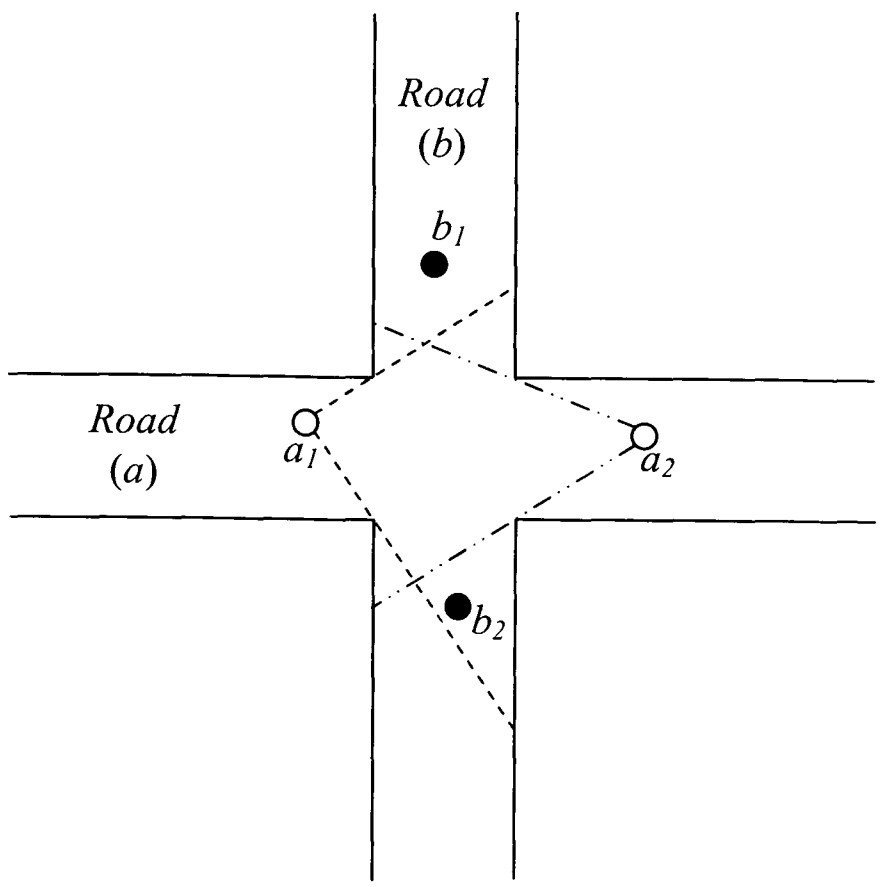

Figure (5.24): Topology of a Junction

1	(a_1,b_1) & (a_1,b_2) & (a_2,b_1) & (a_2,b_2) disconnected
2	(a_1,b_2) & (a_2,b_1) & (a_1,a_2) & (b_1,b_2) disconnected
3	(a_1,b_1) & (a_2,b_2) & (a_1,a_2) & (b_1,b_2) disconnected
4	(a_1,b_1) & (a_1,b_2) & (a_1,a_2) disconnected
5	(a_2,b_1) & (a_2,b_2) & (a_1,a_2) disconnected
6	(a_1,b_1) & (a_2,b_1) & (b_1,b_2) disconnected
7	(a_1,b_2) & (a_2,b_2) & (b_1,b_2) disconnected

Table (5.1): Conditions for a Disconnected Junction

Figure (5.25) shows the probability of full connectivity for the topology of figure (5.24). The simulations are for single lane roads, 10R long and R = 250m. As with curves, we observe that the connectivity improves as the road width increases since the communication areas of the nodes increase. We also note that the probability of full connectivity for a junction is better that the probability for a curve with 90° turn. The reason for this improvement is in junction, alternative routes, other than the direct route, may exist between the nodes. For instance, nodes a_2 and b_1 in figure (5.24) may communicate via the route a_2-a_1-b_2-b_1. Such alternative routes do not exist in turns and hence the probability is worse than the probability for junctions.

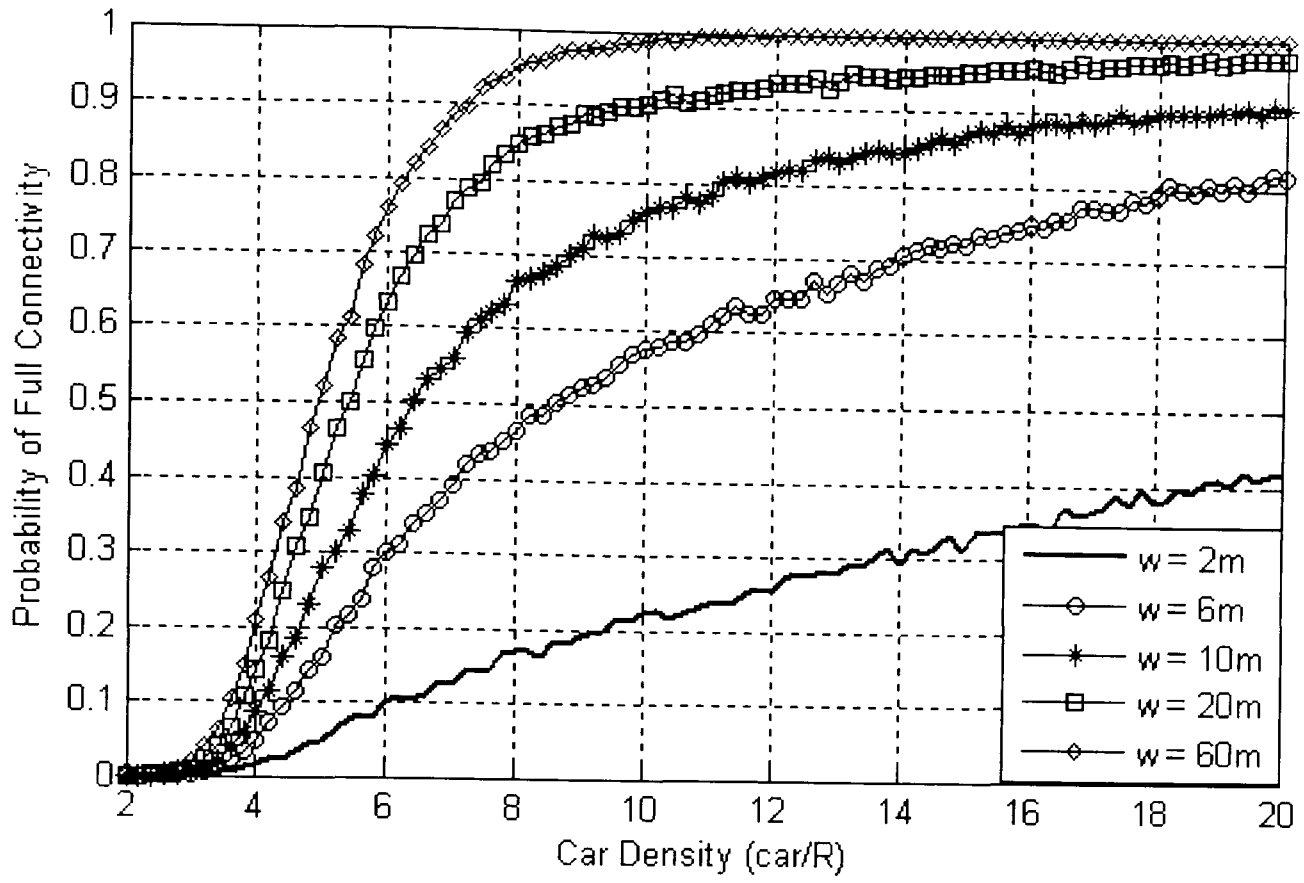

Figure (5.25): Probability of Full Connectivity for Junctions

5.5.3. Roundabouts

Although roundabouts have the same topology as junctions, statues or trees on the roundabout may block the line of sight. Assuming the line of sight between nodes a_1 and a_2, and the line of sight between nodes b_1 and b_2 are always blocked, i.e. (a_1, a_2) and (b_1, b_2) are always disconnected, the conditions of table (5.1) reduce to:

1	(a_1,b_2) & (a_2,b_1) disconnected
2	(a_1,b_1) & (a_2,b_2) disconnected
3	(a_1,b_1) & (a_1,b_2) disconnected
4	(a_2,b_1) & (a_2,b_2) disconnected
5	(a_1,b_1) & (a_2,b_1) disconnected
6	(a_1,b_2) & (a_2,b_2) disconnected

Table (5.2): Conditions for a Disconnected Roundabout

Figure (5.26) shows the probability of full connectivity for roundabouts when the line of sight is blocked. Comparing the results with figure (5.25), we note that the blockage of line of sight reduces the probability of full connectivity since the number of

possible routes is reduced. As with junctions and turns, the probability improves as the road width increases.

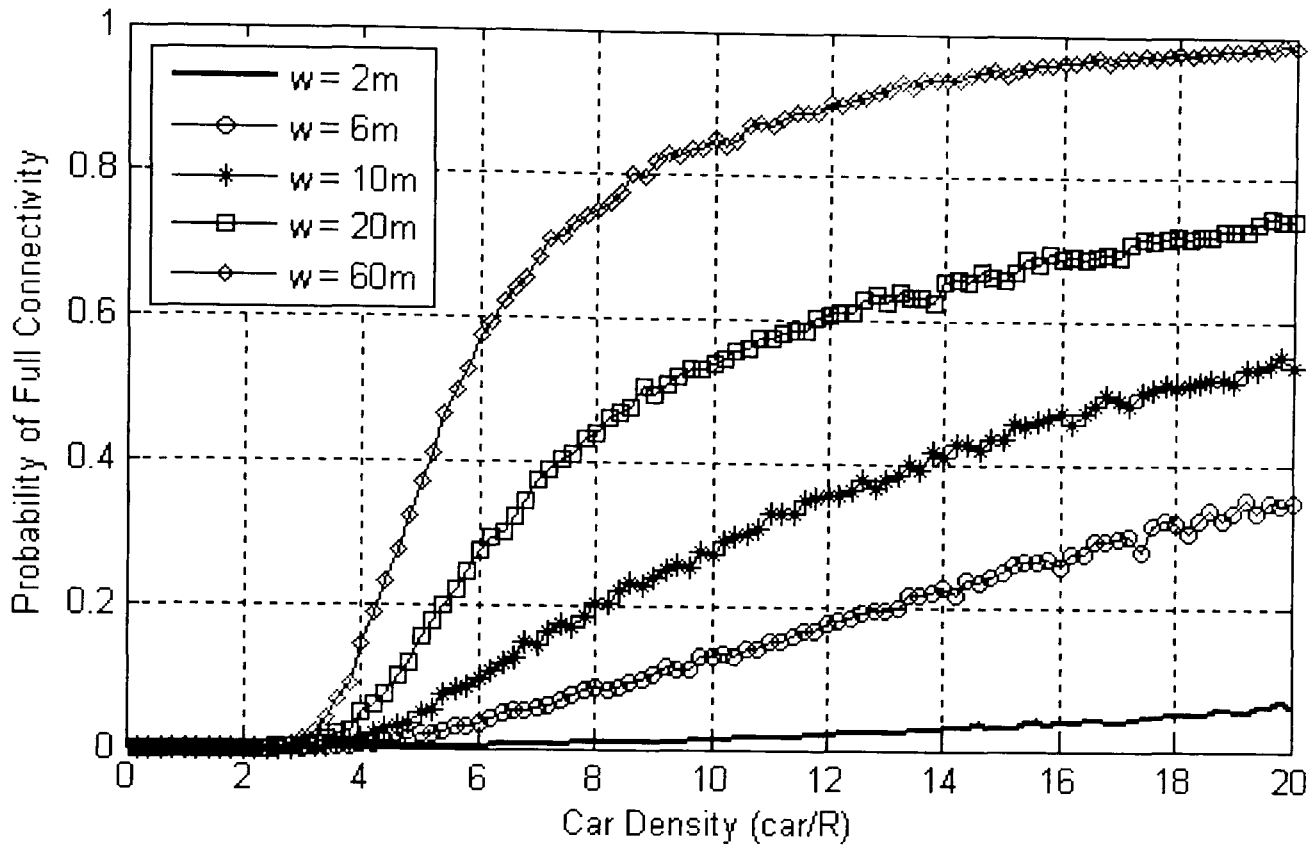

Figure (5.26): Probability of Full Connectivity for Roundabouts

5.6. Connectivity and Penetration Rate

Penetration rate is the percentage of the cars having the necessary hardware and software to participate in VANET. So far we assumed all cars in the road are equipped with communication devices and are able to communicate. However the deployment of vehicular communication equipments will take time, hence not all cars will be equipped at the beginning. In this section we investigate the effects of penetration rate on connectivity. We consider in our simulations penetration rates of 5%, 10%, 20%, 50%, and 70% and compare them to the previous results which represent 100% penetration in figure (5.27). The analysis is for a single lane road, 10R long and a range of 250m.

As observed from figure (5.27), for penetration rates of 50% or more the probability of achieving full connectivity is greater than 80% for a car density of 10cars/R. However at low penetration rates (5-20%) this density is insufficient even to maintain 10% probability. We conclude from this that in the early stages of VANET deployment,

the network will provide little service for drivers on the road unless a large number of road side units are installed. Similar conclusion were reached in [151] and the authors suggest the provision of home-to-vehicle applications, such as download of route information, download of music, acquiring up-to-date traffic conditions (e.g. via the internet), to encourage users to install the system.

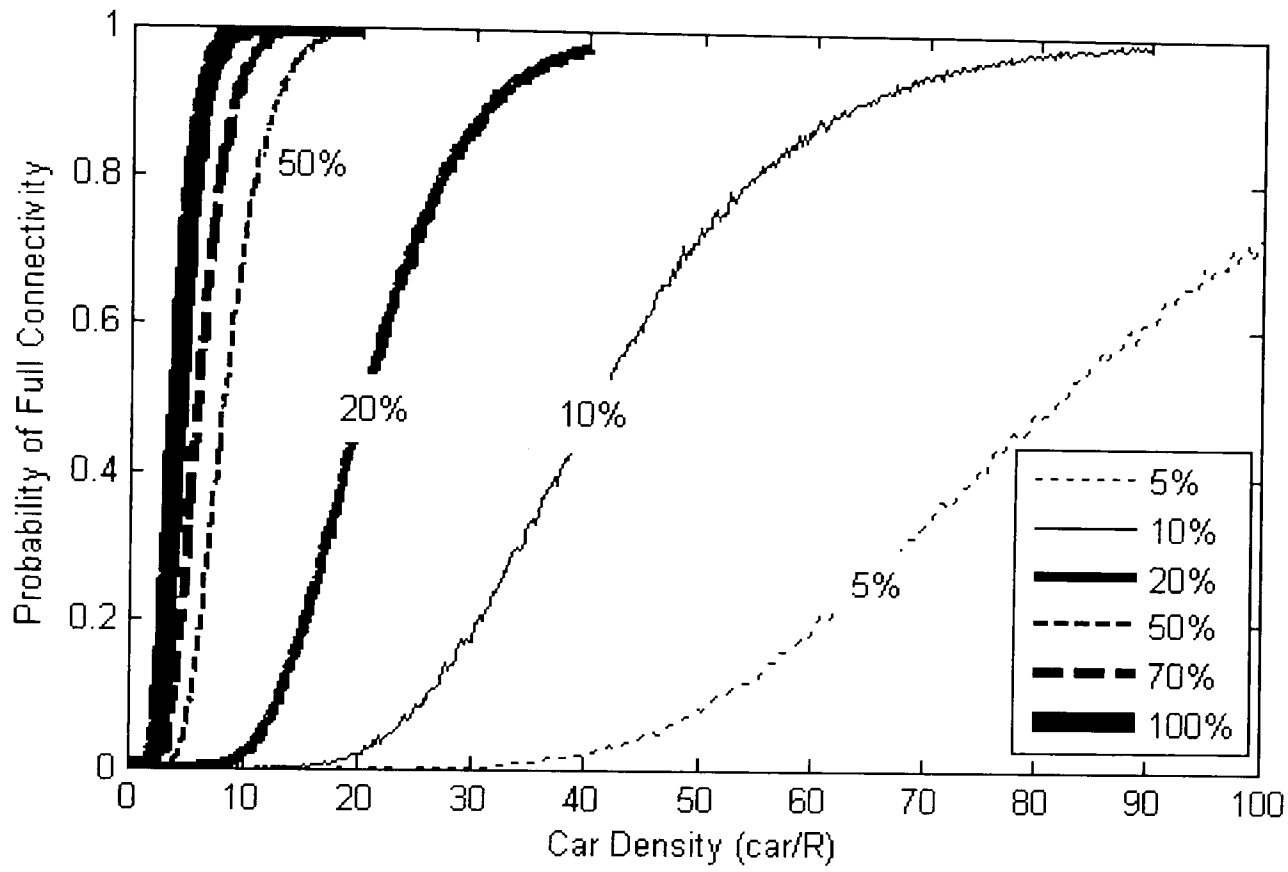

Figure (5.27): Effect of Penetration Rate on Probability of Full Connectivity

5.6. Concluding Remarks

In this chapter we investigated the issue of connectivity in vehicular networks. From the simulation results we conclude that for a 1 dimensional network with communication range of 1 km and 100 km road to be fully connected the node density must be at least 12cars/km. In multilane roads even higher node densities are required since the cars tend to cluster in groups with a large number of nodes per group thus increasing the probability of having isolated groups or even isolated nodes. This last remark is extremely important in the design of the link layer access mechanism since the performance of the link layer depends on the available traffic and the number of nodes. Within the city, a density of 7cars/R is sufficient to guarantee 95% probability of

full connectivity for single lane roads, where R is the communication range. Roads with several lanes have higher average node connectivity but lower probability of full connectivity and number of groups due to the clustering of the nodes. Roads with curves or turns have lower connectivity than straight roads due to the loss of communication between cars before and after the curves. The connectivity drops as the turn angle increases, but improves as the road width increases. Junctions have higher connectivity than turns because several routes exist whereas in roundabouts with obstacles blocking the line of sight the connectivity is lower than in roads with turns. For penetration rates of 50-70% achieving 80% probability of full connectivity requires 10cars/R while for penetration rates of 5-20% the probability for the same node density is less than 10%. This means at the start of VANET deployment, home-to-vehicle applications are essential for market penetration as the network will not be able to provide services on the road with acceptable quality unless a large number of expensive road side units are installed.

Chapter 6

Analysis of 802.11 Medium Access Control

6.1. Overview

The IEEE is working on a MAC layer standard (IEEE 802.11p) which is based on 802.11a and 802.11e standards. 802.11 standards have two modes of operation, a centralised mode which requires an access point, known as the Point Co-ordination Function (PCF), and an ad hoc mode called the Distributed Co-ordination Function (DCF). 802.11e uses an Enhanced DCF (EDCF) to provide quality of service (QoS) by using separate queues and counters for different priority classes. As DCF is a random access mechanism based on Carrier Sense Multiple Access (CSMA), it has an unreliable broadcasting service, provides low throughput as the number of devices increases and has little support for Quality of Service (QoS) [116, 152-154]. A request-to-send clear-to-send (RTS/CTS) handshake, supported in DCF, can be used to improve the performance of point-to-point transfers but is not applicable to broadcast messages. A large number of messages in vehicular networks are broadcasting by nature, e.g. safety messages, location messages, traffic condition messages, therefore the RTS/CTS handshake cannot be used with them. Moreover the number of nodes varies with time and location and peaks in congested areas leading to severe degradation in DCF performance [116, 152-154]. EDCF provides some QoS but packets still contend for the channel and may collide with others having the same QoS requirements (e.g. safety messages from different cars). In this chapter we investigate and analyse the throughput

performance of the 802.11 MAC layer standards. Since DCF is based on CSMA, we start by analysing CSMA.

6.2. Analysis of CSMA

In CSMA, prior to transmission a node senses the channel. If no transmission is sensed, it sends its packet, otherwise it waits for a random amount of time before attempting to transmit again. A slotted version of CSMA can be used in which time is divided into slots and nodes only transmit at the beginning of a slot. The performance of CSMA depends on the available traffic in the network as shown by Kleinrock *et. al.* in [116, 154, 155]. According to their findings the throughput (S) of non-slotted CSMA for a given traffic (G) in a network with an infinite number of nodes, no hidden terminals and fixed packet length is given by:

$$S = \frac{G.e^{-aG}}{G(1+2a)+e^{-aG}} \qquad (6.1)$$

For slotted access the throughput is calculated as [116]:

$$S = \frac{a.G.e^{-aG}}{\left(1-e^{-aG}\right)+a} \qquad (6.2)$$

The parameter (a) is the vulnerable duration of transmission. It is the duration required for all nodes within the system to recognise that a packet is being transmitted normalised to the packet transmission time. The vulnerable period includes the switching time from sensing to transmitting, the maximum propagation delay in the network, and the time required to detect a transmission in the channel. If a node attempts to transmit a packet during the vulnerable period of another packet, a collision will occur. After the vulnerable period, all nodes are aware that the channel is busy and therefore defer their transmissions. G is the offered network traffic per packet transmission duration assuming fixed packet size.

We used equations (6.1) and (6.2) to plot the throughput performance of non-slotted CSMA, figure (6.1), and slotted CSMA, figure (6.2) for various values of (a). As can be seen from figure (6.1), the value a = 0, which corresponds to all nodes sensing the

transmission immediately, gives the best results. The reason for this is when $a = 0$, two packets can collide if and only if they were transmitted at the same time. Since the probability of this event is generally very small, collisions rarely occur and the performance is high. On the other hand for $a = 1$, some of the nodes can sense the packet only at its end since the vulnerable period is equal to the packet transmission time. In this case a collision occurs if another packet arrives at any time between the beginning and end of the transmission. Since the probability of this event is generally high especially at heavy loads, a large number of collisions occur leading to low performance.

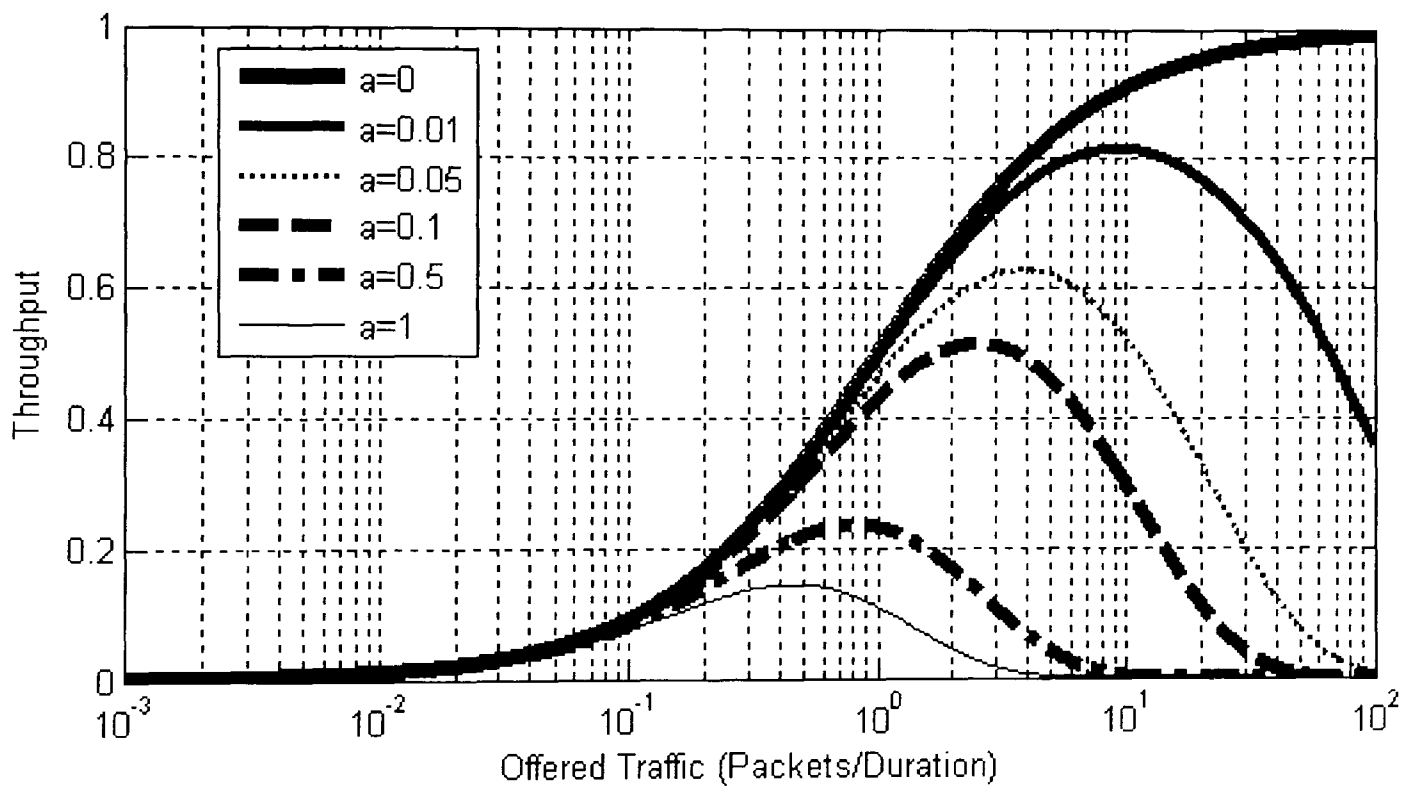

Figure (6.1): CSMA Throughput vs. Traffic, non-slotted CSMA

Figure (6.2) is the throughput for slotted CSMA. Here the channel is decimated into time slots and nodes access the channel at the beginning of a slot. The performance is improved compared to non-slotted access since a packet arriving in the middle of a slot is deferred till the next slot. During this additional waiting time it is possible for the node to detect an ongoing transmission and therefore avoid collision [116].

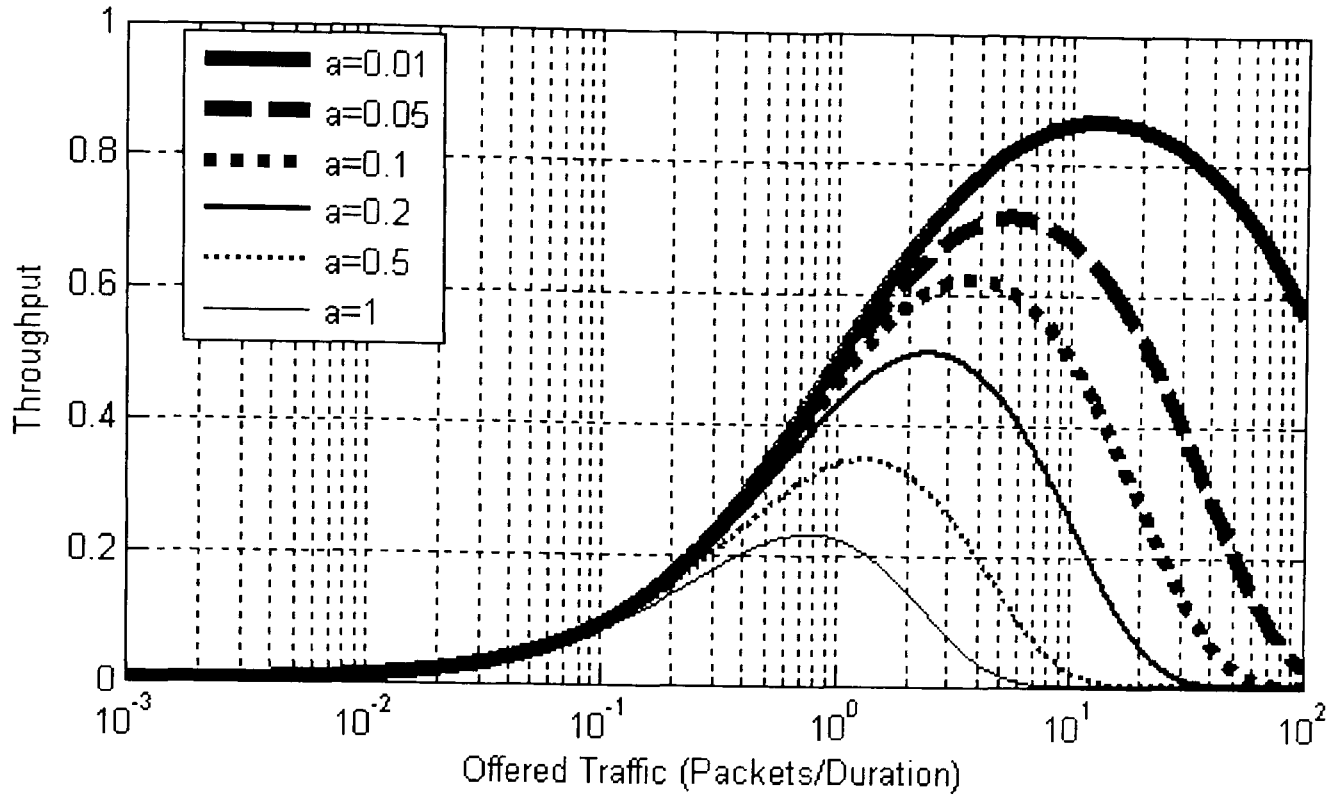

Figure (6.2): CSMA Throughput vs. Traffic, slotted CSMA

6.3. Analysis of IEEE 802.11

The IEEE 802.11 uses the Distributed Co-ordination Function (DCF) for channel access in ad hoc environments. The standard also defines an optional Point Co-ordination Function (PCF) which supports quality of service and traffic with time constraints but requires the use of a central point for polling. Generally PCF is not suitable for ad hoc networks and, therefore, DCF will be our main focus. DCF defines two types of operation both based on slotted CSMA. In the first type, known as basic access, a node senses the channel and if it is idle for a period known as distributed inter-frame space (DIFS), it sets a transmission counter to a random value, uniformly distributed between 0 and a value known as the contention window (CW). The contention window takes a value from CW_{min} to $2^m CW_{min}$, CW_{min} and m are predefined fixed numbers. It starts from CW_{min} and doubles every time a collision occurs until it reaches its maximum value. CW_{min} and m are physical layer dependent and specified in the standard. The value of the transmission counter is decremented every idle time slot and when it reaches zero the packet is transmitted. This is known as the back off procedure and it is used to avoid collisions. After receiving the packet correctly, the

destination waits for a duration known as short inter-frame space (SIFS), which is less than DIFS, and then transmits an acknowledgement (ACK). If no ACK is received, the transmitter assumes a collision occurred and schedules the packet for retransmission. In the other access mode, commonly known as the RTS/CTS mode, the node attempts to reserve the channel prior to transmission. A node sensing the channel idle sets the transmission timer exactly as in the basic mode, however when the timer expires, it transmits a request to send (RTS) packet. The destination node will reply, after an SIFS, with a clear to send (CTS) packet if it senses the channel idle. All nodes sensing the RTS and/or CTS will defer their transmission till the end of the transmission duration specified in the RTS and CTS packets. The source then is free to transmit its data as all the nodes are aware of the transmission and again if it is received correctly, the destination will reply with an ACK after an SIFS period. The source assumes a collision occurred if no CTS or ACK were received [95, 97, 98]. The time is divided into slots in DCF with each slot designed to account for the propagation delay and switching time of the nodes from receive to transmit, i.e. the slot time is closely related to the vulnerable period a [95, 116].

The performance of both access modes of DCF is different from the simple CSMA introduced previously. This is mainly due to the back off procedure of DCF and also the channel reservation handshake of the RTS/CTS mode. Several papers attempted to analyse the performance of DCF but of special interest are [152] which mathematically analysed the saturation throughput of DCF, i.e. throughput when nodes always have packets ready for transmission, and [153] which extended that analysis to unsaturated conditions.

In [152], Bianchi introduced a Markov chain model to approximate the back off procedure in DCF. In his analysis, he assumed no hidden terminals and saturation load conditions. By solving the Markov chain, the probability (τ) that a node transmits at a random time slot was found to be:

$$\tau = \frac{2(1-2p)}{(1-2p)(W+1)+pW\left(1-(2p)^m\right)} \qquad (6.3)$$

Where W is the minimum window size ($W = CW_{min}$), m defines the maximum window size ($CW_{max}=2^m \times CW_{min}$) and p is the probability of collision. In a network with n nodes a collision occurs for an ongoing transmission, say from node 1, if any of the other n-1 nodes transmits. Hence [152]:

$$p = 1-(1-\tau)^{n-1} \tag{6.4}$$

Equations (6.3) and (6.4) can then be solved to find the probability of transmission and probability of collision for each node. The probability (P_{tr}) of at least one transmission in the network is given by [152]:

$$P_{tr} = 1-(1-\tau)^{n} \tag{6.5}$$

The probability (P_s) that the transmission is successful is the probability that only one station transmits in the channel conditioned on the fact that at least one station transmits. This is given by [152]:

$$P_s = \frac{n\tau(1-\tau)^{n-1}}{1-(1-\tau)^{n}} \tag{6.6}$$

The throughput of the system S is the expected time used for successfully transmitting payload divided by the total time. This is calculated as [152]:

$$S = \frac{P_s.P_{tr}.E[P]}{(1-P_{tr})\sigma + P_{tr}.P_s.T_s + P_{tr}(1-P_s)T_c} \tag{6.7}$$

Where σ is the empty slot duration, T_s is the average channel busy time due to successful transmissions, T_c is the average channel busy time due to collisions and $E[P]$, is the average packet duration for successful transmission. The T_s and T_c times for basic and RTC/CTS access are calculated as [152]:

$$T_s^{bas} = H + E[P] + SIFS + \delta + ACK + DIFS + \delta \tag{6.8}$$

$$T_c^{bas} = H + E[P^*] + DIFS + \delta \tag{6.9}$$

$$T_s^{rts} = RTS + SIFS + \delta + CTS + SIFS + \delta + H + E[P] + SIFS + \delta + ACK + DIFS + \delta \tag{6.10}$$

$$T_c^{rts} = RTS + DIFS + \delta \tag{6.11}$$

H is the header transmission duration, $E[P^*]$ is the average duration of collision, δ is the propagation delay, RTS, CTS and ACK are the transmission durations of RTS, CTS and ACK packets. This model calculates the saturation throughput of the network, i.e. when every node always has a packet to transmit. It was extended in [153] to calculate the throughput for non saturated conditions by introducing a new parameter (p_0) which is the probability that the node has no packet to transmit. The modified equations are:

$$p = 1 - (1 - (1 - p_0)\tau)^{n-1} \quad (6.12)$$

$$P_{tr} = 1 - (1 - (1 - p_0)\tau)^{n} \quad (6.13)$$

$$P_s = \frac{n(1 - p_0)\tau(1 - (1 - p_0)\tau)^{n-1}}{1 - (1 - (1 - p_0)\tau)^{n}} \quad (6.14)$$

The rest of the equations from [152] remain unaltered.

6.4. 802.11 Performance

Table (6.1) shows the parameters of 802.11 for Frequency Hopping Spread Spectrum (FHSS), Direct Sequence Spread Spectrum (DSSS) and OFDM physical layers. The parameters of OFDM are based on 802.11a standard except the propagation delay which we modified to account for the 1 km range specified for 802.11p [11], instead of 100m as in 802.11a.

Parameter	FHSS	DSSS	OFDM
Packet payload	8184	8184	18768
MAC header	272 bits	272 bits	272 bits
Physical header (PHY)	128 bits	192 μs	32 μs
ACK	112 bits + PHY	112 bits + PHY	112 bits + PHY
RTS	160 bits + PHY	160 bits + PHY	160 bits + PHY
CTS	112 bits + PHY	112 bits + PHY	112 bits + PHY
Channel Bit Rate	1 Mbit/s	1, 2 Mbit/s	6 -54 Mbit/s
Propagation Delay	1 μs	1 μs	3.33 μs
Slot Time	50 μs	20 μs	9 μs
SIFS	28 μs	10 μs	16 μs
DIFS	128 μs	50 μs	34 μs

Table (6.1): Parameters of FHSS, DSSS and OFDM 802.11 PHY layers [96]

Using these parameters and the models introduced in section (6.3), we analysed the throughput of DCF. The throughput performance of DCF is shown in figures (6.3) and (6.4) for the FHSS parameters. As can be seen the performance of RTS/CTS is superior to the performance of the basic mode due to the reservation procedure employed in RTS/CTS which leads to a smaller average collision duration. The performance drops considerably as the number of nodes increases for basic access method due to collisions while for RTS/CTS the performance remains high. Figures (6.5) to (6.8) show the performance for different probability of transmission ($1-p_0$). As can be seen the throughput of basic access versus number of nodes improves as p_0 increase. This is expected since the higher the value of p_0 the lower the probability of transmission per node and therefore the probability of collision. The performance of a network with lightly loaded nodes improves as the number of nodes increase, since the aggregate traffic is increased and the idle time is reduced. RTS/CTS access is less affected by p_0 and the number of nodes than basic access due to the channel reservation handshake which reduces the channel collision time.

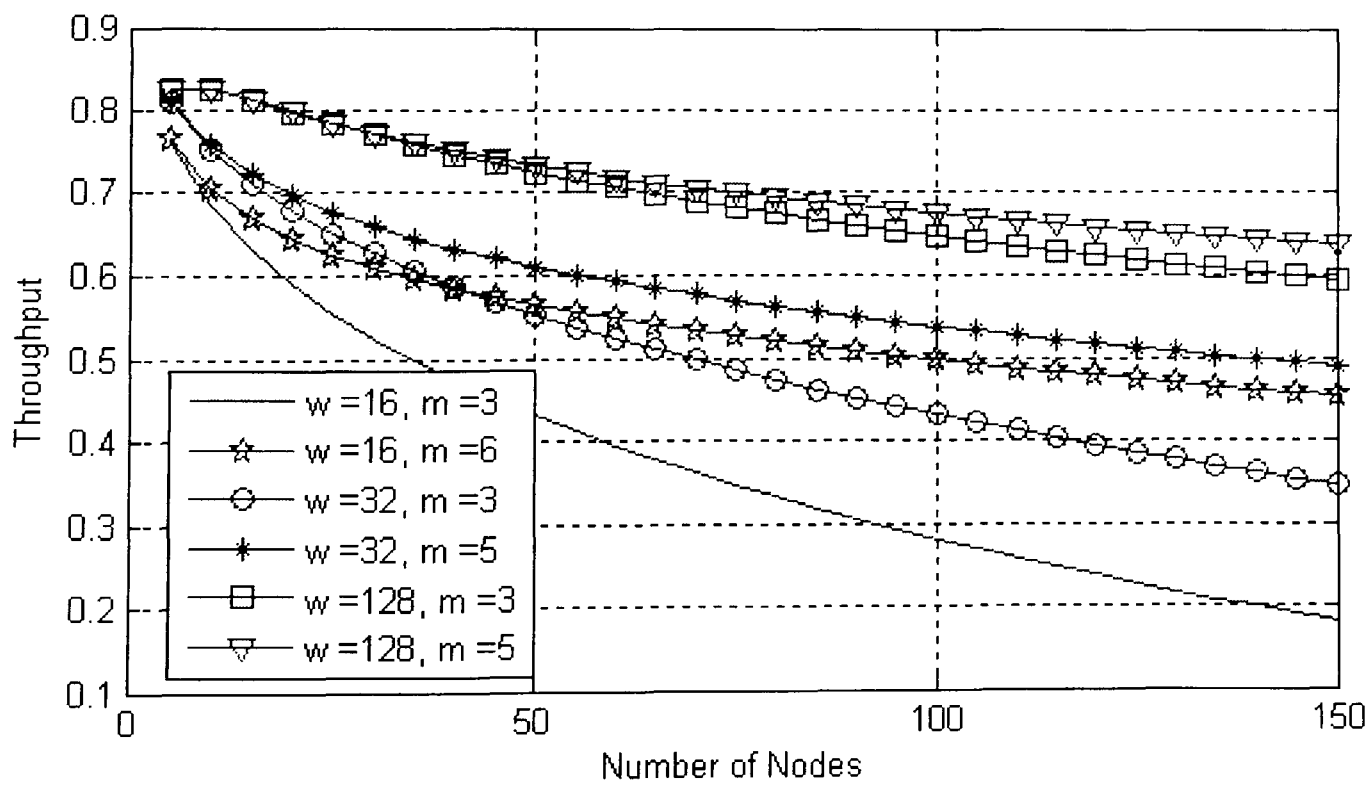

Figure (6.3): Throughput of 802.11 Basic Access vs. No. of Nodes, $p_0 = 0$

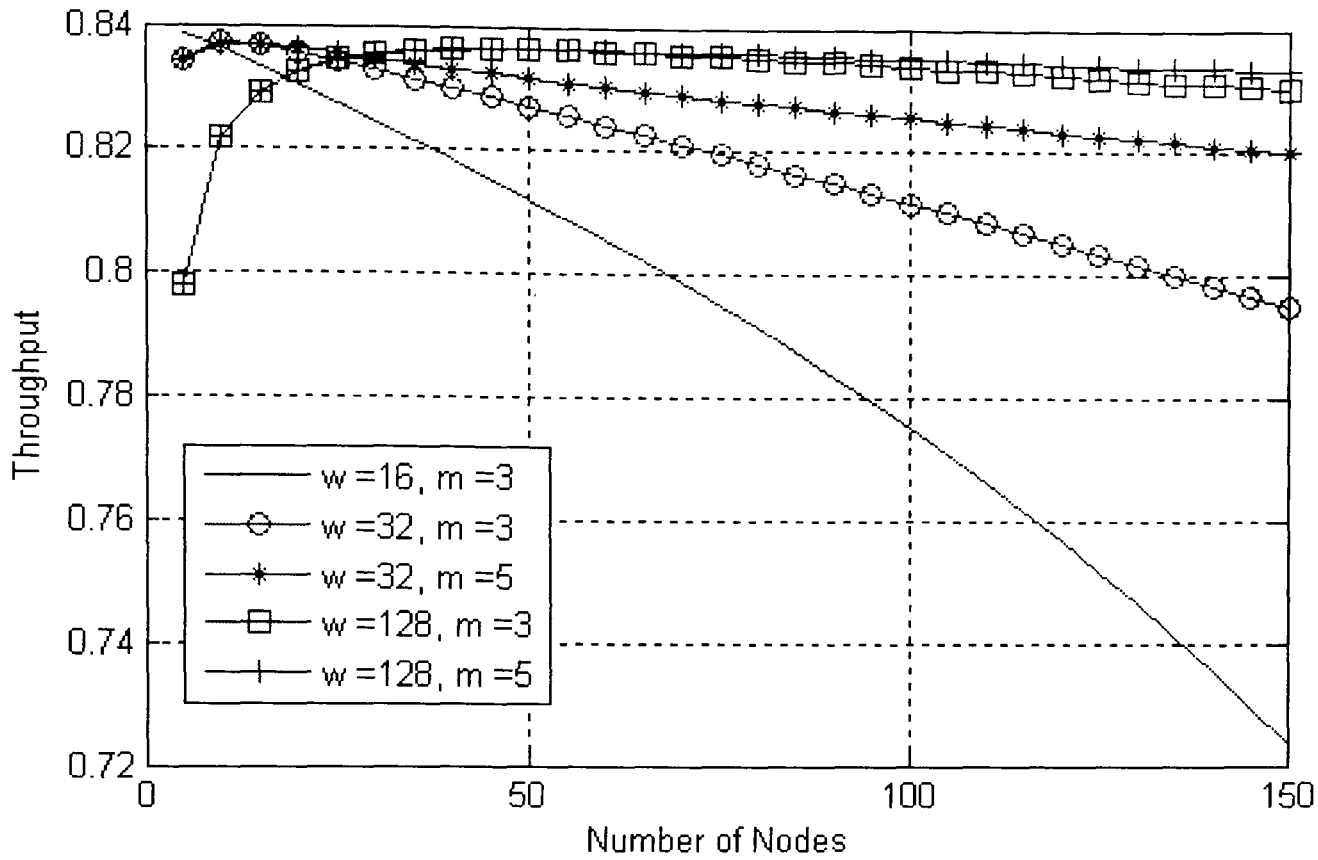

Figure (6.4): Throughput of 802.11 RTS/CTS vs. No. of Nodes, $p_0 = 0$

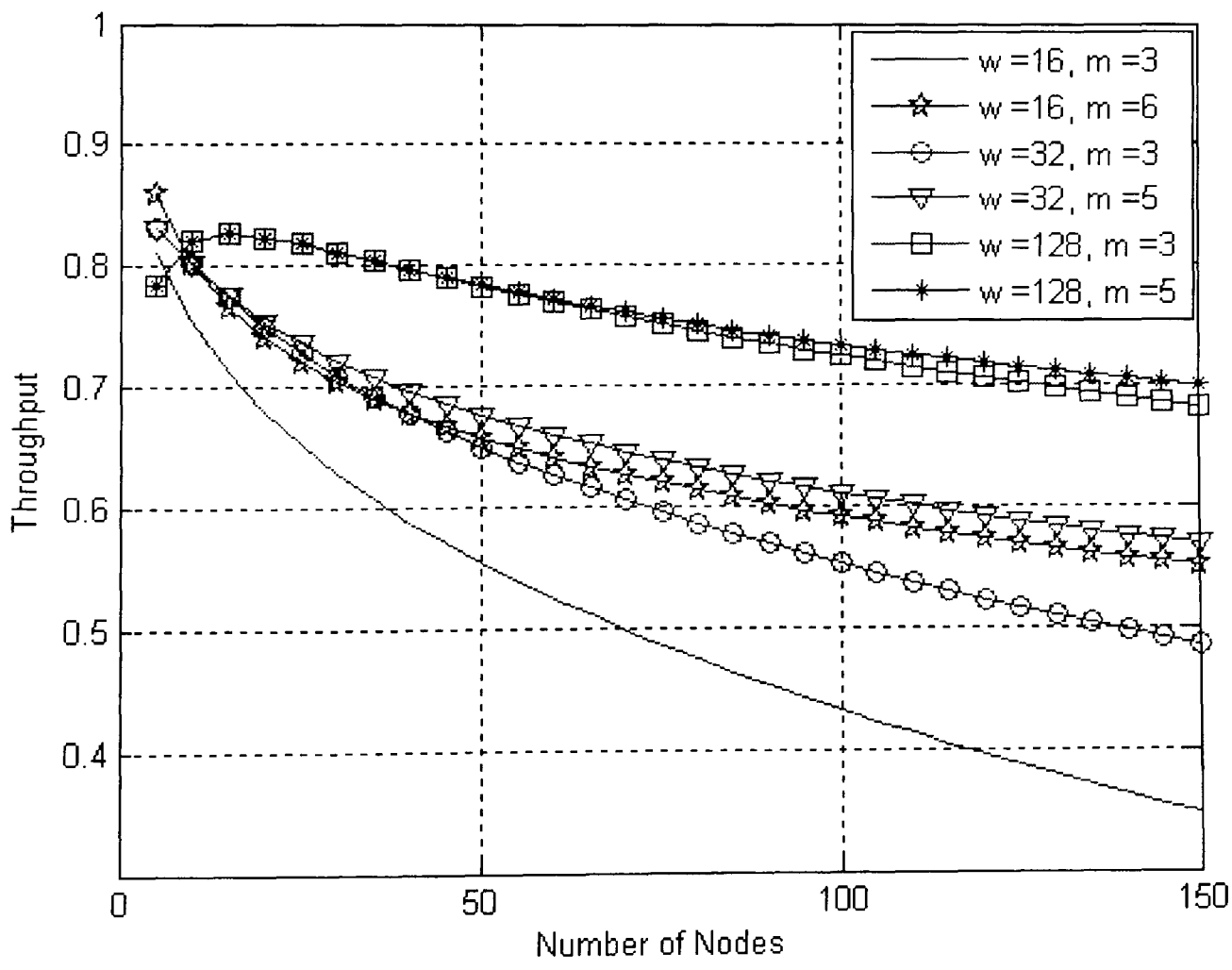

Figure (6.5): Throughput of 802.11 Basic Access vs. No. of Nodes, $p_0 = 0.5$

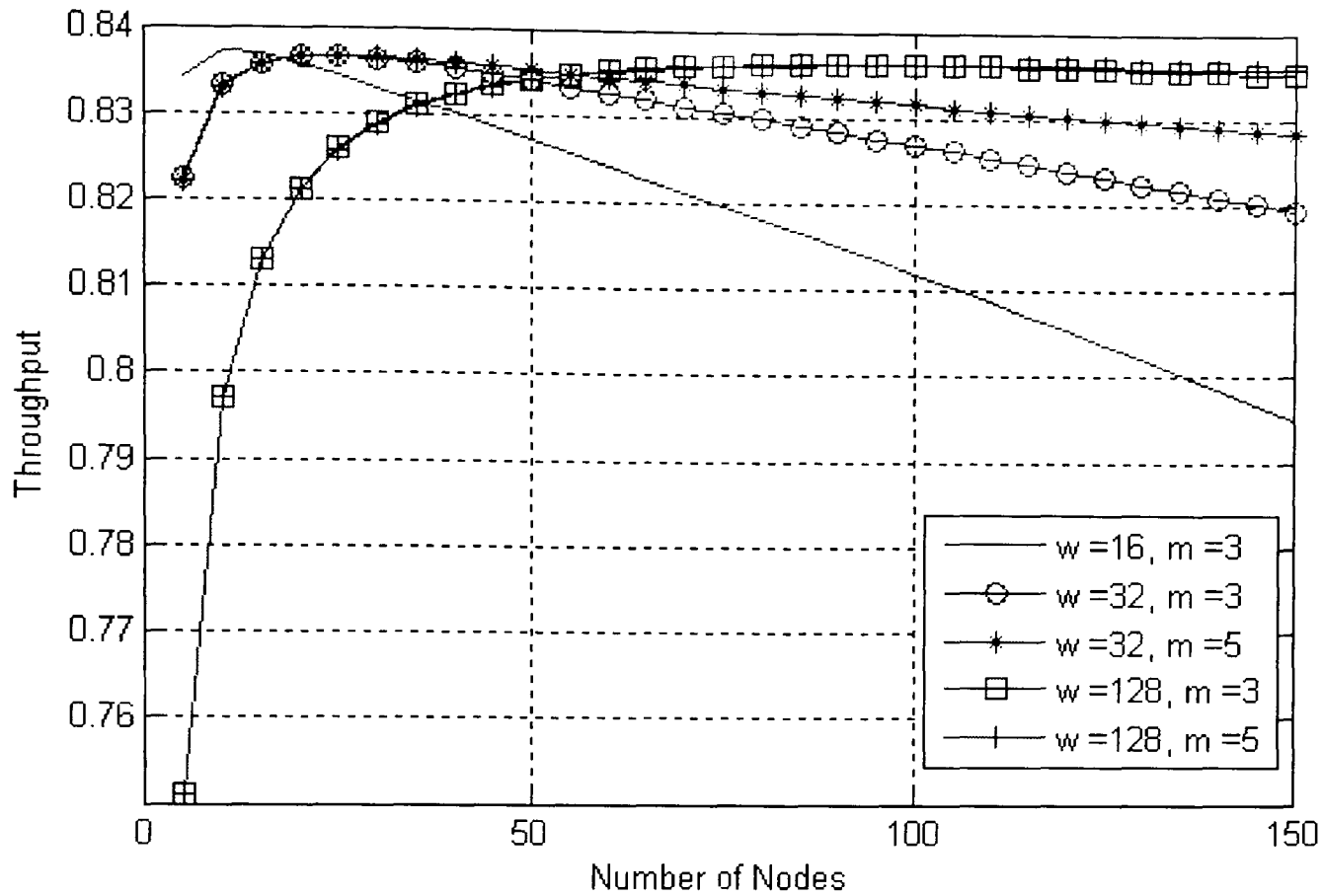

Figure (6.6): Throughput of 802.11 RTS/CTS vs. No. of Nodes, $p_0 = 0.5$

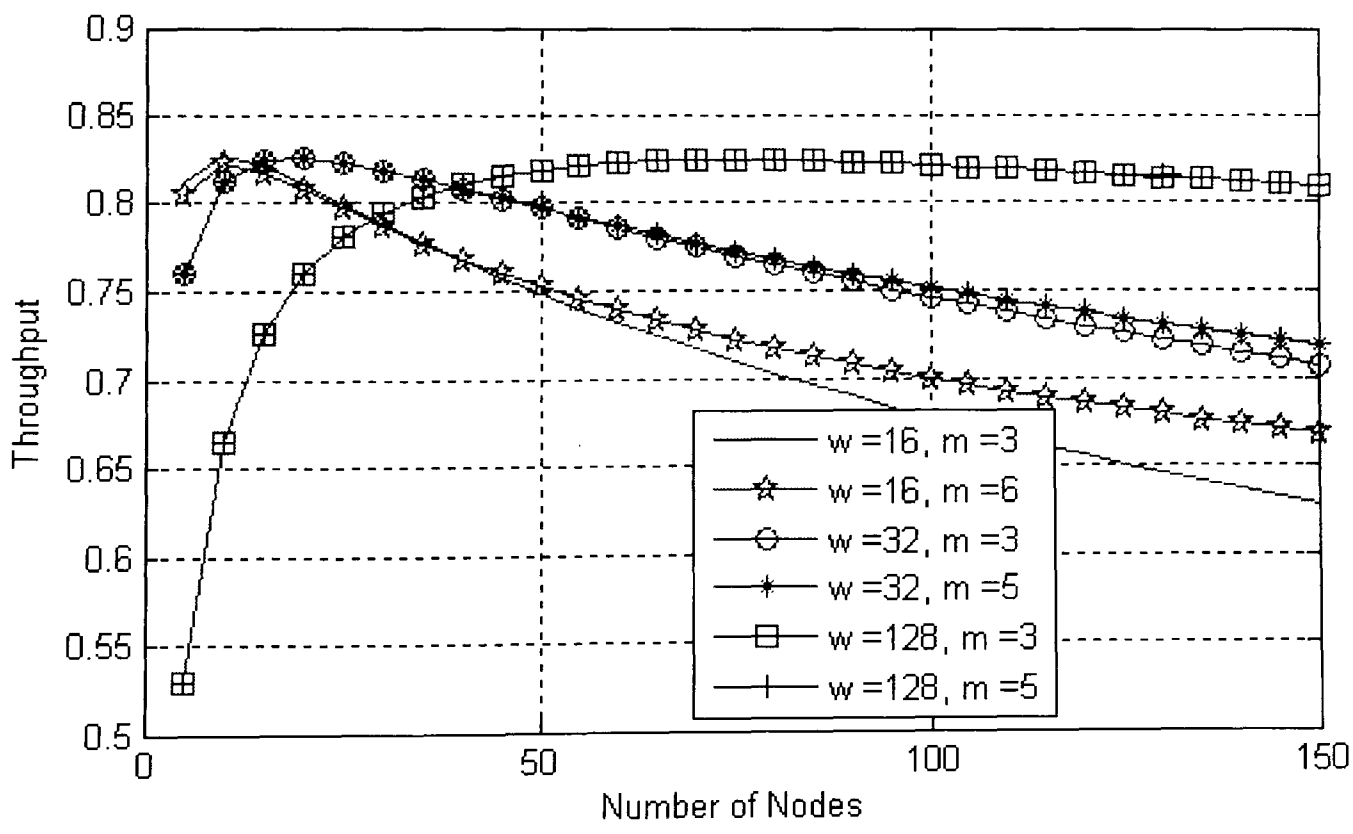

Figure (6.7): Throughput of 802.11 Basic Access vs. No. of Nodes, $p_0 = 0.9$

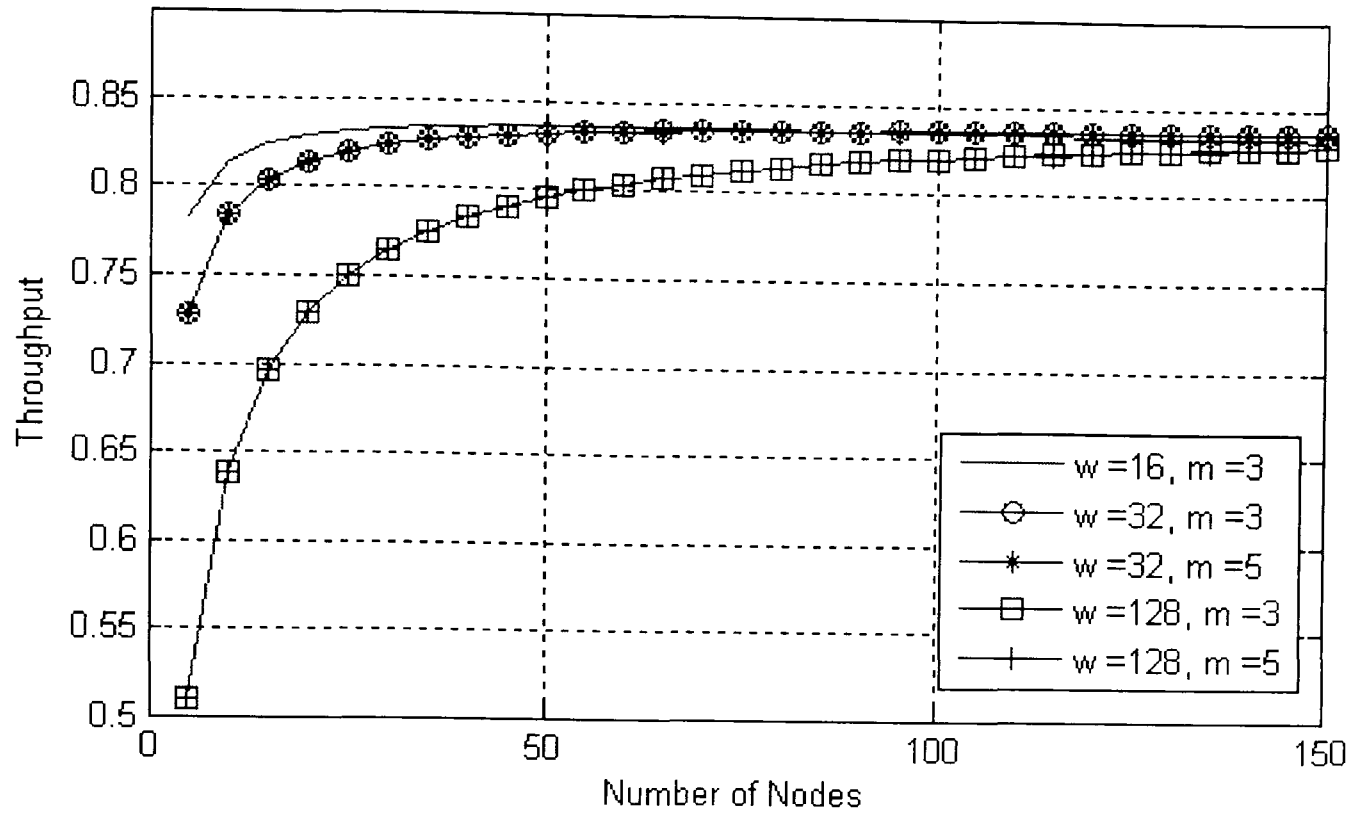

Figure (6.8): Throughput of 802.11 RTS/CTS vs. No. of Nodes, $p_0 = 0.9$

From the figures we note that the performance of DCF basic access is sensitive to the window size. A small window size means quick access to the channel as the range of the random back off counter will be small while for large window sizes a considerable amount of time is wasted before accessing the channel. This is the reason for higher throughput performance with small windows at light load and small number of nodes. As the number of nodes and traffic increase, the probability of collision increases. The back off counters then should take higher values and for this reason the performance of basic access with small contention window (w = 16, m = 3) drops considerably while a window of 128 shows superior performance. For the RTS/CTS access the performance at light load and small number of nodes is better for small windows than for large windows as in basic access. At heavy load the performance is better with larger windows but the improvement is not as large as with basic access (12% compared to 45%). The reason behind this is in RTS/CTS access most of the collisions occur during the channel reservation process, therefore the collision duration is short compared to basic access because RTS and CTS packets are only 20 and 14 bytes long [97, 98, 152].

To study the performance of 802.11 under various traffic conditions, we develop an equation relating the parameter p_0 to the available traffic. We follow the same approach used in [116, 154] to analyse CSMA to compare the two protocols afterwards. When a packet arrives at the MAC layer of a node, the node senses the channel. If the channel is idle the node initiates the transmission process, otherwise the packet is rescheduled for transmission after the ongoing channel transmission elapses. We assume that the traffic in each node is a Poisson process with average packets per node per packet transmission time, including any rescheduled packets, of λ [116]. The aggregate traffic in a network with n nodes is then $n\lambda$. We also assume no hidden terminals and fixed packet length. The probability of a packet arriving in a node within a duration c is given by:

$$P_{packet} = \int_0^c \lambda e^{-\lambda x} dx = 1 - e^{-\lambda c} \qquad (6.15)$$

Therefore the probability of no packet to transmit is:

$$P_{no\ packet} = 1 - P_{packet} = e^{-\lambda c} \qquad (6.16)$$

This is the expression that will be used to calculate the value p_0. However the average channel idle time between two transmissions (c) needs to be determined. For a packet rate of 1packet/packet duration or more for the whole network we expect the average channel idle time between two transmissions (c) to be:

$$c = \frac{1}{T}\left(DIFS + \frac{CW_{\min}}{2} \right) \qquad (6.17)$$

T is the packet transmission time. We use CW_{min} because in DCF if a successful transmission occurs, the CW is reset to CW_{min} so we expect most nodes will have their contention window set to CW_{min} most of the time. For lightly loaded networks, the idle time may be greater than that of (6.17) because the generation rate will be less than 1packet/duration. However as the number of nodes in the network increases, the aggregate packet rate of the network is expected to be much higher than 1packet/packet duration. With this model we analysed the performance of the two modes of DCF for the FHSS parameters of table (6.1) with window size w = 32, m = 3. The results are shown in figures (6.9) and (6.10). Comparing the saturation throughput in figures (6.9)

and (6.10) with the results of figures (6.3) and (6.4), we can see that the achievable saturation throughput from both analytical models is equal, thus validating our analysis. In the next section we analyse the performance of DCF and compare it with CSMA.

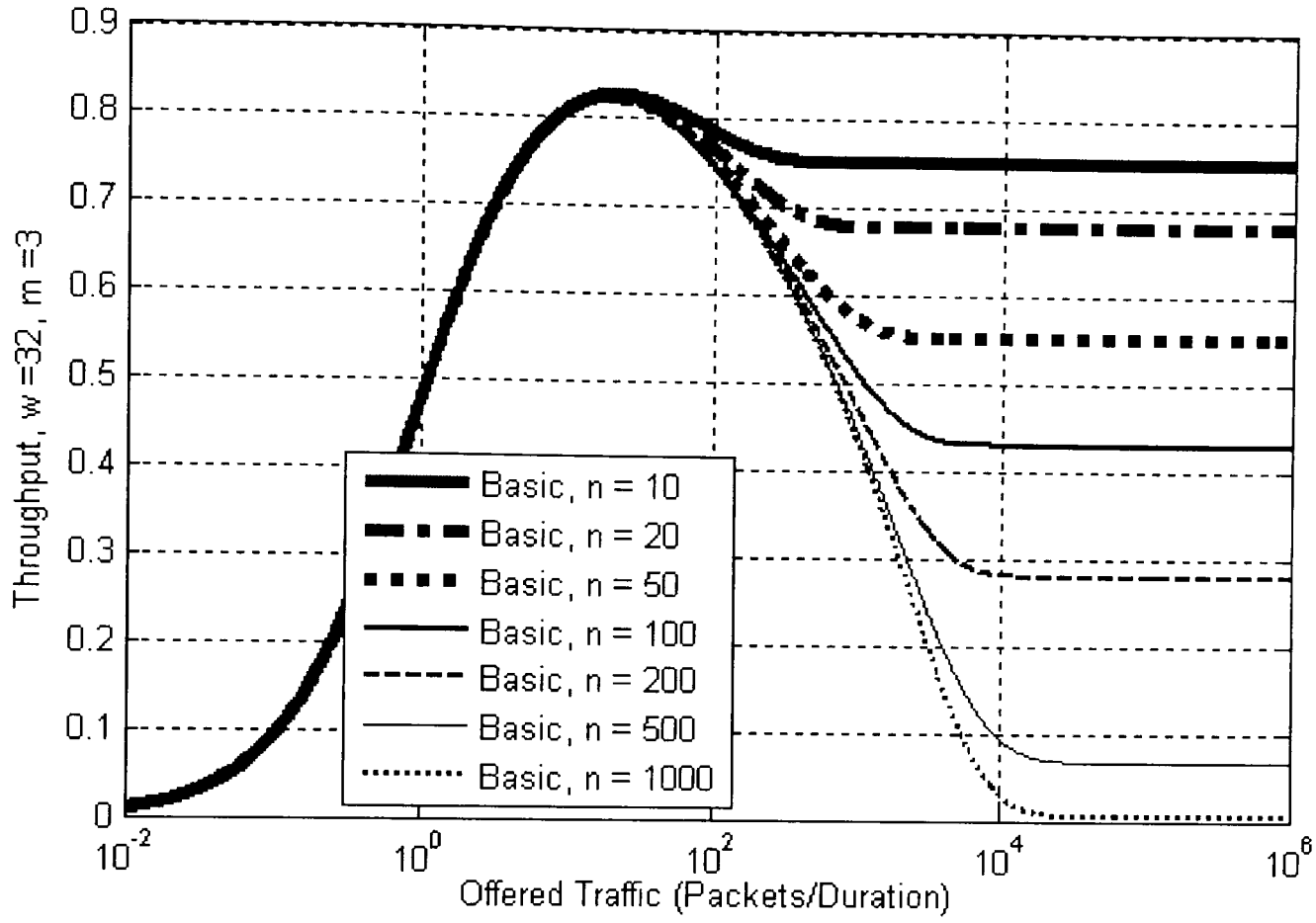

Figure (6.9): Basic Access Throughput vs. Offered Traffic

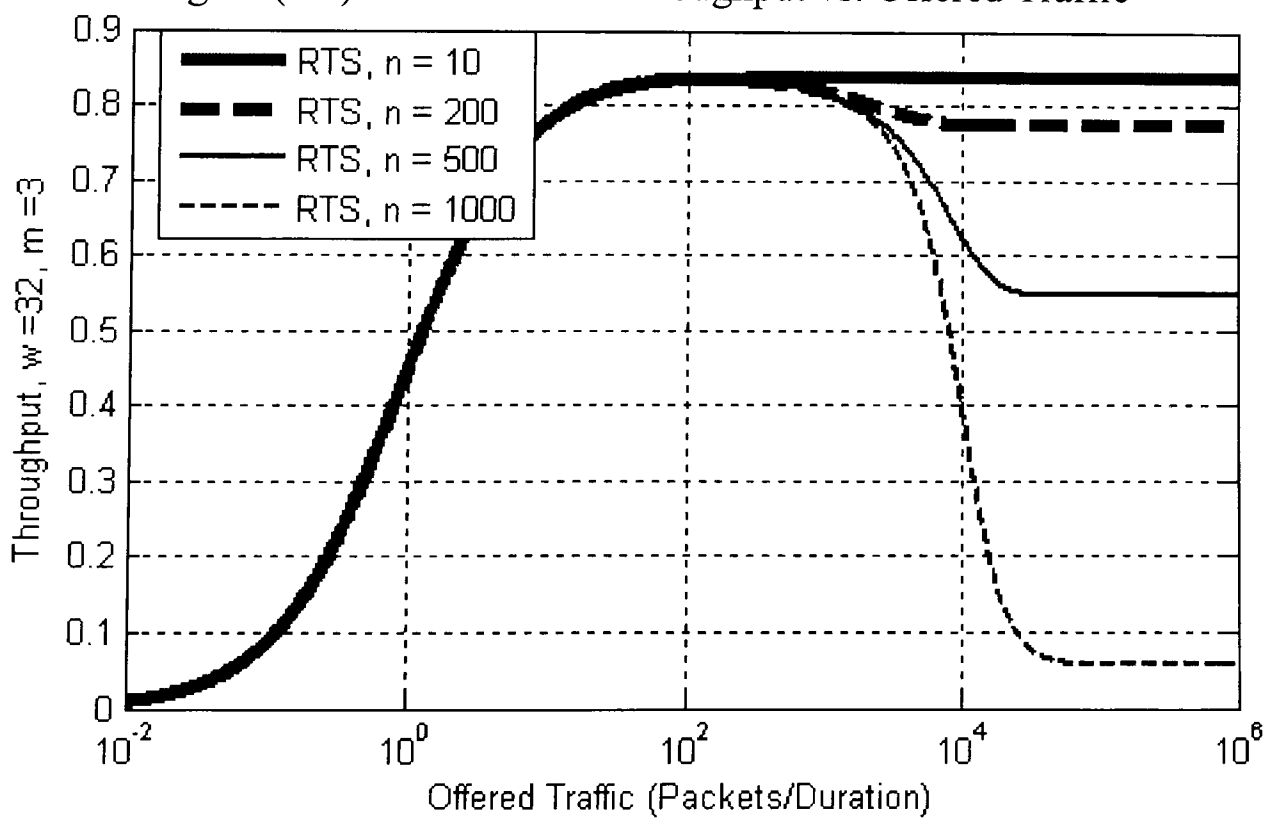

Figure (6.10): RTS/CTS Throughput vs. Offered Traffic

6.5. DCF and CSMA

We now compare the performance of DCF with slotted CSMA. The value of (a) for CSMA equivalent to DCF is the ratio of slot time (σ) to the average successful packet time (T_s) of basic access. This is true because the slot time in DCF (σ) depends on the propagation delay and node switching time which define the vulnerable period of the packet transmission as discussed in section (6.2). We compare DCF with slotted CSMA since time slots are used in 802.11.

Figures (6.11) and (6.12) compare the performance of CSMA with basic access and RTS/CTS access respectively. As observed from the figures, the performance of DCF is similar to that of slotted CSMA under light traffic conditions. At light load we expect a small number of collisions and therefore the contention window size will remain at its minimum value. As the load increases, collisions occur and the backoff procedure increases the window size. This can lead to unnecessary delays in the access to the channel hence the peak throughput of CSMA is higher than basic access and RTS/CTS access. The difference in performance between CSMA and DCF is also partially due to the fact that equations (6.1) and (6.2) do not take into account the capacity wasted in transmitting acknowledgements, RTS and CTS packets. DCF sacrifices this throughput to provide more transmission reliability and to support higher traffic than CSMA. At high traffic the performance becomes independent of the traffic and heavily dependent on the number of nodes. The reason for this is at high traffic the node always has a packet to transmit, i.e. $p_0 \approx 0$. When this occurs, additional traffic has little effects on the value of p_0 and the performance becomes independent of the traffic. However the number of nodes has a major impact on throughput as expected from equations (6.4) to (6.6). As the number of nodes increase the saturation throughput drops gradually. We note from the figures that even with a network of 1000 nodes the RTS/CTS access is able to deliver some packet successfully whereas the throughput of the basic access method reduces to approximately 0.

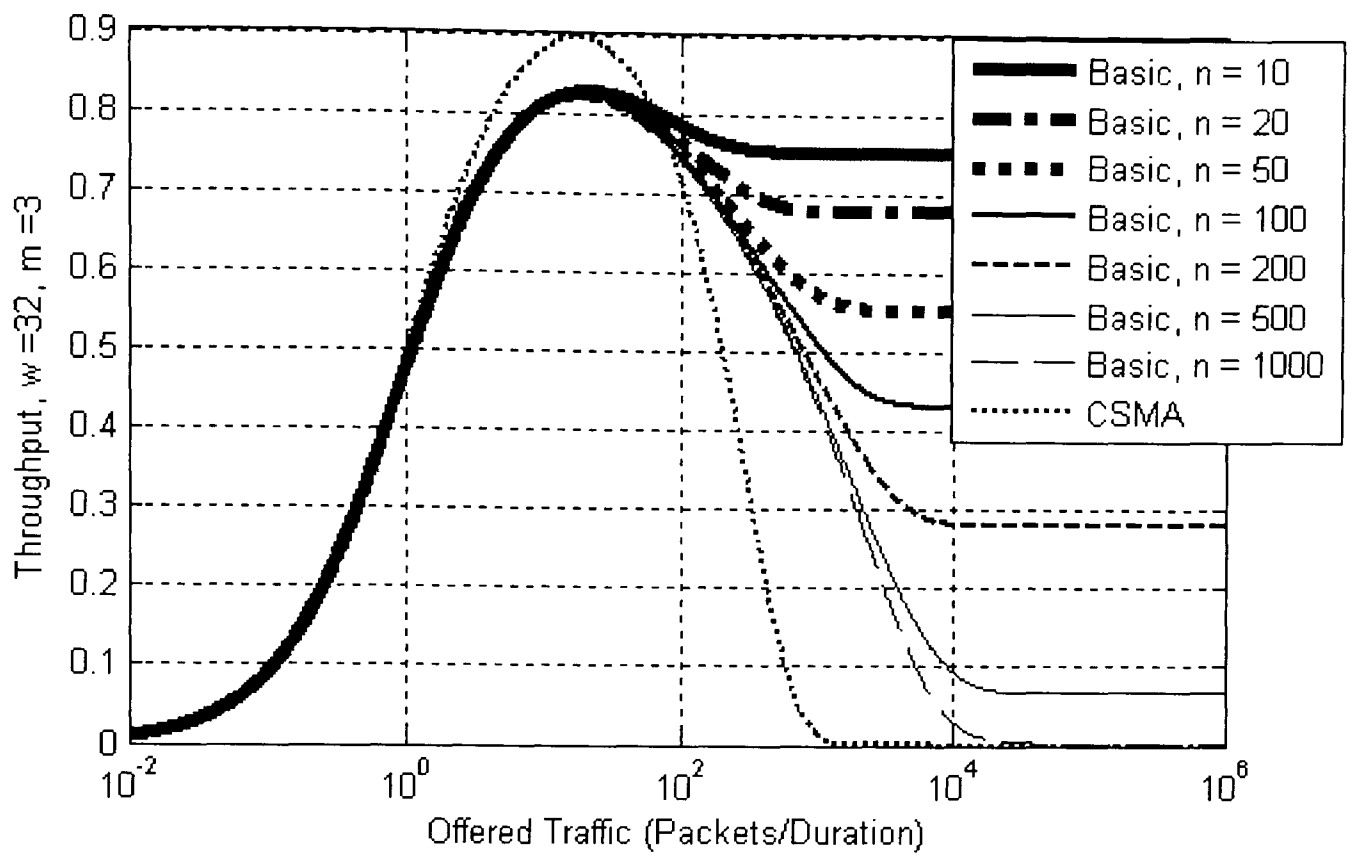

Figure (6.11): Comparison between CSMA and DCF Basic Access

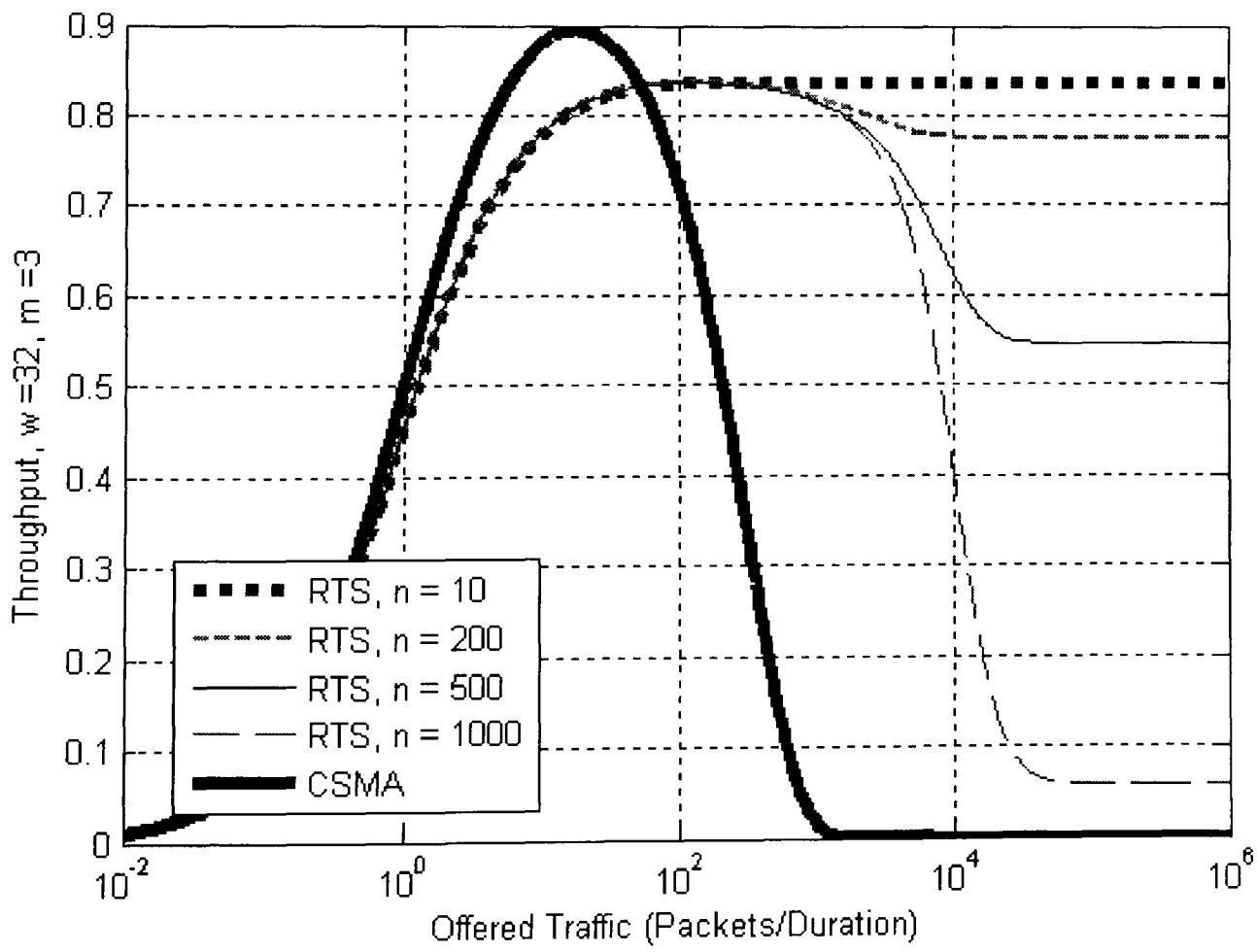

Figure (6.12): Comparison between CSMA and DCF RTS/CTS Access

Figures (6.13) and (6.14) show the expected performance of 802.11p for the OFDM parameters listed in table (6.1). The minimum size of the contention window in 802.11a is 16 and m = 6 [95]. As can be seen, the standard can achieve a slightly higher peak throughput than FHSS due to its small time slot and small initial window size. Both lead to quick channel access and higher performance. Moreover the maximum contention window size is large (1023); therefore the protocol can support a larger number of nodes compared to the w = 32, m = 3 case. However as the number of nodes increase the performance drops gradually especially for basic access. From the figures we note that for a network of 1000 nodes, RTS/CTS mode provides a throughput of approximately 80% whereas the throughput of basic access drops to less than 20%. The channel reservation process of RTS/CTS access considerably improves the throughput performance, but it can be used only for point-to-point transmissions.

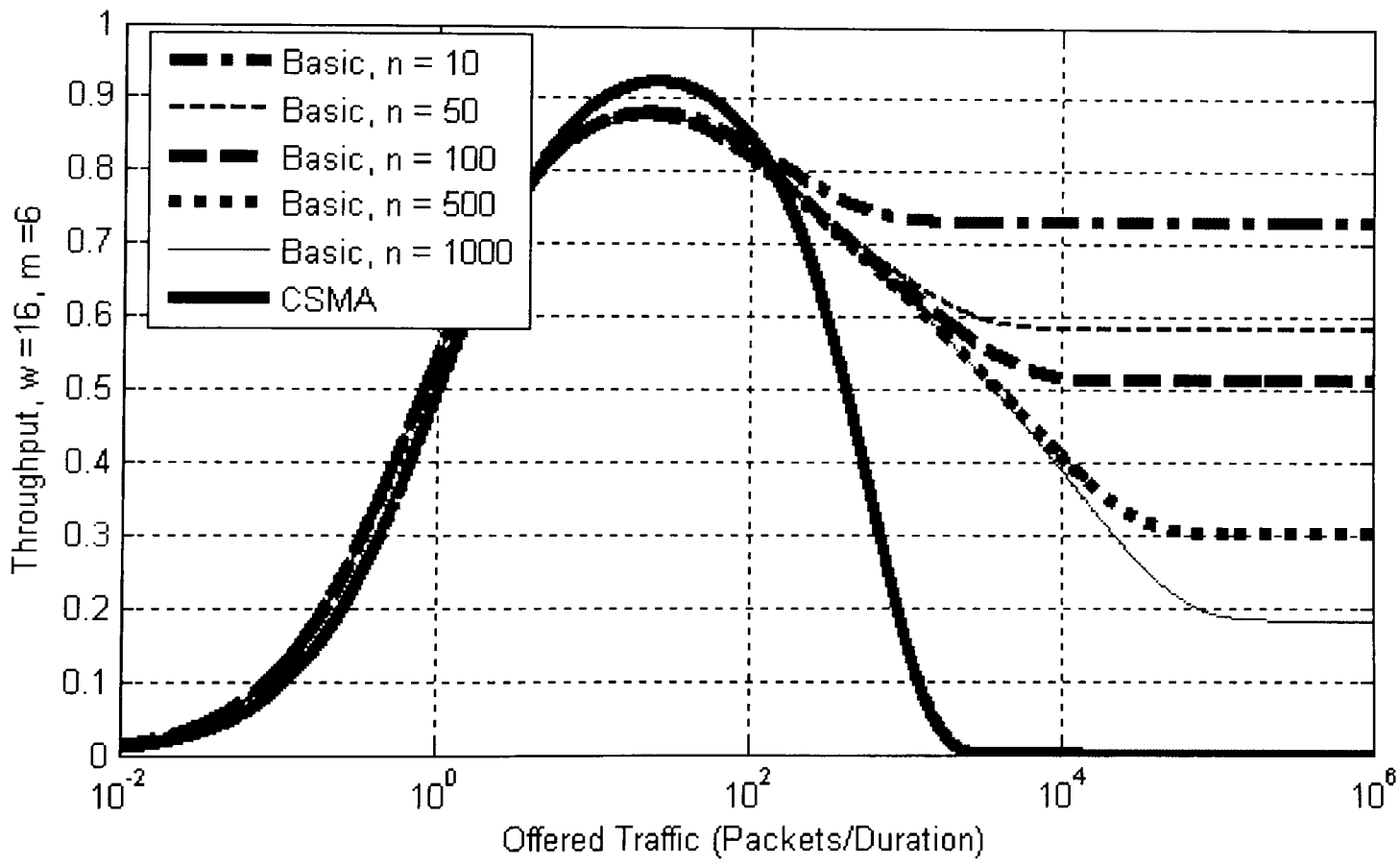

Figure (6.13): 802.11p Basic Access Throughput vs. Offered Traffic

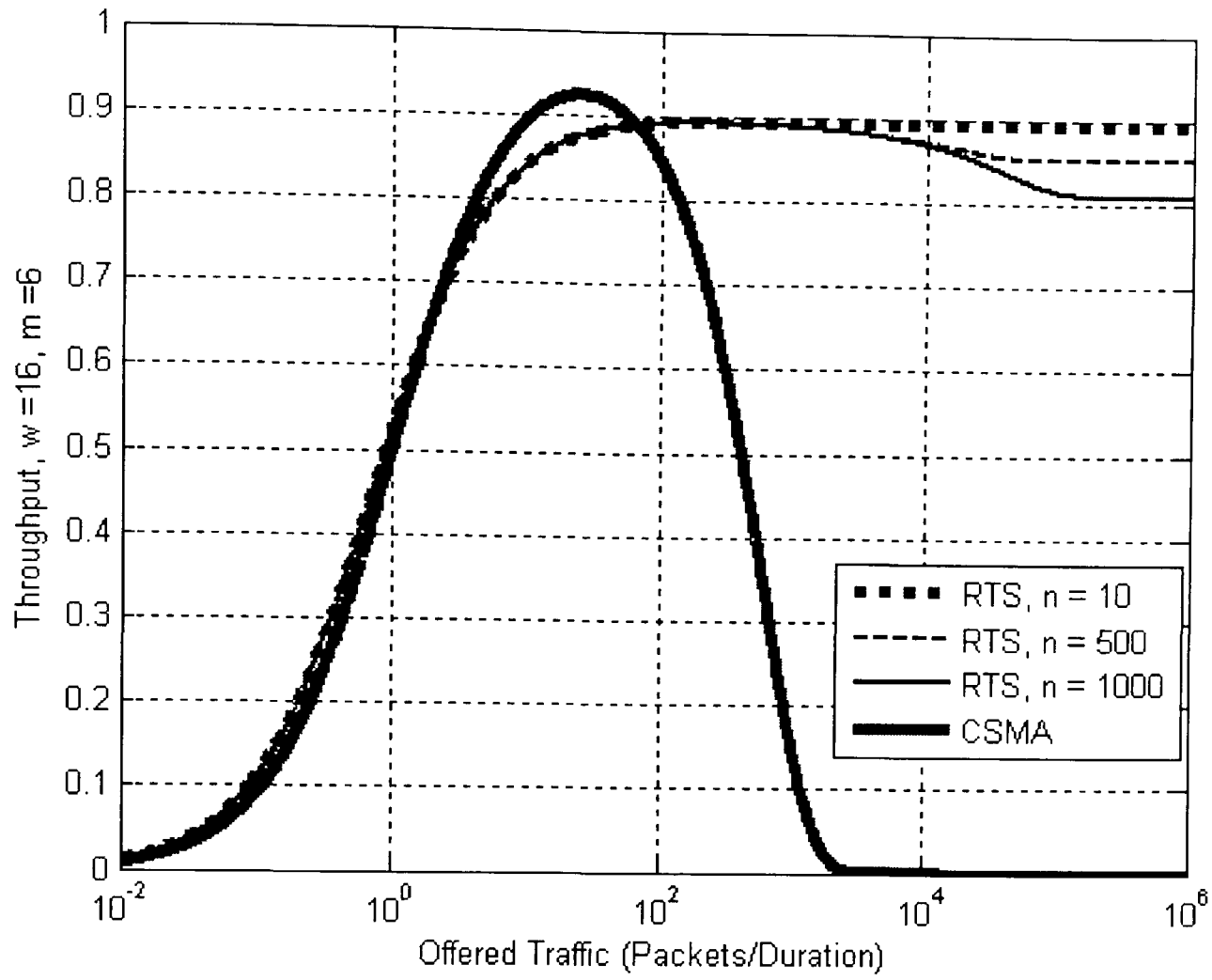

Figure (6.14): 802.11p RTS/CTS Throughput vs. Offered Traffic

6.6. Performance in VANET

We studied the throughput performance of 802.11 basic access in VANET via simulations. We used NS2 version 2.31 to simulate a network of 100 nodes in a single lane road. The traffic generator used is a constant bit rate (CBR) generator, with packets 1000 bytes long, over the UDP transport protocol. Each node communicates with the node in front of it and a "DumbAgent" routing protocol was used to avoid the routing overhead. The bit rate is 3Mbit/s, the frequency is 5.9GHz and the window size used is w = 16, m = 3. The spaces between the nodes follow an exponential distribution and the speed is uniformly distributed in the interval [30m/s, 50m/s]. Each point in our results is the average from 10 runs each 100 seconds long. Goodput is the average data bytes/s successfully received by the destinations.

Figure (6.15) shows the goodput performance versus load for various transmission ranges and a sample average inter-space of 45m. As the transmission range increases,

the number of nodes within the transmission range also increases leading to more nodes competing for the channel and hence more collisions. For this reason the goodput is reduced as the transmission range increases. Similar conclusions were obtained for different average inter-space distances.

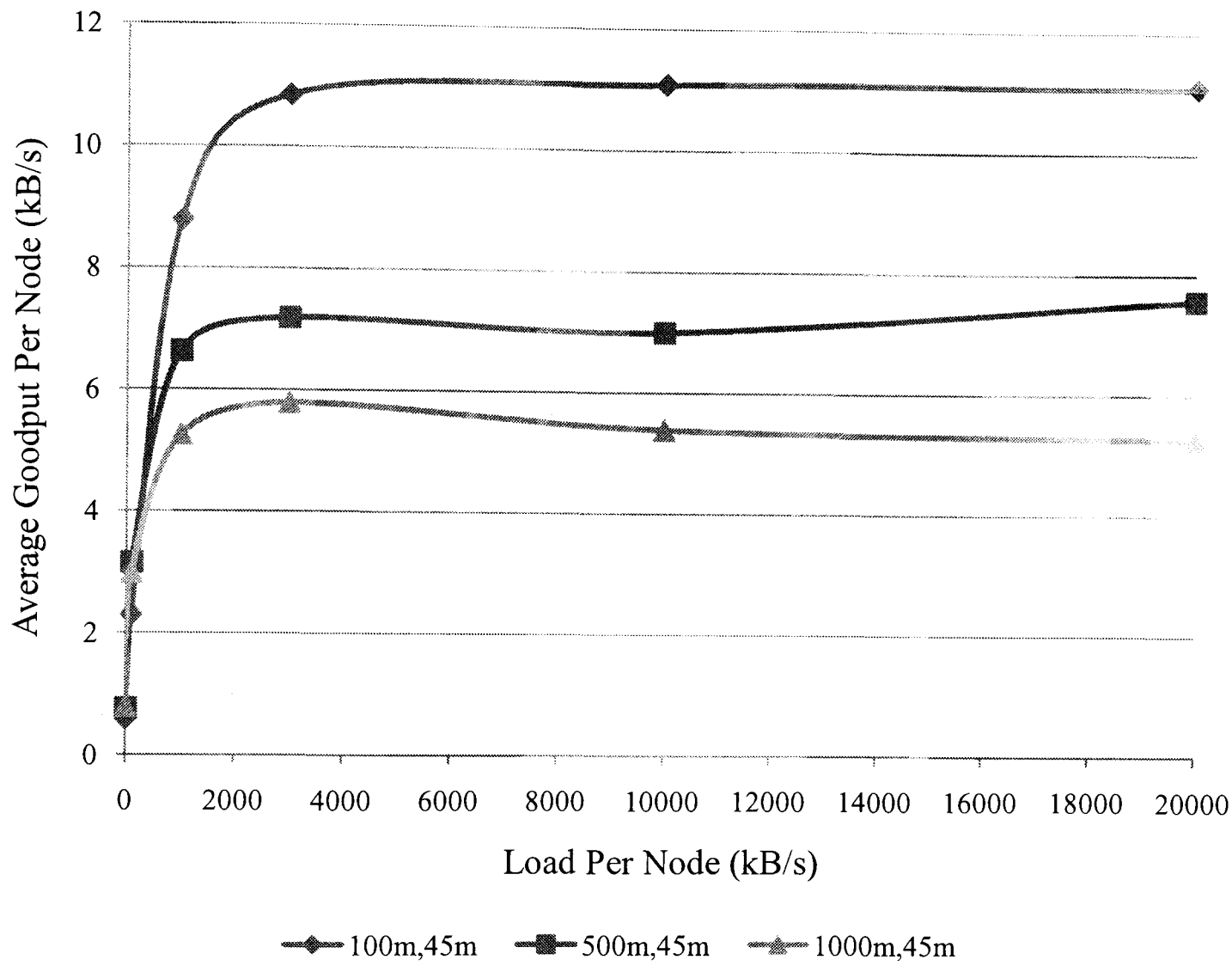

Figure (6.15): Effect of Transmission Range on Throughput

Figure (6.16) compares the achievable goodput with 100m transmission range and various average inter-space distances. As can be seen increasing the interspace distance increases the average goodput per node since the number of nodes within the communication range is reduced, thus reducing collisions. Comparing these results with the results of chapter 5 for connectivity we conclude that although higher densities improve the connectivity of the network and, therefore, the performance of the network

layer, the MAC layer achieves lower throughput due to the higher contention to access the channel.

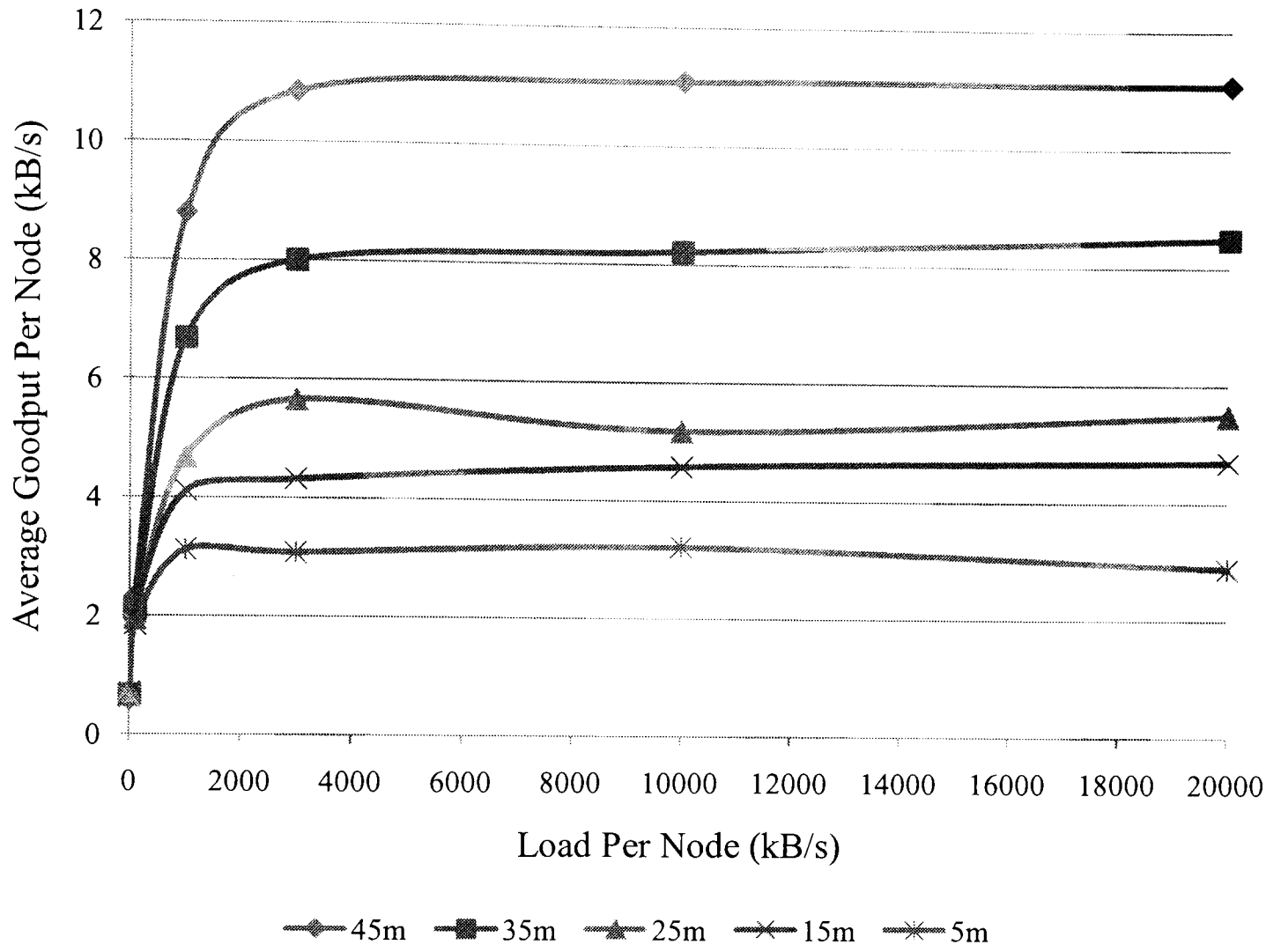

Figure (6.16): Effect of Inter-space Distance on Throughput

6.7. Concluding Remarks

In this chapter we reviewed and analysed the 802.11 DCF basic and RTS/CTS access modes. The throughput performance of DCF basic access is affected by the contention window size, available traffic and number of nodes. A small window size leads to quick access to the channel and therefore less delay and waiting time and higher performance in networks with low traffic. At high traffic and high number of nodes a large contention window achieves less collisions and higher performance. The throughput performance of RTS/CTS showed less dependency on the window size than basic access. This is a result of the channel reservation process used in RTS/CTS which

reduces the channel collision time and organises the access to the channel hence reducing the need for large window sizes. DCF attempts to dynamically optimise the window size by doubling its current value whenever a collision occurs and reducing its value after a successful transmission. Due to this backoff procedure, the basic access mode of DCF showed better performance when compared to CSMA at heavy load. Beside the backoff procedure, RTS/CTS access uses a short channel reservation handshake prior to transmission. This handshake reduces the average collision time and hence provides better performance than basic access. DCF sacrifices the maximum achievable throughput via CSMA for higher throughput at saturation; this is why it shows a more stable performance as the traffic increases. The performance, however, drops gradually as the number of nodes in the network increases. Although RTS/CTS access achieves high performance it applies only to unicast transmissions. Higher node densities improve the connectivity of the network and, hence, the performance of the network layer while reducing the throughput of the 802.11 link layer at high traffic due to collisions. A MAC layer that can support a large number of nodes and provide high throughput is essential to ensure the functionality of VANET particularly in areas with traffic congestions.

Chapter 7

Space-Orthogonal Frequency-Time Medium Access Control

7.1. Overview

IEEE 802.11 provides good performance in networks with low to medium traffic but its throughput drops considerably when the number of nodes increases. This will lead to severe degradation in VANET performance at congested areas. Moreover, 802.11 have poor support for quality of service. Our aim is to ensure high throughput, by controlling the number of nodes using the channel and organising the channel access, while providing good support for traffic with strict quality of service requirements. TDMA have been considered for VANET [77, 78] as it provides guaranteed QoS and high performance in high traffic conditions. However under light load, it encounters unnecessary delays and large overhead leading to lower performance compared to CSMA. Moreover in TDMA the number of nodes that can access the channel is limited by the number of slots whereas random access techniques do not have such constraints. An attempt to combine TDMA and CSMA was introduced in [105]. The nodes use CSMA as long as the traffic is below a certain threshold. Once the traffic exceeds the threshold, nodes switch to TDMA and do not switch back to CSMA unless the traffic drops below the threshold. However different nodes will have different traffic conditions, therefore some will prefer TDMA while for the others CSMA will be the best choice. In this chapter we propose a MAC protocol for VANET which is a combination of Space, Orthogonal Frequency and Time Division Multiple Access

techniques (SDMA, OFDMA and TDMA) called Space-Orthogonal Frequency-Time Medium Access Control (SOFT MAC). In SOFT MAC the space (road) is divided into cells and a portion of the available subcarriers is assigned to each cell. These subcarriers are then shared between nodes within the cell via a TDMA protocol. The TDMA protocol has two periods, a reserved transmission period and a reservation period. The reserved period can be accessed only after a successful reservation while the reservation period can be accessed by any node via random access techniques. The reservation process is accomplished in a distributed manner without the need for a central node or a cluster head. This chapter is based in part on the publications [3, 8, 9].

7.2. SOFT MAC

SOFT MAC uses a combination of SDMA, OFDMA and TDMA. Instead of defining the cells in SDMA to occupy only one node as proposed in the literature [90, 91, 107], a cell in SOFT MAC usually contains several nodes. Each cell is assigned a number of subcarriers and nodes within the cell share these subcarriers in time. Time is divided into frames and each frame is divided into slots. However unlike R-ALOHA and ADHOC MAC there are two types of slots/periods, reserved transmission slots (TS slots) and reservation (RS) slots/period. TS slots cannot be accessed without prior reservation whereas the RS period is accessed via random access schemes (e.g. DCF, CSMA or slotted ALOHA). The number of TS slots varies with the number of reservations, as will be explained, and the RS period occupies the rest of the frame. Under low traffic most of the frame will be RS, accessed via DCF for instance, while at heavy traffic most of the nodes will have a large amount of data and hence will reserve TS slots. Hence, in these high load conditions, most of the frame will be TS slots and therefore the performance will approach that of TDMA systems. Thus the protocol will provide the performance of random access methods under low traffic and the performance of TDMA under high traffic. Our method is different from that of [105]. In our protocol nodes may use TDMA, DCF/CSMA or both in the same frame without the need for all the nodes to switch to the same transmission mode as in [105].

7.2.1. SDMA-OFDMA in SOFT MAC

We assume the system uses N subcarriers, each node knows its location and the network is time and frequency synchronised via Global Positioning System (GPS). In the SDMA scheme roads are divided into cells of radius R and a portion N_c of the subcarriers is allocated to each cell as shown in figure (7.1). Maps identifying which subcarriers are allocated to each portion of the road are pre-installed at the nodes. The radii of the cells and the number of subcarriers per cell are design parameters. At the physical layer, using more subcarriers per cell means higher data rates but smaller number of cells with different subcarriers since the number of subcarriers is limited. Using a large cell radius means longer reuse distance since higher power is required and hence the interference will be higher in adjacent cells. The radius also has a major impact on MAC layer performance. By increasing the radius we decrease the handoff process when nodes move between cells. However a large cell radius means more nodes within the cell and, hence, more traffic and channel contention. We expect a large radius will improve the efficiency in low car traffic areas but cause more collisions in high traffic. There should be an optimum radius for a given expected car density. We can, therefore, optimise the radii of the cells to provide the best performance for the expected car density at a given time. A set of allocation maps can then be used with each map optimised for the expected car density. For instance the city centre at peak hours should use small cells, while highways at night should use large cells. Using this scheme we can improve the efficiency of SDMA in a distributed manner with small hardware complexity.

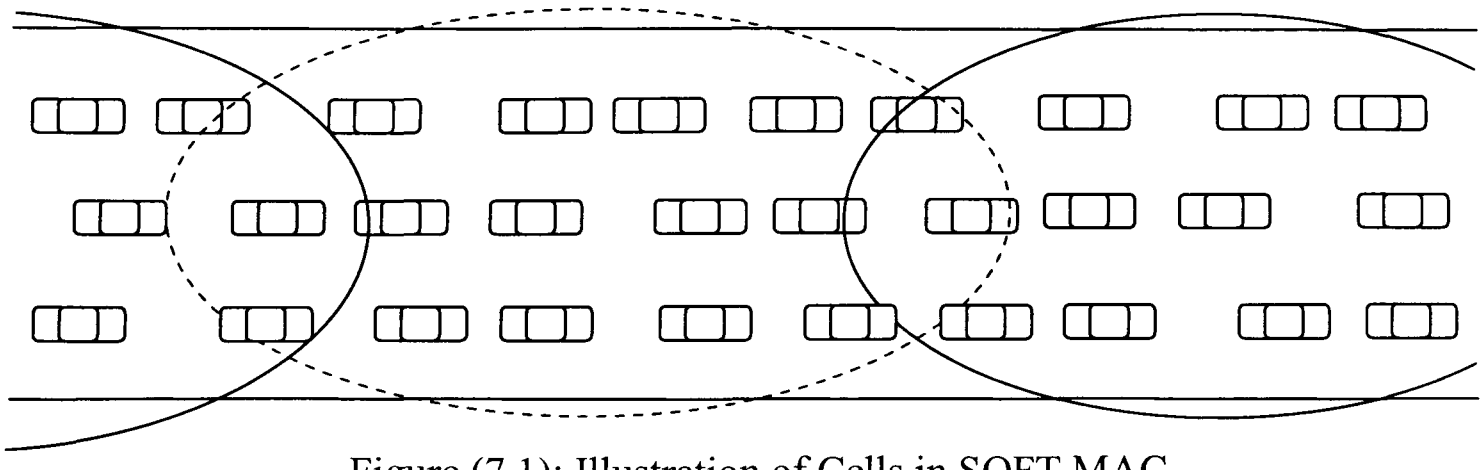

Figure (7.1): Illustration of Cells in SOFT MAC

An important advantage of using OFDMA over frequency division multiple access (FDMA) is that nodes belonging to two cells can receive from or transmit at both cells using a single transceiver whereas in FDMA this is not possible since the node must tune to one of the frequencies used in the cells. This feature can be easily proven. Consider a system of two slightly overlapped-cells. Nodes in cell 1 transmit at subcarriers a_1 to b_1 while the nodes in cell 2 transmit at subcarriers a_2 to b_2 with no common subcarriers. Let's assume a node ($n1$) in cell 1 and another ($n2$) in cell 2 transmit at the same time. Node $n1$ will formulate the signal:

$$x(n)=\frac{1}{N}\sum_{k=a_1}^{b_1} d_1(k).e^{j\frac{2\pi}{N}nk} \tag{7.1}$$

Where $d_1(k)$ is the data from $n1$ at subcarrier k and n is the time index. The summation is from a_1 to b_1 instead of 0 to N-1 because all $d(k)$ values are set to zero except for the subcarriers the node is allowed to transmit in. At the same time node $n2$ will formulate the signal:

$$y(n)=\frac{1}{N}\sum_{k=a_2}^{b_2} d_2(k).e^{j\frac{2\pi}{N}nk} \tag{7.2}$$

A node $n3$ at the intersection of both cells then receives the signal $z(n)$ given by:

$$z(n)=h_1(n)\otimes x(n)+h_2(n)\otimes y(n)+w(n) \tag{7.3}$$

Where $h_i(n)$ is the channel response from node i to $n3$, $w(n)$ is the noise sample and $\otimes$ denotes convolution. Node $n3$ then calculates the FFT of equation (7.3) to get:

$$\begin{aligned} r(k)&=\sum_{n=0}^{N-1} z(n).e^{-j\frac{2\pi}{N}nk}=\sum_{n=0}^{N-1}(h_1(n)\otimes x(n)+h_2(n)\otimes y(n)+w(n)).e^{-j\frac{2\pi}{N}nk} \\ &=\sum_{n=0}^{N-1}(h_1(n)\otimes x(n)).e^{-j\frac{2\pi}{N}nk}+\sum_{n=0}^{N-1}(h_2(n)\otimes y(n)).e^{-j\frac{2\pi}{N}nk}+\sum_{n=0}^{N-1} w(n).e^{-j\frac{2\pi}{N}nk} \end{aligned} \tag{7.4}$$

which is the superposition of the FFT of the transmitted signals. Using (7.1) and (7.2) with an analysis identical to that of section (4.3), equation (7.4) becomes:

$$r(k)=H_1(k)d_1(k)+H_2(k)d_2(k)+W(k) \tag{7.5}$$

Where $H_i(k)$ and $W(k)$ denote the N point FFT of the channel response $h_i(n)$ and noise $w(n)$, and i represents the transmitting node number. Equation (7.5) can be written as:

$$r(k)=\begin{cases} H_1(k)d_1(k)+0+W(k), & a_1 \le k \le b_1 \\ 0+H_2(k)d_2(k)+W(k), & a_2 \le k \le b_2 \\ 0+0+W(k), & otherwise \end{cases} \quad (7.6)$$

With knowledge of the channel response H_i from each node i and as long as each cell uses a unique set of subcarriers, it is possible to decode the transmitted signals successfully.

A node wishing to transmit needs to identify which subcarriers it may use. First the node determines its position using GPS and then uses this position to find the subcarriers allocated for its position using the pre-installed maps. However since more than one node can exist within the same cell, nodes must co-operate to share the available subcarriers. This is done through the TDMA protocol discussed in the next section. To avoid collisions due to the hidden terminal problem at least four different subcarriers sets are needed as will be proven. We assume there are four unique sets of subcarriers S1 to S4. If we assign 64 subcarriers per cell then the total number of subcarriers should be 256 subcarriers. Figure (7.2) shows an example for how subcarriers are assigned to cells. Nodes in the intersection of two cells may transmit using the subcarriers of either or both cells.

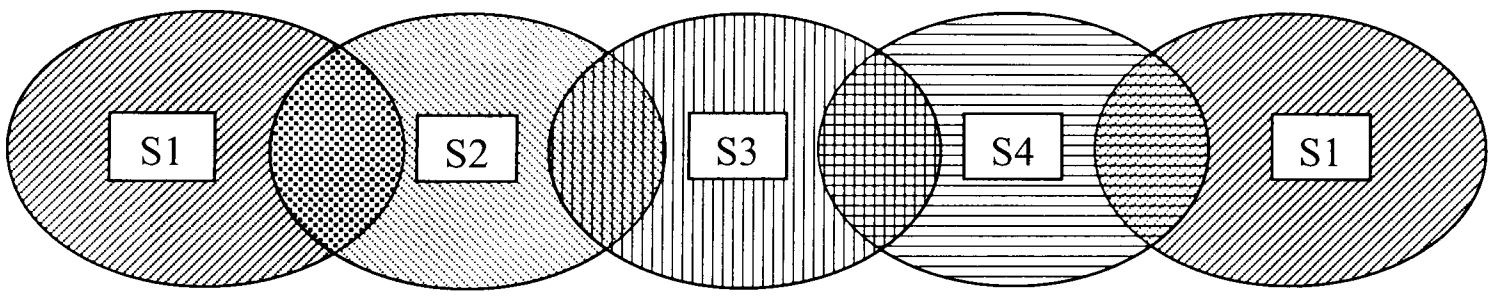

Figure (7.2): Subcarrier Assignment to Cells

To illustrate why at least four groups of subcarriers are required, consider the four left cells of figure (7.2) and assume there were only three sets (i.e. S4 = S1). The nodes in the intersections of cells S1 and S2 may use subcarriers S1. At the same time the nodes in the intersections of S3 and S4 can use subcarriers S3 and S1. Transmissions

using S1 will collide at nodes in the intersection of S2 and S3. By using at least four groups we ensure the same subcarriers are not used for a distance of two hops which is the necessary condition to avoid collisions [156].

The subcarriers assigned to a cell may be adjacent subcarriers or randomly distributed. By using adjacent subcarriers the channel estimation is simplified as the correlation between the channel responses of adjacent subcarriers is high. However this can be a drawback when the channel experiences deep fading. Another possible scheme that can be used is to distribute the allocated subcarriers either uniformly or randomly. This scheme provides frequency diversity and may reduce inter-carrier-interference (ICI), but the channel must be estimated for each subcarrier individually. Several algorithms have been developed in the literature [37] to allocate subcarriers to users randomly. These algorithms aim at maximising the performance by allocating, depending on the channel response, the best subcarriers the user can transmit in. The algorithms are suitable for node to basestation (uplink) transmissions and, therefore, are not directly applicable to ad-hoc networks since the channel response will be different between different node pairs. We assume the scheme used is a uniformly distributed group of subcarriers since it provides diversity and is easy to implement [37].

7.2.2. TDMA in SOFT MAC

TDMA has been the most popular medium access mechanism and several link access protocols are based on it. Its reliability and ease of implementation makes it a very attractive option. TDMA provides efficient, guaranteed and delay constraint access to the medium and therefore has been adopted for voice traffic standards, such as GSM as well as for data traffic in the Point Co-ordination Function (PCF) of IEEE 802.11 standard. There are several ways to implement TDMA. The method used in PCF is a polling service in which the basestation polls each node for possible data. Another implementation is the Token ring method where each node receives a Token when it is its turn for transmission and after it transmits its data it releases the Token to the next node. Under heavy traffic TDMA shows superior performance in terms of throughput,

delay, fairness and efficiency compared to the Carrier Sense Multiple Access (CSMA), used in the Distributed Coordination Function (DCF) of IEEE 802.11. However in light load situations TDMA has larger overhead and longer delays compared to CSMA since a node can only transmit at its designated slots thus incorporating unnecessary delays. Another limitation of TDMA is the need for a central node, typically a basestation, to assign slots to the nodes and provide time synchronisation. Moreover the number of supported nodes in TDMA is bounded by the number of slots.

The proposed TDMA frame consists of two periods, a reservation (RS) period of duration d_R and a transmission period of N_{TS} transmission slots (TS) as shown in figure (7.3). We will assume a constant TS slot duration, constant frame duration and the reservation period has a minimum duration ($d_{R,min}$). We propose to set $d_{R,min}$ either to 10% of the total frame size as in [93], or to the minimum DCF period of 802.11a when PCF is employed [95]. The RS period is used by the nodes to reserve one or more of the TS slots and to transmit short messages.

Access to the RS period is accomplished via DCF, Slotted ALOHA (S-ALOHA) or any other random access technique while access to the TS period is granted only via reservation. For the rest of this chapter, we assume DCF is used to access the RS period. Each node should decide whether a TS slot is required or not based on some or all of the following parameters:

- The amount of queued data to be transmitted. If the data exceeds a certain threshold a TS request is initiated. In this case the long data sequence justifies the additional overhead required by the reservation process. A similar approach is used in IEEE 802.11 to determine whether to use the RTS/CTS handshake and fragmentation or not [95].
- Required QoS (e.g. maximum delay, data rate, etc). TDMA provides reliable QoS therefore QoS requests should initiate a TS reservation.
- A request for a connection from higher layers. This is left as an option to support higher layer implementations.

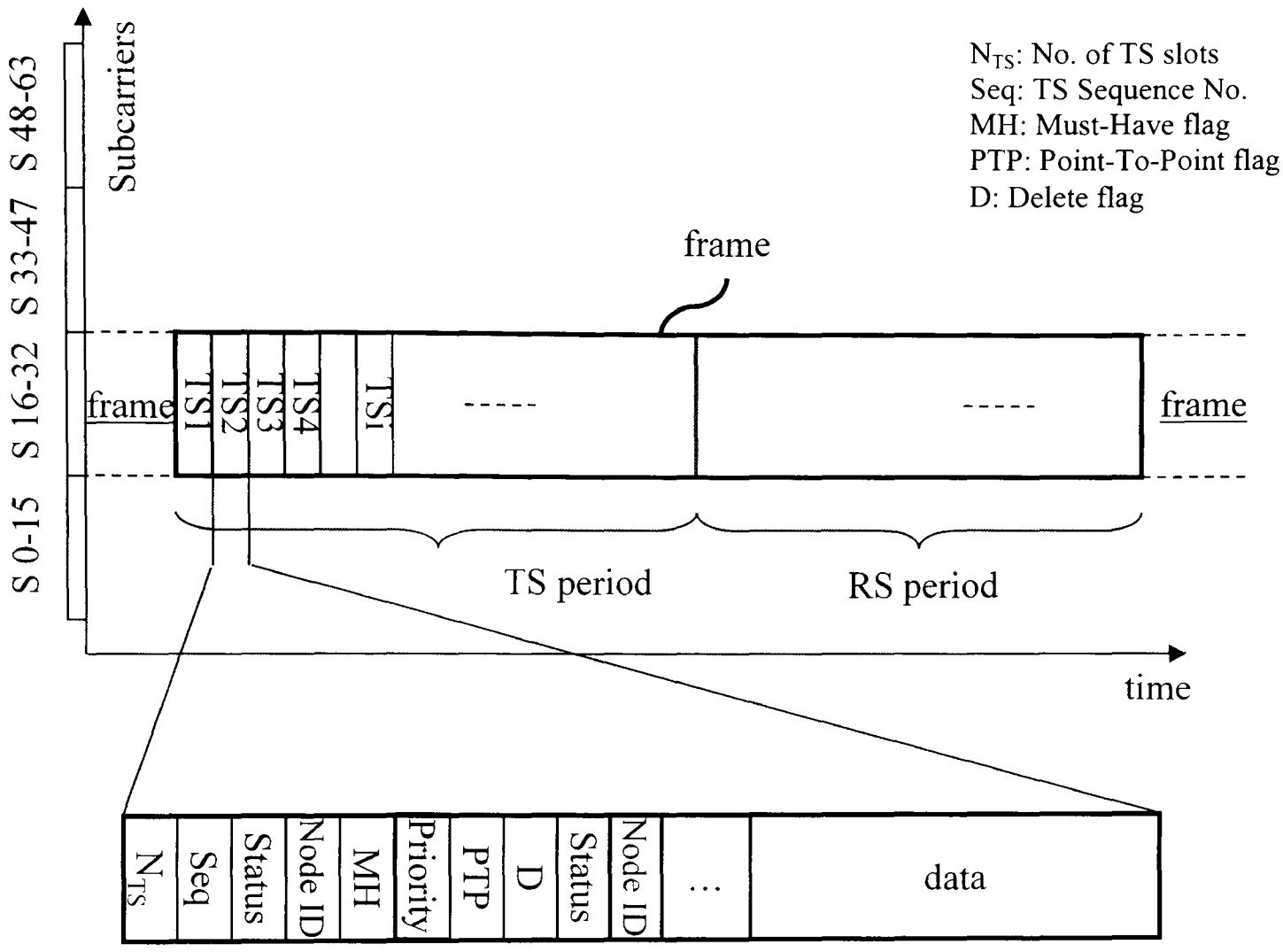

Figure (7.3): SOFT MAC Frame Structure

Once a node has determined it should reserve a TS slot it listens for transmissions in the channel. All transmissions in the frame carry the current number of TS slots (N_{TS}) available in the frame. Transmissions in TS slots, additionally, contain information about the state of each TS slot, BUSY or IDLE, and the ID of the node transmitting in BUSY slots. This is known as Frame Information (FI). A node sets the status of a slot to BUSY in its FI if it can correctly decode a message transmitted in that slot and sets it to IDLE otherwise. The following set of rules organise the reservation and transmission processes.

Rule 1 A node wishing to transmit has two options, either to transmit in the RS period using random access techniques, suitable for small amounts of data, or to reserve a transmission slot and transmit in the reserved TS, ideal for long and quality of service (QoS) transmissions. Initially the RS period occupies the whole frame with no TS slots.

As reservation requests are sent, the number of TS slots increases till the maximum number of TS slots is reached. The number of TS slots is announced in all transmissions in TS as well as in RS. A node wishing to reserve a TS slot checks the number of TS slots in the current frame and initiates a reservation request (Res-Req). Each TS slot has a unique sequence number (Seq). If the maximum number of TS slots is reached, all nodes cease from sending reservation requests for new TS slots but requests for existing TS slots (e.g. IDLE slots) can still be sent. Nodes with no reserved slots access the channel in the RS period. When a node powers up it sets its TS to zero, starts a listening timer and listens for transmissions. There are three possible scenarios:

- The node receives a packet in TS or RS containing the current number of TS slots. It then modifies its TS to the new value and may reserve or transmit in the RS period as required.
- A timeout occurred without receiving any messages. In this case the node assumes the maximum number of TS slots and transmits in the RS period a Hello-New message. Then it sets a counter for repeating this process r times, r a predefined fixed number, before it gives up.
- The node receives a Hello-New message. In this case the node assumes N_{TS} is zero. If it has data, it may either transmit in the RS period or send a Res-Req. If it does not have data, it sends a Re-Hello-New packet which contains the FI, node ID, position, speed, etc. Other nodes use the FI in these packets to update their FIs.

Rule 2 To reserve a TS slot the node broadcasts in the RS a reservation request (Res-Req) packet to reserve the slot that has the sequence number:

$$Seq = Max(N_{TS} + winning\ Res\_Req\ \ received, Seq\ requested\ in\ Res\_Req\ received) + 1 \quad (7.7)$$

The two numbers within the *Max* function should be equal if all nodes are aware of all reservation requests, the first is greater if this node can detect reservation(s) missed by other nodes and the second is greater if the node misses some reservation requests. The term "winning Res-Req" will be explained in rule 3, for now assume all Res-Req are winning Res-Req. After the transmission of the Res-Req, the node waits for one frame

after the frame it initiated the reservation in. The reservation is assumed successful if a slot is assigned as reserved for the node in succeeding received FIs. The reservation is also assumed successful if Seq = 1 and no FI was received during the waiting period. The reservation is assumed to have failed otherwise. A node may also request a slot which has been marked as IDLE in all received FIs for k consecutive frames, k a predefined fixed number. All Res-Req packets contain FI of current and new successfully reserved TS slots within the same frame. If a node has a TS slot and wishes to reserve another, this can be done either via the RS period or by signalling in the TS period.

To illustrate rule 2 let there be 4 TS slots and 2 new nodes (1 and 2) wishing to reserve. Assume the first node (1) accesses the RS period without collision. It will announce the number of TS slots as 4 and request slot number 5. The second node accessing the RS period will announce the number of TS slots as 5, the frame information (FI) will indicate TS slot with Seq = 5 is reserved for node (1), and request TS number 6. In the next frame the nodes at TS 1 to 4 will also announce the slot allocation and increase the number of TS slots, however the new nodes will delay their transmission for this frame to avoid any hidden terminals as will be explained in rule 8. Note that if a collision occurred during the reservation process, the reservation either fails and the process is restarted, or one of the reservations is successfully detected by some node(s) and is announced in subsequent transmissions, or both reservations are detected, each by a different group of nodes, in which case these groups announce two different reservations for the same slot. This is resolved using rule 8.

Rule 3 A node belonging to two cells and having a TS slot in cell 1 may reserve a TS slot in cell 2 and keep the reserved slot in cell 1 if the new slot satisfies one or more of the following conditions:

- It has the same sequence number as the reserved TS in cell 1
- The equivalent TS slot in the frame of cell 1 is marked as Point-To-Point (PTP) and this node is not the destination
- It is in the RS period of the frame of cell 1

If more than one slot satisfy different conditions, the slot satisfying the first condition is preferred followed by the second then the third. If two or more slots satisfy the same condition one of the slots is chosen randomly. If no free slots satisfy the conditions the must-have flag is used, as explained next, to force the reservation. If the must-have reservation fails, it is not possible to reserve a new slot in cell 2 along with that of cell 1, the node needs to release the slot in cell 1 before transmitting in the TS of cell 2.

If a TS slot is free, even if a reservation request has been sent for it by another node, or BUSY but a must-have (MH) flag is not set, a node may send a reservation request for this slot with the MH flag set. This is used only by nodes belonging to two cells. The slot is then allocated to one of the nodes that have set the MH flag on a first come first serve basis and the MH flag of the slot in the FI is set. The node that occupied, or first requested, the slot with the MH flag unset is allocated another slot if possible. Nodes which have requested the slot and set the MH flag but failed the first come first serve process are not allocated a slot. These are 'failing Res-Req' and all the others are 'winning Res-Req'. The MH flag remains set as long as the node has reserved slots in the frames of two, or more, cells otherwise it is unset. A node may have several slots in the same frame but only one of them can have the MH flag set. This rule provides seamless handoff between cells. The conditions for reserving an additional slot in a new cell ensure the node does not miss any TS broadcast messages in the original cell since typically a node cannot transmit and receive at the same time.

Rule 4 If a node correctly decodes a packet in a TS slot, it announces this slot as BUSY and reserved for the source node (destination of an ACK packet). Otherwise it announces the slot as IDLE.

Rule 5 A broadcast transmission is assumed successful if all the frame information (FI) received by the source indicate the slot is reserved for it. If this is not true a collision is assumed, the slot is released and a new reservation is started.

Rule 6 A node modifies its FI information to include any new TS slots if it receives an FI with the new slot(s) allocated to certain node(s). This is a case when a node cannot

sense some reservation(s) but another node within the cell can (hidden terminal problem).

Rule 7a In the FI each TS slot has a delete (D) flag. An active node broadcasts a delete request by setting in its FI the D flag of a slot to delete the assignment of that unused TS slot to an inactive node if for q consecutive frames, q a predefined fixed number greater than k, the slot was sensed idle and declared IDLE in all received frame information (FI). Each node checks its own FI to determine the slots it can occupy in the frame and broadcasts this in its own transmission. A node declares it can occupy a slot if it is IDLE in all received FI and in its own FI.

Rule 7b The active node that broadcasted the delete request rearranges the slot allocation in the frame so that the last TS slot becomes IDLE and broadcasts the new slot assignment to the active nodes in its TS slot. The number of TS slots is reduced for each unassigned TS slot while the RS period increases, i.e. deleted TS slots become part of the RS period. If a node declares it cannot occupy a slot, e.g. slot declared busy by one of its neighbours, then the slot cannot be re-assigned to it but can be re-assigned to another node that can occupy it. If a slot cannot be re-assigned, the delete counter is reset to q. If there are no hidden terminals, the simplest implementation of this algorithm is to move the node occupying the last TS slot to the TS slot to be deleted, and decrement the number of TS slots.

Rule 8 An active node with no reserved TS sets a timer (Gateway counter) if it detects two successful reserve requests for the same TS slot (at least the second request has the MH flag unset, which may be generated by a hidden node). Let's call this case double reservation. The node reduces the Gateway counter to half its current value for each additional successfully detected reserve request for the same slot. Note that a reserve request refers to reservations via Res-Req messages in the RS as well as new TS assignments in the FI of other nodes. If the Gateway counter expires, the node sends a message (Gateway-Hello). In the Gateway-Hello message the number of TS slots is set to be:

$$N_{TS} = Max(N_{TS}\ in\ Res\_Req, N_{TS}\ in\ node) + No\ of\ received\ double\ Reservations \quad (7.8)$$

The FI field in the Gateway-Hello message arranges the assignment of the slots to nodes based on a first come first serve basis. If the Gateway already has a reserved slot it transmits in its TS slot. The node resets its Gateway counter and does not transmit a Gateway-Hello message if there are no more free TS slots or if all the following conditions are satisfied:

1. A Gateway-Hello message or FI sent from another node is received
2. The received Gateway-Hello or FI has an N_{TS} equal to or greater than that of equation (7.8)
3. The received Gateway-Hello or FI assigned slots to all the nodes requesting new reservations

To illustrate rule 8 consider the network shown in figure (7.4). The nodes in figure (7.4) are represented by circles while the ovals are clusters. Assume each node within a cluster can correctly receive packets from all the nodes within the same cluster but not from nodes in other clusters. For instance node 2 can receive from 4, 5 and 6 but not from the other nodes while 4 can sense the transmissions of all the nodes.

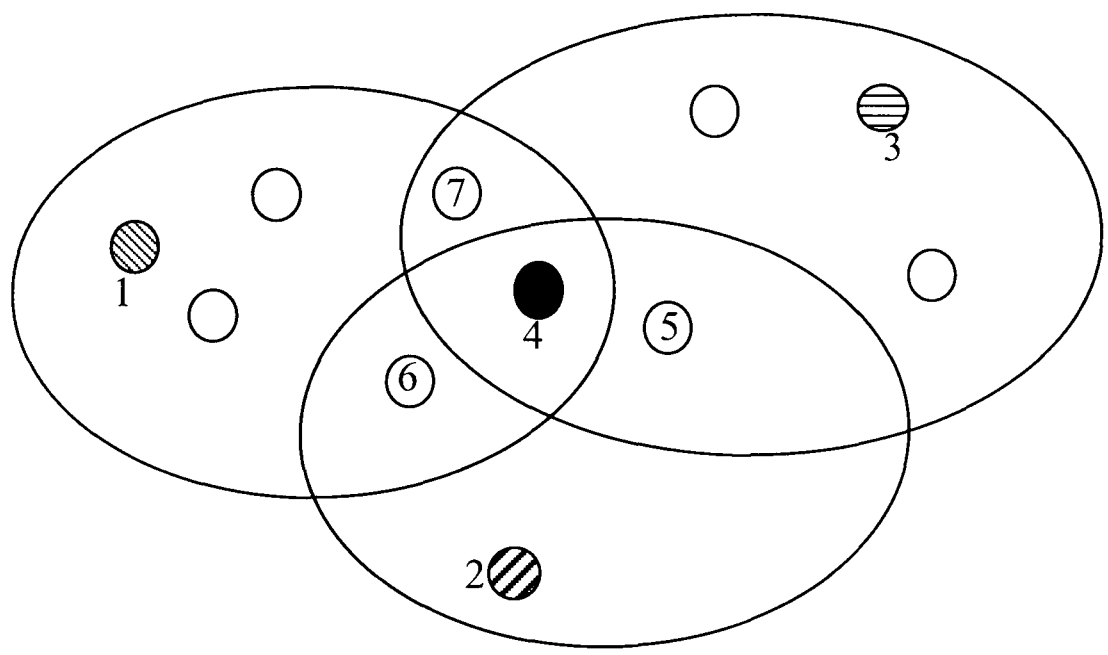

Figure (7.4): Illustration of Double Reservation

Let the number of TS slots = 0 and assume nodes 1, 2 and 3 each want to reserve a slot and each of them successfully accessed the RS period without collision. Since none of them can sense the reservation request of the others, they will all request the same slot i.e. TS 1. Let node 1 be the first to transmit a reservation, this will be sensed by

nodes 4, 6 and 7. Then node 2 broadcasts a reservation for the same slot. Nodes 4 and 6 both now detect a double reservation and each of them sets its own Gateway counter to resolve this double reservation whereas 5 and 7 have only detected a single reservation. Now node 3 announces its reservation thus nodes 5 and 7 start their Gateway counters since they detected double reservation, however 4 now has detected 3 reservations for the same slot, so it reduces its counter to half its value to access the channel before nodes 5, 6 and 7 and announce an N_{TS} of 3, assigned to nodes 1, 2 and 3 respectively (first come first serve). Nodes 5, 6 and 7 receiving the FI of node 4 and realising the N_{TS} announced is 3, which is greater than their N_{TS} (= 2), and all reservation requests have been resolved, cease from transmitting the Gateway Hello packet and update their FIs. Note that even if node 4 does not exist, node 6 will access the channel to resolve the double reservation between 1 and 2. Nodes 5 and 7 will then become aware of the additional hidden node from the FI of node 6 and reduce their counters. Now nodes 5 and 7 both have the information of all the reserving nodes and any one of them upon announcing the reservation will reset the other. If node 4 has a TS slot reserved then it simply waits for its reserved TS to announce the slot allocation without the need to set a Gateway counter.

7.2.3. Point-to-Point Transmission in SOFT MAC

For point-to-point (PTP) communications we adapt the approach proposed in [92] to work with our protocol. A Point-to-Point (PTP) flag is used to differentiate between a broadcast transmission and a PTP transmission.

Rule 9 A node sets the PTP flag for a TS slot in its own FI to 1 if:

1. The message received in that slot is a broadcast message or
2. It is the destination of this packet in PTP communications

The PTP flag is set to 0 otherwise. If the destination does not have a reserved slot it must reply with an acknowledgement packet (explicit ACK) in the same TS slot. The source can determine whether to expect an ACK or not by checking its FI. If the destination has a reserved BUSY slot the ACK packet is not expected but the PTP flag

of the source's slot in the FI of the destination is checked and the transmission is successful if PTP equals 1 (implicit ACK). If the destination has no TS slot an ACK is expected and the source must adjust its packet length so that the duration of the packet + ACK + any waiting time does not exceed the TS slot duration.

Rule 10 A busy TS slot can be accessed for PTP communication if the following conditions are satisfied:

1. The PTP flag in set to 0 in all received FIs
2. The FI received from the intended destination declares the slot as IDLE
3. An ACK cannot be sensed in the specified slot.

The first and third conditions ensure that the ongoing communication in the slot is PTP and the destination of this transmission is not within the range of the transmitter. The second condition ensures the new destination is not within the range of the transmitter or the receiver of the original transmission.

Rule 11 The transmission is considered successful if the slot is set to BUSY with the correct node ID and PTP set in the FI of the destination terminal or if an ACK was received; otherwise it is assumed that the transmission has failed.

7.2.4. Multi-hop broadcast service

Each node within the cluster can identify the neighbours of the other nodes by checking the FI information received from each node. This is true since a node sets the state of a TS slot to BUSY only if it correctly decodes the transmission. The node ID in the FI will be that of the source of the transmission. Each node receiving a broadcast message should check its set of neighbours against those of the nodes around it before forwarding. It does not forward the message according to the following rule [77]:

Rule 12 If a terminal (i), which has a reserved slot and a set of neighbours (C_i), receives a broadcast message, it does not rebroadcast the message if:

1. Its set of neighbours that did not receive the message (S_i) is empty ($S_i = \phi$)
2. There exists any other node j ($j \neq i$), for which ($S_i \subseteq C_j$) and ($|C_i| < |C_j|$)

In the first condition all the neighbours received the message and therefore a rebroadcast is not necessary. In the second condition the node does not forward if its set of neighbours which did not receive the message is a subset of that of another node with higher number of neighbours.

Rule 13 If the number of reserved slots is 0 or there is only one TS slot and it is reserved for the broadcasting source, we propose two approaches. In the first each node sets a counter inversely proportional to its distance from the source, if it expires and no retransmission was sensed it retransmits the packet [157]. In the second approach the message is not relayed and it is up to higher layers to decide whether to forward or not.

Rule 14 If a broadcast safety message is transmitted in the RS period from a node with no reserved TS slot, the node includes a partial FI with only the state of each slot (BUSY or IDLE). This is then used by nodes having reserved slots to rebroadcast the message, if necessary, based on rule 12.

7.2.5. Priority in SOFT MAC

We adapt the 2-bit priority field of the IEEE 802.11e standard to identify the type of traffic in a given TS slot [97, 98]. Nodes then use this field, along with the MH flag, to request TS slots occupied by lower priority traffic. Table (7.1) shows the proposed priority scheme in descending order.

MH flag	Priority	Type of Traffic
1	X	Handoff
0	3	Safety
0	2	Road Traffic data
0	1	Multimedia
0	0	Best Effort

Table (7.1): Priority in SOFT MAC

The priority of the traffic transmitted in the TS is announced in the header. If a node wishes to overtake a TS slot, it checks its traffic priority against that announced in the TS. If its traffic has higher priority, it may send a reservation request and the TS will be reassigned to it. If the priority is lower, the reservation will be declined. The MH flag has the highest priority since it indicates the node is moving from one cell to another,

thus it is necessary to perform the handoff between cells. Other than the handoff case, reservation requests for BUSY TS slots are not sent unless the maximum number of TS slots is reached.

7.2.6. SOFT MAC and WAVE

The WAVE standard divides time into segments and each segment consists of two 50ms time periods. Within the segment, all nodes tune to the control channel in one period and may switch to another channel in the other [111]. In our proposed MAC each of the seven channels of DSRC will have its independent frame and reservations. The frame duration is fixed but should be optimised for best performance. For each channel, the frame can occupy only one period per segment but may extend to several segments. To illustrate how this works assume a node transmits in one channel (we will call it service channel) beside the control channel. At the beginning of a segment the node will tune to the control channel where nodes use the control channel MAC frame to organise access to the channel. After the time-period elapses, the node will switch to the service channel and the nodes transmitting in the service channel use the service channel MAC frame to organise access to the channel. After the time period elapses, all nodes will switch to the control channel (a new segment). This current control channel frame can be either a new frame, if the frame duration is one period, or a continuation of the previous frame, if the frame length is more than one period. The frame in the second case extends over multiple segments. For convenience and ease of implementation, the frame duration should be an integer number of periods. As nodes switch between channels, they keep records of the status of the frames of the control channel and the channel(s) they switch to. Figure (7.5) illustrates a two-segment frame.

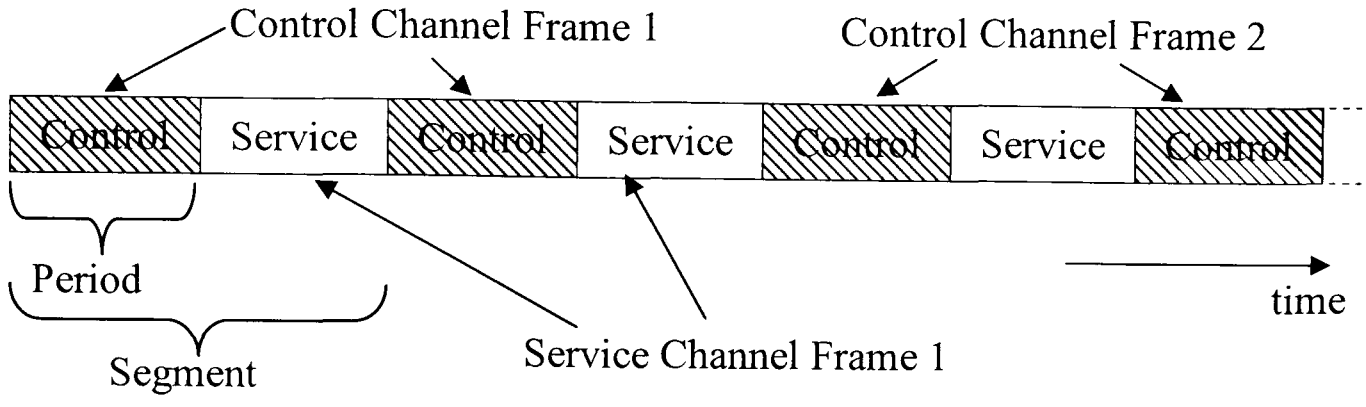

Figure (7.5): Illustration of a Two-Segment Frame

7.3. Implementation of SOFT MAC using 802.11

The 802.11 standard has two modes of operation, Distributed Co-ordination Function (DCF) and Point Co-ordination Function (PCF). PCF is implemented using an Access Point (AP). In PCF there are two intervals, Contention Period (CP) and Contention Free Period (CFP). During the CP, nodes access the channel using the DCF in a distributed manner without the intervention of the AP. In the CFP, the AP polls the nodes for data. A node must register itself with the AP to enter the polling list [95, 97, 98]. The frame structure is shown in figure (7.6) [97].

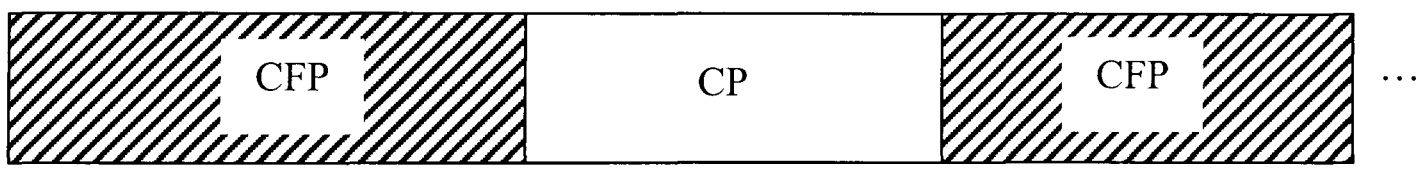

Figure (7.6): PCF Frame Structure

There are four basic time units in 802.11, the slot time (σ), Short Inter Frame Space (SIFS), Priority Inter Frame Space (PIFS) and Distributed Inter Frame Space (DIFS). The slot time is the time unit used for the back-off counters. SIFS is the smallest of the Inter Frame Spaces and is used between a transmission and its acknowledgement as well as in request to send/clear to send handshakes (RTS-CTS-data-ACK). PIFS (=SIFS+σ) is used only by the AP while the DIFS (=SIFS+2σ) is used by all nodes.

In PCF the AP waits for the channel to be idle for a PIFS before broadcasting a beacon packet. This beacon indicates the start of the CFP period and announces the channel to be busy for the maximum CFP period. All nodes then update their Network

Allocation Vectors (NAV) to indicate that the channel will be busy for the duration specified in the beacon. During this period no node will attempt to access the channel unless the AP polls it for data. After the AP finishes polling, even if the maximum CFP duration has not elapsed, it broadcasts another beacon that terminates the CFP (starts the CP). The nodes then reset their NAV and contend for the channel using DCF [95, 97, 98].

SOFT-MAC can be easily implemented using the features of PCF. When the TS period starts, the node that reserved TS 1 waits for a PIFS before transmission. This will ensure the node gains access to the channel before any other node. Subsequent nodes follow the same strategy to access their TS slots. All nodes transmitting in the TS will broadcast the time left in the TS period. This is used by nodes which did not reserve a TS to update their NAV and hence do not attempt to access the channel during this period. After the TS period, all nodes wait for a DIFS before attempting to access the channel. Although the PCF mode is optional, the 802.11 standard specifies that all nodes must be able to co-operate with the PCF function even if they do not support the polling service of the AP. This ensures that SOFT MAC can coexist with 802.11 [95, 97, 98]. Figure (7.7) shows this access scheme.

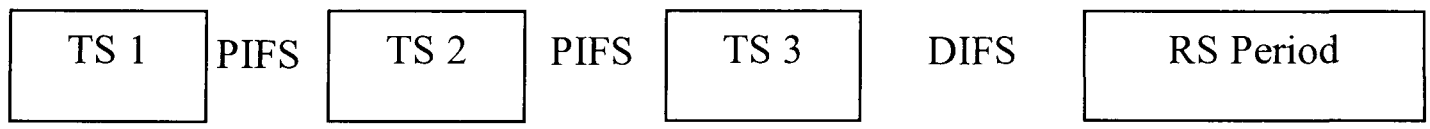

Figure (7.7): SOFT MAC Implementation Using 802.11

7.4. SDMA-OFDMA Design

We derive equations for the design of the cell overlapping distance of the SDMA cells in SOFT MAC. Considering figure (7.8), the number of subcarrier groups is four, the cell diameter is D_c, the subcarrier reuse distance is D_r and the overlap distance (handoff distance) between two cells is ε. To simplify the analysis we assume these values are equal for all the cells.

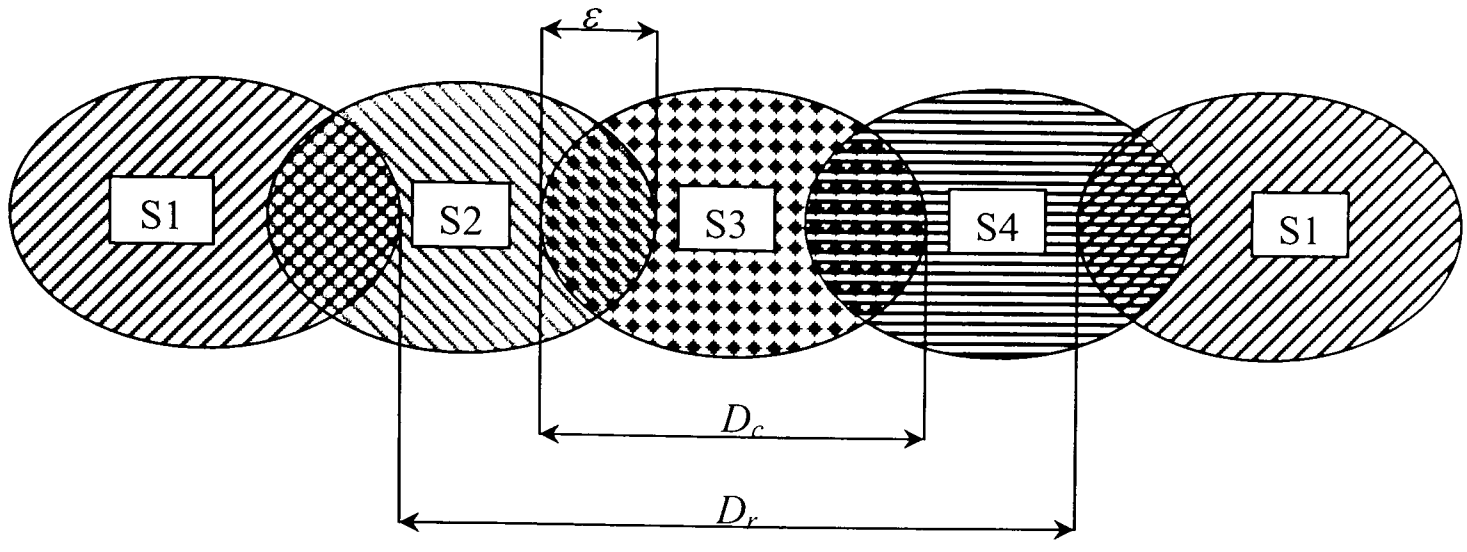

Figure (7.8) SDMA-OFDMA Implementation in SOFT MAC

From figure (7.8), the reuse distance D_r is given by:

$$D_r = 3D_c - 4\varepsilon \qquad (7.9)$$

which can be generalised for N_g subcarrier groups as:

$$D_r = (N_g - 1)D_c - N_g\varepsilon \qquad (7.10)$$

The minimum handoff distance ε should be long enough for the car to receive information about the TDMA frame in the next cell. The maximum distance for ε is half the cell radius to avoid the overlapping of 3 cells. We therefore set the bounds for ε as:

$$\frac{D_c}{2} \geq \varepsilon \geq T_{frame} \times v_{\max} \qquad (7.11)$$

T_{frame} is the TDMA frame duration and v_{max} is the maximum allowed speed. For the N_g = 4 system, consider a node in the intersection of S1 and S2 and assume the node uses the subcarriers specified in S1. This is equivalent to having 3 groups instead of 4. Since the interference increases with ε we assume the worst case of $\varepsilon = 0.5D_c$. The reuse distance D_r, from equation (7.10), is then $0.5D_c$. Thus four groups are sufficient to avoid collisions. Assuming frame duration of 100ms and a maximum speed of 120 km/hr, the minimum handoff distance from equation (7.11) is then 3.33m.

7.5. Throughput Analysis of SOFT MAC

In this section we mathematically analyse the performance of SOFT MAC. In the next section we compare its performance with 802.11. The following assumptions will be used for our analysis:

- Both SOFT MAC and 802.11 have the same bandwidth (20MHz) and number of subcarriers (64) per cell
- The data rate is 6Mbps
- Nodes share a single channel
- SOFT MAC is implemented using 802.11 as discussed in section 7.3
- The frame duration (T_{frame}) is fixed and equal to 100ms
- All transmissions start and finish within the frame (i.e. no transmission extends between two frames)
- We adopt the specifications of 802.11a (5.8GHz)
- All TS slots have been reserved
- Nodes always have data to transmit (saturation throughput)
- Implicit ACK is used
- No hidden terminals

7.5.1. Throughput of the TS period

Since the TS period is contention free, its throughput (S_{TS}) is given by:

$$S_{TS} = \frac{Data/rate}{(Header + Data)/rate + Wait\_time} \tag{7.12}$$

Where *Data* is the total transmitted data, *rate* is the data rate, *Header* is the total header (control bits) and *Wait_time* is any idle time (e.g. PIFS). The header size in each TS slot is given by:

$$H_{TS} = N_{TS}(TSstatus + PTP + MH\_Pri + NodeID) + NoTS + Seq + FrCON + FrDU + DestID \tag{7.13}$$

Where N_{TS} is the number of TS slots. The other parameters of (7.13) are listed in table (7.2). Their size is based on the 802.11 header.

Field	Use	Number per TS slot	Size (bits)
TSstatus	State of each TS slot in the frame (BUSY/IDLE)	N_{TS}	1
PTP	Point-To-Point flag	N_{TS}	1
MH_Pri	MH flag/Priority of each TS slot	N_{TS}	3
D	Delete Flag	N_{TS}	1
NodeID	MAC Address of node transmitting in a TS	N_{TS}	48
NoTS	Announces the current number of TS slots in frame	1	8
Seq	Sequence No. of the current TS slot	1	8
FrCON	Frame Control	1	16
FrDU	Frame Duration (Time left in TS period)	1	16
DestID	MAC Address of the destination of the current TS slot	1	48

Table (7.2): Fields of TS Header

Since there are N_{TS} slots per frame, the parameters of (7.12) are given by:

$$\begin{aligned} Header &= N_{TS} \times H_{TS} \\ Data &= N_{TS} \times P_{TS} \\ Wait\_time &= N_{TS} \times PIFS \end{aligned} \tag{7.14}$$

Where P_{TS} is the average payload size per TS slot. The TS period duration (T_{TS}) must satisfy:

$$T_{frame} \geq T_{TS} \geq \frac{(Header + Data)}{rate} + Wait\_time \tag{7.15}$$

After the TS period all nodes must wait for a DIFS before attempting to access the channel. Therefore the duration of the RS period (T_{RS}) is given by:

$$T_{RS} = T_{frame} - T_{TS} - DIFS \tag{7.16}$$

Nodes access the RS period using DCF. Equations (7.13) to (7.16) are the key to the design of the frame as they specify the possible number of TS slots for specific frame duration, TS duration and packet size. As the packet size increases, the possible number of TS slots decreases while improving the throughput since less header and wait time is needed. On the other hand a smaller number of TS slots means less nodes can reserve TS slots.

7.5.2. Throughput of the RS period

The theoretical saturation throughput (S_{RS}) of the RS period depends on the random access scheme used. Since we assume DCF is used, the throughput of the RS period is found from equations (6.3) to (6.11) as discussed in the chapter 6. The total throughput of the frame is then calculated as:

$$S = \frac{S_{TS} \times T_{TS} + S_{RS} \times T_{RS}}{T_{frame}} \qquad (7.17)$$

Note that if the RS period is smaller than the time required to transmit a packet, the throughput of the RS period is set to zero.

7.6. Evaluation of SOFT MAC

Using the previous analysis we now study the performance of SOFT MAC. Figure (7.9) shows the number of possible TS slots in the frame versus the payload size. As the payload size increases the duration of the TS slot increases. This means, for a fixed TS period, the number of possible slots decreases and therefore fewer nodes can access the channel. On the other hand increasing the payload size increases the efficiency as shown in figure (7.10). As the number of TS slots decreases, the header also decreases as expected from equations (7.13) and (7.14). Since the header is a waste of resources, the smaller the header the higher the efficiency of the protocol, therefore the efficiency improves as the payload increases. For 2312 bytes payload and 100ms TS period, the maximum number of TS slots is 29 and the efficiency is approximately 92%. If the payload is 1000 bytes the number of slots increases to 51 but the efficiency drops to approximately 73%.

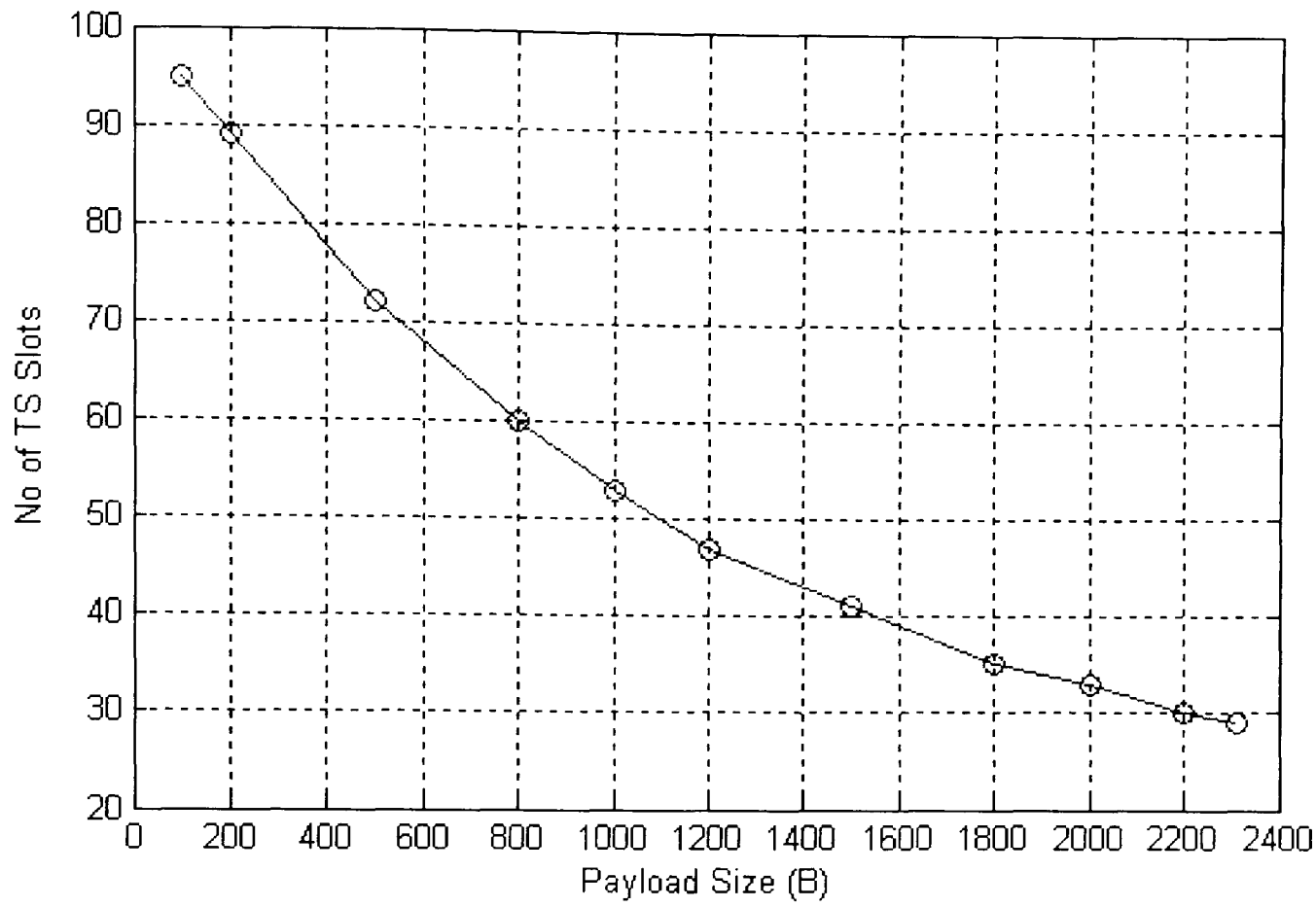

Figure (7.9): Number of TS Slots vs. Payload Size

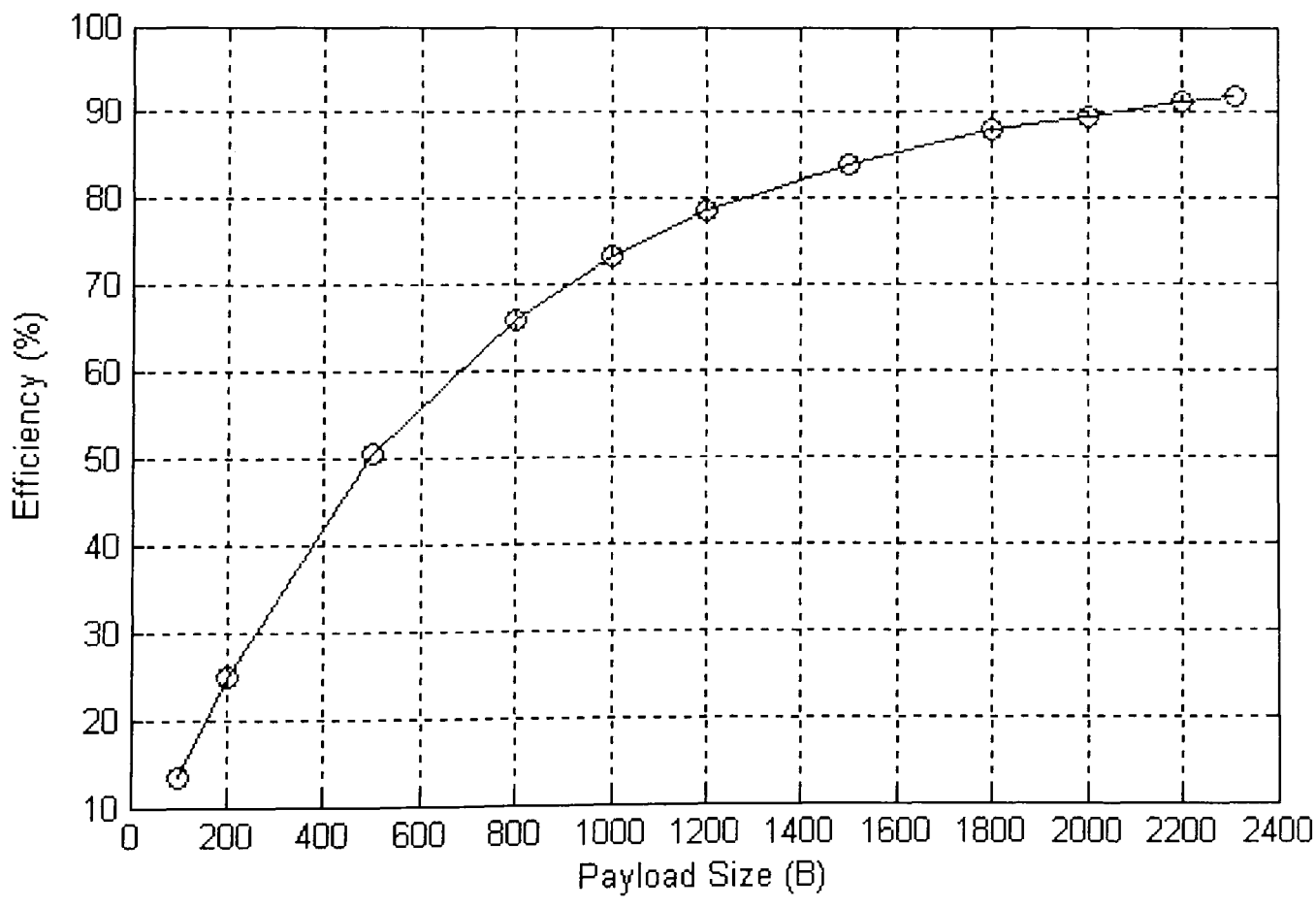

Figure (7.10): Slot Efficiency vs. Payload Size

Figure (7.11) shows the saturation throughput of SOFT MAC versus the number of nodes using DCF basic access. We assume a node having a reserved TS slots may also transmit data in the RS period. The payload size was set to 2312 bytes which is the maximum frame payload specified in the 802.11 standard [95]. When the TS period is 0% of the frame period, i.e. all the frame is RS period, nodes access the channel using the DCF basic access. As can be seen, the performance improves as the TS period increases till it reaches a maximum throughput of approximately 90% when the TS period occupies the whole frame. In this case, the rest of the bandwidth (10%) is wasted in header transmission and waiting time. This waste in bandwidth is feasible compared to that caused by the collisions incorporated by the basic access of the DCF (0 slots curve). However with the TS period occupying the entire frame, only 29 nodes are able to transmit in the channel. Changing the payload size to 1000B reduces the maximum achievable throughput, as shown in figure (7.12), but increases the maximum number of slots to more than 50 slots, hence, more nodes can reserve TS slots. The performance of the TDMA protocol is then a trade-off between the maximum achievable throughput and maximum number of nodes. By combining TDMA with the SDMA-OFDMA scheme it is possible to control the number of nodes using the channel and hence enhance the throughput without denying channel access to nodes. The maximum TS duration in the frame should be optimised for the number of nodes, traffic and quality of service requirements expected. When the TS period occupies the entire frame only nodes with reserved slots can access the channels, hence the throughput is independent of the number of nodes. However when the frame consists of TS and RS periods, the throughput drops as the number of nodes increase. In this case, nodes compete for the channel in the RS period and thus collisions occur. The throughput of the RS period is the throughput of the DCF access which drops as the number of nodes increases as discussed in chapter 6. The TS period is a collision-free period, hence as the TS period increases, the throughput improves.

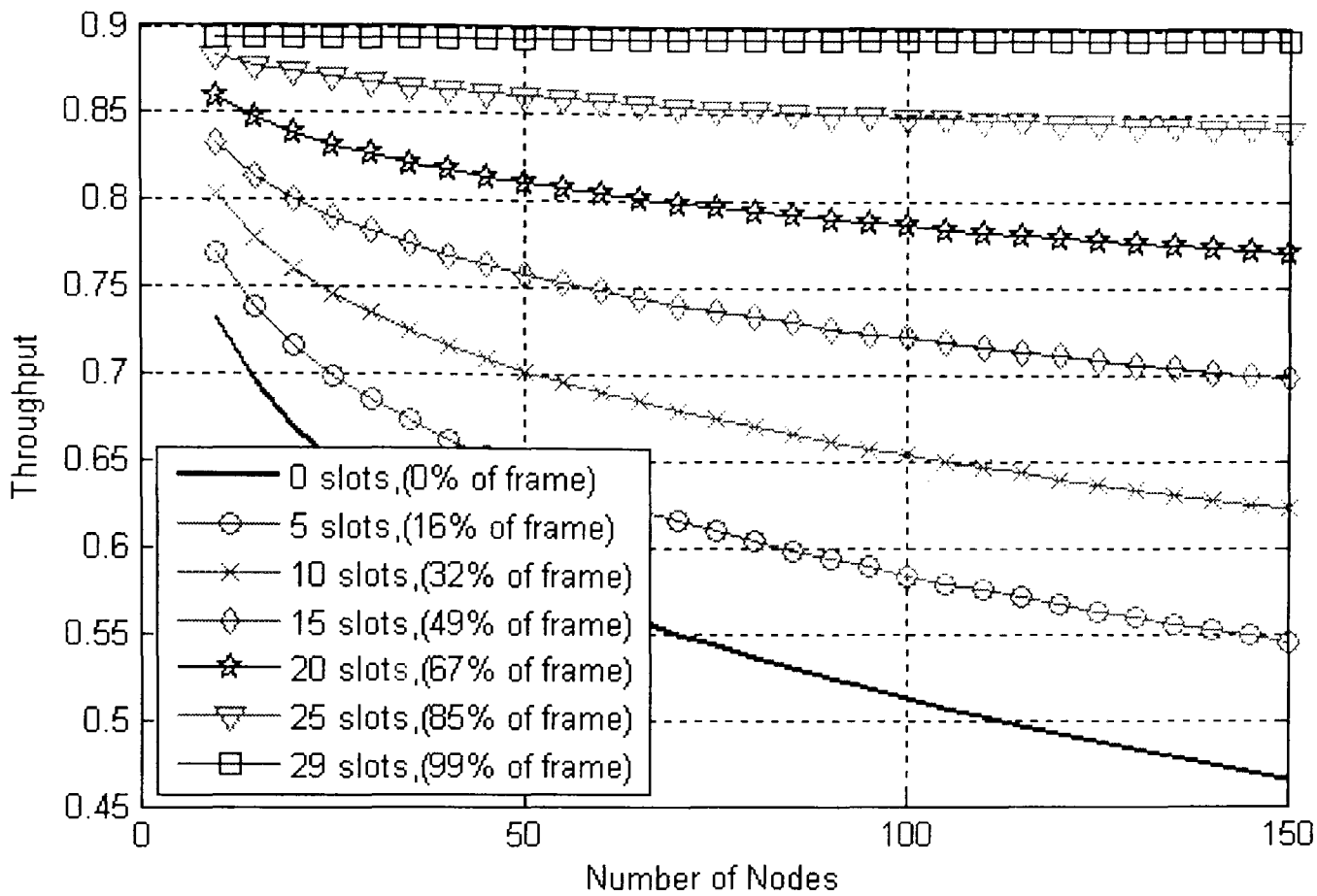

Figure (7.11): Throughput (Basic Access) vs. No. of Nodes (Payload = 2312B)

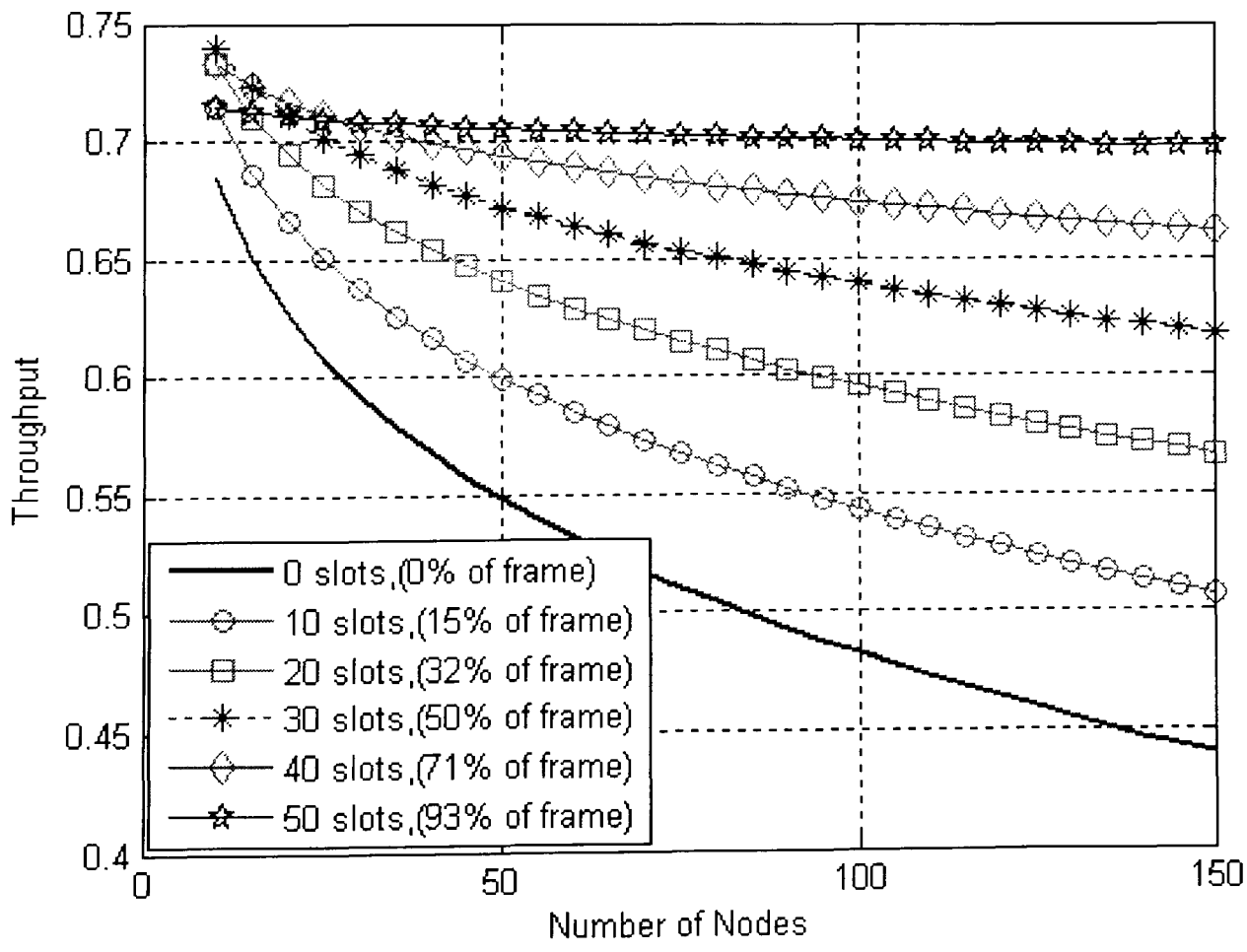

Figure (7.12): Throughput (Basic Access) vs. No. of Nodes (Payload = 1000B)

Figures (7.13) to (7.15) show the saturation throughput of SOFT MAC versus payload length with different network sizes. At small payload lengths and small number of nodes the performance of DCF is superior to SOFT MAC. However as the network size increases, the performance of DCF drops considerably due to collisions whereas the collision-free TS slots of SOFT MAC maintain high performance. As the payload size increases, the performance of SOFT MAC becomes superior since, from figure (7.10), its efficiency improves with payload size. The minimum payload for SOFT MAC to perform better than DCF depends on the network size. DCF provides good performance in small networks. We observe from figure (7.13) that for a payload size of approximately 800B or more SOFT MAC shows higher throughput than DCF. As the number of nodes increase, the contention for the channel and, hence, collisions deteriorate the performance of DCF and therefore the performance of SOFT MAC becomes superior even with small payloads. From figures (7.14) and (7.15) we note that for networks with 50 nodes or more and payload size of 500B or more SOFT MAC provides higher throughput than DCF compared to 800B for 10 nodes.

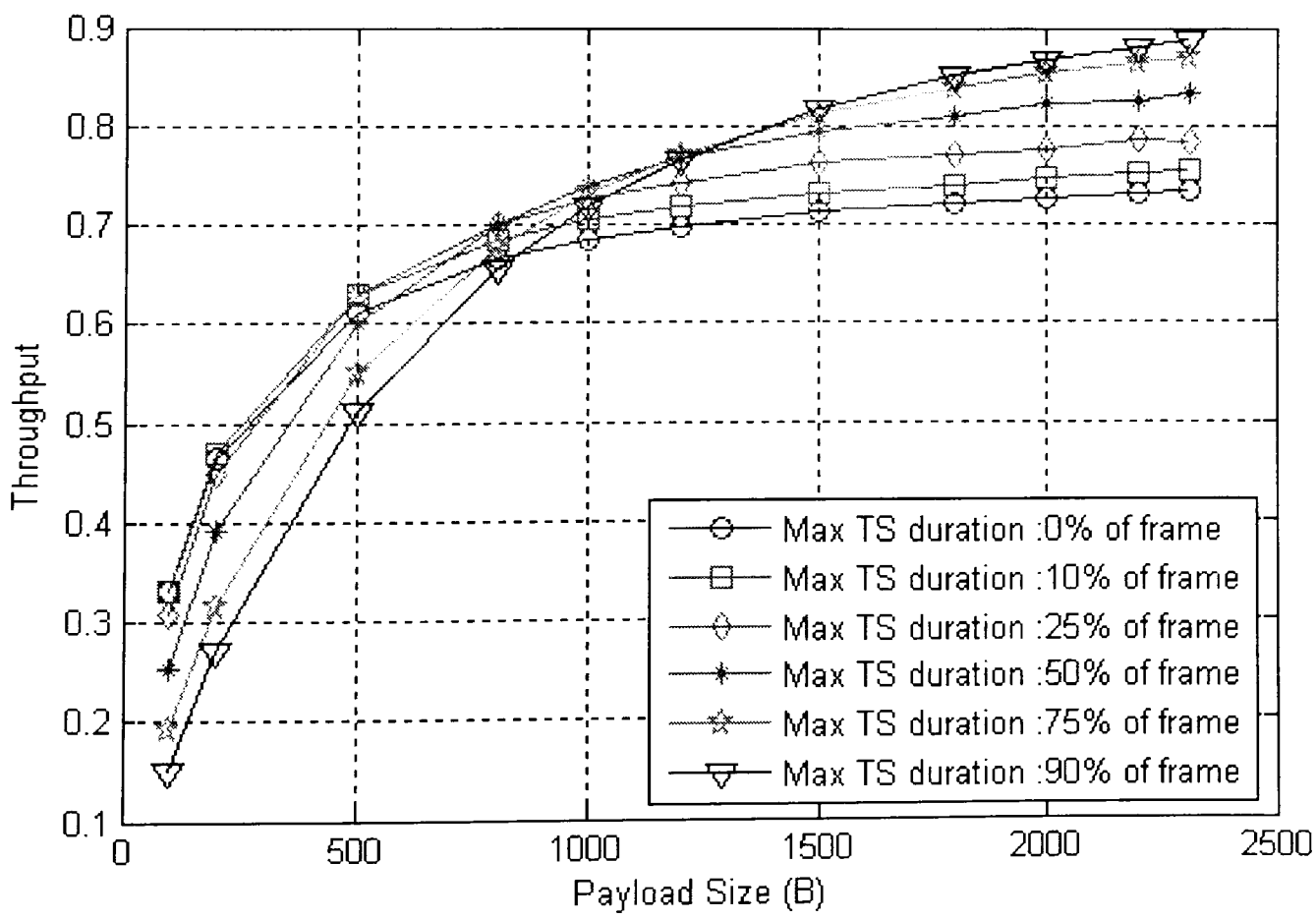

Figure (7.13): Throughput (Basic Access) vs. Payload Size (10 Nodes)

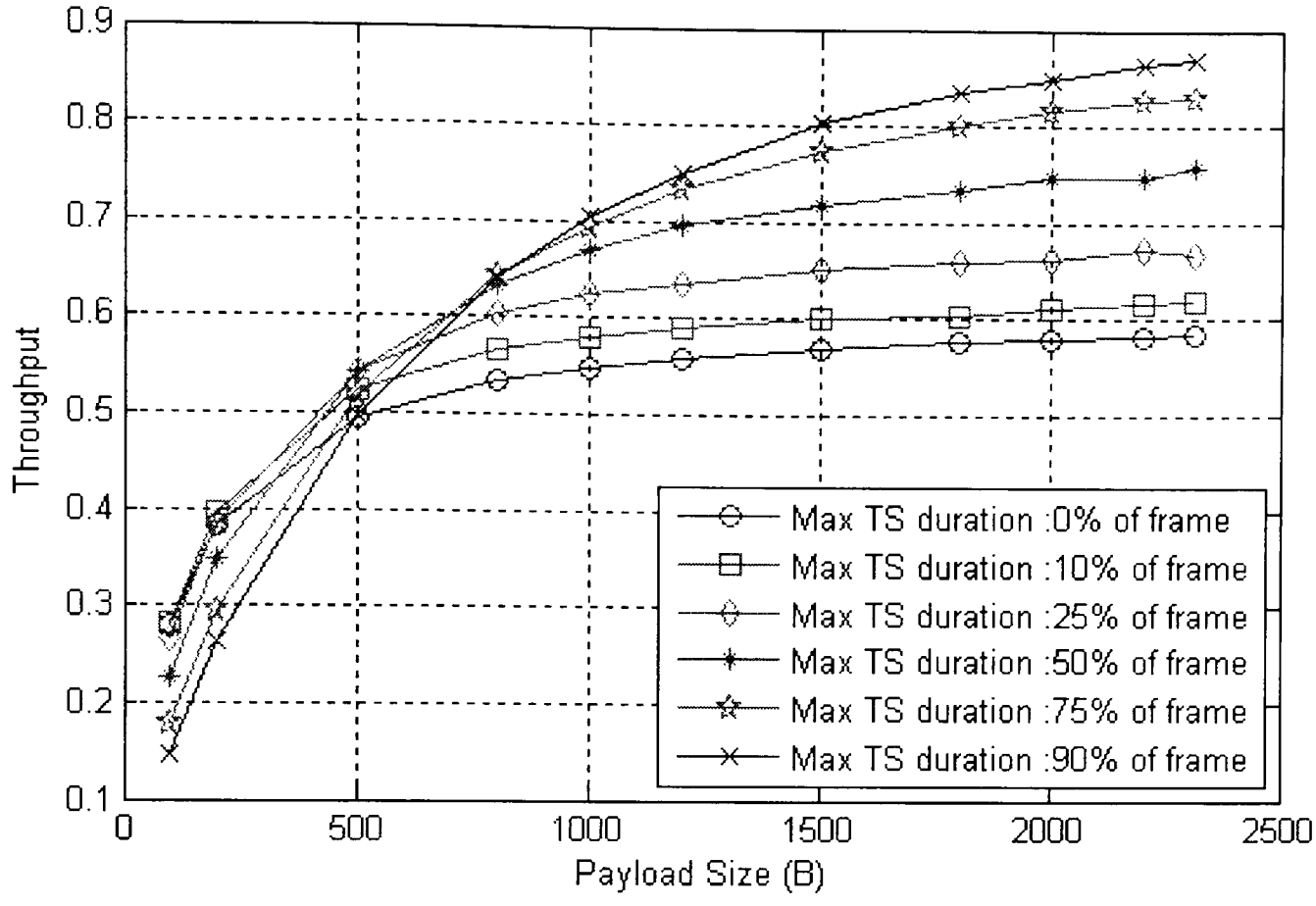

Figure (7.14): Throughput (Basic Access) vs. Payload Size (50 Nodes)

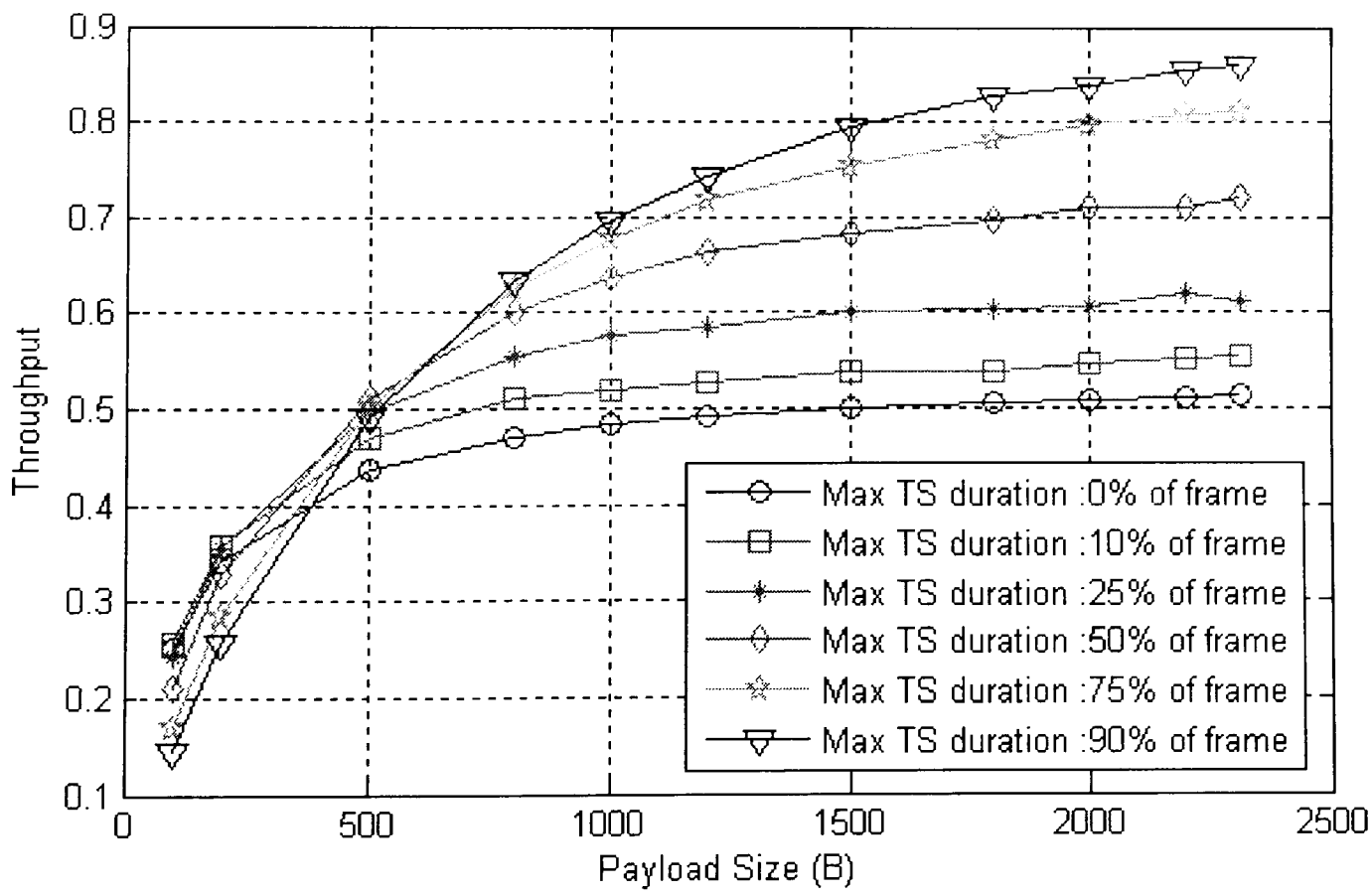

Figure (7.15): Throughput (Basic Access) vs. Payload Size (100 Nodes)

Figure (7.16) is the saturation throughput of SOFT MAC versus the number of nodes using DCF RTS/CTS access and 2312 byte payload. As shown, the performance first improves as the number of TS slots increases then deteriorates as the number of TS slots increase. As the number of TS slots in SOFT MAC increase the header consumes a significant portion of the bandwidth and the efficiency of the protocol drops. This loss of bandwidth is less than the bandwidth wasted due to collisions in basic access. The channel reservation process of RTS/CTS reduces the contention in the channel and organises the access to the channel leading to less collisions compared to the basic access mode. Thus SOFT MAC does not provide considerable improvement for RTS/CTS. From figure (7.16), the maximum improvement is throughput less than 3%. Similar conclusions can be reached from figure (7.17) which is for a payload of 1000 bytes. In this case the small payload makes the protocol inefficient that the bandwidth used to transmit the header for 50 slots exceeds that lost due to collisions.

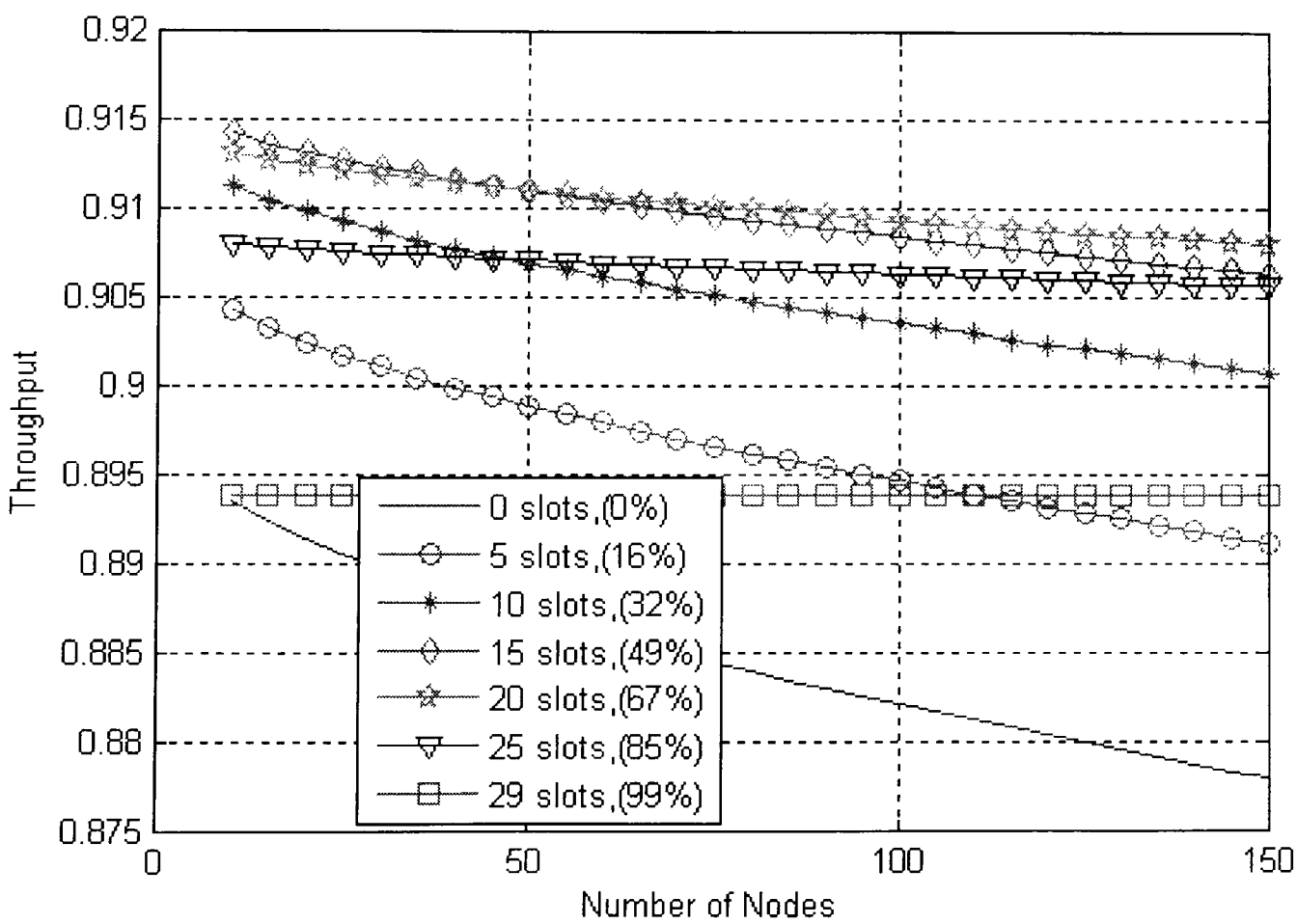

Figure (7.16): Throughput (RTS/CTS) vs. No. of Nodes (Payload size = 2312B)

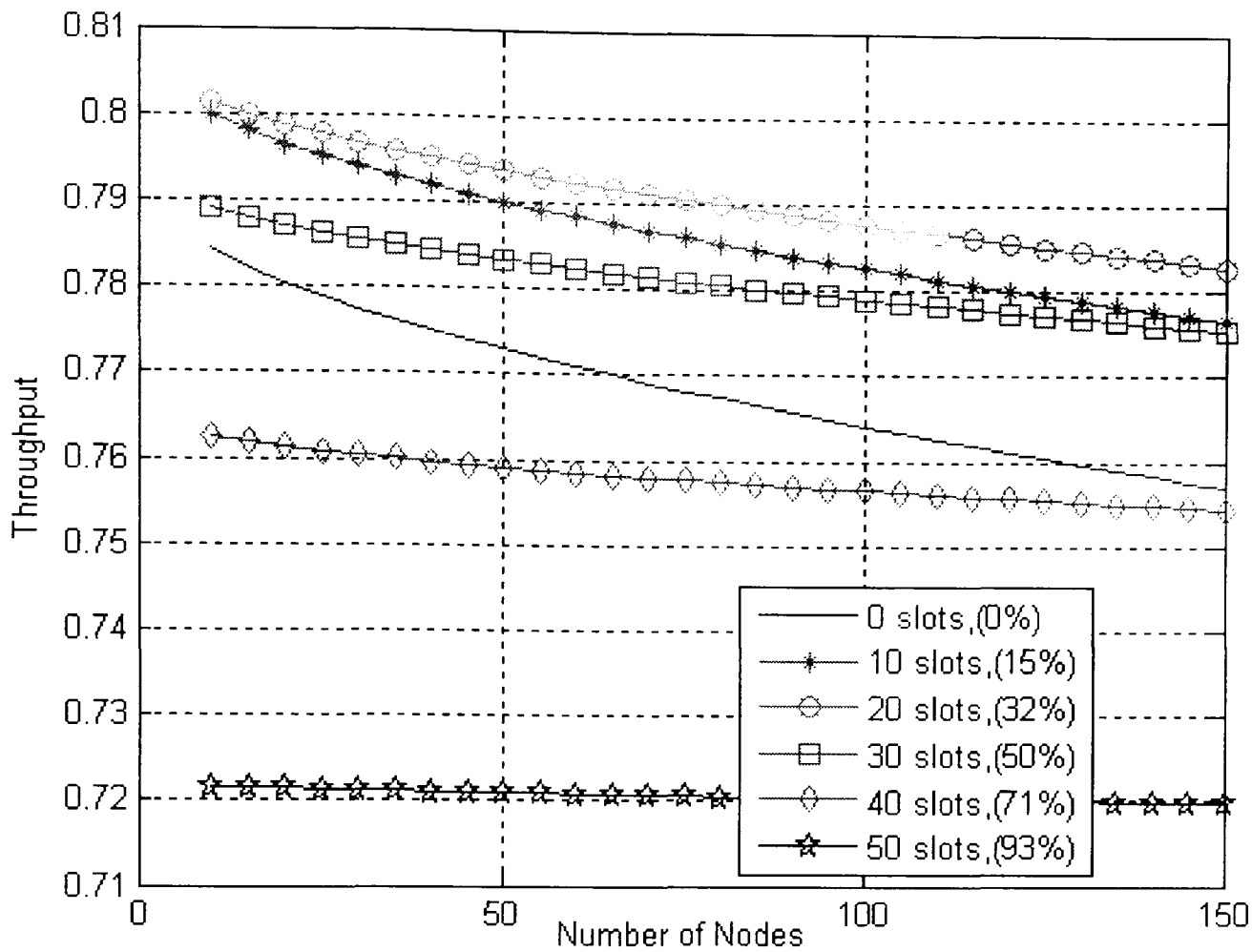

Figure (7.17): Throughput (RTS/CTS) vs. No. of Nodes (Payload size = 1000B)

Figures (7.18) and (7.19) show the saturation throughput of SOFT MAC versus the payload size for networks of 10 and 100 nodes. As with basic access, the throughput improves as the payload size increases. From figures (7.16) to (7.19) we expect that an optimum number of TS slots will depend on the number of nodes and payload size. However the expected improvement over RTS/CTS performance is less than 5%. On the other hand for small packet sizes the performance of SOFT MAC will be worse than RTS/CTS if the TS period exceeds 50% of the frame. This is due to the large overhead since the number of slots, and therefore header, increase as the payload size decreases. The maximum loss in throughput is less than 15%. An important advantage of SOFT MAC over RTS/CTS access, however, is that RTS/CTS handshake is applicable only for point to point transmissions whereas SOFT MAC can be used for broadcast as well as point to point transmissions.

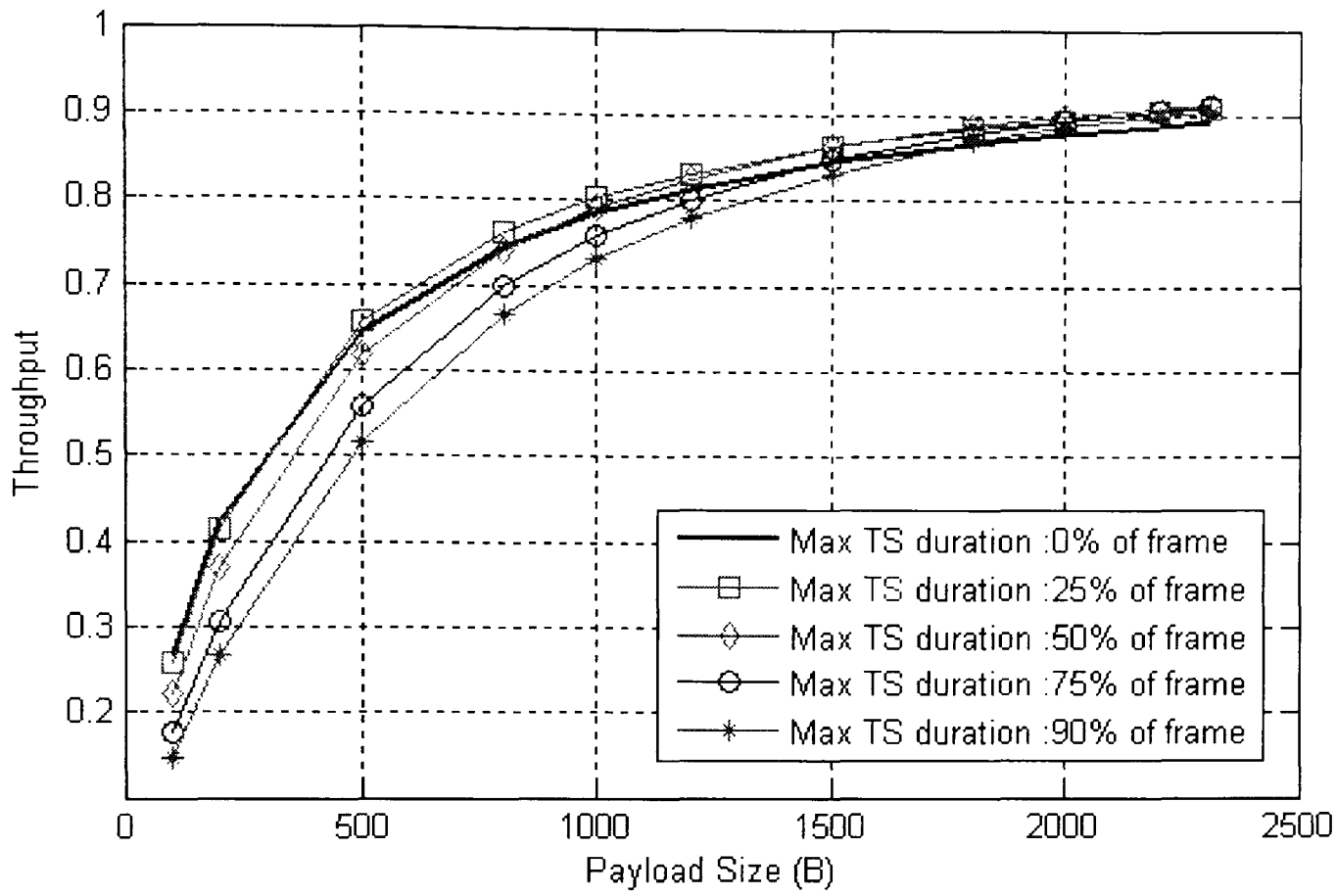

Figure (7.18): Throughput (RTS/CTS) vs. Payload Size (10 Nodes)

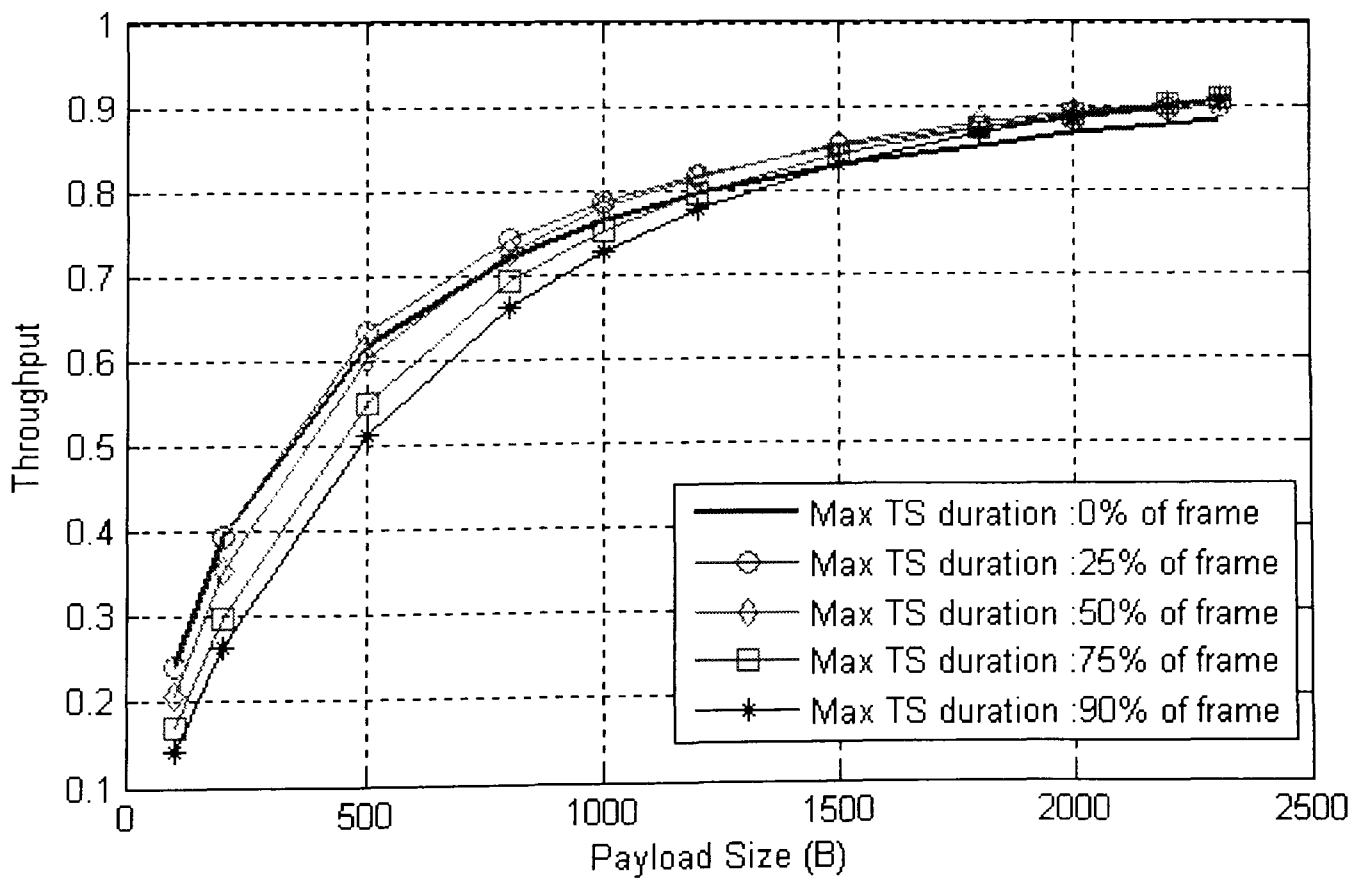

Figure (7.19): Throughput (RTS/CTS) vs. Payload Size (100 Nodes)

7.7. Concluding Remarks

In this chapter a new MAC protocol for VANET known as SOFT MAC was introduced and analysed. SOFT MAC is a combination of Space, Orthogonal Frequency and Time medium access techniques. The SDMA, OFDMA part of the protocol divides the road into cells and allocates each cell a group of subcarriers. By using OFDMA, nodes in the intersection of two, or more, cells can receive or transmit using the subcarriers of both cells with a single transceiver.

The cell radii and number of subcarriers per cell are design parameters and should be optimised for the expected traffic density. Each node determines its position using GPS and consults pre-installed maps to determine the subcarriers it is allowed to use. Within the cell, nodes share the available subcarriers using a combined TDMA-DCF protocol. In SOFT MAC time is divided into equal frames and each frame has two periods. The first period consists of transmission slots (TS period) and is accessed after reservation. The second period is the reservation (RS) period and is accessed using a random access technique such as DCF. The RS period is used to send reservation requests as well as data. Initially the duration of the TS period will be zero. As nodes send reservation requests, the duration of the TS period increases up to a prefixed maximum value.

A mathematical analysis of the saturation throughput was derived and used to analyse the protocol. Compared to 802.11 basic access, SOFT MAC shows improvement in the saturation throughput of medium to large networks as long as the payload size exceeds 500 bytes. As the payload size and TS period increase the performance improves but the number of nodes that can successfully access the channel is reduced. The performance of the RTS/CTS access method is comparable to that of SOFT MAC. However the RTS/CTS access is restricted to point to point transmissions only whereas SOFT MAC can be used for unicast and broadcast traffic. Our analysis assumes no hidden nodes and no mobility. Further investigation and simulation to analyse the protocol with mobility and hidden terminals is required to examine its performance under various conditions.

Chapter 8

Conclusions

In this chapter we summarise and discuss the project findings and investigate some open research issues that require further analysis.

8.1. Project Aims

The aim of the project was to study the physical and link layer challenges and limitations in VANET and develop bandwidth efficient solutions to provide high data rates particularly for commercial applications. Towards these aims we reviewed the literature to identify the latest proposals and standards for VANET. We then investigated the use of MIMO techniques in VANET to provide high data rates at the physical layer. Afterwards we studied the performance of 802.11 standards and designed a MAC protocol to provide efficient link layer access in a distributed manner. In the next sections we summarise our findings and results.

8.2. Contribution to Knowledge

- Development and verification of an accurate channel model for VANET.
- Analysis of the antenna correlation in VANET.
- Study of the effects of correlation and line of sight on VBLAST transmission.
- Performance analysis of VBLAST in VANET with perfect channel knowledge and training-based channel estimation.
- Derivation and evaluation of a channel tracking algorithm for VBLAST in flat fading channels.
- Derivation and evaluation of a channel tracking algorithm for VBLAST-OFDM systems in frequency selective channels.

- Analysis of the MIMO-OFDM Inter-Carrier-Interference (ICI) problem.
- Design and analysis of an ICI cancellation algorithm for VBLAST-OFDM.
- An investigation of the connectivity of VANET in highways and within the city.
- Throughput analysis of 802.11 standards.
- Design and evaluation of a new link layer protocol for VANET that achieves high throughput and supports quality of service in a distributed manner.

8.3. Summary of Literature Review

The main motivation behind VANET was providing a safe, fast, efficient and comfortable journey for people on the road. Safety was the main aim of VANET but several governmental and commercial applications were also proposed. Vehicle networks are a mix of ad hoc and architectural networks since road side units will be installed to cover only portions of the road network. Current physical layer standards use multiple channels at 5.9GHz and the proposed modulation is OFDM-QAM. The performance of OFDM, however, is limited by inter-carrier interference when the nodes move at high speeds. MIMO systems in rich Rayleigh fading have higher capacities compared to single antenna systems. Several MIMO techniques have been discussed. Diversity and space-time coding systems can be used to increase the reliability of the transmission whereas BLAST systems provide higher data rates. Among the available BLAST systems, VBLAST has the lowest computational complexity hence we adopted it in our project. The performance of BLAST systems degrades considerably due to inaccurate channel information at the receiver, and also when the correlation between the antennas is high. An accurate channel model is essential to study the performance of MIMO or any physical layer system for VANET. Existing VANET models define two zones, an urban zone with rich Rayleigh fading and a suburban zone for open areas with high probability of line of sight. However the models do not specify well defined criteria as to when to switch from one model to the other. Furthermore these models do not consider the correlation between the antennas and, hence, will not accurately simulate the channel for MIMO systems. For the MAC layer, the IEEE 802.11p

standard is been developed. IEEE 802.11 standards are CSMA based, best effort protocols and their performance becomes quite poor in highly congested networks. The RTS/CTS handshake can be used to improve the performance but it only applies to unicast transmissions. Several link layer proposals for VANET were introduced based on SDMA, TDMA and CDMA. Proposed SDMA solutions have low efficiency and are sensitive to location errors. TDMA solutions have a large overhead and can support a limited number of nodes. CDMA requires power control to solve the near-far problem but power control is difficult to implement in ad hoc networks since the power level will be different for different nodes. In some proposals, a node is elected, known as cluster head, to take the role of a basestation and organise access to the channel. However the election process requires some overhead and issues of clusters merging/emerging and loss of connection to the cluster head are of concern. Access to the multichannel band of VANET is organised by the IEEE WAVE standard which specifies that all nodes must switch to the control channel for a 50ms period every 100ms and may switch to any other channel in the other 50ms.

8.4. Concluding Remarks about Channel Model and VBLAST Performance

To study the performance of MIMO systems in VANET, an accurate channel model that takes into account the correlation between the elements in an antenna array was required. Existing channel models were designed to simulate either city or suburban environments and assume fixed surroundings and a single antenna. Our channel model extends to VANET the single bounce geometrical channel model originally developed to study the performance of antenna arrays in microcells. The scatterers in our model are not stationary, as in existing models, causing the Doppler spectrum to extend beyond Jakes' spectrum. These conclusions agree with the findings in the literature obtained via measurements. We studied the correlation between receive antennas for different array configurations and designed a 4 elements antenna array for VANET. We found the correlation increases for small delay spreads and/or under strong line of sight

conditions leading to higher bit error rates. The bit error rate (BER) of VBLAST for rich Rayleigh fading and perfect channel knowledge was analysed theoretically and via simulations and the results from both methods showed reasonable agreement. VBLAST requires accurate channel information to decode the signal correctly. As the nodes in VANET move at high speeds the channel response changes rapidly leading to an error floor in BER performance. Channel tracking techniques are needed to update the channel matrix at the receiver and maintain high performance.

8.5. Concluding Remarks about Channel Tracking and ICI Equalisation

We developed a simple recursive algorithm to track the changes in the channel response and update the channel estimation matrix for VBLAST in flat fading channels. After decoding, the algorithm calculates the difference between the received signal and expected received signal. This is multiplied by the pseudoinverse of the transmitted symbols and an update factor, then added to the current estimate. The update factor is optimised to minimise the mean square error of the estimation and takes into account the noise power. The update algorithm enhances the channel estimation on a symbol by symbol basis, but this can be relaxed for high symbol rates and/or slow fading as the channel coherence time will be large compared to the symbol duration. The proposed algorithm improves the system BER and channel estimate MSE via continuous and accurate channel updating and has low computational complexity as a result of using a set of simple single tap filters. Simulation results showed improvements in MSE and BER when using the update algorithm compared to the training only channel estimation. We also analysed the inter-carrier interference (ICI) problem and introduced algorithms for channel tracking and ICI equalisation in VBLAST-OFDM systems. ICI was found to increase with the number of subcarriers used, antennas transmitting and speed. The analysis showed that ICI causes an error floor at high SNR. The channel update algorithm was extended to OFDM and it showed improvement in BER performance when compared to the ordinary training based channel estimation. Both methods,

however, experience an error floor at high SNR due to ICI. An equalisation technique to reduce ICI for SISO was extended to VBLAST and evaluated. Our channel tracking algorithm updates the channel and estimates the slope of the channel response. This estimate is then fed to an equaliser to reduce ICI. The BER performance improves as the number of subcarriers included in the equaliser increases at the expense of more receiver complexity.

8.6. Concluding Remarks about Connectivity

We investigated the issue of connectivity in vehicular networks. Connectivity is a measure of how many nodes in the network are able to communicate. A network is defined to be fully connected, i.e. has a connectivity of 1, if a path exists between any two nodes regardless of the number of intermediate hops. The connectivity of Mobile Ad hoc Networks (MANET) was studied in the literature and was found to improve as the node density increases. VANET however are different from MANET because the nodes in VANET are distributed in a linear topology (road) whereas in MANET the nodes are typically distributed in an unconstraint two dimensional area. An expression for the probability of full connectivity of VANET was derived in the literature [117] but assumed uniformly distributed nodes, whereas typically the interspaces between cars follow an exponential distribution [114, 117]. We developed a simulation model to study the connectivity in VANET. The inter-space distribution used was the exponential distribution. The results showed that for a single lane highway road 100 km long and a communication range of 1 km, a node density of at least 12cars/km is required for the network to be fully connected. In multilane roads even higher node densities are required since the cars tend to cluster in groups with a large number of nodes per group thus increasing the probability of isolated groups or even isolated nodes. These results are particularly important in the design of the link layer since the performance of the link layer depends on the available traffic and the number of nodes. They also have a major impact on the network layer as a route many not exist between some groups. Within the city where roads are short, a density of 7cars/R is sufficient to guarantee a

95% probability of full connectivity for single lane roads, where R is the communication range. Roads with several lanes have higher average node connectivity but lower probability of full connectivity and number of groups. Roads with curves and turns showed lower connectivity than straight roads. The turn may lead to blockage of line of sight between cars before and after the turn, thus causing loss of connection. As the road width increases and/or the turn angle decreases, the area within the communication coverage of cars before the turn increases. Hence the connectivity improves as the turn angle decreases and/or the road width increases. Junctions also have lower probability of full connectivity than straight roads due to the 90° turns in the junction. However junctions have higher connectivity compared to turns because alternatives routes are possible other than the direct route. Some roundabouts have statues and trees which may block the line of sight. Such cases showed very low connectivity, even lower than turns. The connectivity in junctions and roundabout also improves as the road width increases due to the increase in coverage area. We also investigated the impact of penetration rate where not all nodes have the communication system installed. For penetration rates of 50-70% achieving 80% probability of full connectivity requires 10cars/R while for penetration rates of 5-20% the probability for the same density is less than 10%. This means at the start of VANET deployment, home-to-vehicle applications are essential for market penetration as the network will not be able to provide services on the road with acceptable quality unless a large number of roadside units are installed which is very expensive.

8.7. Concluding Remarks about 802.11 Throughput

The 802.11p standard under development by the IEEE for VANET is based on the 802.11a physical layer specification and uses the Enhanced Distributed Co-ordination Function (EDCF) to support quality of service. The difference between EDCF and the original Distributed Co-ordination Function (DCF) is that EDCF provides quality of service by using separate queues and contention windows for each QoS class. This QoS scheme is not reliable as packets still contend for the channel. We analysed the

throughput performance of the basic and RTS/CTS access methods of the 802.11 DCF. It was shown that the performance is affected by the contention window size, number of nodes and available traffic. For basic access, using a small window size leads to fast access to the channel in small networks with light traffic, whereas a large window size gives superior performance in large networks with heavy traffic. The throughput of RTS/CTS access is less dependent on the window size than basic access because the channel reservation handshake reduces the collision duration and organises access to the channel. The window size specified for 802.11a ranges from 16 to 1024. Each node in DCF attempts to optimise its window size for the available network traffic by doubling the current window whenever a collision is detected and reducing its size when the transmission is successful. This is known as the back off scheme of DCF. DCF basic access provides better saturation throughput compared to CSMA due to the back off procedure used in DCF. RTC/CTS access provides even better performance by combining the back off algorithm with a channel reservation handshake. DCF sacrifices the maximum achievable throughput via CSMA for higher throughput at saturation; this is why it shows a more stable performance as the traffic increases. The performance, however, drops gradually as the number of nodes in the network increases. Higher network densities lead to poor DCF performance whilst improving the connectivity of the network.

8.8. Concluding Remarks about SOFT MAC

To improve the throughput performance of VANET and support QoS traffic, we designed and analysed a new MAC protocol for VANET known as Space-Orthogonal Frequency-Time Medium Access Control (SOFT MAC). SOFT MAC is a combination of Space, Orthogonal Frequency and Time medium access techniques. The SDMA-OFDMA part of the protocol divides the road into cells and allocates each cell a group of subcarriers. By using OFDMA, nodes in the intersection of two, or more, cells can receive or transmit using the subcarriers of both cells with a single transceiver. The cell radii and number of subcarriers per cell are design parameters and should be optimised

for the expected traffic density. Each node determines its position using GPS and consults pre-installed maps to determine the subcarriers it is allowed to use. Within the cell, nodes share the available subcarriers using a combined TDMA-CSMA protocol. In SOFT MAC time is divided into equal frames and each frame has two periods. The first period consists of transmission slots (TS period) and is accessed after reservation. The second period is the reservation (RS) period and is accessed using a random access technique such as DCF. The RS period is used to send reservation requests as well as data. Initially the duration of the TS period will be zero. As nodes send reservation requests, the duration of the TS period increases up to a prefixed maximum value. A mathematical analysis of the saturation throughput was derived and used to analyse the protocol. Compared to 802.11 basic access, SOFT MAC shows improvement in saturation throughput as long as the payload size exceeds 500 bytes. As the payload size and TS period increase the performance improves but the number of nodes that can successfully access the channel is reduced. The performance of the RTS/CTS access method is comparable to that of SOFT MAC. However the RTS/CTS access is restricted to point to point transmissions only whereas SOFT MAC can be used for unicast and broadcast traffic. Moreover, nodes with reserved slots in SOFT MAC have a known fixed delay between transmission durations whereas the delay in 802.11 is random.

8.9. Future work

In this section we identify the open issues and limitations that require further investigation.

8.9.1. Channel Tracking and Error Correcting Codes

The performance of the channel tracking and ICI cancellation algorithms was studied with uncoded data. Error correcting codes, such as convolutional codes, can be employed to enhance the bit error rate of the system. For instance, if the decision of the Viterbi decoder is used in the update algorithm instead of using the decision before the

Viterbi decoder, the performance of the algorithm may improve. This is true since the update algorithm assumes correct decoding. The Viterbi decoder, however, encounters some delay before a decision is obtained. Further investigation is required to study the impact of using the decision of the Viterbi decoder and the optimum error correcting codes.

8.9.2. Simplified ICI Equalisation

The ICI equalisation scheme introduced in chapter 4 cancels the ICI contribution of adjacent subcarriers by inverting a large matrix. The matrix size increases with the number of antennas transmitting and/or number of subcarriers to be cancelled. In [72] the authors proposed the use of decision feedback filters to reduce this complexity. A similar approach can be applied in our ICI equalisation algorithm to reduce its complexity but may lead to error propagation if the detection was incorrect. This scheme needs more evaluation to identify its advantages if any.

8.9.3. Dynamic Optimisation of Capacity

We investigated the performance of 2 and 3 transmitting antennas with QPSK modulation. In a real system the number of antennas and modulation used should be optimised to achieve the highest capacity. The optimum selection depends on the signal to noise ratio, correlation between the antennas, Doppler shift and possibly the error correcting code used. An algorithm to dynamically select the optimum combination of antenna, modulation and error correcting code is required to provide best performance.

8.9.4. SOFT MAC Simulation and Handoff Analysis

Further investigation of the performance of SOFT MAC should be carried via simulation. The theoretical analysis derived in chapter 7 assumes no hidden terminals, no mobility and all the TS slots have been successfully reserved. In a highly dynamic network such as VANET, hidden terminals are quite common and the implication of this on the reservation process and throughput requires further investigation. Moreover

the handoff process and the overhead encountered as nodes move between cells should be assessed.

8.9.5. Optimum Cell Radius and Subcarrier Assignment

The cell radius and number of subcarriers per cell in SOFT MAC should be optimised for the expected traffic density. At low traffic density the cell radius should be large to minimise the handoff process when cars move between cells while keeping the number of nodes small to limit the number of nodes competing for the channel. At high traffic small cells should be used to maintain acceptable quality of service. In congested areas cars move at low speeds, hence even with small cells, we expect the enhancement in throughput due to the small cell size to exceed the loss due to the handoff overhead. The relationship between expected traffic density, cell size and number of subcarriers should be analysed and optimized to achieve the highest throughput.

8.9.6. Synchronisation

SOFT MAC assumes the nodes are synchornised via GPS. Synchronisation via GPS is hard to implement. A scheme similar to that proposed in [101, 102] can be used where nodes use GPS for coarse synchronisation and a midample for fine synchronisation. More research is required to investigate the impact of this or any other synchronisation solutions on performance.

Appendix I: Derivation of the Optimum Update Parameter

In this appendix we derive the optimum value (γ_i^{opt}) of the update parameter (γ_i). Equation (4.84) can be expanded for the elements within the matrices as:

$$\hat{h}_{ri}(F+1,k)=\hat{h}_{ri}(F,k)+\gamma_i\Delta h_{ri}(F,k) \qquad \text{(I.1)}$$

The mean square error of the estimation is found by:

$$E\left[\left|\varepsilon_{ri}(F+1,k)\right|^2\right]=E\left[\left|h_{ri}(F+1,k)-\hat{h}_{ri}(F+1,k)\right|^2\right]$$

$$=E\left[\left|h_{ri}(F,k)+(N+CP)a_{ri}(F,k)-\hat{h}_{ri}(F,k)-\gamma_i\Delta h_{ri}(F,k)\right|^2\right] \qquad \text{(I.2)}$$

CP is the cyclic prefix. To calculate the mean square error we need to find the autocorrelation function of $a_{ri}(F, k)$. This is given by [40]:

$$E\left|a_{ri}(t,k)\times\bar{a}_{ri}(t+\tau,k)\right|=-\frac{\partial^2 AC(\tau)}{\partial\tau^2} \qquad \text{(I.3)}$$

Where $AC(\tau)$ is the autocorrelation function of the channel for a delay τ and ($\bar{}$) represents complex conjugate. The autocorrelation function for Rayleigh fading channels is [26]:

$$AC(\tau)=J_0(2\pi f_d\tau) \qquad \text{(I.4)}$$

Where J_0 is the zero order Bessel function and f_d is the maximum Doppler shift. $J_0(x)$ can be approximated for small values of x by [26, 40, 143]:

$$J_0(x)\approx 1-\left(\frac{x}{2}\right)^2 \qquad \text{(I.5)}$$

Using this approximation, equation (I.3) for discrete time can be written as:

$$E\left|a_{ri}(F,k)\times\bar{a}_{ri}(F+m,k)\right|=-\frac{\partial^2 J_0(2\pi f_d mT_s)}{\partial m^2}\approx 2(\pi f_d T_s)^2 \qquad \text{(I.6)}$$

T_s is the symbol duration. mT_s is used instead of the delay (τ) for discrete time.

Now substituting (I.1) and (4.83) in (I.2) we get:

$$E\left[\left|\varepsilon_{ri}(F+1,k)\right|^2\right]=E\left[\left|\begin{array}{l}(1-\gamma_i)\varepsilon_{ri}(F,k)+(N+CP)a_{ri}(F,k)- \\ \gamma_i\left[\sum_{\substack{b=1\\b\neq i}}^{A}\frac{d_b(F,k)}{d_i(F,k)}\varepsilon_{rb}(F,k)+\frac{1}{N}\sum_{b=1}^{A}\sum_{\substack{p=0\\p\neq k}}^{N-1}\frac{d_b(F,p)}{d_i(F,k)}a_{rb}(F,p)C_{pk}+\frac{W_r(F,k)}{d_i(F,k)}\right]\end{array}\right|^2\right] \quad (I.7)$$

Let:

$$g_{ri}(F,k)=\sum_{\substack{b=1\\b\neq i}}^{A}\frac{d_b(F,k)}{d_i(F,k)}\varepsilon_{ri}(F,k)+\frac{1}{N}\sum_{b=1}^{A}\sum_{\substack{p=0\\p\neq k}}^{N-1}a_{rb}(F,p)\frac{d_b(F,p)}{d_i(F,k)}C_{pk}+\frac{W_r(F,k)}{d_i(F,k)} \quad (I.8)$$

Assuming the data on each antenna and subcarrier are independent and identically distributed (i.i.d) white data with equal average power (P), we can treat the terms in (I.8) as noise with average power [143]:

$$N_T=E\left[\left|g_{ri}(F,k)\right|^2\right]=\sum_{\substack{b=1\\b\neq i}}^{A}\sigma_{rb}{}^2(k)+2A(2\pi f_d T_s)^2\sum_{\substack{p=0\\p\neq k}}^{N-1}\left|C_{pk}\right|^2+\frac{N_{oise}}{P} \quad (I.9)$$

Where N_{oise} is the noise power and:

$$\sigma_{rb}{}^2(F,k)=E\left[\left|\varepsilon_{rb}(F,k)\right|^2\right] \quad (I.10)$$

We then rewrite (I.7) as:

$$E\left[\left|\varepsilon_{ri}(F+1,k)\right|^2\right]=E\left[\left|(1-\gamma_i)\varepsilon_{ri}(F,k)+(N+CP)a_{ri}(F,k)-\gamma_i.g_{ri}\right|^2\right] \quad (I.11)$$

This can be split into two uncorrelated errors as [143]:

$$E\left[\left|\varepsilon_{ri}{}^C(F+1,k)\right|^2\right]=E\left[\left|(1-\gamma_i)\varepsilon_{ri}{}^C(F,k)+(N+CP)a_{ri}(F,k)\right|^2\right] \quad (I.12)$$

$$E\left[\left|\varepsilon_{ri}{}^N(F+1,k)\right|^2\right]=E\left[\left|(1-\gamma_i)\varepsilon_{ri}{}^N(F,k)-\gamma_i.g_{ri}\right|^2\right] \quad (I.13)$$

Where $\varepsilon_{ri}{}^C$ is the error due to the change in the channel and $\varepsilon_{ri}{}^N$ is the error due to the noise and ICI. Equations (I.12) and (I.13) can be written as:

$$E\left[\left|\varepsilon_{ri}{}^C(F+1,k)\right|^2\right]=E\left[(N+CP)^2\sum_{u=0}^{F}\sum_{v=0}^{F}(1-\gamma_i)^u.(1-\gamma_i)^v a_{ri}(u,k).\bar{a}_{ri}(v,k)\right] \quad (I.14)$$

$$E\left[\left|\varepsilon_{ri}{}^N(F+1,k)\right|^2\right]=E\left[\gamma_i{}^2\sum_{u=0}^{F-1}\sum_{v=0}^{F-1}(1-\gamma_i)^u.(1-\gamma_i)^v g_{ri}(u,k).\bar{g}_{ri}(v,k)\right] \quad (I.15)$$

Since the noise and data are assumed white, for large F equation (I.15) becomes:

$$E\left[\left|\varepsilon_{ri}{}^{N}(F+1,k)\right|^{2}\right]=\frac{\gamma_i}{2-\gamma_i}N_T\approx\frac{\gamma_i}{2}N_T \tag{I.16}$$

Using equation (I.6), for large F equation (I.14) becomes:

$$E\left[\left|\varepsilon_{ri}{}^{C}(F+1,k)\right|^{2}\right]=2\left(\frac{\pi f_d T_s(N+CP)}{\gamma_i}\right)^{2} \tag{I.17}$$

Combining (I.16) and (I.17) we have:

$$E\left[\left|\varepsilon_{ri}(F+1,k)\right|^{2}\right]\approx 2\left(\frac{\pi f_d T_s(N+CP)}{\gamma_i}\right)^{2}+\frac{\gamma_i}{2}N_T \tag{I.18}$$

Which is independent of the receive antenna r since we assume i.i.d fading and equal average SNR for the receive antennas. The optimum value of γ_i , denoted (γ_i^{opt}) , for transmit antenna i is obtained by differentiating the mean square error (equation (I.18)) and setting the derivative equal to zero to minimise the MSE. We then find:

$$\gamma_i{}^{opt}=\sqrt[3]{\frac{8\left[\pi f_d T_s(N+CP)\right]^{2}}{N_T}} \tag{I.19}$$

Substituting this value in equation (I.18) we get:

$$\sigma_i{}^{2}(F,k)=E\left[\left|\varepsilon_{ri}(F,k)\right|^{2}\right]=E\left[\left|\varepsilon_{i}(F,k)\right|^{2}\right]=2\left[\frac{\pi f_d T_s(N+CP)}{\gamma_i{}^{opt}}\right]^{2}+\frac{\gamma_i{}^{opt}}{2}N_T \tag{I.20}$$

Appendix II: Flow Charts of SOFT MAC

Initialise: Called when a node joins a cell for the first time.

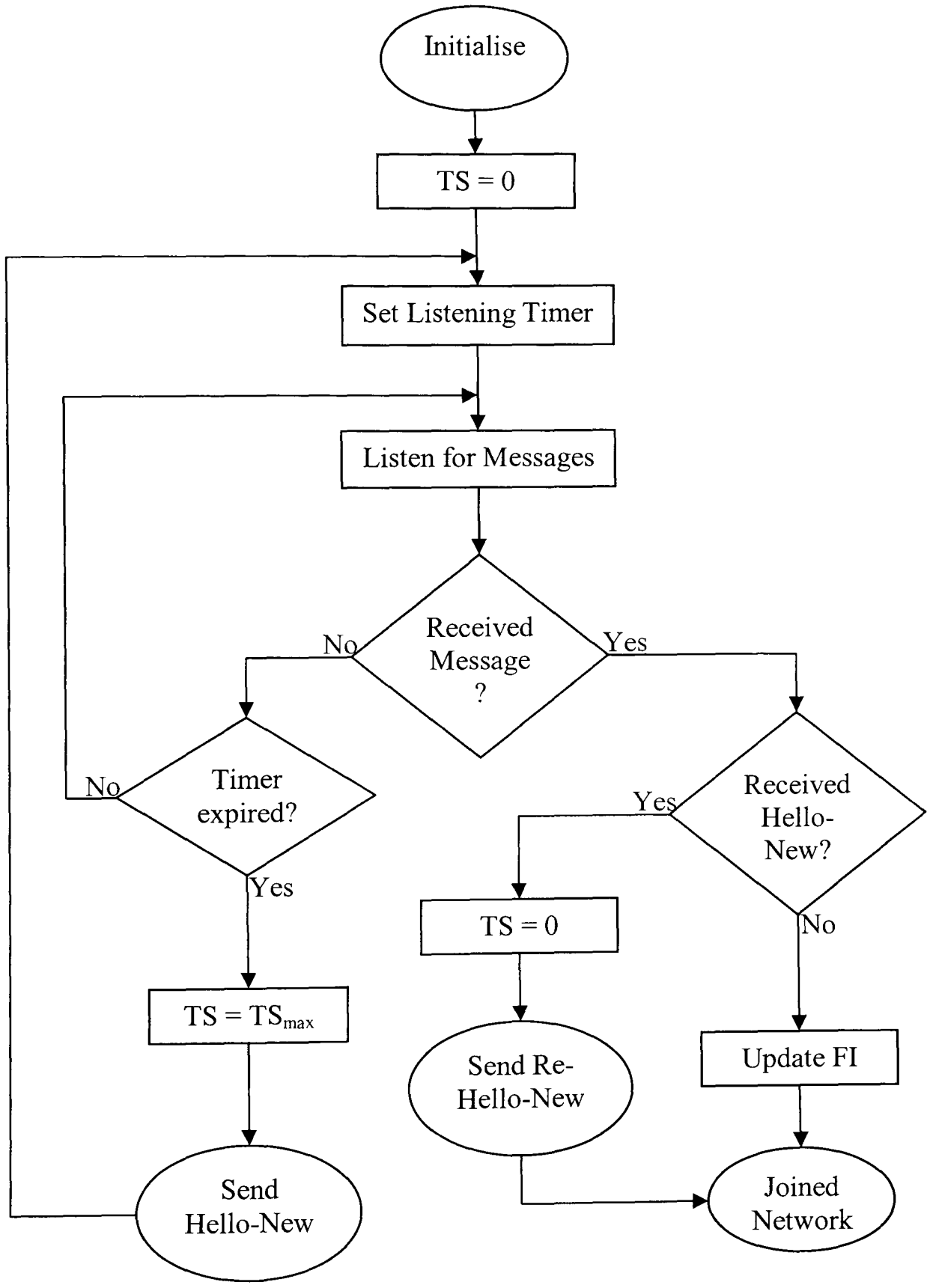

Receive: Called when the node receives a packet.

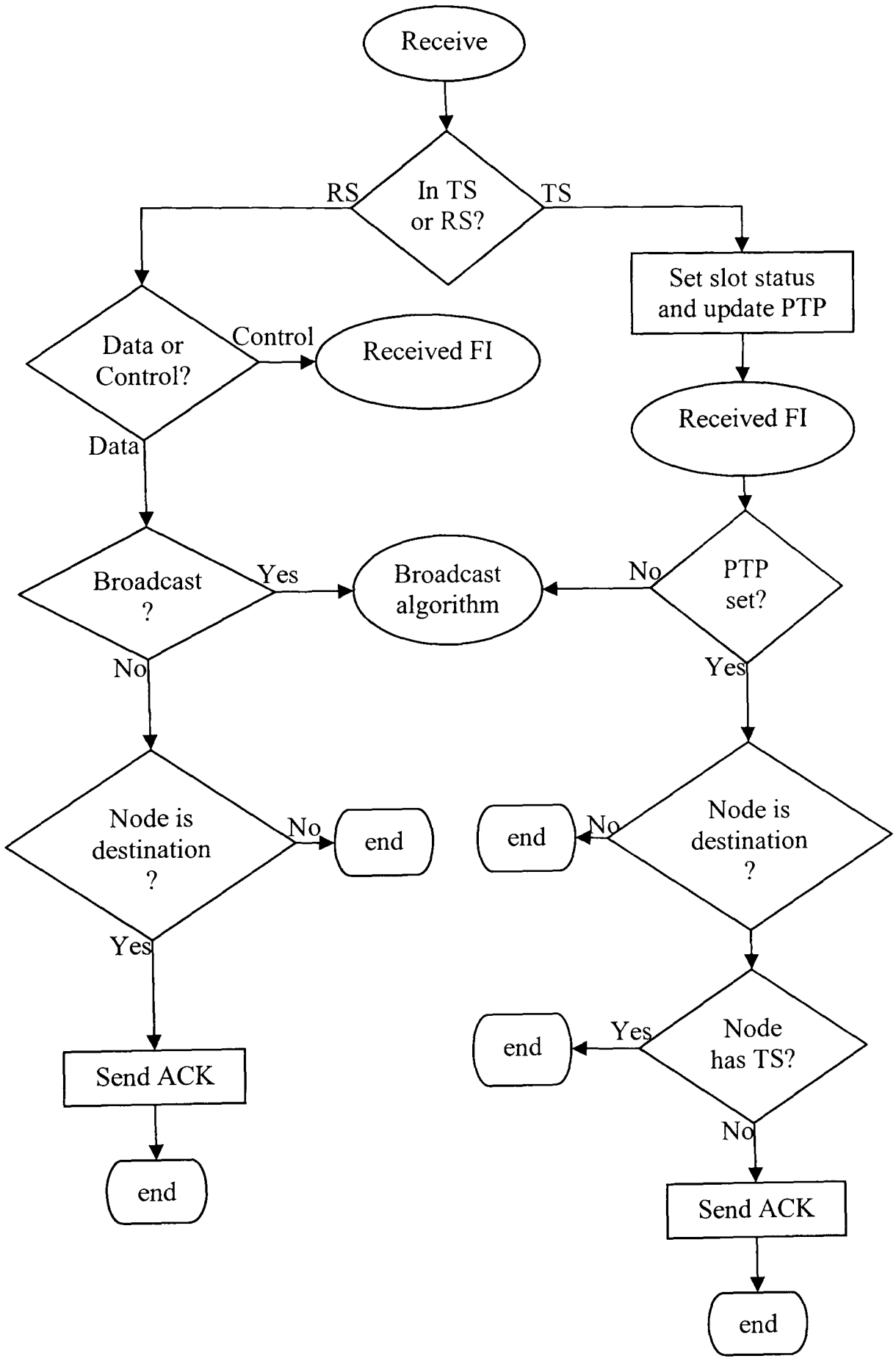

Received FI: Called when the node receives frame information.

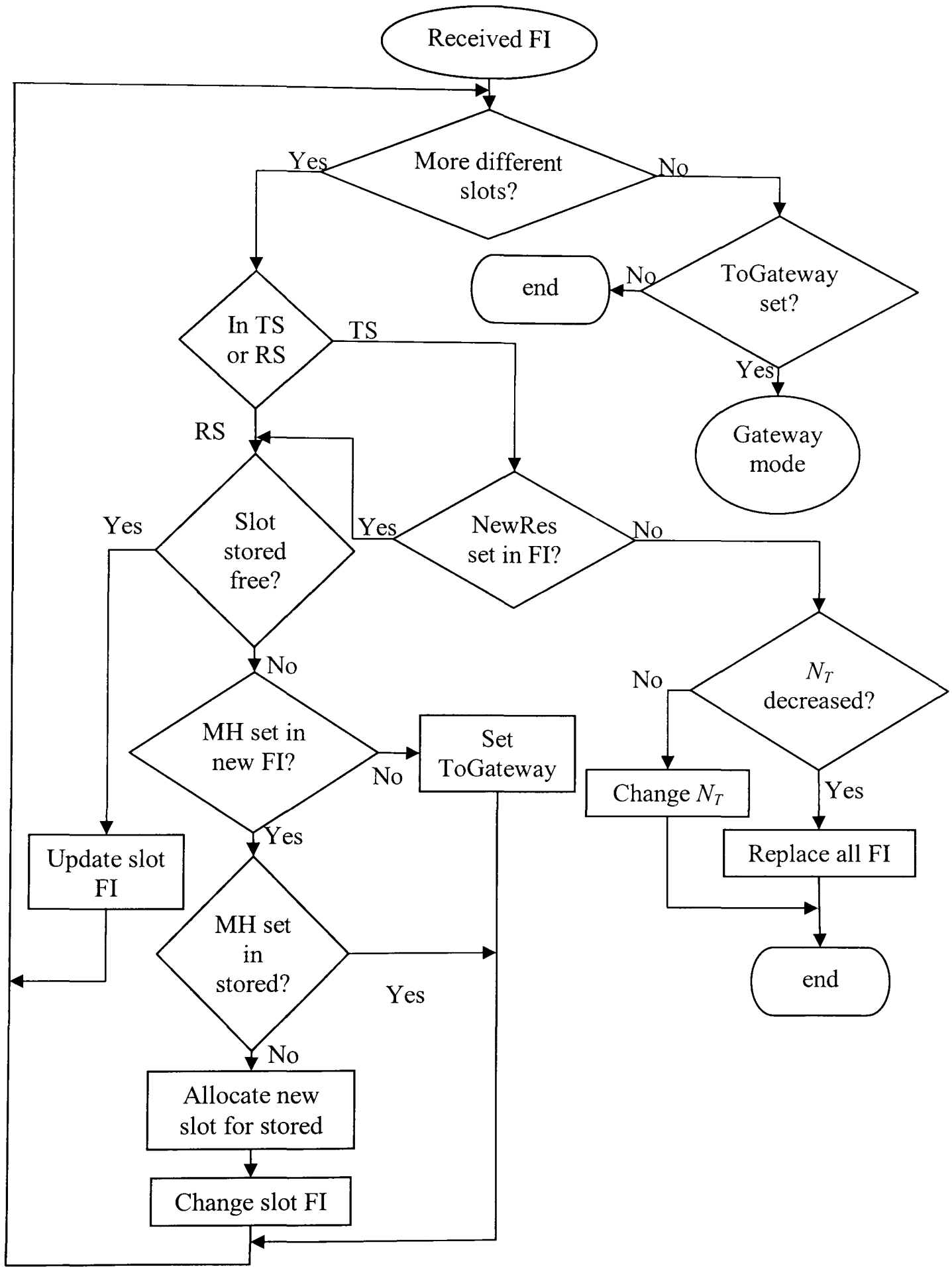

Gateway Mode: Called when the node detects double reservation.

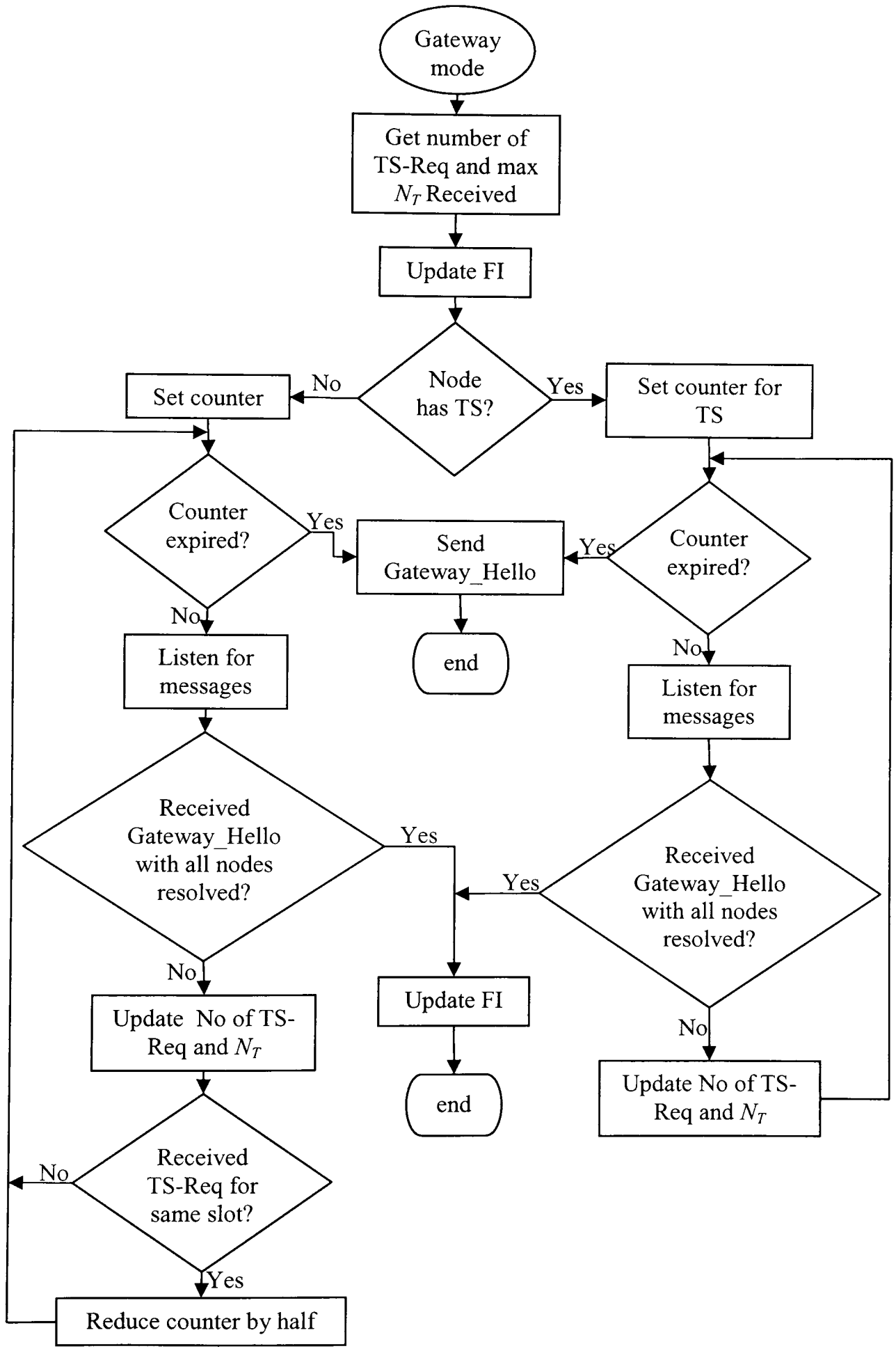

Send: Called when the node has a packet to send.

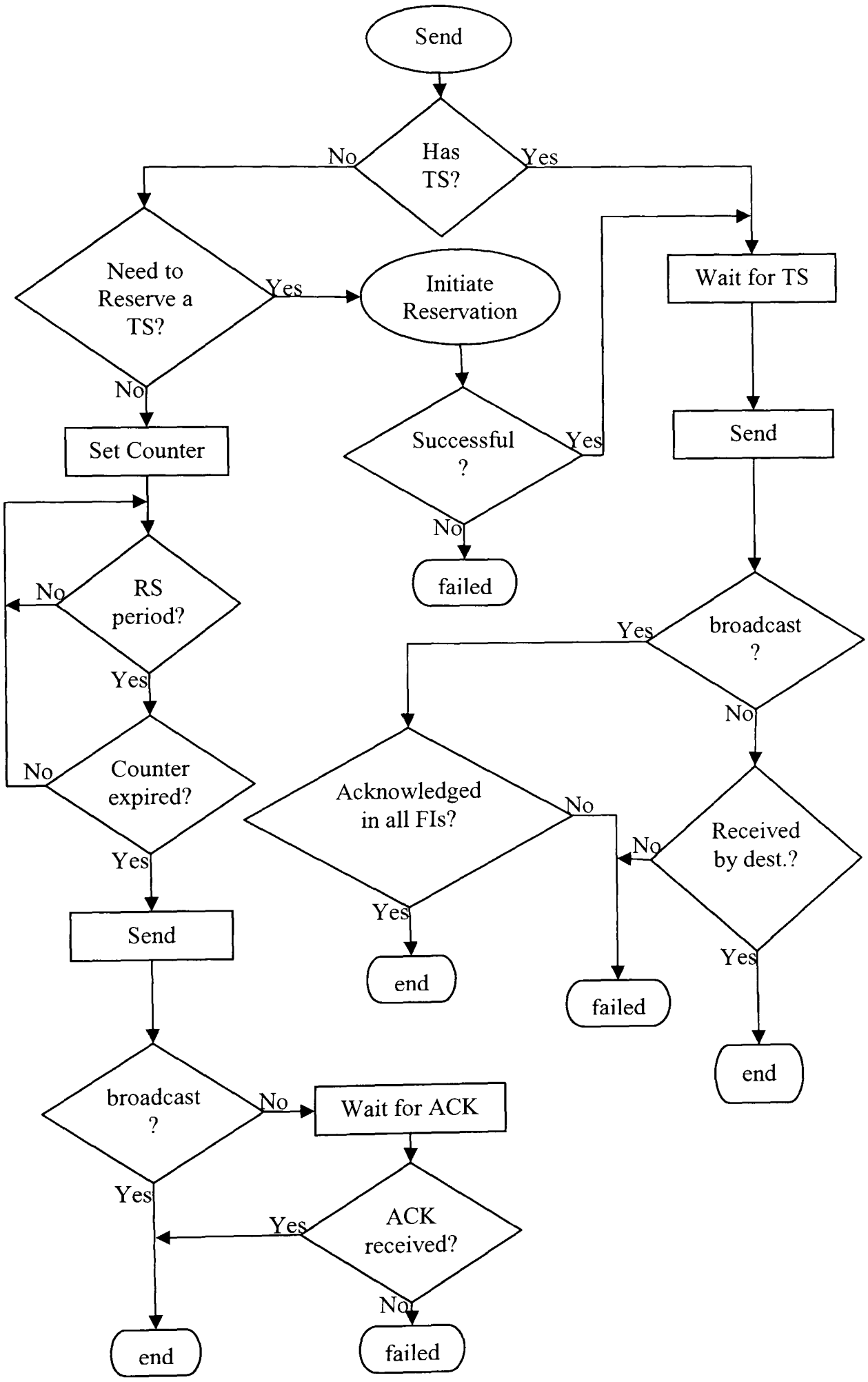

Initiate Reservation: Called when the node intends to reserve a TS slot.

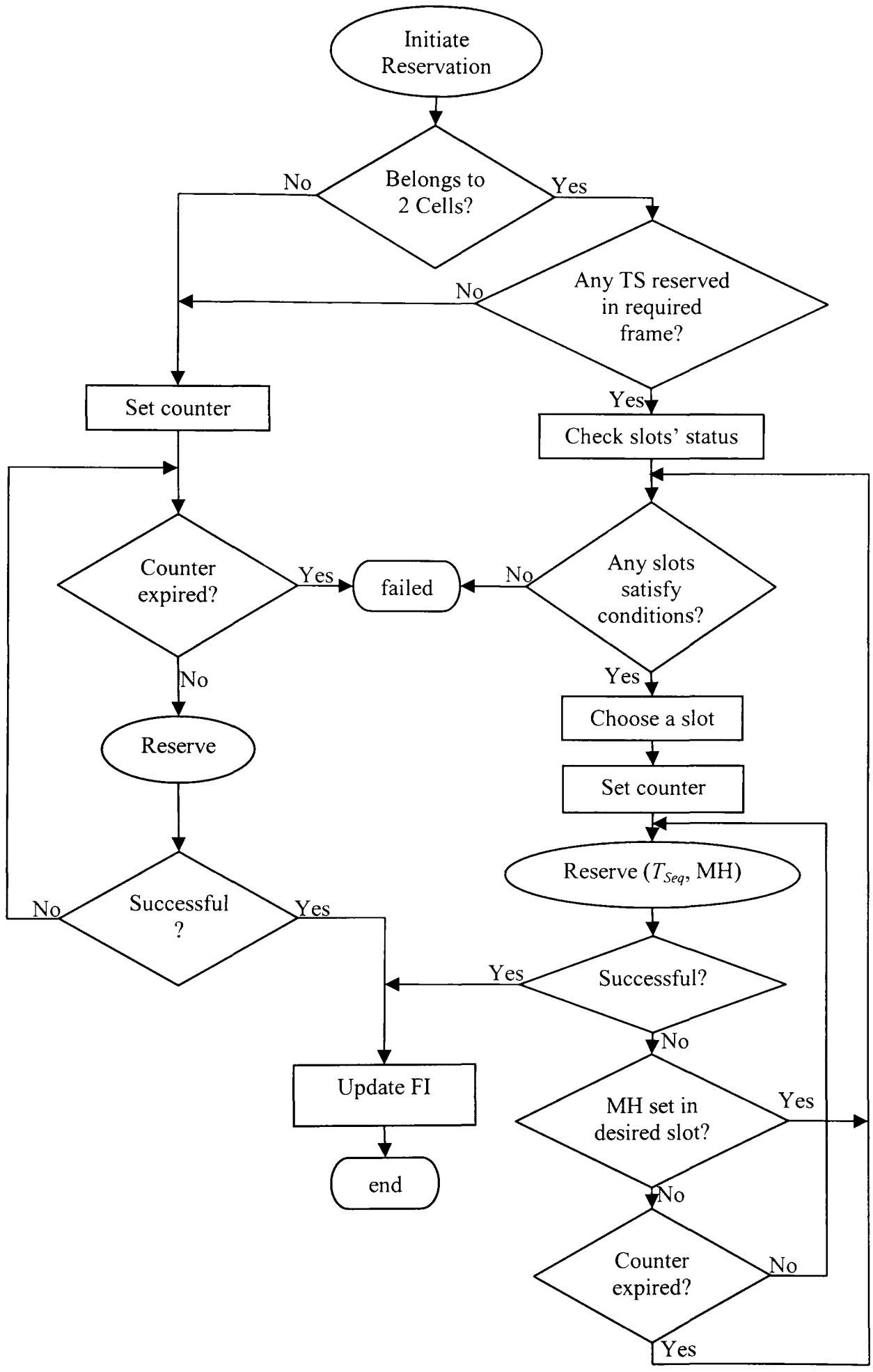

Reserve: Performs the reservation of a TS slot.

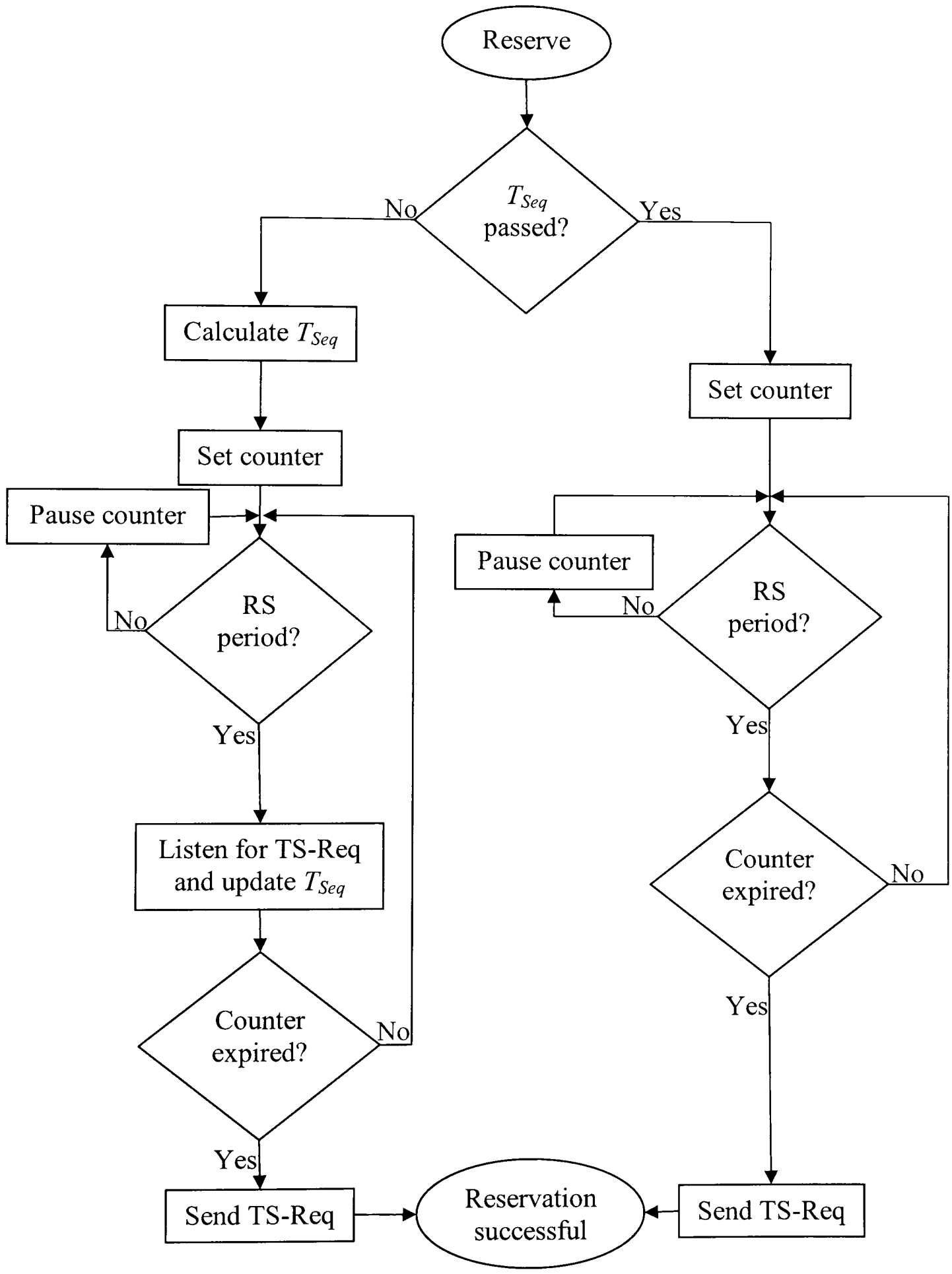

Reservation Successful: Checks whether the reservation was successful or not.

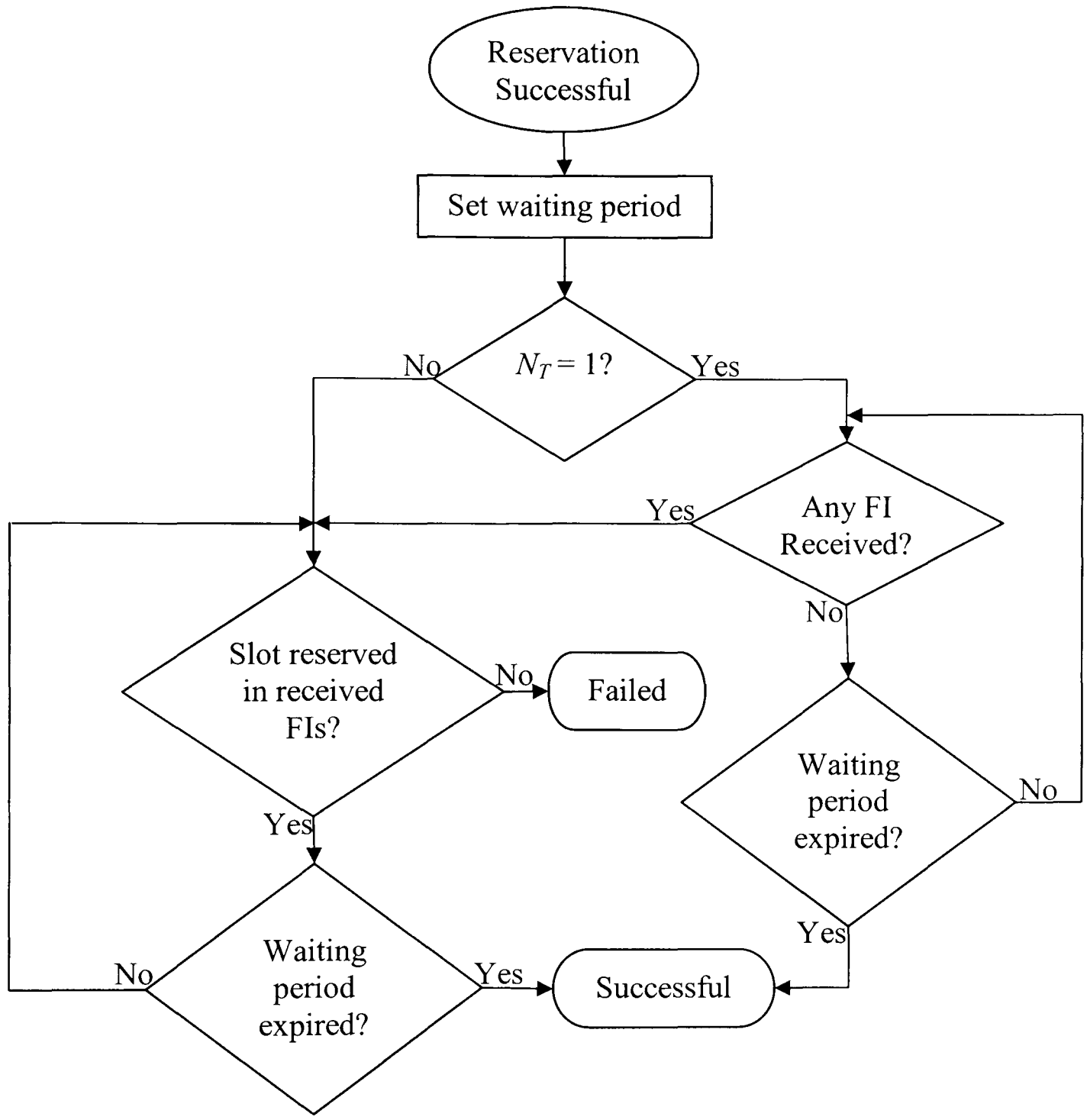

Initiate Delete: Called to delete a TS slot when the slot has been sensed IDLE and reported IDLE in received FI for the maximum number of frames (q) a TS slot can remain inactive (see section (7.2.2) rules (7.a) and (7.b)).

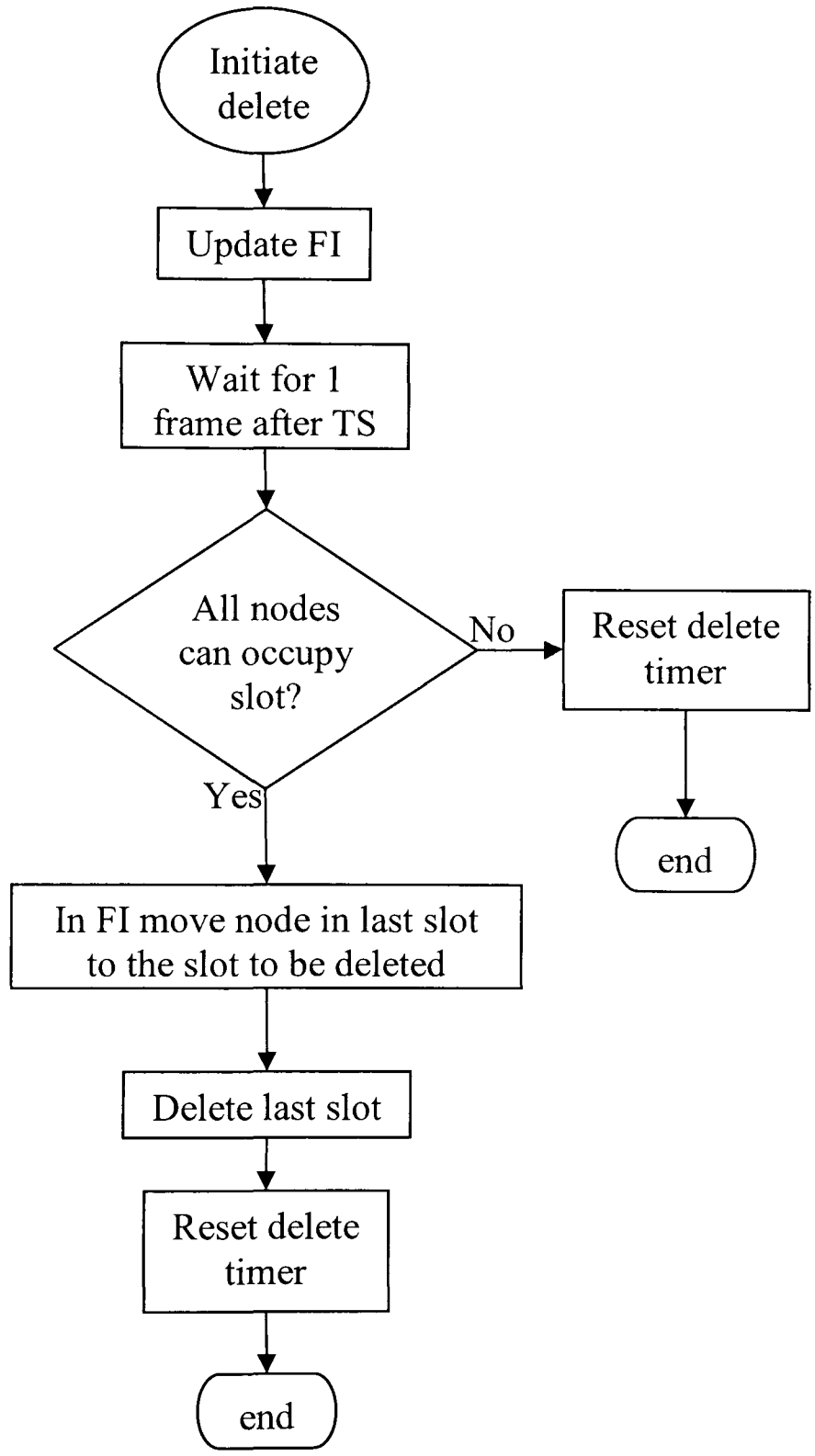

Broadcast Algorithm: Called when the node receives a broadcast packet to rebroadcast it.

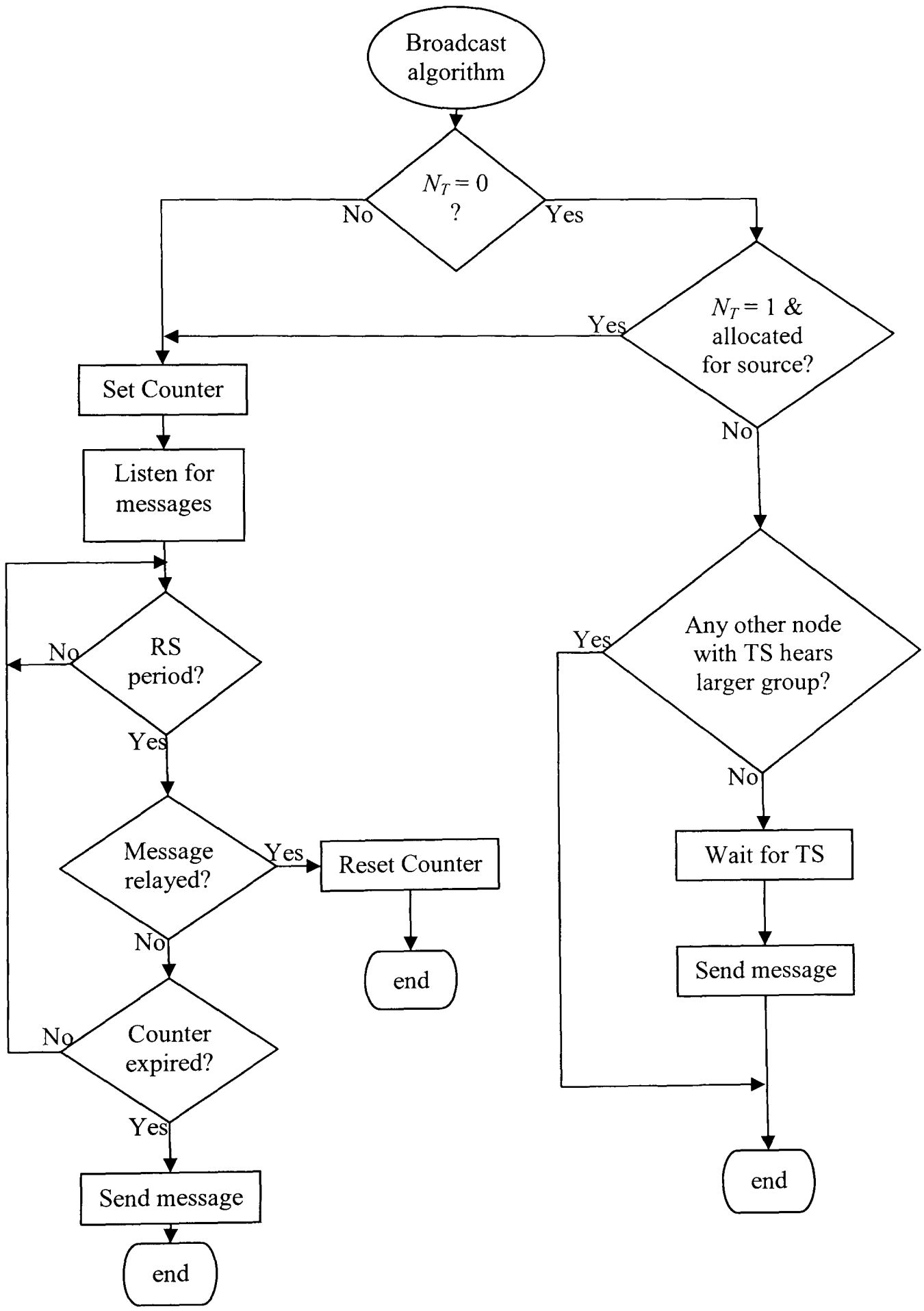

References

[1] G. M. T. Abdalla, M. A. Abu-Rgheff, and S.-M. Senouci, "Current Trends in Vehicular Ad Hoc Networks", UBIROADS Workshop, IEEE GIIS Conference,, Marrakech, Morocco,2-6 July 2007.

[2] G. M. T. Abdalla, M. A. Abu-Rgheff, and S. M. Senouci, "A Channel Update Algorithm for VBLAST Architecture in Vehicular Ad-hoc Networks", Wivec 2008, Calgary, Canada,21–22 Sep 2008.

[3] G. Abdalla, M. A. Abu-Rgheff, and S. M. Senouci, "Space-Orthogonal Frequency-Time Medium Access Control (SOFT MAC) for VANET," in *IEEE GIIS*, Hammamet, Tunisia, 22-26 June 2009.

[4] G. M. T. Abdalla, M. A. Abu-Rgheff, and S. M. Senouci, "Current Trends in Vehicular Ad Hoc Networks," in *UbiCC Journal-Special Issue of UbiRoads 2007*. vol. UbiRoads -Special Issue, March 2008.

[5] G. M. T. Abdalla, M. A. Abu-Rgheff, and S. M. Senouci, "An Adaptive Channel Model for VBLAST in Vehicular Networks," *EURASIP Journal on Wireless Communications and Networking,* vol. 2009, 2009.

[6] G. Abdalla, M. A. Abu-Rgheff, and S. M. Senouci, "Channel Tracking for VBLAST," *IEEE Vehicular Technology Magazine,* vol. 4, pp. 71-77, March 2009.

[7] G. M. T. Abdalla, M. A. Abu-Rgheff, and S. M. Senouci, "Joint Channel Tracking and ICI Equalisation for VBLAST-OFDM in VANET," *Accepted for IET Intelligent Transport Systems*.

[8] G. M. T. Abdalla, M. A. Abu-Rgheff, and S. M. Senouci, "Evaluation of SOFT MAC for VANET," *Submitted for IET Communications*.

[9] M. A. Abu-Rgheff, G. M. T. Abdalla, and S.-M. Senouci, "Space-Orthogonal Frequency-Time Medium Access Control (SOFT MAC) for VANET", France, INDI FR #0951620

[10] "FleetNet," *http://www.et2.tu-harburg.de/fleetnet/*.

[11] "IEEE Draft P802.11p/D2.0, November 2006."

[12] "IEEE Draft P1609.0/D01, February 2007."

[13] K. Tokuda, "DSRC-Type Communication System for Realizing Telematics Services," *Oki Technical Review,* vol. 71, No.2, pp. 64-67, April 2004.

[14] "IEEE Draft P802.11p/D0.25, November 2005."

[15] L. Armstrong, "Dedicated Short Range Communications (DSRC) at 5.9 GHZ," *Presentation, http://www.leearmstrong.com/DSRC%20Home/Standards%20 Programs/North%20American/DSRC%20Summary.ppt*.

[16] "American Society for Testing and Materials (ASTM)," *www.astm.org*.

[17] "COMeSafety Forum," *http://www.comesafety.org*.

[18] S. Hess, "Frequency spectrum for ITS," COMeSafety July 2006.

[19] S. Haykin and M. Moher, *Modern Wireless Communications*. USA: Pearson Prentice Hall, 2005.

[20] L. Cheng, B. E. Henty, D. D. Stancil, F. Bai, and P. Mudalige, "Mobile Vehicle-to-Vehicle Narrow-Band Channel Measurements and Characterisation of the 5.9 GHz Dedicated Short Range Communication (DSRC) Frequency Band," *IEEE Journal On Selected Areas In Communications,* vol. 25, pp. 1501-1516, Oct 2007.

[21] A. Polydoros, K. Dessouky, J. M. N. Pereira, C. Sun, K. Lee, T. D. Papavassiliou, and V. O. K. Li, "Vehicle to Roadside Communications Study," California Partners for Advanced Transit and Highways (PATH), California, Research Reports UCB-ITS-PRR-93-4, June 1993.

[22] J. G. Proakis, *Digital communications*, 4th ed. Singapore: McGraw Hill, 2001.

[23] T. P. Gill, *The Doppler Effect*. New York: Logos Press Limited, 1965.

[24] B. Sklar, "Rayleigh Fading Channels in Mobile Digital Communication Systems Part I: Characterization," in *IEEE Communications Magazine*. vol. 35, July 1997, pp. 90-100.

[25] B. Sklar, "Rayleigh Fading Channels in Mobile Digital Communication Systems Part II: Mitigation," in *IEEE Communications Magazine*. vol. 35, July 1997, pp. 102-109.

[26] W. C. Jakes, "Microwave Mobile Communications," USA: IEEE Press, 1994.

[27] R. B. Ertel, P. Cardieri, K. W. Sowerby, T. S. Rappaport, and J. H. Reed, "Overview of Spatial Channel Models for Antenna Array Communication Systems," in *IEEE Personal Communications*. vol. 5, Feb. 1998, pp. 10-22.

[28] W. C. Y. Lee, *Mobile Communications Engineering*. USA: McGraw Hill, 1982.

[29] J. C. Liberti and T. S. Rappaport, "A Geometrically Based Model for Line-of-Sight Multipath Radio Channels," in *Vehicular Technology Conference*, Atlanta, 1996, pp. 844-848.

[30] C. S. Patel, G. L. Stuber, and T. G. Pratt, "Simulation of Rayeligh-Faded Mobile-to-Mobile Communication Channels," *IEEE Transactions On Communications,* vol. 53, no. 11, pp. 1876-1884, Nov. 2005.

[31] L. Cheng, B. E. Henty, D. D. Stancil, and F. Bai, "Doppler Component Analysis of the Suburban Vehicle-to-Vehicle DSRC Propagation Channel at 5.9 GHz," in *IEEE Radio and Wireless Symposium*, 22-24 Jan 2008, pp. 343-346.

[32] A. G. Zajic and G. L. Stuber, "A Three-Dimensional MIMO Mobile-to-Mobile Channel Model," in *IEEE WCNC 2007 proceedings*, 2007, pp. 1885-1889.

[33] W. Wiesbeck and S. Knorzer, "Characteristics of the Mobile Channel for High Velocities," in *International Conference on Electromagnetics in Advanced Applications (ICEAA 2007)*, 17-21 Sep 2007, pp. 116-120.

[34] D. W. Matolak, I. Sen, W. Xiong, and N. T. Yaskoff, "5 GHz Wireless Channel Characterization For Vehicle To Vehicle Communications," in *IEEE Military Communications Conference*, 2005, pp. 3016-3022.

[35] J. Maurer, T. Fugen, and W. Wiesbeck, "Narrow-Band Measurement and Analysis of the Inter-Vehicle Transmission Channel at 5.2 GHz," in *Vehicular Technology Conference*, 6-9 May 2002, pp. 1274-1278.

[36] A. Paier, J. Karedal, N. Czink, H. Hofstetter, C. Dumard, T. Zemen, F. Tufvesson, A. F.Molisch, and C. F.Mecklenbrauker, "Car-to-car radio channel measurements at 5 GHz: Pathloss, power-delay profile, and delay-Doppler spectrum," in *IEEE ISWCS 2007*, 2007, pp. 224-228.

[37] A. R. S. Bahai, B. R. Saltzberg, and M. Ergen, *Multi-Carrier Digital Communications Theory and Applications of OFDM*, 2nd ed. USA: Springer, 2004.

[38] M. C. D. Maddocks, "An Introduction to Digital Modulation and OFDM Techniques," BBC Research Department Report No RD 1993/10 1993.

[39] Y. Chiu, D. Markovic, H. Tang, and N. Zhang, "OFDM Receiver Design," University of Berkeley Dec 2000.

[40] T. Wang, J. G. Proakis, E. Masry, and J. R. Zeidler, "Performance Degradation of OFDM Systems Due to Doppler Spreading," *IEEE Transactions On Wireless Communications,* vol. 5, pp. 1422-1432, June 2006.

[41] G. J. Foschini and M. J. Gans, "On Limits of Wireless Communications in a Fading Environment when Using Multiple Antennas," *Wireless Personal Communications,* vol. 6, pp. 311-335, March 1998.

[42] G. J. Foschini, "Layered Space-Time Architecture for Wireless Communication in a Fading Environment When Using Multi-element Antennas," *Bell Labs Technical Journal,* pp. 41-59, 1996.

[43] V. Tarokh, N. Seshadri, and A. R. Calderbank, "Space-Time Codes for High Data Rate Wireless Communication: Performance Criterion and Code Construction," *IEEE Transactions On Information Theory,* vol. 44, pp. 744-765, March 1998.

[44] P. W. Wolniansky, G. J. Foschini, G. D. Golden, and R. A. Valenzuela, "V-BLAST: An Architecture for Realizing Very High Data Rates Over the Rich-Scattering Wireless Channel," in *IEEE Proceedings of International Symposium on Signals, Systems, and Electronics*, Pisa, Italy, Sep. 1998, pp. 295-300.

[45] S. M. Alamouti, "A Simple Transmit Diversity Technique for Wireless Communications," *IEEE Journal on Selected Areas in Communications,* vol. 16, pp. 1451-1458, Oct 1998.

[46] V. Tarokh, H. Jafarkhani, and A. R. Calderbank, "Space-Time Block Codes from Orthogonal Designs," *IEEE Transactions On Information Theory,* vol. 45, pp. 1456-1467, July 1999.

[47] X. Li and Z. Nie, "Performance Losses in V-BLAST Due to Correlation," *IEEE Antennas and Wireless Propagation Letters,* vol. 3, pp. 291-294, 2004.

[48] G. J. Foschini, G. D. Golden, R. A. Valenzuela, and P. W. Wolniansky, "Simplified Processing for High Spectral Efficiency Wireless Communication Employing Multi-Element Arrays," *IEEE Journal On Selected Areas In Communications,* vol. 17, pp. 1841-1852, Nov 1999.

[49] D. Chizhik, G. J. Foschini, M. J. Gans, and R. A. Valenzuela, "Keyholes, Correlations, and Capacities of Multielement Transmit and Receive Antennas,"

IEEE Transactions On Wireless Communications, vol. 1, pp. 361-368, April 2002.

[50] D. Chizhik, F. Rashid-Farrokhi, J. Ling, and A. Lozano, "Effect of Antenna Separation on the Capacity of BLAST in Correlated Channels," *IEEE Communications Letters,* vol. 4, pp. 337-339, Nov. 2000.

[51] S. Loyka and A. Kouki, "On MIMO Channel Capacity, Correlations, and Keyholes: Analysis of Degenerate Channels," *IEEE Transactions On Communications,* vol. 50, pp. 1886-1888, Dec. 2002.

[52] K. Liu and A. M. Sayeed, "An Iterative Extension of BLAST Decoding Algorithm for Layered Space-Time Signals," *IEEE Transactions On Communications,* vol. 53, pp. 1754-1761, Oct. 2005.

[53] H. Lee, B. Lee, and I. Lee, "Iterative Detection and Decoding With an Improved V-BLAST for MIMO-OFDM Systems," *IEEE Journal On Selected Areas In Communications,* vol. 24, pp. 504-513, Mar. 2006.

[54] A. A. Rontogiannis, V. Kekatos, and K. Berberidis, "A Square-Root Adaptive V-BLAST Algorithm for Fast Time-Varying MIMO Channels," *IEEE Signal Processing Letters,* vol. 13, pp. 265-268, May 2006.

[55] M. Sellathurai and S. Haykin, "TURBO-BLAST for Wireless Communications: Theory and Experiments," *IEEE Transactions on Signal Processing,* vol. 50, pp. 2538-2546, Oct 2002.

[56] J. Hagenauer, "The Turbo Principle: Tutorial Introduction and State of the Art," in *Proc. Internationl Symposium on Turbo Codes*, Best, France, Sep. 1997.

[57] C. Berrou and A. Glavieux, "Near Optimum error-correcting coding and decoding: Turbo codes," *IEEE Transactions on Communications,* vol. 44, pp. 1261-1271, Oct 1996.

[58] M. Biguesh and A. B. Gershman, "Training-Based MIMO Channel Estimation: A Study of Estimator Tradeoffs and Optimal Training Signals," *IEEE Transactions on Signal Processing,* vol. 54, pp. 884-893, March 2006.

[59] H. Minn and N. Al-Dhahir, "Optimal Training Signals for MIMO OFDM Channel Estimation," *IEEE Transactions On Wireless Communications,* vol. 5, no. 5, pp. 1158-1168, May 2006.

[60] B. Park and T. F. Wong, "Optimal Training Sequence in MIMO Systems with Multiple Interference Sources," in *IEEE Communications Society Globecom 2004*, 2004, pp. 86-90.

[61] Q. Sun, D. C. Cox, H. C. Huang, and A. Lozano, "Estimation of Continuous Flat Fading MIMO Channels," *IEEE Transactions On Wireless Communications,* vol. 1, pp. 549-553, Oct. 2002.

[62] I. Barhumi, G. Leus, and M. Moonen, "Optimal Training Design for MIMO OFDM Systems in Mobile Wireless Channels," *IEEE Transactions on Signal Processing,* vol. 5, pp. 1615-1624, June 2003.

[63] Y. Li, "Simplified Channel Estimation for OFDM Systems With Multiple Transmit Antennas," *IEEE Transactions On Communications,* vol. 1, pp. 67-75, Jan 2002.

[64] C. Lin, W. Zhang, Y. Guo, and Y. Xu, "Co-Cyclic Jacket Matrix Based Optimal Training Design and Placement for MIMO OFDM Channel Estimation," in *IEEE International Conference on Circuits and Systems for Communications (ICCSC 2008)*, 26-28 May 2008, pp. 392-396.

[65] H. Minn and N. Al-Dhahir, "Optimal Training Signals for MIMO OFDM Channel Estimation," in *GLOBECOM 2004*, 29 Nov-3 Dec 2004, pp. 219-224.

[66] V. Pohl, P. H. Nguyen, V. Jungnickel, and C. v. Helmolt, "How often channel estimation is needed in MIMO systems," in *GLOBECOM 2003*, 1-5 Dec 2003, pp. 814-818.

[67] B. Balakumar, S. Shahbazpanahi, and T. Kirubarajan, "Joint MIMO Channel Tracking and Symbol Decoding Using Kalman Filtering," *IEEE Transactions on Signal Processing,* vol. 55, no. 12, pp. 5873-5879, Dec 2007.

[68] E. Karami and M. Shiva, "Maximum Likelihood MIMO Channel Tracking," in *IEEE VTC 2004*, May 2004, pp. 876-879.

[69] G. Yanfei and H. Zishu, "MIMO Channel Tracking Based on Kalman Filter and MMSE-DFE," in *Communications, Circuits and Systems, 2005 Proceedings*, May 2005, pp. 223-226.

[70] L. Li, H. Li, H. Yu, B. Yang, and H. Hu, "A New Algorithm for MIMO Channel Tracking Based on Kalman Filter," in *WCNC 2007 proceedings*, 2007, pp. 164-168.

[71] W. G. Jeon, K. H. Chang, and Y. S. Cho, "An Equalization Technique for Orthogonal Frequency-Division Multiplexing Systems in Time-Variant Multipath Channels," *IEEE Transactions on Communications,* vol. 47, pp. 27-32, Jan 1999.

[72] W. S. Hou and B. S. Chen, "ICI Cancellation for OFDM Communication Systems in Time-Varying Multipath Fading Channels," *IEEE Transactions On Wireless Communications,* vol. 4, pp. 2100-2110, Sep 2005.

[73] Y. Zhao and S.-G. Häggman, "Intercarrier Interference Self-Cancellation Scheme for OFDM Mobile Communication Systems," *IEEE Transactions on Communications,* vol. 49, pp. 1185-1191, July 2001.

[74] K. W. Park and Y. S. Cho, "An MIMO-OFDM Technique for High-Speed Mobile Channels," *IEEE Communications Letters,* vol. 9, pp. 604-606, July 2005.

[75] J. Kim, J. Robert W. Heath, and E. J. Powers, "Receiver Design for Alamouti Coded OFDM Systems in Fast Fading Channels," *IEEE Transactions On Wireless Communications,* vol. 4, pp. 550-559, March 2005.

[76] J. G. Andrews, A. Ghosh, and R. Muhamed, *Fundamentals of WiMax*. New Jersey: Prentice Hall, 2007.

[77] F. Borgonovo, A. Capone, M. Cesana, and L. Fratta, "ADHOC MAC: a new, flexible and reliable MAC architecture for ad-hoc networks," in *IEEE Wireless Communications and Networking*, 2003, pp. 965-970 vol.2.

[78] A. Ebner, H. Rohling, L. Wischhof, R. Halfmann, and M. Lott, "Performance of UTRA TDD Ad Hoc and IEEE 802.11b in Vehicular Environments", IEEE Vehicular Technology Conference, Jeju, South Korea,April 2003.

[79] M. Ergen, D. Lee, R. Sengupta, and P. Varaiya, "WRTP-Wireless Token Ring Protocol," *IEEE Transactions on Vehicular Technology,* vol. 53, pp. 1863-1881, Nov 2004.

[80] T.-K. Liu, J. A. Silvester, and A. Polydoros, "Performance Evaluation of R-ALOHA in Distributed Packet Radio Networks with Hard Real-time Communications", IEEE 45th Vehicular Technology Conference,1995.

[81] F. Yu and S. Biswas, "A Self Reorganizing MAC Protocol for Inter-vehicle Data Transfer Applications in Vehicular Ad Hoc Networks," in *IEEE 10th International Conference on Information Technoogy (ICIT 2007)*, 17-20 Dec 2007, pp. 110-113.

[82] R. Jurdak, C. V. Lopes, and P. Baldi, "A Survey, Classification and Comparative Analysis of Medium Access Control Protocols for Ad Hoc Networks," in *IEEE Communications Surveys & Tutorials*. vol. 6, Final Quarter 2004.

[83] S. Kumar, V. S. Raghavan, and J. Deng, "Medium Access Control protocols for ad hoc wireless networks: a survey," in *ARTICLE IN PRESS*, 2004.

[84] J. J. Blum, A. Eskandarian, and L. J. Hoffman, "Challenges of Intervehicle Ad Hoc Networks," *IEEE Transactions On Intelligent Transportation Systems,* vol. 5, pp. 347-351, Dec 2004.

[85] C. L. Fullmer and J. J. Garcia-Luna-Aceves, "Floor Acquisition Multiple Access (FAMA) for Packet-Radio Networks," in *Proceedings of ACM SIGCOMM 95 Conference*, 1995, pp. 262-273.

[86] P. Karn, "MACA - A New Channel Access Method for Packet Radio", ARRL/CRRL Amateur Radio 9th Computer Networking Conference,Sep 1990.

[87] V. Bharghavan, "MACAW: A Media Access Protocol for Wireless LAN's," *ACM SIGCOMM Computer Communication Review,* 1994.

[88] C.-s. Wu and V. O. K. Li, "Receiver-Initiated Busy-Tone Multiple Access in Packet Radio Networks," in *ACM SIGCOMM'94*, 1994, pp. 336-342.

[89] Z. J. Haas and J. Deng, "Dual Busy Tone Multiple Access (DBTMA)—A Multiple Access Control Scheme for Ad Hoc Networks," *IEEE Transactions on Communications,* vol. 50, pp. 975-985, June 2002.

[90] S. V. Bana and P. Varaiya, "Space Division Multiple Access (SDMA) for Robust Ad hoc Vehicle Communication Networks," in *IEEE Intelligent Transportation Systems Conference*, Oakland (CA) USA, 25-29 Aug 2001, pp. 962-967.

[91] J. J. Blum and A. Eskandarian, "A Reliable Link-Layer Protocol for Robust and Scalable Intervehicle Communications," *IEEE Transactions on Intelligent Transportation Systems,* vol. 8, pp. 4-13, March 2007.

[92] F. Borgonovo, A. Capone, M. Cesana, and L. Fratta, "ADHOC MAC: New MAC Architecture for Ad Hoc Networks Providing Efficient and Reliable Point-

to-Point and Broadcast Services," *Wireless Networks,* vol. 10, pp. 359-366, 2004.

[93] Y. Gunter, B. Wiegel, and H. P. Grossmann, "Cluster-based Medium Access Scheme for VANETs," in *IEEE Intelligent Transportation Systems Conference*, Seattle, USA, Oct 2007, pp. 343-348.

[94] H. Su and X. Zhang, "Clustering-Based Multichannel MAC Protocols for QoS Provisionings Over Vehicular Ad Hoc Networks," *IEEE Transactions on Vehicular Technology,* vol. 56, pp. 3309-3323, Nov 2007.

[95] B. O'Hara and A. Petrick, *IEEE 802.11 Handbook A Designer's Companion.* New York: Institute of Electrical and Electronics Engineers Inc., 1999.

[96] "IEEE Standard for Information technology— Telecommunications and information exchange between systems— Local and metropolitan area networks—Specific requirements." vol. Part 11: Wireless LAN Medium Access Control (MAC) and Physical Layer (PHY) Specifications: IEEE, June 2007.

[97] J. Larocca and R. Larocca, *802.11 Demystified.* USA: McGraw-Hill, 2002.

[98] N. Reid and R. Seide, *802.11 (Wi-Fi) Networking Handbook.* USA: McGraw-Hill, 2003.

[99] Y.-L. Kuo, C.-H. Lu, E. H.-K. Wu, G.-H. Chen, and Y.-H. Tseng, "Performance Analysis of the Enhanced Distributed Coordination Function in the IEEE 802.11e," in *VTC 2003*, 6-9 Oct 2003, pp. 3488-3492.

[100] M. Lott, "Performance of a Medium Access Scheme for Inter-vehicle Communication," in *Proc. of International Symposium on Performance Evaluation of Computer and Telecommunication Systems (SPECTS'02)*, San Diego, California, July 2002.

[101] A. Ebner, H. Rohling, R. Halfmann, and M. Lott, "Synchronization in Ad Hoc Networks Based on UTRA TDD," in *Proceedings of the 13th IEEE International Symposium on Personal, Indoor and Mobile Radio Communications (PIMRC 2002)*, Lisbon, Portugal, 2002.

[102] A. Ebner, H. Rohling, M. Lott, and R. Halfmann, "Decentralized Slot Synchronization In Highly Dynamic Ad Hoc Networks," in *Proceedings of the 5th International Symposium on Wireless Personal Multimedia Communications (WPMC'02)*, Honolulu, Hawaii, 2002.

[103] M. Lott, "Performance of a Medium Access Scheme for Inter-Vehicle Communication", International Symposium on Performance Evaluation of Computer and Telecommunication Systems SPECTS 2002, San Diego, CA, USA,July 2002.

[104] M. Lott, R. Halfmann, and M. Meincke, "A Frequency Agile Air-Interface for Inter-Vehicle Communication", ICT 2003, Tahiti,Feb 23 - March 1, 2003.

[105] C. Chih-Min, S. Jang-Ping, and I. C. Chou, "A load awareness medium access control protocol for wireless ad hoc network," in *IEEE International Conference on Communications*, 2003, pp. 438-442.

[106] F. Yu and S. Biswas, "Self-Configuring TDMA Protocols for Enhancing Vehicle Safety With DSRC Based Vehicle-to-Vehicle Communications," *IEEE Journal On Selected Areas In Communications,* vol. 25, pp. 1526-1537, Oct 2007.

[107] S. Katragadda, C. N. S. Ganesh Murthy, M. S. Ranga Rao, S. Mohan Kumar, and R. Sachin, "A decentralized location-based channel access protocol for inter-vehicle communication," in *The 57th IEEE Semiannual Vehicular Technology Conference, 2003. VTC 2003-Spring*, 22-25 April 2003, pp. 1831-1835.

[108] X. Zhang, H. Su, and H.-H. Chen, "Cluster-Based Multi-Channel Communications protocol in Vehicle Ad Hoc Networks," in *IEEE Wireless Communications*, Oct 2006, pp. 44-51.

[109] S.-L. Wu, C.-Y. Lin, Y.-C. Tseng, and J.-L. Sheu, "A new multi-channel MAC protocol with on-demand channel assignment for multi-hop mobile ad hoc networks," in *International Symposium on Parallel Architectures, Algorithms and Networks (I-SPAN 2000)*, 2000, pp. 232-237.

[110] J. So and N. H. Vaidya, "A Multi-channel MAC Protocol for Ad Hoc Wireless Networks," University of Illinois, Illinois Jan 2003.

[111] Y. Zang, L. Stibor, B. Walke, H. J. Reumerman, and A. Barroso, "A Novel MAC Protocol for Throughput Sensitive Applications in Vehicular Environments," in *IEEE Vehicular Technology Conference*, 22-25 April 2007, pp. 2580-2584.

[112] Y. Zang, L. Stibor, B. Walke, H.-J. Reumerman, and A. Barroso, "Towards Broadband Vehicular Ad-Hoc Networks - The Vehicular Mesh Network (VMESH) MAC Protocol," in *WCNC 2007*, 11-15 March 2007, pp. 417-422.

[113] M. Desai and D.Manjunath, "On the Connectivity in Finite Ad Hoc Networks," *IEEE Communications Letters,* vol. 6, pp. 437-439, Oct 2002.

[114] O. Dousse, P. Thiran, and M. Hasler, "Connectivity in ad-hoc and hybrid networks," in *IEEE INFOCOM 2002*, 2002, pp. 1079-1088.

[115] D. Yu and H. Li, "On The Definition of Ad Hoc Network Connectivity," in *Proceedings of ICCT2003*, 2003, pp. 990-994.

[116] L. Kleinrock and F. A. Tobagi, "Packet Switching in Radio Channels: Part I-Carrier Sense Multiple-Access Modes and Their Throughput-Delay Characteristics," *IEEE Transactions on Communications,* vol. COM-23, pp. 1400-1416, Dec 1975.

[117] C. H. Foh and B. S. Lee, "A Closed Form Network Connectivity Formula for One-Dimensional MANETs," in *IEEE International Conference on Communications*, June 2004, pp. 3739-3742.

[118] A. Ghasemi and S. Nader-Esfahani, "Exact Probability of Connectivity in One-Dimensional Ad Hoc Wireless Networks," *IEEE Communications Letters,* vol. 10, pp. 251-253, Apr 2006.

[119] C. H. Foh, G. Liu, B. S. Lee, B.-C. Seet, K.-J. Wong, and C. P. Fu, "Network Connectivity of One-Dimensional MANETs with Random Waypoint Movement," *IEEE Communications Letters,* vol. 9, pp. 31-33, 2005.

[120] I. W. H. Ho, K. K. Leung, J. W. Polak, and R. Mangharam, "Node Connectivity in Vehicular Ad Hoc Networks with Structured Mobility," in *IEEE 32nd Conference on Local Computer Networks (LCN 2007)*, 15-18 Oct 2007, pp. 635-642.

[121] S. Schnaufer, H. F¨ußler, M. Transier, and W. Effelsberg, "Vehicular Ad-Hoc Networks: Single-Hop Broadcast is not enough," in *3rd International Workshop on Intelligent Transportatio (WIT)*, Hamburg, Germany, March 2006, pp. 49-54.

[122] M. Torrent-Moreno, A. Festag, and H. Hartenstein, "System Design for Information Dissemination in VANETs," in *3rd International Workshop on Intelligent Transportation(WIT)*, Hamburg, Germany, March 2006, pp. 27-33.

[123] M. Torrent-Moreno, F. Schmidt-Eisenlohr, H. Füßler, and H. Hartenstein, "Packet Forwarding in VANETs, the Complete Set of Results," Dept. of Computer Science Universität Karlsruhe (TH) 2006.

[124] M. Meincke, P. Tondl, M. Dolores, P. Guirao, and K. Jobmann, "Wireless Adhoc Networks for Inter-Vehicle Communication", Zukunft der Netze - Die Verlezbarkeit meistern, 16. DFN-Arbeitstagung \über Kommunikationsnetze,2002.

[125] M. Jerbi, S.-M. Senouci, and Y. Ghamri-Doudane, "Towards Efficient Routing in Vehicular Ad Hoc Networks", UBIROADS 2007 workshop, GIIS, Marrakech, Morocco,July 2007.

[126] M. Mabiala, A. Busson, and V. e. V`eque, "On the capacity of Vehicular Ad Hoc Networks", UBIROADS 2007 workshop, GIIS, Marrakech, Morocco,July 2007.

[127] W. Stallings, *Data and Computer Communications*, 8th ed. New Jersey: Prentice Hall, 2007.

[128] "ITS Applications Overview," *http://itsdeployment2.ed.ornl.gov/ technology_overview/.*

[129] "eSafety Forum," *http://www.escope.info/.*

[130] T. Yamamoto, "Transportation and Safety In Japan," *IATSS Research,* vol. 29, pp. 110-113, 2005.

[131] J. Njord, J. Peters, M. Freitas, Bruce Warner, K. C. Allred, R. Bertini, R. Bryant, Robert Callan, M. Knopp, L. Knowlton, C. Lopez, and T. Warne, "Safety Applications of Intelligent Transportation Systems in Europe and Japan," American Trade Initiatives Jan. 2006.

[132] "SAFESPOT Project," *http://www.safespot-eu.org/pages/page.php.*

[133] "innovITS," *http://www.innovits.com/.*

[134] "Co-operative Systems for Intelligent Road Safety " *http://www.coopers-ip.eu/.*

[135] "CELTIC Initiative," *http://www.celtic-initiative.org/Projects/CARLINK/ default.asp.*

[136] "CARLINK Project," *http://carlink.lcc.uma.es/.*

[137] D. Khadraoui and F. Zimmer, "Carlink Project", UBIROADS 2007 workshop, GIIS, Marrakech, Morocco,July 2007.

[138] I. Sarris and A. Nix, "Design and performance assessment of maximum capacity MIMO architectures in line-of-sight," *IEE Proceedings-Communications,* vol. 153, pp. 482-488, Aug 2006.

[139] J. D. Parsons, *The Mobile Radio Propagation Channel*: John Wiley & Sons, 2001.

[140] Wikipedia, "http://en.wikipedia.org/wiki/Normal_distribution," 30 June 2009.

[141] S. Loyka, "V-BLAST Outage Probability: Analytical Analysis", Vehicular Technology Conference,2002.

[142] S. Loyka and F. Gagnon, "Performance Analysis of the V-BLAST Algorithm: An Analytical Approach," *IEEE Transactions On Wireless Communications,* vol. 3, pp. 1326-1337, July 2004.

[143] H. Meyr, M. Moeneclaey, and S. A. Fechtel, *Digital Communication Receivers*. USA: John Wiley & Sons, 1998.

[144] C. R. Rao and M. B. Rao, *Matrix Algebra and Its Applications to Statistics and Econometrics*. Singapore: World Scientific Publishing Co., 1998.

[145] J. R. Schott, *Matrix Analysis for Statistics*. New York: John Wiley & Sons, 1997.

[146] Wikipedia, "http://en.wikipedia.org/wiki/Moore-Penrose_pseudoinverse," 16 June 2009.

[147] J. J. Komo, *Random Signal Analysis in Engineering Systems*. London, UK: Academic Press, 1987.

[148] "http://integrals.wolfram.com/index.jsp."

[149] J. Nzouonta, N. Rajgure, G. Wang, and C. Borcea, "VANET Routing on City Roads Using Real-Time Vehicular Traffic Information," *IEEE Transactions on Vehicular Technology,* vol. 58, pp. 3609-3626, Sept 2009.

[150] M. Jerbi, "IVC-Analytic Studies," France Telecom R&D Feb 2008.

[151] K. Matheus, R. Morich, and A. Lübke, "Economic Background of Car-to-Car Communication," http://www.network–on–wheels.de/documents.html, 2004.

[152] G. Bianchi, "Performance Analysis of the IEEE 802.11 Distributed Coordination Function," *IEEE Journal on Areas in Communications,* vol. 18, pp. 535-547, March 2000.

[153] H. Fattah, "Analysis of the Channel Access Mechanism in IEEE 802.11 Wireless Local Area Networks," in *IEEE Pacific Rim Conference on Communication, Computing and Signal Processing*, Aug 2007, pp. 74-77.

[154] L. Kleinrock and F. A. Tobagi, "Packet Switching in Radio Channels: Part II-Carrier Sense Multiple-Access Modes and Their Throughput-Delay Characteristics," *IEEE Transactions on Communications,* vol. COM-23, pp. 1417-1433, Dec 1975.

[155] L. Kleinrock and F. A. Tobagi, "Packet Switching in Radio Channels: Part III-Carrier Sense Multiple-Access Modes and Their Throughput-Delay Characteristics," *IEEE Transactions on Communications,* vol. COM-23, pp. 832-845, Aug 1976.

[156] F. Borgonovo, L. Campelli, M. Cesana, and L. Fratta, "Impact of User Mobility on the Broadcast Service Efficiency of the ADHOC MAC protocol," in *IEEE 61st Vehicular Technology Conference*, 30 May -1 June 2005, pp. 2310-2314.

[157] H. Füßler, A. Leibscher, J. Widmer, M. Transier, and W. Effelsberg, "Contention-Based Distance-Vector Routing (CBDV) for Mobile Ad-Hoc Networks," http://www.informatik.uni-mannheim.de/pi4/publications/single/Fuessler2004e, Dec 2006.